Tuning sensory mechanotransduction to wind down neuropathic pain

Dissertation zur Erlangung des akademischen Grades des Doktors der Naturwissenschaften (Dr. rer. nat.)

Eingereicht im Fachbereich Biologie, Chemie, Pharmazie
der Freien Universität Berlin

vorgelegt von

Johannes Kühnemund

aus Deutschland

14.12.2020

1. Gutachter: Prof. Dr. Gary R. Lewin

2. Gutachter: Prof. Dr. Peter Robin Hiesinger

Disputation am: 21.06.2021

Directory

List of Figures

List of abbreviations

aa	amino acid
AM	A-mechanonociceptor
AMPA	α-Amino-3-Hydroxy-5-Methyl-4-Isoxazolepropionic acid
ANOVA	analysis of variance
AP	action potential
BDNF	brain derived neurotrophic factor
BiFC	bi-molecular fluorescence complementation
C.elegans	Caenorhabditis elegans
cAMP	cyclic adenosine monophosphate
CCI	chronic constriction injury
CFA	complete Freund's adjuvants
C-M	C-mechanonociceptor
C-MC	C-mechano-cold nociceptor
C-MH	C-mechano-heat nociceptor
C-MHC	C-mechano-heatcold nociceptor
CNS	central nervous system
CRPS	complex regional pain syndrome
CV	conduction velocity
DH	dorsal horn
D-hair	down hair
DRG	dorsal root ganglion
e.g.	exempli gratia(lt.) - for example
ECM	extracellular matrix
EM	electron microscopy
ES	embryonic stem cells
fTIR	frustrated total internal reflection
GABA	gamma-Aminobutyric acid
HEK	human embryonic kidney cell line
HIV	human immunodeficiency virus
HTMR	high-threshold mechanoreceptor
i.p.	intraperitoneal
IASP	international association for the study of pain
IL	interleukin
K2p	2-pore domain potassium channel

LTMR	low-threshold mechanoreceptor
MSC	mechanosensitive ion channel
MscL	mechanosensitive channel of large conductance
MscS	mechanosensitive channel of small conductance
N2A	neurobalstoma cell line
NGF	nerve growth factor
NMDA	N-Methyl-D-aspartate
NNT	numbers needed to treat
OB-1,2	oligomerisation blocker 1,2
ORF	open reading frame
PAR2	protease activated receptor 2
PFA	paraformaldehyde
PKA	protein kinase A
PKC	protein kinase C
PWT	paw-withdrawal threshold
RA	rapidly-adapting
RAM	rapidly-adapting mechanoreceptor
SA	slowly-adapting
SAM	slowly-adapting mechanoreceptor
SC	spinal cord
SIF	synthetic inerstitial fluid
SNI	spared nerve injury
SNL	spinal nerve ligation
STOML3	stomatin-like protein 3
TEM	transmission electron microscopy
TG	trigeminal ganglion
TNFa	timor necrosis factor alpha
TRP-V	transient receptor potential vanilloid
TTX	tetrodotoxin
VGCC	voltage-gated calcium channel
VGSC	voltage-gated sodium channel
WDR	wide dynamic range

Abstract

Neuropathic pain is caused by lesion or disease of the somatosensory nervous system. It is a multifactorial condition with common symptoms and disease mechanisms (allodynia and hyperalgesia) that causes severe suffering in patients and a high burden to society.

We wanted to gain a deeper understanding of disease contributions of the peripheral nervous system with the goal to develop new analgesic substances. We performed chronic constriction injury (CCI) on experimental animals which produced robust mechanical hypersensitivity. Gait analysis was established to provide an additional experimenter-independent read-out for mechanical hypersensitivity following neuropathic injury. Light- and electron microscopy were used to quantify the damage subjected to the peripheral nerve. An e*x-vivo* skin nerve preparation from the glabrous skin of experimental animals was used to characterize mechanoreceptors and nociceptors in neuropathic skin and uncover possible sensitization effects linking behavioural data with nerve recordings and therefore compile an integrative dataset. STOML3 is upregulated after nerve injury, therefore I additionally investigated the effects of *in vivo* overexpression of STOML3 on sensory mechanotransduction, as well as *stoml3* conditional deletion specifically in sensory neurons.

I found that the physiological properties of low-threshold mechanoreceptors (LTMRs) are not altered following CCI, except a diminished static phase activity in slowly-adapting mechanoreceptors (SAMs). However, sensitization following neuropathic injury could be shown in C-fibers, displaying a significant reduction in transduction thresholds as well as emerging dynamic-phase coding properties that resulted from the injury. These alterations in physiological properties could explain in part the phenomenon of mechanical allodynia. Stimuli that would under normal circumstances not induce activity in the nociceptive C-fiber system, now do so following CCI. Following neuropathic injury proportionately more nociceptors are activated by low intensity mechanical stimuli therefore nociceptive input plays a more pronounced role in the overall sensory barrage into the spinal cord in animals with neuropathic pain.

The *in vivo* overexpression of STOML3 has immense effects on the physiological properties of mechanoreceptors and nociceptors. LTMRs (RAMs and SAMs) were clearly sensitized and again C-fibers displayed prominent changes in their mechanosensitivity. Polymodal C-fibers displayed marked sensitization phenotypes: increased activity, lowered mechanical thresholds as well as dynamic-phase coding properties emerged after induced STOML3 overexpression. CMs increased their activity as well but only for the largest suprathreshold force stimuli. Overall, the overexpression of STOML3 in sensory neurons phenocopied the physiological

changes emerging following CCI. Animals acquired mechanical hypersensitivity and the changes in the C-fiber nociceptive system were very similar to neuropathic injury.

STOML3 is essential for the emerging sensitization of C-fibers following neuropathic injury proven by genetic ablation of *stoml3* in sensory neurons. C-fibers recorded from conditional knockouts did not display elevated physiological activity (CMs) or showed intermediate phenotypes (polymodal C-fibers) following CCI. Interestingly, polymodal C-fibers showed increased activity immediately (<1s) after a mechanical stimulus, however in CMs this physiological abnormality was completely abolished. STOML3 seems to be essential for CM sensitization after neuropathic injury and for polymodal C-fibers partially responsible in producing the sensitization phenotype. Finally, I showed that sensitized C-fibers acquired the ability to follow low frequency (5Hz) vibrations. In some cases, to the extent of phase-locking, and in some cases with less accuracy. High stimulation strengths were necessary to induce activity in CMs in the conditional knockouts, polymodal C-fibers lacking STOML3 did not respond to this type of stimulation at all, further evidence that STOML3 is important for onset activity, that STOML3 is essential for peripheral sensitization following neuropathic injury and that the changes in C-fiber physiology might be the driver for mechanical hypersensitivity displayed by experimental animals after induced neuropathy.

Zusammenfassung

Neuropathischer Schmerz wird durch eine Verletzung oder Krankheit des somatosensorischen Nervensystems verursacht. Es handelt sich um ein multifaktorielles Krankheitsbild mit gemeinsamen Symptomen und Krankheitsmechanismen (Allodynie und Hyperalgesie) welches ernstes Leid in Patienten hervorruft und eine schwere Belastung für die Gesellschaft darstellt.

Wir wollten ein tiefgründiges Verständnis für den Anteil des peripheren Nervensystems an dieser Krankheit erlangen, mit dem Ziel neue Analgetika zu entwickeln. Wir haben die „chronic constriction inury (CCI)“ in Versuchstieren zur Anwendung gebracht und damit robuste mechanische Hypersensitivität herbeigeführt. Gangartanalyse wurde etabliert, um einen zusätzlichen Experimentator-unabhängigen Messwert für mechanische Hypersensitivität nach neuropathischer Verletzung zu bekommen. Licht- und Elektronenmikroskopie wurde angewandt, um den zugefügten Schaden im peripheren Nerven zu quantifizieren. Eine e*x-vivo* Hautnerv-Präparation von der unbehaarten Haut von Versuchstieren wurde benutzt, um Mechanorezeptoren und Nozizeptoren aus neuropathischer Haut zu vermessen und vermutete Sensitisierungseffekte zu entdecken und Daten aus Verhaltensexperimenten mit Nervableitungen zu verbinden, um somit einen integrativen Datensatz zu erlangen. STOML3 ist nach Nervenverletzung hochreguliert, deswegen wurde zusätzlich der Effekt von *in vivo* Überexprimierung von STOML3 auf die Mechanotransduktion untersucht, sowie die für sensorische Neurone spezifische Entfernung von *stoml3*.

Ich habe herausgefunden, dass sich die physiologischen Eigenschaften von low-threshold Mechanorezeptoren (LTMRs) nach CCI nicht ändern, bis auf eine reduzierte Aktivität in der statischen Phase von langsam adaptierenden Mechanorezeptoren (SAMs). Jedoch konnte auf neuropathische Verletzung folgende Sensitisierung in C-Fasern nachgewiesen werden, welche eine signifikant herabgesetzte Reiztransduktionsschwelle, sowie die auftretende Eigenschaft dynamische Phasen von mechanischen Stimulationen zu transduzieren, zeigten. Diese Änderungen von physiologischen Eigenschaften könnten das Phänomen der mechanischen Allodynie erklären. Reize, die unter normalen Umständen keine Aktivität im nozizeptiven C-Faser-System auslösen würden, tun dies nun nach erfolgter CCI-Operation. Nach neuropathischer Verletzung werden proportional mehr Nozizeptoren von schwachen mechanischen Reizen aktiviert und somit spielt der Anteil des nozizeptiven Einganges von Peripherie ins Rückenmark des Nervensystems eine größere Rolle bei Versuchstieren mit neuropathischem Schmerz.

Die *in vivo* Überexprimierung von STOML3 hat einen immensen Effekt auf die physiologischen Eigenschaften von Mechanorezeptoren und Nozizeptoren. LTMRs (RAMs und SAMs) waren eindeutig sensitisiert und wieder zeigten C-Fasern deutliche Änderungen in ihrer Mechanosensitivität. Polymodale C-Fasern zeigten einen starken Sensitisierungsphänotyp: erhöhte Aktivität, erniedrigte Schwellenwerte für mechanische Reiztransduktion sowie die Eigenschaft dynamische Phasen von mechanischen Stimulationen zu transduzieren erschienen nach induzierter STOML3 Überexprimierung. CMs erhöhten ihre Aktivität auch, aber eher, wenn mit den stärksten mechanischen Reizen stimuliert. Zusammenfassend lässt sich festhalten, dass die Überexprimierung von STOML3 in sensorischen Neuronen die auftretenden physiologischen Änderungen nach CCI-Operation reproduziert. Versuchstiere entwickelten mechanische Hypersensitivität und physiologische Änderungen im nozizeptiven C-Faser System waren sehr ähnlich zu denen nach neuropathischer Verletzung.

STOML3 ist essenziell für die aufkommende Sensitisierung in C-Fasern nach neuropathischer Verletzung, bewiesen durch die genetische Entfernung von *stoml3* in sensorischen Neuronen. C-Fasern abgeleitet von konditionellen Knockouts nach CCI-Operation haben keine gesteigerte physiologische Aktivität gezeigt (CMs) oder aber einen abgeschwächten Phänotyp (polymodale C-Fasern). Interessanter weise zeigten polymodale C-Fasern trotzdem erhöhte Aktivität in der ersten Sekunde der mechanischen Stimulation, in CMs war diese physiologische Abnormalität komplett verschwunden. STOML3 scheint essenziell für CM Sensitisierung nach neuropathischer Verletzung zu sein und für polymodale C-Faserns teilweise verantwortlich für den Sensitisierungs-Phänotyp. Schlussendlich habe ich gezeigt, dass C-Fasen die Fähigkeit gewinnen niedrig-frequente Vibration zu transduzieren. In manchen Fällen sogar bis zum vollumfänglichen Phasenlock, in manchen Fällen mit weniger Genauigkeit. Große Stimulationsstärken waren nötig, um Aktivität in CMs der konditionellen Knockouts zu induzieren, polymodale C-Fasern ohne STOML3 haben auf diese Art von Stimulation überhaupt nicht reagiert, zusätzliche Beweise, dass STOML3 essentiell für die Aktivität zu Beginn der Reiztransduktion ist, sowie für periphere Sensitisierung nach neuropathischer Verletzung und, dass die Änderungen in der C-Faser Physiologie möglicherweise die treibende Kraft für aufkommende mechanische Hypersensitivität darstellt, welche von Versuchstieren nach neuropathischer Verletzung zur Schau gestellt werden.

1 Introduction

1.1 Aims and hypothesis

The aim of this work was to investigate physiological changes in somatosensory mechanotransduction following nerve injury to uncover new targets for pharmacological intervention - as well as the establishment of an experimenter-independent assay to measure pain-progression / alleviation of pain after drug treatment.

Neuropathic pain is caused by lesion or disease of the somatosensory nervous system [IASP-Definition, (Murnion, 2018)]. It is a multifactorial condition that causes severe suffering in patients and a high burden to society. It can be caused by viral infection (e.g. shingles), microvascular injuries in diabetic cases, trauma, or emerge as a side-effect of chemotherapy. While the cause of pain onset is multifactorial there are common symptoms and disease mechanisms present in most cases – allodynia and hyperalgesia (Baron, 2006). Hyperalgesia is an elevated pain response to noxious stimuli whereas in allodynia normally innocuous stimuli are suddenly perceived as painful. Allodynic patients can perceive tiny stimuli such as the brush of a feather as painful and current therapeutic strategies are not sufficient, since they in general require high NNTs (numbers needed to treat) between 6 to 10 (Finnerup et al., 2015). Patients may receive centrally acting opioid analgesics as well as anti-convulsive drugs which only mask the symptoms and have severe side effects (e.g. the opioid crisis, USA). Our lab has been working on new strategies to address this problem. Since allodynia and hyperalgesia are both forms of hypersensitivity caused by injury or disease, we hypothesize that following nerve injury physiological properties of mechanoreceptors and/-or nociceptors within the somatosensory system may be altered. For example, peripheral nerve terminals could be sensitized and therefore upon stimulation produce enhanced sensory input, that when relayed into the central nervous system becomes a percept with painful paraesthetic quality. We want to counteract this harmful process by modulating sensory mechanotransduction in the periphery and investigate if this leads to alleviation of pain.

To test this hypothesis, the chronic constriction injury (CCI) was applied to experimental animals. CCI produces robust mechanical hypersensitivity quantifiable using a modification of the classical von Frey assay (Chaplan, Bach, Pogrel, Chung, & Yaksh, 1994; Dixon, 1980). Gait analysis was established in the lab to provide an additional experimenter-independent read-out. We hypothesized that experimental animals would display differences in weight-bearing behaviour, since any contact with the constricted hind-paw will cause pain, animals will try to prevent self-stimulation by minimising contact time with the walkway. Light- and electron microscopy were used to quantify the damage to the peripheral nerve and to

investigate if the integrity of the myelin sheath of sensory neurons remained intact. *Ex-vivo* skin nerve recordings were performed in the glabrous skin of experimental animals to characterize mechanoreceptors and nociceptors in neuropathic skin and uncover possible sensitization effects linking behavioural data with sensory recordings. In many studies nerve injury models are applied to experimental animals and behavioural data acquired by stimulating the glabrous skin of the animals, but electrophysiological recordings are performed on the hairy skin which has not been tested in the behaviour. This approach is unreasonable since there is no direct connection between behavioural and electrophysiology data. Here, I compile an integrative dataset ultimately linking behaviour and electrophysiology.

Furthermore, I investigated the effects of *in vivo* overexpression of STOML3 on sensory mechanotransduction, as well as *stoml3* ablation in sensory neurons specifically using a wnt1-Cre conditional knockout to determine STOML3s effect on mechanotransduction and nociception.

1.2 Introduction

In order to interact with and experience their surrounding world, living organisms have developed sensory systems to see, hear, smell, taste and feel physical objects and assign pleasant or unpleasant characteristics to them. One of these five sensory modalities is touch mediated through humans' largest sensory organ – the skin. Touch can have various qualities: weak or vibrating- as well as strong, painful or pleasant stimuli which when detected are transduced into electrical signals by specialized receptors in our skin (signal transduction). There is a high degree of specialisation in touch-receptors. One population is dedicated to transducing weak and vibrating stimuli (low-threshold mechanoreceptors) and another transduces strong and potentially harmful stimuli (high-threshold mechanoreceptors / nociceptors). Multiple subclasses of receptive end-organs as well as innervating neurons belong to both categories.

The molecular mechanisms of mechanotransduction are currently poorly understood. How can external force, acting on receptors, gate ion-channels and initiate action potential (AP) generation and -propagation? It is not only mechanotransduction that needs to be researched further – the aim of my thesis work is to investigate what happens to the disordered somatosensory system in disease states. I investigated potential physiological alterations in mechanotransduction as a possible mechanism for the emergence of pathological pain states and aim to alleviate hypersensitivity-based pain disorders through modulation of afferent sensory mechanotransduction.

Neuropathic pain is caused by lesion or disease of the somatosensory nervous system [IASP-definition]. It is a serious problem diminishing the quality of life of patients. The most common symptoms following traumatic nerve injury in humans are paraesthesias: allodynia and hyperalgesia. Hyperalgesia is an elevated pain response to noxious stimuli whereas in allodynia normally innocuous stimuli are suddenly perceived as painful. Currently there are very limited therapeutic strategies to treat these conditions. The current view is that these pathological states originate from aberrant excitation in damaged peripheral sensory nerves which drives central sensitisation in somatosensory pathways (Gold & Gebhart, 2010; M Koltzenburg, Torebjörk, & Wahren, 1994; Kuner & Flor, 2016; Meacham, Shepherd, Mohapatra, & Haroutounian, 2017).

1.2.1 Sensory mechanotranduction in glabrous skin (general introduction)

The recognition and processing of mechanical stimuli is mediated by cells located in the dorsal root- (DRG) and trigeminal ganglia (TG). These ganglia house the somata of a diverse cell

population with pseudunipolar neurites. One branch extends to the periphery to form free nerve endings, hair follicle afferents or to innervate specialized end organs in the skin whereas the second branch connects to secondary neurons in the dorsal horn (DH) of the spinal cord (SC). This special anatomy illustrates their function: Information is transferred from the periphery to higher order integrative centers in the central nervous system (CNS).

Diverse mechanical, thermal and chemical stimuli act on the skin and are transformed into the language of our nervous system: the action potential. For mechanical stimuli this process is termed mechanotransduction. A supra-threshold stimulus acts on receptor-endings in the periphery resulting in a graded receptor-potential which eventually triggers action potential initiation (Hu & Lewin, 2006) and subsequently -propagation into the CNS. An important question that received a lot of attention from multiple research groups in the last decades is: which proteins are involved in this process?

Mechanotransduction is extremely fast (Corey & Hudspeth, 1979). Based on the observation that movement of a hair bundle produced electrical signals just 40µs after deflection it was hypothesized that mechanotransduction must be a process that works via direct gating of a channel-protein facilitating ion-influx, no chemical intermediates could play a role (except for maybe a modulatory role) because of its incredible speed. Here, I will at first introduce the various receptive end organs as well as innervating neurons of the glabrous skin with their physiological characteristics before reviewing the current information about the mechanosensitive ion channels mediating their activity.

The glabrous skin of mammals is a highly specialized type of skin most often used to explore, experience and interact with the tactile world. The palms and fingertips for instance are comprised of glabrous skin – providing us with an incredibly sensitive sensory organ to detect the texture of objects as well as thermal qualities such as warmth or cold. If a stimulus is harmful, specialized high-threshold receptors or nociceptors will be activated giving us the means to avoid further contact through the initiation of pain sensation as a protective mechanism. Pain can unfortunately also emerge if no potentially harmful stimulus is present due to pathological processes in the peripheral nervous system – this phenomenon is termed neuropathic pain and will be addressed in a later part of the introduction. I will start with introducing the so-called low-threshold mechanoreceptors that transduce tiny mechanical stimuli such as vibration, before introducing high-threshold receptors or nociceptors and pain sensation.

1.2.2 LTMRs (end organs and physiology)

Low-threshold mechanoreceptors (LTMR) as their name suggests, respond to mechanical stimuli and exhibit low detection thresholds. They can be associated with thickly- or thinly myelinated fibers of the A-ß or A-δ categories respectively or some with C-fibers. Depending on the grade of myelination, fast (A-ß: >10m/s in mice (Adriaensen, Gybels, Handwerker, & Van Hees, 1983; Martin Koltzenburg, Stucky, & Lewin, 1997)), intermediate (between 10 - 1.3m/s in mice (Martin Koltzenburg et al., 1997)) or slow (< 1.3m/s in mice (Martin Koltzenburg et al., 1997)) conduction velocity of signal propagation is achieved. Furthermore, adaptation properties to mechanical stimuli differ along with end-organs in the skin (the actual receptor or mechanotransducer) that are innervated by the aforementioned fiber-types, resulting in a complex pattern of preferred modality transduction as sensory basis for haptic percepts.

Meissner's corpuscles are the specialized end-organs of rapidly-adapting low-threshold mechanoreceptors (RAMs) associated with A-ß fiber neurons in mammalian glabrous skin (Fig.1). A second RA population associated with Pacinian corpuscles was additionally described (Joong Woo Leem, Willis, & Jin Mo Chung, 1993; A. Zimmerman, Bai, & Ginty, 2014), however this end-organ is not vastly abundant in mouse glabrous skin (Cain, Khasabov, & Simone, 2001; Gary R. Lewin & Moshourab, 2004). RAMs are so-called velocity-indicators (Johansson & Westling, 1984; Westling & Johansson, 1984; Sanders & Zimmermann, 1986; Vega-Bermudez & Johnson, 1999a, 1999b). They are sensitive to vibrations (e.g. a phasic velocity stimulus such as a sinusoidal wave) and generate neuronal activity rapidly after the onset of an appropriate stimulus. Increasing neuronal firing is produced with increasing velocity, whereas static indentations are not transduced. The classical stimulation of mechanoreceptors consists of mechanical indentations comprised of a dynamic-phase (the stimulator makes contact with the skin causing a small indentation during which movement occurs) and a static phase (the stimulus is kept constant to test adaptation properties). RAMs adapt rapidly, meaning that the static phase of the stimulus is not coded by APs.

Slow adaptation (SA) or persistent generation of neuronal activity in the dynamic- and static phase of aforementioned stimulus is the defining characteristic of a second population of sensory receptors, associated with the Merkel cell (-complex) in glabrous skin (Fig.1). Like the Meissner's corpuscle they are associated with A-ß fiber neurons. A second SA population associated with Ruffini endings was additionally described (Amanda Zimmerman, Bai, & Ginty, 2014), however again in mouse glabrous skin, these receptors are not very abundant (Cain et al., 2001; Gary R. Lewin & Moshourab, 2004). SAMs are sensitive to vibration as well and generate APs rapidly after onset of mechanical indentation.

The third member of the LTMR category are the D-hair mechanoreceptors (Rutlin et al., 2014; Walcher et al., 2018). Hair shafts were found in the center of the glabrous skin in mice. These hairs are innervated by so-called hair-follicle afferents displaying rapidly-adapting properties and innervation by A-δ neurons (Fig.1).

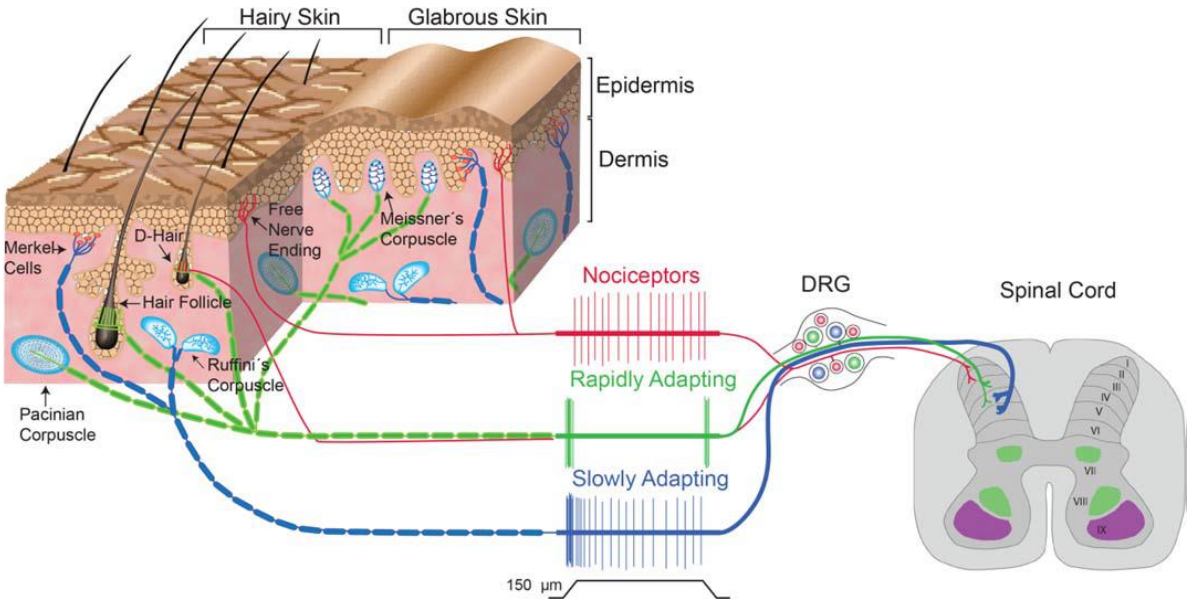

Figure 1 – Mechanoreceptors and nociceptors in glabrous- and hairy skin

A plethora of mechanoreceptors mediating light touch as well as nociceptors mediating noxious stimuli can be found in mammals glabrous- and hairy skin. Merkel cells, Pacinian corpuscle, Ruffini's corpuscle and free nerve endings can be found in both skin types (as well as D-hair receptors). The Meissner's corpuscle is a specialized end organ only found in glabrous skin, whereas hair follicle afferents are found in hairy skin (again, the exception is the D-hair receptor). The scheme shown here additionally illustrates the type of somatic afferent fiber associated with the end-organs as well as its adaptation properties. LTMRs are associated with myelinated afferents (blue or green) and can be slowly- or rapidly adapting. C-fiber nociceptors are associated with unmyelinated afferents. The soma of the sensory neurons is in the DRG, nociceptive input is relayed to the superficial layers of the dorsal horn, whereas LTMR input is relayed to deeper laminae. Figure illustrated by Dr. Bernal Sierra, Yinth Andrea

Meissners' corpuscle

In 1853 Meissner and Wagner first described a corpuscular structure in the dermal-epidermal border region of the glabrous skin (Meissner et. al., 1853; Cauna, 1881). Meissner's corpuscles were found to be ellipsoid, Schwann cell lamellar-layered cells (similar in appearance to scaly armour) covered by a connective tissue capsule linked to collagen that spans and connects the upper layer of the dermis to the epidermis (Takahashi-Iwanaga & Shimoda, 2003). They were found to be innervated by up to three thickly myelinated neurons with a spiral ending (winding through and around the lamellar cells). How can this structure mediate rapidly-

adapting physiological properties observed in sensory afferents? Firstly, the receptor potential (inward current) is produced by mechanosensitive ion channels (MSC) present in the plasma membrane of the sensory endings close to the central discs, displaying extremely smooth surfaces covered with a basal lamina-like matrix. As of now it is not known how the gating of the MSCs occurs, there is speculation that collagen mediated stretch might be the modus. A physical indentation stimulus impinging on the glabrous skin will result in its' deformation, which will cause the corpuscle to be moved, the attached collagen fibers to be stressed and the lamellar cells to transfer that stress (force) onto the ion channels in the sensory neuron endings, generating rapidly-adapting receptor potentials. A recent comparison of Meissners' corpuscles in glabrous hindpaw vs. forepaw skin revealed a higher innervation density in forepaw glabrous skin along with smaller mechanical thresholds and higher activity to comparable stimuli (Walcher et al., 2018). Meissners' corpuscles are essential for fine motor skills such as handling of objects and grip control (Guinard, Usson, Guillermet, & Saxod, 2000; Johansson & Westling, 1984; Macefield, Häger-Ross, & Johansson, 1996; Paré, Elde, Mazurkiewicz, Smith, & Rice, 2001; Vallbo & Johansson, 1984).

Merkel cell

The second end-organ implicated in fine touch was discovered in 1875 by Friedrich Merkel (Merkel, 1875). Merkel cells are derived from the epithelium and located in the basal layer of the epidermis. Following mechanical indentation of the skin, these receptors display an immediate burst of activity followed by persistent generation of neural activity to static pressure (Hartschuh & Weihe, 1980; Johnson, 2001; Maricich, Morrison, Mathes, & Brewer, 2012; Muir, 1969; Wellnitz, Lesniak, Gerling, & Lumpkin, 2010) and therefore are also classified as slowly-adapting low-threshold mechanoreceptors (SAMs) (Morrison, Miesegaes, Lumpkin, & Maricich, 2009). Merkel cells are essential for texture discrimination and shape recognition (Blake, Hsiao, & Johnson, 1997; Johnson, 2001; Maricich et al., 2012; W. H. Talbot, Darian-Smith, Kornhuber, & Mountcastle, 1968; Vallbo & Johansson, 1984). However, the Merkel cells are not solely responsible for the emerging SA physiology. Recent studies of the MSC *Piezo2* have shown, that the initial rapid burst of activity in SA afferents is due to *Piezo2* mediated activity following skin-stretch. Upon stimulation the Merkel cells then release neurotransmitters which excite the nerve fiber of the innervating sensory neuron which is observed as a maintained static phase activity, mediated through voltage-gated calcium channel activity (Ranade et al., 2014; S.-H. Woo et al., 2014; Amanda Zimmerman et al., 2014).

D-hair receptor

D-hair receptors are the second class of rapidly-adapting low-threshold mechanoreceptors and therefore similar in physiology to the previously described RAMs (Meissners' corpuscles); they also generate activity rapidly upon stimulation with an appropriate stimulus and do not transduce static indentation. There are, however, many differences between the two RA receptors such as innervation, receptive end-organ and receptive field size. D-hairs are so-called hair follicle afferents initially described in the hairy skin of cats (Brown & Iggo, 1967).

The hairy skin of mammals consists of three types of hairs, the guard hairs (1-3% of the fur; Driskell, Giangreco, Jensen, Mulder, & Watt, 2009; Dry, 1926; Duverger & Morasso, 2009) innervated by thickly myelinated A-ß fibers, awl-/auchene hairs (30% respectively 1% of the fur; Driskell et al., 2009; Dry, 1926; Duverger & Morasso, 2009) also innervated by A-ß fibers and additionally A-δ- and C-fibers. Lastly, zigzag hairs (approximately 65% of the fur; Driskell et al., 2009; Dry, 1926; Duverger & Morasso, 2009). Every hair is innervated by circumferential- and or lanceolate endings (Li & Ginty, 2014; Millard & Woolf, 1988; Yamamoto, 1966) and associated with terminal Schwann cells (Brown & Iggo, 1967; Li & Ginty, 2014; Zotterman, 1938).

D-hairs possess large receptive fields (in contrast to Meissners' corpuscle receptors), experimentally stimulating the receptor, one can evoke responses by brushing over more than half of the skin of the foot, which results from the ability of a single A-δ fiber to innervate many awl-/auchene hairs. Furthermore, D-hairs display directional sensitivity. Deflecting the hair-shaft in the direction of its growth results in the generation of significantly more activity compared to deflection in the direction against its growth (Rutlin et al., 2014; Walcher et al., 2018). These two studies do not agree with each other in terms of directional activity, however the Walcher et al. study shows actual *ex-vivo* deflections coupled to activity recordings in a skin nerve preparation, providing the stronger evidence.

1.2.3 HTMRs (end organs and physiology)

High-threshold mechanoreceptors (HTMR) or nociceptors which display high thresholds for the detection of mechanical stimuli, represent a population of receptors that are not used for the tactile exploration of our surrounding world, but rather to protect mammals from overexposure to harmful or noxious stimuli and possible tissue damage. They can be associated with thinly myelinated fibers of the A-δ category or C-fibers and therefore have intermediate (between 10 - 1.3m/s in mice) or slow (< 1.3m/s in mice) conduction velocities for AP propagation. The stimulation of nociceptors is associated with the sensation of pain.

Nociceptors associated with A-δ neurons are called A-fiber mechanonociceptors (AMs) and terminate in “free nerve endings” (same as unmyelinated nociceptors); meaning that the neuron of the A-δ category loses its myelin sheath in the epidermis and forms “free (of myelin)” branches connected to terminal Schwann cells (Fig.1) (Kruger, Perl, & Sedivec, 1981). AMs are thought to mediate the percept of the so-called first pain (Ploner, Gross, Timmermann, & Schnitzler, 2002; Price, 1972, 1977; Taylor, 1950; Torebjörk & Hallin, 1973). They possess large receptive fields and a fraction can be excited by thermal stimuli in addition to mechanical stimulation (Cain et al., 2001; Caterina et al., 2000; P. R. B. and E. R. Perl, 1972). Challenged with mechanical indentations they generate activity only in the static phase of the stimulation and display slowly-adapting properties (Garell, McGillis, & Greenspan, 1996).

Finally, there are nociceptors associated with C-fiber neurons, which are non-myelinated and therefore display slow AP propagation, also terminating in free nerve endings. C-fibers are thought to mediate the percept of the so-called second pain (Fig.1) (Ploner et al., 2002; Price, 1972, 1977; Taylor, 1950). Most C-fibers are polymodal, meaning that in addition to mechanical stimuli, they fire to stimuli like heat, cold or chemical irritants. This discovery resulted in a systematic classification of C-fiber nociceptors according to the stimuli that excite them. There are C-fibers only transducing mechanical stimuli (C-mechanonociceptor (C-M)), C-fibers transducing mechanical and heat stimuli (C-mechano-heat nociceptor (C-MH)), C-fibers transducing mechanical and cold stimuli (C-mechano-cold nociceptor (C-MC)) or C-fibers transducing mechanical and heat- as well as cold stimuli (C-mechano-heatcold nociceptor (C-MHC)) (Fleischer, Handwerker, & Joukhadar, 1983; Kress, Koltzenburg, Reeh, & Handwerker, 1992; G. R. Lewin & Mendell, 1994; Paricio-Montesinos et al., 2020). Additionally, low-threshold C-fiber mechanoreceptors and mechanically-insensitive (or silent) C-fibers were described (Iggo, 1960; Meyer, Davis, Cohen, Treede, & Campbell, 1991; Prato et al., 2017). But they do not seem to be of large abundance in rodent skin (Handwerker, Forster, & Kirchhoff, 1991; Kress et al., 1992; G. R. Lewin & Mendell, 1994) and will therefore not be discussed further here. Similar to AMs, C-fibers challenged with mechanical indentations generate activity only in the static phase of the stimulation and display slowly-adapting properties (Garell et al., 1996). Most recently nociceptive Schwann-cells were discovered, a specialized type of glia-cells forming a tight mesh-like network and tightly associated with free nerve endings of nociceptors in the subepidermal region of the skin. These Schwann-cells were demonstrated to have a direct excitatory function on sensory neurons (mainly nociceptors) and might therefore play an important role in initiation of nociceptive activity (Abdo et al., 2019).

1.2.4 Mechanosensitive ion channels (focus on Piezo2)

The quest for the identification of mechanosensitive ion channels (MSCs) has unfortunately not been fruitful until recently. In bacteria the mechanosensitive channels of large- and small conductance have been identified (MscL and MscS repectively) (Lett et al., 1994; Sukharev, 1994). Additionally, the TRAAK and TREK-1 K^+ channels (Berrier et al., 2013; Maingret, Fosset, Lesage, Lazdunski, & Honoré, 1999; Maingret, Patel, Lesage, Lazdunski, & Honoré, 1999), Swell1 (Qiu et al., 2014), Piezo 1 and 2 (Coste et al., 2010) and very recently OSCA1 (Murthy, Dubin, et al., 2018), TACAN (Beaulieu-Laroche et al., 2020; Christin & Agosti, 2019) as well as TMC1 and 2 (Jia et al., 2020) associated with TMIE (Cunningham et al., 2020) and Elkin-1 (Patkunarajah et al., 2020) have been described. The general strategy applied to uncover these mechanosensitive channels was mutagenesis of model organisms and complex proteomic screens for transmembrane proteins based on following criteria:

1. expression in mechanosensitive cells (such as DRG or TG neurons)
2. localisation to the plasma membrane
3. deletion causes mechanosensing defects (phenotype)
4. increasing mechanosensitivity when expressed in heterologous systems
5. decreasing mechanosensitivity when expression in heterologous systems is reduced
6. rapid-opening properties
7. gating required through mechanical stimulus (such as stretch or indentation)
8. formation of ion-conducting pore when reconstituted in artificial bilayer membranes

Early studies using the mutagenesis approach were conducted in the model organism *C.elegans* (nematode). C.elegans is particularly suited for studying the nervous system since the connections of all of its neurons (302 out of 959 cells in total) were mapped using electron microscopy in 1986 (White et al., 1986). Therefore, genetic ablation experiments could be performed, ablating specific circuits in the nervous system which resulted in the identification of 6 touch receptors. Consecutive screening for abnormal phenotypes applying various mechanical stimuli such as brush, gentle or intense touch with mutagenized worms yielded the identification of 16 genes involved in touch. Some of those genes were found to have supporting roles such as maintenance of structural integrity as well as development and differentiation, some had very interesting effects on motor behaviour such as *unc-86* (uncoordinated). The most interesting genes for mechanosensation were *mec-4*, *mec-10* and *mec-6*. The gene-products from *mec-4* and *mec-10* form an ion channel and *mec-6* encodes an accessory subunit involved in channel assembly (Driscoll & Tavernarakis, 1997; M, MA, & MX, 1993). The *mec-2* protein was found to act as a link with the *mec-4* and *mec-10* encoded channel to the cytoskeleton and was proposed to directly influence its gating-properties (M.

Huang, Gu, Ferguson, & Chalfiet, 1995). Interestingly, the functional mammalian homolog of *mec-4*, *mec-10* and *mec-6* were later discovered to be Piezo2 the principal MSC involved in touch and the *mec-2* homolog is STOML3 its modulator (Fig.2) (Poole, Herget, Lapatsina, Ngo, & Lewin, 2014a; Poole, Moroni, & Lewin, 2014).

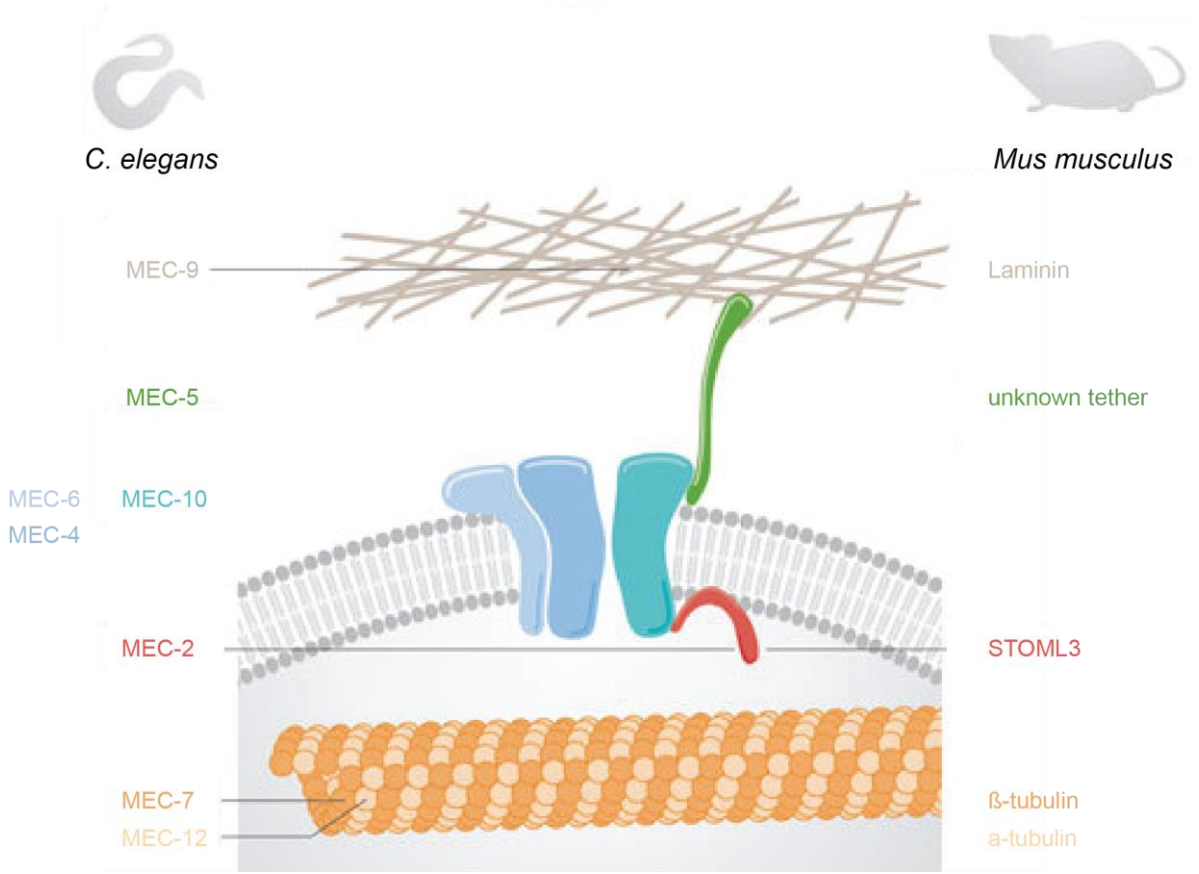

Figure 2 – Identified components of the mechanosensory molecular machinery

Studies in the nematode *C. elegans* revealed parts of the apparatus necessary for mechanotransduction. A central ion channel (MEC-4, MEC-6, MEC-10) is gated by deflection of the extracellular matrix. The transfer of force is thought to be mediated by a still unknown tether protein. MEC-2 is tuning the sensitivity of the central ion channel. Functional homologs of these genes in mouse were later to be identified as Piezo2 and its modulator: STOML3. Figure adapted from Lechner and Siemens, 2011

The mammalian Piezo proteins were discovered in an RNAi knockdown screen in N2A cells (neuroblastoma cell line) of genes with suspected roles in generating mechanically gated currents (Coste et al., 2010). FAM38A and FAM38B renamed Piezo1 and Piezo2 respectively, have since their discovery been extensively studied and proven to be essential for the function of various physiological processes absolutely necessary for mammalian life. They are multimeric (trimeric subunits) pore-forming ion channels of ~2500 amino acids (aa) per subunit that upon gating allow the influx of sodium and calcium (non-selective cation channels) for the initiation of action potential generation and propagation along the axon (Murthy, Dubin, & Patapoutian, 2017). Piezo1 and -2 share ~50% sequence identity and diverge in expression

localisation. Piezo1 is expressed mainly in non-neuronal cells and is involved in for instance vascular development, blood pressure regulation and apoptosis (Retailleau et al., 2015; Wang et al., 2016). Piezo2 is expressed mainly in sensory neurons and will therefore be described in more detail in this introduction.

Macroscopic currents induced by mechanical stimulation activate and inactivate within milliseconds of the channel's stimulation due to physiological mechanisms still unknown and both Piezo1 and -2 are blocked by GsMTx4 (a spider toxin), known to block stretch activated channels (Alcaino, Knutson, Gottlieb, Farrugia, & Beyder, 2017; Bae, Sachs, & Gottlieb, 2011). But how exactly does the gating of Piezo channels work?

There are two hypotheses regarding how gating of MSCs occurs, the "force-from lipids" model and the "force-from filaments" model. In the "force-from lipids" model, protein interaction of the ion channel and the lipid membrane it is embedded in are altered through tension in the membrane (induced by a mechanical stimulus). Force acting upon the membrane results in its deformation, this tension causes a rearrangement of lipids surrounding the ion channel and ultimately its activation (channel opening). This mechanism of action was described for members of the K_{2P} family (2-pore domain potassium channels) (Brohawn, Campbell, & MacKinnon, 2014). The second model requires the presence of a so-called tether protein essential for channel gating by mediating the transfer of force from the ECM or intracellular cytoskeleton proteins onto the channel.

Proteins modulating membrane properties such as curvature or stiffness have been shown to tune Piezo channel mechanosensitivity. Piezo activity is modulated by cytoskeletal proteins (actin, dynamin and filamin A) due to their influence on the rigidity of the plasma membrane (Cox et al., 2016; Lee et al., 2014; Retailleau et al., 2015). A proposed mechanism of how the previously described mammalian *mec-2* homolog STOML3 acts is by reducing activation thresholds of Piezo1 and -2 through binding of cholesterol, recruiting it to lipid rafts in the ECM and therefore increasing membrane stiffness (Poole, Herget, Lapatsina, Ngo, & Lewin, 2014b; Qi et al., 2015a). Ultimately tension acting on the membrane would more easily gate the channel. Due to the importance of STOML3 to this thesis work and mechanosensation, the stomatins will be introduced properly in the following section.

Piezo2 is implicated in the detection of light touch, proprioception, respiratory physiology and recently also nociception (Murthy, Loud, et al., 2018a; Szczot et al., 2018a). It is critical for the detection of light touch and vibration as it is expressed in LTMR-associated fibers as well as Merkel Cells. Studies with genetically ablated *piezo2* in mice sensory neurons and Merkel Cells showed severe deficits in touch sensation (Ikeda et al., 2014; Maksimovic et al., 2014; Ranade

et al., 2014; S.-H. Woo et al., 2014). Similarly, genetic ablation studies in proprioceptors revealed severe deficits in limb positioning and body coordination due to the lack of stretch-induced activity in these neurons (Florez-Paz, Bali, Kuner, & Gomis, 2016; Woo, S.H., 2015). The most astonishing effect and argument for Piezo2's critical role in mammalian physiology is probably the fact, that global *piezo2* knockouts are embryonically lethal due to respiratory distress (Nonomura et al., 2017). It was proposed that in the absence of Piezo2 the initial inflation of the lung after birth failed to occur, resulting in death.

1.2.5 Modulators of sensory mechanotransduction – STOML3

The stomatin domain family of proteins is abundant in all phyla and well conserved (Green & Young, 2008; Tavernarakis, Driscoll, & Kyrpides, 1999). In mammals there are five members: Stomatin, StomL1-3 and Podocin. Except for StomL2 all family members are integral membrane proteins with a short hydrophobic core-domain (similar between members) (Green & Young, 2008) and variable N- and C-termini (Salzer, Ahorn, & Prohaska, 1993).

Stomatin, first identified in erythrocytes, is ubiquitously expressed as well as highly expressed in DRG neurons in mice (Mannsfeldt, Carroll, Stucky, & Lewin, 1999; Wetzel et al., 2007). It can self-oligomerize and associate to lipid-rafts in the ECM (Snyers, Umlauf, & Prohaska, 1998). Stomatin plays a role in sensory mechanotransduction, since knockout studies in mice revealed impaired mechanosensory properties in D-hair receptors recorded using *ex-vivo* skin nerve experiments (Martinez-Salgado et al., 2007). The proposed mechanism was a regulation or tuning of MSCs essential for signal transduction in LTMRs. StomL1's core-domain is located closer to the N-terminus (in all other family members, it's closer to the C-terminus), it's expression is higher in the brain and adipocytes and even though an effect on gating-properties of Piezo ion channels was proven *in vitro* (Poole, Herget, et al., 2014a), StomL1 knockout mice did not show the same sensory phenotype as stomatin transgenic animals, no deleterious effect on mechanotransduction could be proven. StomL2 is mainly localized in mitochondria (inner membrane) where it has a proposed protective role against oxidative mitochondrial stress (Tondera et al., 2009). StomL2 has not been tested for a potential role in mechanotransduction. Podocin is specifically expressed in the kidney, where it localizes to the podocyte slit diaphragm (Roselli et al., 2002). It can also self-oligomerize and interact with cholesterol as well as the ion channel TRP V6. With the actin part of the cytoskeleton and nephrin it can form lipid-protein domains (Huber et al., 2006; Saleem et al., 2002). However, since it is specific to podocytes, it is probably not relevant for somatosensory mechanotransduction. Finally, StomL3 and its role in mechanotransduction:

StomL3 expression levels are low compared to other members of the stomatin family (Liudmila Lapatsina, Smith, et al., 2012). Like other stomatin family members, StomL3 possesses a stomatin core-domain, allowing it to self-oligomerize as well as a hairpin structure (hydrophobic) that enables interaction with the plasma membrane. To date the structure of StomL3 has not been resolved, but Brand et. al. (Liudmilla Lapatsina, Brand, Poole, Daumke, & Lewin, 2012) solved the crystal structure of stomatin giving insight into the stomatin-domain protein oligomerization mechanism. Stomatin exists as a banana-shaped dimer, a valine residue is essential for dimer formation and when mutated prevents dimerization (V190P). Three banana-shaped dimers can form a higher order cylindrical structure. Formation could also be inhibited introducing another mutation (R90A). Two forms of StomL3 exist, one being post-translationally modified (N-glycosylated) representing the single span transmembrane protein, whereas the smaller 32 kDa form is associated with the cytosolic side of the plasma membrane (James Hall, PhD thesis).

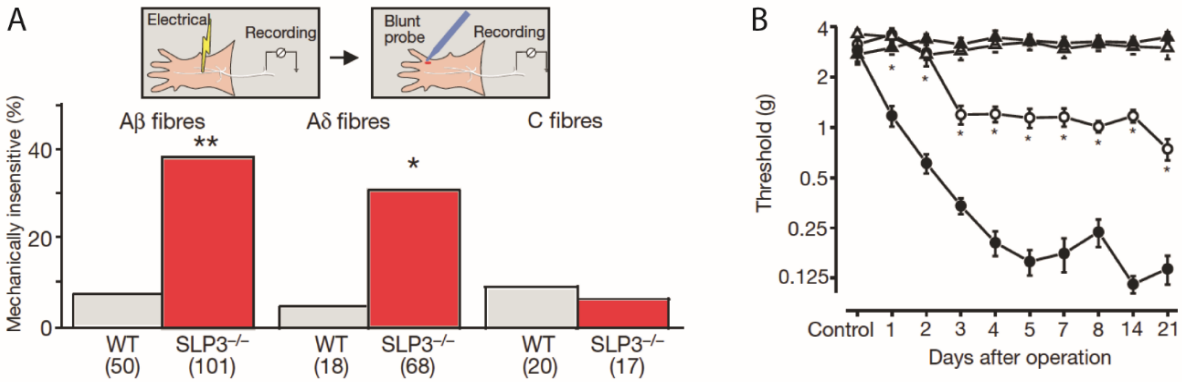

Figure 3 – Physiological properties of STOML3 knock-out mice: sensory afferents and pain behaviour

An electrical search protocol was applied to determine the mechanical sensitivity of mechanoreceptors and nociceptors in a saphenous nerve preparation (hairy skin). The nerve was stimulated electrically, the afferent fiber traced to its receptive field and then stimulated with a blunt probe. Approximately 35% of Aβ fibers lost their ability to transduce mechanical stimuli as well as 30% of Aδ fibers. C-fibers were unaffected (A). Following CCI STOML3 knock-out mice developed significantly less mechanical allodynia represented by the white circles in B (circles: CCI, triangles: sham-OPs; in white: STOML3 knockouts, black: C57BL6/N). Data from Wetzel et al., 2007, Figures 1 and 4

StomL3 is present in DRG neurons (Wetzel et al., 2007) and the generation and subsequent investigation of global knockout mice revealed that it is absolutely essential for proper mechanotransduction in up to 40% of A-ß fiber neurons (RAMs and SAMs) as well as 35% of A-δ fiber neurons (D-hairs and AMs, (Fig.3)). The absence of StomL3 renders neurons “silent”, meaning that it was possible to electrically excite the neurons and localize their receptive field, but mechanical stimuli were not able to consecutively induce AP firing (Wetzel et al., 2007). In addition, effects of *stoml*3 ablation could be observed on the organismal level using

behavioural assays. Firstly, a so-called tactile acuity test was performed in which animals were put into boxes with two central rectangular areas in which tactile cues could be introduced.

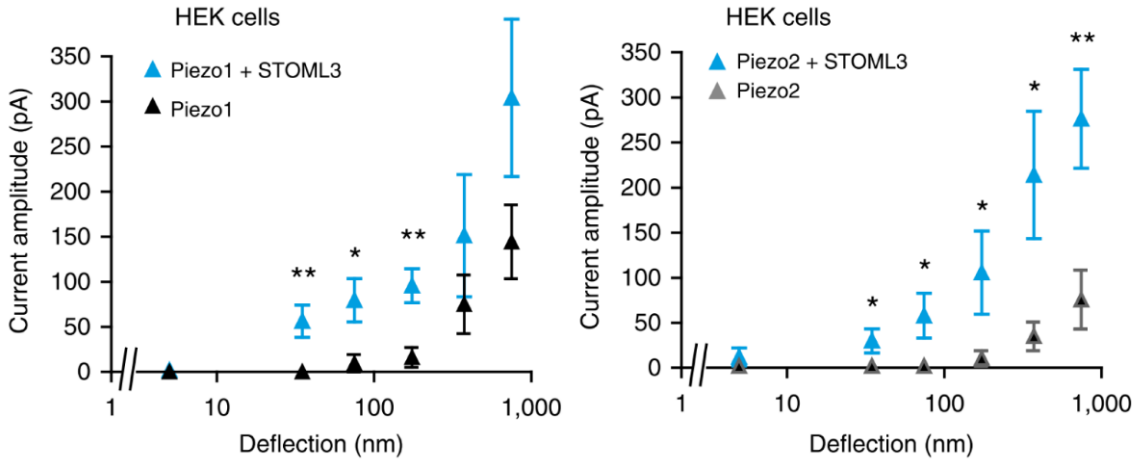

Figure 4 – The effect of STOML3 on the mechanotransduction properties of Piezo ion channels

The presence of STOML3 yields increased current amplitude in both Piezo1 and 2 ion channels in response to mechanical stimulation. Furthermore, tiny deflections (ranging below 100nm) only induce Piezo1 and 2 currents if STOML3 is present. Hence STOML3 increases the sensitivity of Piezo ion channels. Data from Poole, Herget, et al., 2014b, Figure 5

One area was always equipped with a grated surface (with varying widths from 250µm to 750µm) and the other kept empty. StomL3 knockout animals were not able to detect the finer gratings as indicated by untargeted exploratory behaviour whereas control animals detected the mechanical cue and spend significantly more time on it. Tactile exploration (relying on fine touch perception) was impaired (Wetzel et al., 2007).

Like StomL1, StomL3 sensitizes Piezo ion channel activity (both Piezo1 and 2) as proven by the significantly lower deflection magnitudes required to gate the MSCs using an elastomeric pillar array *in vitro* assay (Fig.4) (Poole, Herget, et al., 2014a). By mutating conserved residues in STOML3 that mediate self-association (Brand et al., 2012) its sensitization properties on Piezo ion channels were abolished. It could be, that proper StomL3 function depends on its oligomerization and formation of higher order structures. A concept that was utilized later in the development of small-molecule oligomerization blockers of StomL3 (OB-1,2) in the context of neuropathic pain (Wetzel et al., 2017). Subjecting global StomL3 knockout animals to neuropathic injury did not produce severe symptoms of mechanical hypersensitivity as shown by reduced paw-withdrawal thresholds using the von Frey assay (Fig.3). The absence of STOML3 seems to have a protective role in certain forms of peripheral neuropathies and since it is also a modulator of MSCs it was hypothesized that neuropathic pain emerges as a consequence of peripheral sensitization in sensory neurons. How does StomL3 modulate

MSCs? Hu and colleagues. (Qi et al., 2015b) found, that StomL3 facilitates membrane stiffening in a cholesterol dependent manner and therefore less force is required to gate MSCs if StomL3 is present in the plasma membrane.

StomL3 was upregulated in neuropathic nervous tissue as shown by Wetzel et. al. 2017. Therefore, its effect on plasma membranes containing MSCs might be potentiated which could translate into emerging allodynia and hyperalgesia (both of which will be introduced properly in the section on neuropathic pain) in neuropathic conditions and therefore targeting StomL3 to try and alleviate pain states represents a reasonable approach.

1.2.6 Neuropathic pain (general introduction)

Neuropathic pain is defined according to the most recent IASP definition as “pain caused by a lesion or disease of the somatosensory system” including central neurons and peripheral fibers (A-ß, A-δ and C-fibers). It is a multifactorial disease affecting up to 7-10% (O. van Hecke, 2013) of the entire human population (Bouhassira, Lantéri-Minet, Attal, Laurent, & Touboul, 2008) with increasing abundance due to longer life expectancies with the emergence of corresponding comorbidities such as diabetes mellitus as well as improved survival of cancer patients and related chemotherapy induced neuropathic pain. It is a condition dramatically affecting the quality of life of patients (e.g. pain, frequent doctor visits, increasing medication) and to date very few effective treatment approaches have been developed, often leading to anxiety and depression in patients, making this field of study highly relevant.

Lesions or diseases of the somatosensory system can affect proper signal transmission influencing our sensory perception of touch. In such cases, an important question is: is it due to altered mechanotransduction in the periphery or a centrally emerging paraesthesia? Various conditions are linked to emerging neuropathic pain, the most common are diabetic neuropathy, infection with HIV, stroke, amputation, postherpetic neuralgia, trigeminal neuralgia and peripheral nerve injury. Patients suffering from these conditions can experience debilitating symptoms such as allodynia (normally innocuous stimuli (light touch) are perceived as intensely painful) and hyperalgesia (an increased pain-sensation caused by normally painful stimuli) as well as burning or electrical sensations. What are the causes of these symptoms?

Since this work is concerned with peripheral neuropathic pain the mechanisms and diseases aetiological for centrally emerging neuropathic pain will not be addressed further. Peripheral neuropathic pain is usually divided into generalized and focal neuropathic pain. Generalized means that the condition (diabetes mellitus, infectious diseases, inflammatory- or inherited diseases or involvement of the immune system) produces pain more widely distributed throughout the body. Most commonly, the distal extremities are involved (feet and hands,

calves and forearms) encompassing a loss of sensitivity and pain that progresses in the proximal-distal direction. Focal neuropathic pain on the other hand is more regionally defined. A peripheral nerve or a nerve root is damaged or involved in pathological processes, therefore pain emerges in the sensory dermatome innervated by the injured peripheral nerves (post-traumatic polyradiculopathies, cervical- and lumbar polyradiculopathies, trigeminal neuralgia, postherpetic neuralgia, leprosy and CRPS). Not entirely relevant for the emerging phenotype I studied in this PhD work but very interesting because they offer insight to the molecular basis of pain are the rare inherited channelopathies. Mutations in the gene *SCN9A* that encodes the VGSC $Na_V1.7$ (voltage-gated sodium channel involved in the generation and propagation of action potentials) are the cause for inherited erythromelalgia. It is a disease characterized by reddening of the extremities (erythema) and pain intensified by heat (Yang et al., 2004). *SCN9A* mutations are the cause of other pain syndromes (paroxysmal extreme pain disorder) highlighting the significance of proper functioning ion channels being crucial for a sensory system working within normal parameters.

Animal studies genetically ablating *SCN9A* produced animals incapable of sensing noxious stimuli (Gingras et al., 2014; Minett et al., 2012; Nassar et al., 2004). Being able to feel and experience pain is essential for viability because it functions as a warning sign and motivates avoidance of further contact and/or exposure to the cue inducing the pain sensation. What is known so far about changes in the nociceptive signalling pathway?

According to gate-control theory (Melzack & Wall, 1967), there is a balance between input from small fibers (usally nociceptors) and large fibers (mechanoreceptors). This means that LTMR input can modulate nociceptive input and only if the nociceptive input is exaggerated, will pain be experienced. Similarly, there is central inhibitory and excitatory signalling that in neuropathic states is changed due to altered electrical properties of peripheral nerves, which lead to an impairment of inhibitory interneurons at the spinal cord level as well as control systems of the descending pathways. Bluntly put, loss of inhibition and gain in facilitation produce a state of hyperexcitability in the somatosensory system linked to the various neuropathic pain states. Changes maintained for a longer time might be aetiological for chronification of said neuropathic pain.

1.2.6.1 Peripheral mechanisms in neuropathic pain

Mechanisms underlying nerve-injury-induced neuropathic pain are complex. Peripheral sensitisation represents altered input to the somatosensory system via increased responsiveness or reduced neuronal firing thresholds (C J Woolf & Salter, 2000; Clifford J Woolf & Mannion, 1999). This electrical hyperexcitability can manifest as ectopia (an abnormal,

erratic excitability of C-fiber sprouts at the injury site (Patrick D. Wall & Gutnick, 1974; Zimmermann, 2001)). Trauma can cause sensory neuron de-afferentiation, with a loss of peripheral innervation but a remaining intact central terminal. The site of lesion is called the neuroma and C-fibers were especially shown to generate bouts of activity when de-afferentiated. But this increased activity in injured fibers is not all that contributes to the pathology. There is crosstalk between injured and uninjured neurons, rendering the uninjured fibers hyperexcitable (irritable nociceptors) (Fields, Rowbotham, & Baron, 1998; Tesfaye, Boulton, & Dickenson, 2013). These irritable nociceptors are thought to be the cause of ongoing and evoked pain in patients. The application of so-called nerve blocks (lidocaine patch, blocks VGSCs) yielded relief of pain (Haroutounian, 2014; Kleggetveit, 2012; Serra, 2011; Vaso et al., 2014) suggesting that peripheral input is a driver for neuropathic pain (Fig.5). So how does ectopia or in general activity in peripheral nerves emerge?

One identified mechanism is the increased function and expression of VGSCs in peripheral nerve terminals of the spinal cord (dorsal horn) that is accompanied by enhanced alpha2-delta subunits of calcium channels. These alterations lead to increased neurotransmitter release in addition to a state of heightened excitability and signal transduction. These changes occur hand in hand with a loss of modulatory activity facilitated by a loss of potassium channels and overall cause heightened excitatory input into the nociceptive circuits (Fig.5).

Alterations in excitability especially in spinal cord interneurons (of the WDR type) is a consequence of their activation by neurons of the A-ß and A-δ type. They increase their modality specificity and expand their receptive fields resulting in sensory input being able to excite more second order nociceptive neurons which relay nociceptive information to the brain. This process is called central sensitization (Baron, Hans, & Dickenson, 2013; Clifford J. Woolf, 2011).

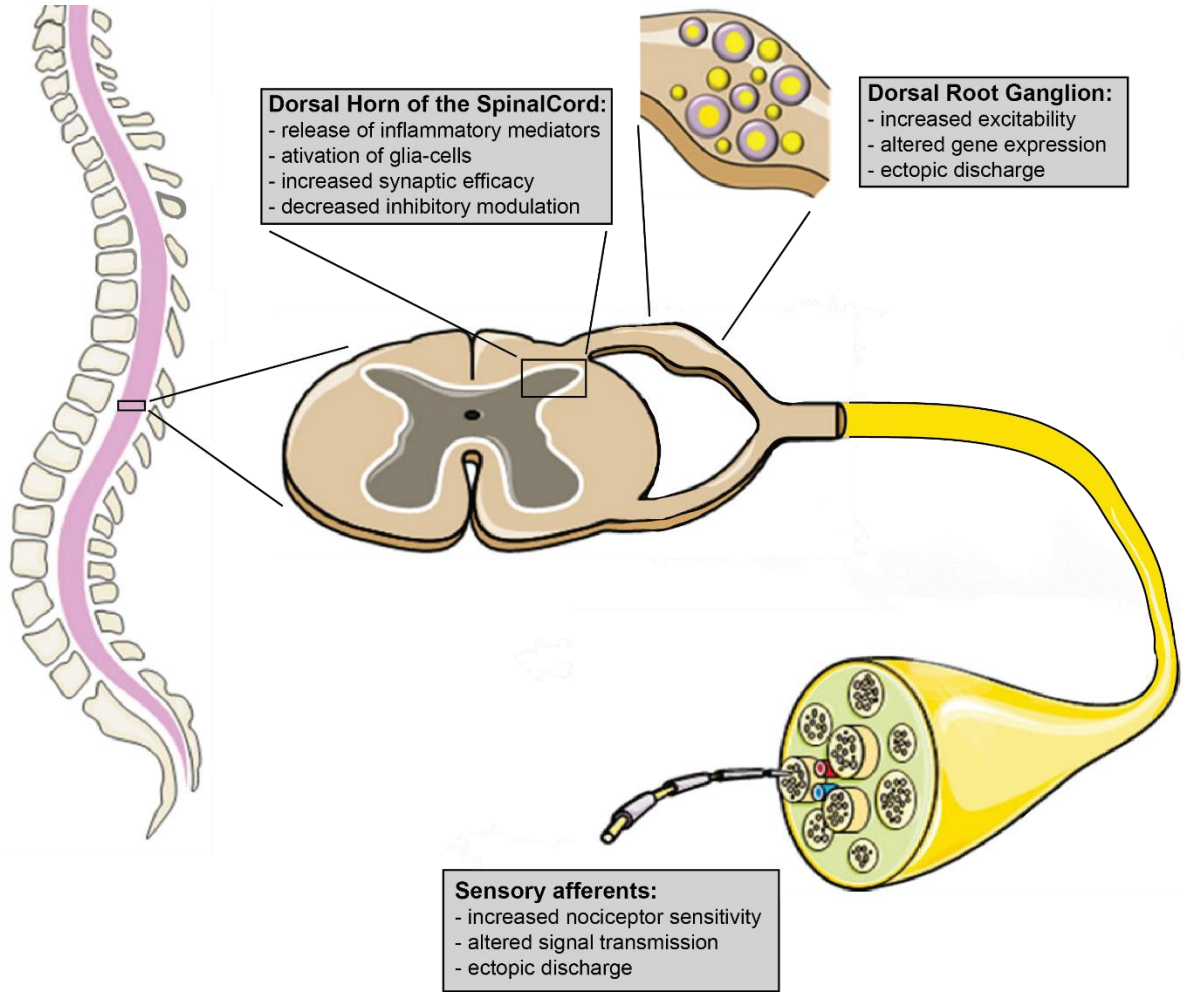

Figure 5 – Pathological changes along the sensory axis following neuropathic injury

Sensory afferents relay information from the periphery to our central nervous system. The soma of the sensory afferents lay in the DRG, the central branch of the pseud-unipolar neurons connects to the dorsal horn of the spinal cord. Along these stations of the sensory axis, pathological processes occur which are thought to be aetiological for neuropathic pain. Nociceptors display increased sensitivity, ectopic discharge emerges in the axon as well as in the cell body (DRG), where gene expression is altered, leading to increased excitability. Inflammatory mediators are released in the spinal cord, glia cells activated and a net increase in synaptic efficacy as well as decrease in descending inhibitory modulation are believed to contribute to neuropathic pain. Figure adapted from (Meacham et al., 2017) Previous studies have until now disregarded the receptor properties in the periphery, an important component of the sensory axis I address here in this thesis work.

Central sensitization was investigated in a number of studies, and it was shown that peripheral input induced release of neuropeptides and amino acids (excitatory) leads to phosphorylation of NMDA and AMPA receptors that cause increased thalamic activity (Patel & Dickenson, 2016; Peyron, 2016). A second possible mechanism is the loss of GABAergic interneurons generating an overall loss of inhibition, contributing to emerging hypersensitivity (Gagnon et al., 2013).

1.2.6.2 Current treatment approaches

Pharmacological treatment of neuropathic pain is problematic. The molecular mechanisms underlying the various diseases are not sufficiently understood, the recommended first-line treatments consist of antidepressants and antiepileptic drugs (pregabalin, gabapentine), tricyclic antidepressants (amitriptyline) and serotonin-noradrenalin reuptake inhibitors (duloxetine). Their proposed mechanism of action is in modulating the descending modulatory inhibitory controls as well as decreasing central sensitization through interference with VGCCs (voltage-gated calcium channels) (Luo et al., 2001). Most commonly, patients are treated with a combination therapy consisting of multiple drugs, especially if they do not respond well to high dose monotherapy (Tesfaye, Wilhelm, et al., 2013).

Second-line treatments consist of capsaicin patches, lidocaine patches and/or tramadol (an opioid agonist). Lidocaine blocks sodium channels and therefore counteracts ectopic discharge in sensory neurons ultimately yielding only a moderate relief (Binder et al., 2009).

And third-line treatments consist of strong opioids and botulinum toxin A. Oxycodone and morphine are amongst the most famous opioid agonists, unfortunately associated with misuse and overdose resulting in death especially at present in the USA (opioid crisis) and only displaying moderate efficacy according to the NNTs (Finnerup et al., 2015).

There is a need for new analgesics, specific to the different diseases summarized as neuropathic pain, but in order to develop specific treatments, the basic research of the various diseases needs to be expedited.

1.2.6.3 Models

The study of neuropathic pain and its pathological mechanisms required the use of tractable laboratory models, usually rats and mice. Over the years numerous models have been introduced which will be reviewed here. The aim is to gain a deep understanding of the pathologies to be able to invent new therapeutic approaches since commonly used pharmacotherapy has limited success. Experimental procedures should induce an easily reproducible phenotype characterized by common sensory deficits observed in neuropathic pain patients such as allodynia, hyperalgesia and/or spontaneous pain. Pain aetiology is incredibly diverse and in order to meet these criteria models for peripheral nerve injuries, spinal cord injuries, chemotherapy, cancer and other diseases were developed. Because this work aims to unravel peripheral pain mechanisms, I will focus on animal models of peripheral neuropathic pain.

The first model to be developed was the axotomy model in rats. The entire sciatic nerve is transected by applying tight nylon sutures proximal to the sciatic trifurcation with approximately 1cm of spacing in between. Approximately 5mm of nerve is cut between the sutures to prevent reinnervation. The saphenous nerve is transected as well producing denervation of the entire hind-limb. This model produces anaesthesia dolorosa, ongoing pain in a body area that has lost its sensitivity. A consequence of this procedure is autotomy (self-mutilation) due to excessive grooming without sensory feedback or in order to try and alleviate the ongoing intense pain (Kauppila, 1998; P. D. Wall et al., 1979). However, a complete loss of all sensitivity in an extremity is rare (amputations) and the induced pain and behaviour (autotomy) gruesome, raising the ethical question if the amount of induced pain is in line with the knowledge gained and clinical relevance. As a consequence, the axotomy model was refined and numerous partial axotomy models were developed.

Partial nerve ligation (also known as the Seltzer model (Seltzer, Dubner, & Shir, 1990)) only ligates 1/3 to ½ of the sciatic nerve using fine silk-gut ligatures (8-0). Behavioural signs of neuropathic pain emerge in this model approximately one week after surgery. Paw licking and guarding (paw elevated from ground, sometimes placed onto the tail but not the ground of the cage) as well as chemical, mechanical and cold paraesthesias were observed and persist for 6 weeks (Dowdall, Robinson, & Meert, 2005; Mitchell, White, & Cousins, 1999; Seltzer et al., 1990). Later on, this model was applied in mice with similar behavioural outcomes. The model is used to study causalgiform pain (also termed CRPS type 2), associated with burning pain and pain increasing with sensory stimulation (Shir & Seltzer, 1991).

Another refinement of the axotomy model is the spared nerve injury (SNI) developed by Isabel Decosterd and Clifford Woolf (Decosterd & Woolf, 2000). It involves a more distal incision (through the biceps femoris muscle and not access to the sciatic nerve in the popliteal fossa) to expose the 3 terminal branches of the sciatic nerve (tibial nerve, common peroneal nerve and sural nerve). From those 3 terminal branches 2 (the common peroneal and the tibial nerve) are tightly ligated with silk-gut ligatures (5-0) and approximately 2mm of nerve axotomized. The sural nerve remains undamaged. Different combinations of spared nerves and axotomized nerves were made subsequently (Bourquin et al., 2006; Kohno, Moore, Baba, & Woolf, 2003). The model produces robust mechanical and thermal hyperalgesia and allodynia for up to 6 months after surgery (Bourquin et al., 2006; Decosterd & Woolf, 2000) and later on the model was also transferred to mice with the same behavioural outcomes (Bourquin et al., 2006; Shields, Eckert, & Basbaum, 2003). The main new feature of this model is the ability to study and compare non-injured and injured skin territories providing the chance to investigate sensory cross-talk between injured and uninjured nerves. These criteria make it on paper a

perfect model of peripheral neuropathies to answer specific questions. However, since the injured territories represent complete axotomies, the peripheral contribution of mechanoreceptive and nociceptive end-organs cannot be studied, only changes in electrical properties of sensory neurons influenced by axotomized fibers and denervation induced changes in the central terminals of sensory neurons as well as possible effects on second order neurons (interneurons), which may exclude an important driver of neuropathic pain – changes in the periphery.

The spinal nerve ligation (SNL) was developed by Kim and Chung (Kim & Chung, 1992) and utilizes ligations on a more proximal level – the spinal nerve roots. L5 and L6 are tightly ligated just distal to the DRG using silk-gut ligatures (6-0). It is crucial not to ligate L4 since interfering with it produces severe motor-deficits that will make behavioural assessment of pain states impossible (Kim & Chung, 1992; Komori et al., 2007; Lin et al., 2007) and sparing L4 preserved motor function. Behavioural signs of neuropathic pain (in this case: mechanical- and cold allodynia as well as thermal hyperalgesia and spontaneous pain) develop incredibly fast, just 48 hours after surgery persisting for up to 16 weeks (Kim & Chung, 1992; LaBuda & Little, 2005; Yoon, Young Wook, Heung Sik, Sun Ho, & Jin Mo, 1994).

The main difference between the SNL model and the previously described axotomy models is that in SNL intact and damaged afferents are present in the same nerve segment, making it possible to investigate peripheral contributions to neuropathic pain as well as neuronal cross talk rendering it a more accurate model of most traumatic injuries, since again usually complete axotomies are rare, however the surgical procedure is quite extensive being the reason for us to have chosen the chronic constriction injury (CCI).

The CCI model was developed by Bennett and Xie in rats (Bennett & Xie, 1988). Three to four loose (initially chromic gut ligatures) silk-gut ligatures (4-0) are tied around the common sciatic nerve proximal to the sciatic trifurcation with approximately 1mm of spacing between each suture. This injury produces intraneural edema resulting in pressure that damages parts of the nerve while others are left intact. Similar to SNL neuronal cross talk as well as peripheral contribution to neuropathic pain can be studied. Animals in this model display paw guarding and licking, limping and an avoidance behaviour (weight bearing behaviour). Mechanical- and thermal hyperalgesia and allodynia as well as chemical hyperreactivity have been documented to occur 1 week after surgery persisting for at least 7 weeks (Bennett & Xie, 1988; De Vry, Kuhl, Franken-Kunkel, & Eckel, 2004; Dowdall et al., 2005). Histological studies suggest that the damage through constriction affects myelinated afferents to a larger degree than unmyelinated C-fibers (Carlton, Dougherty, Pover, & Coggeshall, 1991). However, different studies find a large degeneration of C-fiber axons as well (Basbaum, Gautron, Jazat, Mayes,

& Guilbaud, 1991). It is still controversially discussed which sensory fiber system is responsible for the maintenance and development of the pain phenotype, is it the loss of A-fibers or C-fibers? One problem with the CCI model is reproducibility. Since loose ligatures are tied by hand, this will always introduce some degree of variation in constriction force (L. S. Ro & Jacobs, 1993) (and therefore degree of damage). Also, the type of suture has been reported to introduce variability (Maves, Pechman, Gebhart, & Meller, 1993).

Even more models have been developed, to briefly mention some: tibial- and sural nerve transection, ligation of the common peroneal nerve, sciatic cryoneurolysis and caudal trunk resection (…and even more). Of those briefly mentioned the common peroneal nerve ligation is interesting, since it is well suited to investigate sensory defects without an interfering motor component (on behaviour). However, the skin innervated by the common peroneal nerve is just a small area on the dorsal side of the hindpaw (hairy skin), which once again would not permit the experimenter to correlate behavioural effect such as von Frey paw-withdrawal thresholds or thermal plate assays with electrophysiology. For these kind of studies CCI is a better model, since the physiological properties of sensory afferents can be directly compared with behavioural observations.

1.2.7 Small-molecule oligomerisation blockers that inhibit STOML3

In 2017 the Lewin lab published a study showing that interfering with STOML3 self-oligomerization yielded a beneficial effect on neuropathic pain (Wetzel et al., 2017). The self-association ability of STOML3 was monitored using a BiFC assay (bi-molecular fluorescence complementation) and mutations (of STOML3) were introducing that interfered with oligomerisation. This assay was used to screen the central compound collection of the FMP (Leibnitz Institute for Molecular Pharmacology) for molecules decreasing the BiFC signal and therefore interfering with self-association in a manner similar to that observed after mutation of residues critical for oligomerisation.

The screen yielded a few interesting candidates of which OB-1 and OB-2 were studied further and found to be effective in interfering with STOML3 self-oligomerisation. These oligomerisation blockers modulated mechanotransduction currents in cell lines as well as DRG neuron cultures and most interestingly proved to be effective in attenuating tactile allodynia following CCI.

The downside of OB-1 however was, that it had to be applied subcutaneously into the neuropathic hindpaw. Subsequently the small-molecule oligomerisation blockers were chemically refined, and a second generation produced.

In this thesis work I aim to characterize an established model of neuropathic pain in more detail uncovering new mechanistic changes in peripheral sensitisation. Using STOML3 in genetically modified mouse models (overexpression as well as ablation) yields insight into the peripheral mechanosensory driving force of neuropathic symptoms such as allodynia that could help to determine if modulating peripheral input can indeed alleviate neuropathic pain.

2 Materials and Methods

2.1 Materials

2.1.1 Technical equipment

ADInstruments, PowerLab 4/30
Digitimer Ltd., NeuroLog Amplifier
Digitimer ltd., Neurolog Stimulator Modules
Digitimer NL 100 Headstage
Gilson, Minipuls 3 Peristaltic Pump
Heiddolph, Promax 1020 shaker
IKA Labortechnik, RCT basic magnetic stirrer
Julabo, MP and Medingen Waterbaths
Kametec, Magnetic Base
Kleindiek Nanotechnik, MMA3-LS micromanipulator
Kleindiek Nanotechnik, NM nanomotor
Kleindiek Nanotechnik, Ultra-precise Force Measurement System
Leica, IC80 HD camera
Leica, KL1500 LCD- lamp
Leica, MS5/ M26 /MZ 10F dissecting microscope
LG, Monitor
LG, Windows 7 PC
Marzhäuser Wetzlar, MM33 manual micromanipulator
Newport, IG Breadboard table
Physik Instrumente, Piezoaktor
Physik Instrumente, Piezoverstärker
Tektronix, TDS 1002 Two Channel Digital Real Time Oscilloscope
Tetratec, AS30 airstone
Tygon, E-3603 tubing
World Precision Instruments, Magnetic Stand
World Precision Instruments, Mircoelectrode platinum iridium PTM23B10KT (1mΩ)
Weller WS51 soldering iron
Cookson Electronics S-Sn60 Pb40 soldering tin
Advent-Silverstone (No. AG54864) electrode wire
von Frey Filaments (Aesthesio)
Waterbath: P-D Industriegesellschaft mbH – WB-5

Scientific industries: Vortex-Genie2
Mettler Toledo: XS 205 DualRange
Macherey-Nagel:MN 226.90x115mm
Spatula

EM:
Leica Ultracut E4
AC20-Stainer (Leica)

Dissection equipment:
2x FST 5SF Inox. - forceps
2x FST 5HDC Inox. - forceps
FST No. 15023-10 spring scissors
FST No. 15000-10 spring scissors

Surgery equipment:
Anaesthesia unit: Evaporator (Parkland Scientific, No. 1286)
Sugery setup binocular: Leica S6 MEB115
Cold light source: Leica L2
AssuSilk 5-0 USP (EP1) - suture
Syringes: Braun: Omnifix F 100 (1ml)
Terumo: Agani needle 23Gx1
Reflex skin closure system Reflex7 wound clips

Mouse walk (all materials):
2x plate PMMA poured 150mm x 800mm x 10mm (C.A. LOEWE)
Acrylic glass mirror (Modulor)
Square tube (lead), 25mm (RS Components)
12x RS PRO fourfold-connector polymer, lead (RS Components)
4x RS PRO threefold connector (RS Components)
PVC black (C.A. LOEWE)
Magnetic tape (RS Components)
PVC white (hard, 0,3mm) (Modulor)
RS PRO adjustable base (plastic) (RS Components)
RS PRO adjustable base (plastic) square tube 25mm (RS Components)
Aluminum U-profiles (13x20x2,5, (LxHxW)) (Gemmel)

LED stripes with open wire-end, 24V, 100cm cold light (Conrad)
Hose line H03VV-F, 2x 0.75mm (Conrad)
4x4mm built-in socket (red, black) (RS Components)
4x measurement line 4mm (black, red) 2m (RS Components)
4x lemo connector series Redel P, 2 poles, 10A (RS Components)
Lemo connector series Redel P, socket, 2 poles, 10 A (RS Components)
Power supply (GW INSTEK), GPS-2303 (Conrad)
Screws, M3/M4 diverse

RoHS 2.3 MP Mono Grasshopper, FLIR
custom Mount
Canon EF-S 18-55mm 1:3.5-5.6 IS II Zoomobjective, f/3.5-5.6

2.1.2 Analytical software

ADI instruments, Chart v7.3 for Windows
Adobe, CS v5.5
GraphPad, Prism v5
Kleindiek Nanotechnik, Nanocontrol v4.0
Leica, LAS X
Mircosoft, Office 365
MatLab R2018b, R2019b
Mouse walk script for Matlab
ImageJ v1.51j8
iTEM v5.1

2.1.3 Chemicals and reagents

Isofluran (Baxter)
Tamoxifen (Sigma)
AD-3 (synthesized by Analyticon)
Corn Oil (Sigma)
Minearal Oil (Sigma-Aldrich)
Ethanol (30%, 50%, 70%, 90% and 100%) (Merck)
Propylene oxide (Polysciences Inc.)
Epon (Polysciences Inc.)
Osmiumtetroxid (Sigma)
Formvar/coal (Electron Microscopy Sciences)

Uranyl acetate (Serva)
Lead citrate (Leica)
Paraformaldehyde (Fluka)
Glutharaldehyde (EM-grade, Sigma)

2.1.4 Buffers and solutions

SIF (synthetic interstitial fluid):	2 nM CaCl2, 5.5 mM glucose, 10 mM Hepes, 3.5 mM KCl, 0.7 mM MgSO4, 123 mM NaCl, 1.5 mM NaH2PO4, 7.4 mM saccharose, set to pH 8.4 with NaOH

0,1M phosphate buffer
1% osmium tetroxide in 0,1M phosphate buffer (pH 7,5)

2.1.5 Labware and chemistry equipment

Brand, Pasteur pipette
Braun, razor blade
Electron Microscopy Science, silicon isolators
Eppendorf, Falcon tube
Eppendorf, Safe-lock tubes
World Precision Instruments, Sylgard 184 silicon elastomer

2.2 Mouse lines

2.2.1 C57BL6/N

C57BL6/N animals (inbred strain) were obtained from Charles River (CR). As they are the most commonly used wildtype animals used in translational research and therefore suitable for modelling diseases such as peripheral neuropathies. Furthermore, CR guarantees genetically identical individuals with a high degree of uniformity in their inherited phenotypes such as behavioural characteristics and responses to treatment which is ensured by a pyramid mating system in accordance with the international genetic standardization program (IGS). These animals were bought and used from an age of 8 to 10 weeks on for the initial CCI experiments (males only).

2.2.2 Avil-Cre/ERT2::Rosa26Stoml3-tdtomato-Flag

A former colleague (James Hall, PhD thesis) generated animals in which STOML3 could be overexpressed conditionally *in vivo*. He added a 3xFlag tag to the C-terminal of the *stoml3* cDNA, subcloned it into a vector with a CMV promotor and transfected the construct into HEK293 cells. A 2A peptide was inserted downstream between the 3xFlag tag and the red reporter tdTomato. The construct was subcloned into the Rosa26PA plasmid, linearized and electroporated into 129 ES cells. The clones were screened for transgenesis in the Rosa26 locus, cultured and injected into the denucleated blastocyst of a C57BL/6 mouse and implanted into an adult female.

Offspring were genotyped, positives for the transgene cross-bred with littermates and their offspring again genotyped to ensure germline transmission. The following generation was back-crossed with C57BL/6 for 5 generations to establish *Stoml3*$^{\text{LSL-3xFlag-Gt(Rosa26)Glwn}}$ mice. These mice were cross-bred with the Cre recombinase reporter line wnt1 to selectively overexpress STOML3 in wnt1 expressing tissue. Wnt1 is neural crest specific, originating lineages of all peripheral- and enteric nerves, glia and smooth muscle cells among others (X. Huang & Saint-Jeannet, 2004) and thus crossing *Stoml3*$^{\text{LSL-3xFlag-Gt(Rosa26)Glwn}}$ with wnt1-cre reporter mice resulted in selective overexpression of STOML3 in the peripheral nervous system. In a second step *Stoml3*$^{\text{LSL-3xFlag-Gt(Rosa26)Glwn}}$ mice were crossed with the AdvilinCre/ERT2 reporter mouse to confer full temporal control over the onset of overexpression and thus counteract possible compensatory developmental mechanisms. The Cre/ERT2 system uses a modified human estrogen receptor which is inducible by delivery of its agonist (artificial estrogen) such as Tamoxifen (Lau et al., 2011; Metzger & Chambon, 2001). These animals were used in the STOML3 overexpression section, referred to as

induced overexpression of STOML3 or sensory STOML3 OE (AvilCre/ERT2::LSLstoml3-Flag / Tamoxifen) and controls (AvilCre/ERT2::LSLstoml3-Flag / vehicle or LSLstoml3-Flag / vehicle) respectively. Animals from age 13 to 28 weeks were used, 14 females (5 were Cre positive) and 16 males (9 were Cre positive).

2.2.3 Wnt1-Cre::*stoml3*$^{fl/fl}$

Another former member of the Lewin lab (Liudmila Lapatsina, PhD thesis) generated conditional knockout alleles of *stoml3*, called B6.Stoml3^{tm4Glwn} (official nomenclature) and in this work *stoml3*$^{fl/fl}$. The first exon of s*toml3* was flanked by two loxP sites. Initially, a loxP site was introduced into the subcloned DNA fragment upstream of the first *stoml3* exon sequence by introducing a neomycin resistance cassette and subsequent removal with a Cre-deleter, leaving a single loxP site. Subsequently, a second loxP site was introduced ultimately producing floxed s*toml3* animals. Endogenous *stoml3* promotor sequences, subsequent genomic sequences and the UTR-sequence were kept unchanged. Crossing these mice with a line expressing a Cre recombinase such as Tg(Wnt1-cre)11Rth (from JAX: MGI:2386570, Danielian, Muccino, Rowitch, Michael, & McMahon, 1998) excised the exon 1 and produced a frameshift mutation in the open-reading frame (ORF) leading to a complete gene ablation in neural crest derived cells including sensory neurons. The advantage of this approach is in the temporal and spatial control over the STOML3 expression. Analyzing animals with a genetic ablation of *stoml3* spatially restricted to the somatosensory system allows for a differentiated analysis of peripheral contributions of STOML3 in sensory biology as well as an investigation of its potential beneficial effects in neuropathic pain. 10 male animals in the age of 26 to 29 weeks were used for the *stoml3* ablation experiments. Controls in this section will be referred to as controls (*stoml3*$^{fl/fl}$) and conditional knockouts of STOML3 as *stoml3* conditional deletion (wnt1-Cre::*stoml3*$^{fl/fl}$).

2.3 Chronic constriction injury (CCI) model

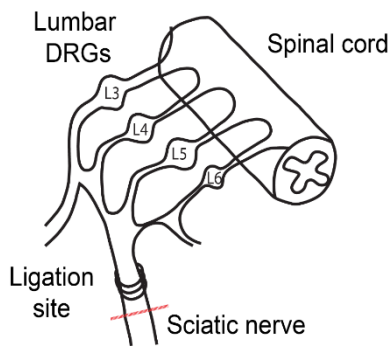

Figure 6 – Schematic of the chronic constriction injury (CCI)

Three silk-gut ligatures (5-0) are tied around the common sciatic nerve proximal to the sciatic trifurcation. The operation is performed under deep isoflurane anaesthesia; behavioural assessment of established neuropathic pain is performed 7 days after surgery. The red line indicates the plane distal to the ligation used for TEM as well as the recording site of the electrophysiological experiments.

To produce a neuropathic condition the chronic constriction injury (CCI) invented and first described by Bennett and Xie (Bennett & Xie, 1988) was applied to adult male Sprague-Dawley rats. Subsequently, this model was applied to mice as well. In my experiments C57BL6/N mice (from Charles River) were anaesthetized by isoflurane inhalation anaesthesia using a Parkland Scientific anaesthesia device. To initiate narcosis a 5% isoflurane-air mixture (Baxter) was flooded into a transparent plastic box containing the experimental animal. After the animal was anaesthetized it was removed from the transparent box and placed in the surgery setup face down, the lower body was mounted on the side – the right hindleg facing up. The nose of the animal was placed into a plastic tube that delivered an isoflurane-air mixture of 2.5% for anaesthetic maintenance. After the animal stopped breathing rapidly and started breathing slowly at a deep and steady rate, its hindpaw was pinched to determine if pain-reflexes were still present. Under incomplete anaesthesia animals withdraw their paw and hindlimb to this pinching stimulation, absence of the reflex proves deep anaesthesia. First the animals right hindlimb was shaved between hip and mid-upper leg. The location of the hip can be determined by palpation of the leg, a bony protrusion – the iliac crest - can be felt and was used as a landmark for the incision. The incision was made approximately 5-7mm distal to the iliac crest on a line between the iliac crest and the knee joint and was approximately 1cm long. The skin was separated from the underlying muscle tissue and connective tissue between ischiocrural muscles and quadriceps femoris was bluntly dissected using forceps. The sciatic nerve was visualized by slightly moving the quadriceps femoris muscle to the side (using forceps with a straight finish angled approximately 45°) and lifted a few millimetres. The position of the forceps was fixed using plastilin. 3 silk-gut ligatures 5-0 (Catgut GmBH, Naturseide-S, schwarz – 5/0 USP (sterile)) were tied around the nerve (with approximately 1mm space in between) proximal to the sciatic trifurcation. It is crucial not to use too much force, that would completely transect the nerve – the tightness of the ligatures was slowly increased until a twitch in the animals' lower leg was noticed then 2 knots were tied with the silk-gut to fix the desired compression strength. After the ligatures were tied, the wound was closed using Refelx 7 stainless steel wound clips (7mm). The animal was removed from

the anaesthesia source and returned to its home cage. A few minutes after terminating the anaesthesia the animals slowly begin to move, explore and interact with its cage-mates – all animals were monitored until they displayed normal exploratory behaviour to ensure they fully recovered from the anaesthesia.

2.4 Behaviour

2.4.1 von Frey Assay

In the classical von Frey assay calibrated monofilaments are used to stimulate an experimental animal's hind paw glabrous skin with an up- and down paradigm. Experimental animals were placed in a mesh-grid box and habituated to the new environment for 30 to 45 minutes. Then the first stimulation was applied using the 400mg von Frey monofilament. This filament was always used as a starting point. In theory 50% of the experimental animals should display aversive behaviour to this gauge filament, such as lifting and or licking of the paw, flinching or toe spreading whereas the other 50% of the population should not. If aversive behaviour was displayed and scored by the experimenter (with an X) the subsequent and weaker stimulus was provided, if no aversive behaviour was displayed and scored by the experimenter (with an O) the next stronger stimulus was provided. I applied the Chaplan (Chaplan et al., 1994) modification of the Dixon (Dixon, 1980) approach – 6 to 9 stimuli are sufficient to calculate the 50% paw-withdrawal thresholds using the log-value of the final von Frey filament, the k-value (that can be found in the Appendix 1 of the aforementioned Chaplan paper) which is produced from the pattern of aversive and non-responses to stimulations and the mean difference between stimuli. Animals were not stimulated more frequently than once a minute to avoid wind-up phenomena.

2.4.2 Mouse walk

Gait analysis was established in the lab using "Mouse walk" technology described by Mendes et. al. (Mendes et al., 2015). An acrylic walkway of approximately 80cm length was produced with white-light LED-strips attached to its sides. Another similar walkway was used as a background light (sky) with white plastic attached to the top to provide a lighter and even background. These two walkways were embedded in a black custom-built rack with a mirror angled 45° below the walkway. On the left side of the walkway a small custom-built plexiglas "house" was introduced to provide shelter for the animals. A monochromatic high-speed camera (FLIR, RoHS 2.3 MP Mono Grasshopper) was used to videotape the animal's walk (the mirror image / reflection was recorded). Experiments were performed with no additional light source present in the room. Animals were initially habituated to the walkway for 15 minutes

– they were put in the setup on the right side, opposite of the shelter and allowed to explore freely. Usually, they spent most of the time in the shelter after the initial exploration of the walkway. At the end of the habituation time the shelter containing the animal was removed, the animal placed on the right side again and the shelter placed on the left side – to make the animal cross the walkway a few times. Each animal was recorded multiple times to obtain recordings with constant velocity and no stops during the crossing – 4 to 5 of these videos were then cropped, converted to single image stacks (every frame was converted into 1 image, the framerate of the camera was 150 frames/s) and analyzed using a MATLAB script provided by Cesar Mendes. The white-LED light transilluminates the walkway creating an effect called fTIR (frustrated total internal reflection) - in brief: the light traveling through the walkway is reflected differently when there is contact of the animals' paw with the walkway. This is visualized through lighting of the contact area – the intensity of the reflected footprint is increasing with pressure / weight. This was used for the annotation of the videos, the paws as well as the head, nose, center of the body and other markers were used to evaluate approximately 26 parameters of the animals' gait.

2.4.3 Induction of *in vivo* overexpression with Cre/ERT2 system

Conditional overexpression animals of STOML3 were injected intraperitoneally with 100µl Tamoxifen (20mg/ml) solubilized in corn oil (Sigma) for 5 consecutive days. The day before the first injection Tamoxifen (Sigma Aldrich) was dissolved on a shaker at 37°C over night and stored at 4°C for the time of injections (5 days). Animals were always injected at the same time using a Braun: Omnifix F 100 (1ml) syringe with a Terumo: Agani needle 23Gx1; injections were made in the left and right lower quadrant alternately. Afterwards the animals were returned to their home cage and quarantined. Control animals received a vehicle injection (corn oil). After the last injection animals were left unhandled in their home cages for at least 5 days in order to achieve a maximal amount of recombination and afterwards tested with behavioural assays and electrophysiology.

2.5 Light microscopy

For the anatomical investigation of the CCIs effect on peripheral nervous tissue. 12 C57BL6/N animals (from Charles River) were operated and evaluated for their neuropathic status using the von Frey assay and then on the 10^{th} post-operative day sacrificed and ipsilateral as well as contralateral sciatic and tibial nerve samples taken (sciatic was proximal to the CCI and tibial distal to it). The samples were put fixed in 4% PFA (Fluka) with 2.5% Glutaraldehyde (EM grade, Sigma) in 0.1M phosphate buffer and then transferred to the EM core facility at the MDC for further processing, where they were post fixed for 3 days at 4°C (in the same buffer). After

fixation, samples were washed in 0.1M phosphate buffer 2x for 20min and then transferred into 1% osmium tetroxide (Sigma) in 0.1M phosphate buffer (pH 7.5) for 2 hours at room temperature. Afterwards samples were washed in 0.1M phosphate buffer 2x for 30min, dehydrated using an ascending concentration of ethanol (Merck) at 4°C (30%: for 15min, 50%: 2x for 30min, 70%: over night, another wash with 70% for 30min on the following day, 90%: 2x for 30min and finally 100%: 2x for 30min) and embedded into Epon (Polysciences Inc.) at room temperature. Initially in propylene oxide (Polysciences Inc.) 2x for 30min, then in propylene oxide/Epon (1:1) 2x for 30min, propylene oxide/Epon (1:2) 2x for 30min and finally in pure Epon. The pure Epon was changed at least once and allowed to infiltrate the sample over night on a shaker (slow movement). On the following day the Epon was changed again (after 3-4 hours), the samples filled into forms and polymerized at 60°C for 2-3 days. After polymerization, the blocks were cut semi-thin (1µm) and dyed with toluidine blue for 5min.

ImageJ was used to process/visualize images and myelinated neurons were counted. Healthy fibers were classified as such if they displayed a clear “lumen” inside the myelin sheath. Injured or degenerating axons were classified as such if the previously mentioned “lumen” was not present. Electron microscopy revealed that neurons without lumen were actually whirls of myelin in the process of degeneration (Wallerian degeneration).

The iTEM software was used to measure circumferences of the entire peripheral nerves (sciatic or tibial).

2.6 Transmission Electron microscopy

The same time course described for light microscopy was applied here. Animals were sacrificed 10 days post-CCI, tibial and sciatic nerve samples taken, put in 4% PFA (Fluka) with 2.5% Glutaraldehyde (EM grade, Sigma) in 0.1M phosphate buffer and then transferred to the EM core facility at the MDC for further processing. The processing was exactly the same as described in the light microscopy section, different after staining with toluidine blue: After trimming, ultra-thin cuts (70µm) were performed using a Leica Ultracut E4 on 100 mesh copper-grids coated with formvar/coal (Electron Microscopy Sciences). Enhancing the contrast of the cuts was achieved using Uranyl acetate (Serva) /lead citrate (Leica) in an AC20-Stainer (Leica). The pictures were taken with a Thermo Fisher EM “Morgagni” equipped with a CCD camera “Morada”.

Ultrastructural images with a 5600x magnification were taken from 3 planes per sample (5 images per plane) on a random basis, yielding 15 images per animal and condition for analysis (15x ipsilateral sciatic, 15x ipsilateral tibial and 15x contralateral sciatic, 15x contralateral

tibial). In every image myelinated- and unmyelinated fibers were counted. Additionally, for myelinated fibers the outer- and inner circumference of the myelin sheath were measured to calculate g-Ratios, a parameter used to judge myelin sheath integrity and therefore estimate the conduction velocity of the neuron.

2.7 *Ex-vivo* skin nerve preparation

After the experimental animal was euthanized the tips of the toes (the entire nail bed) were cut off and the hairy skin of the hindpaw removed. A circumferential cut was made around the ankle, blunt forceps were used to peel the glabrous skin of the foot until approximately mid-foot level. An incision was made at the hip-level and the entire skin of the leg removed as well as superficial fatty tissue. Afterwards the common sciatic nerve was freed from surrounding connective tissue and uncovered from hip to ankle taking care not to nick accompanying blood vessels. The common peroneal- and sural branches were cut off, leaving only the tibial nerve intact. The foot was angled to the side and metacarpal bones cut out (incisions were always placed at the joints) as well as tendons. After the last metacarpal bone was cut out, the foot (with glabrous skin and remaining digital bones) was detached from the ankle by carefully slicing remaining connective tissue “bridges” apart. The foot with the entire tibial nerve (up to the sciatic trifurcation at which point it is named sciatic nerve) was transferred into the organ bath chamber after cutting the sciatic as close to the spinal cord as possible. In the organ bath chamber (with superfused 30°C SIF buffer, Fig.7) the glabrous skin was pinned down temporarily to stretch the tissue in order to prevent cutting or nicking. The remaining muscle tissue, digital bones as well as tendons (plantar aponeurosis and individual finger tendons) were cut out and pins removed, the skin flipped to the “outside-out” configuration and pinned down again. The tibial nerve was transferred to the adjacent insulation chamber filled with mineral oil (Sigma). In the oil chamber the tibial nerve was cleared from surrounding connective tissue as well as the epineural sheath and fine filaments were teased out of the nerve and put on the recoding electrode to perform single unit recordings (Fig.7).

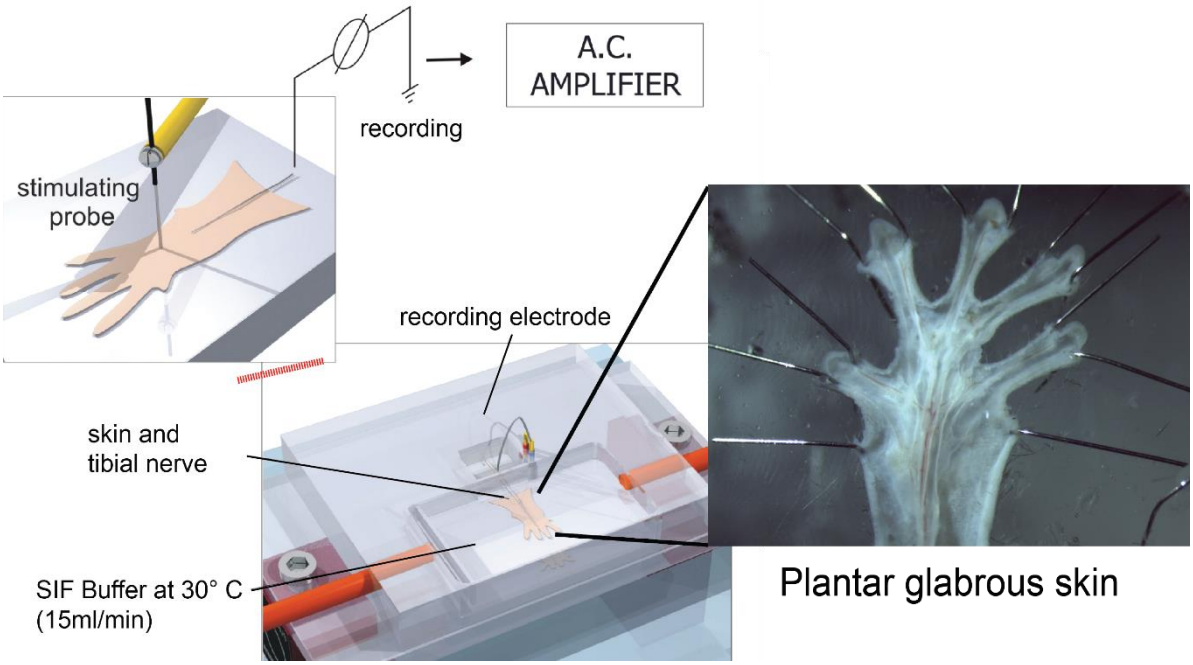

Figure 7 – *Ex-vivo* skin nerve setup

Schematic drawing of the *ex-vivo* skin nerve setup. The glabrous skin with its innervating nerve (tibial nerve) is dissected and pinned down in the organ bath, superfused with 30°C SIF buffer at 15ml/min. The tibial nerve is transferred to the oil chamber where filaments are teased and put onto a recording electrode. Electrical- as well as mechanical stimulations can be applied to map receptive fields in the glabrous skin and record action potentials generated in mechanoreceptors and nociceptors to characterize the receptors. The glabrous skin is shown in the "inside-out" configuration to highlight the nervous innervation of the hindpaw. (Illustration modified from Paul Heppenstall)

2.7.1.1 Isolation of single units

A glass rod was used to "scan" the glabrous skin for receptive fields. To elicit neuronal responses in mechanoreceptors a slight gentle brush or tapping of the skin with the glass rod was sufficient. For nociceptors a more forceful, prolonged and punctate search paradigm was applied. Ideally, the teased filaments were small so that there was no overlap of receptive fields and single units were excited with mechanical stimulation. If more than one receptor was stimulated and their physiological characteristics in terms of amplitude and shape of the action potential were sufficiently distinct, spike sorting could be applied. However especially in case of overlapping nociceptors if post recording differentiation could not satisfactorily be accomplished, these recordings were discarded.

2.7.1.2 Determination of neuronal- and receptor class according to conduction velocity and adaptation properties

An electrical stimulus was applied to the receptive field using a PTI microelectrode. 50 or 150µs stimulations with a frequency of 1Hz were applied to the receptive field with increasing intensity

(1-100mA). Mechanoreceptors usually required very little current injection to elicit action potential generation. For C-fiber nociceptors longer and stronger stimuli were required. Once the electrical threshold was reached and action potentials were generated, the stimulation intensity was reduced to find the minimum amount of current required to excite the neuron of interest. This was important since the injection of too much current reduces electrical latency and results in a higher conduction velocity (CV) which would be problematic for sensory neuron classification. A-ß neurons have conduction velocities of more than 10m/s in mice, A-δ neurons are slower than 10m/s but faster than 1.3m/s and finally C-fibers are slower than 1.3m/s. According to the CV different stimulation protocols were applied. A-ß fibers (and D-hair receptors associated with A-δ fibers) were stimulated with the Piezo actor to present the so-called “velocity” stimulus (description in the following section, Fig.8). Nociceptors (AM, associated with A-δ fibers and C-fibers) were stimulated with the Nanomotor and the “ramp and hold” stimulus (again, the detailed description follows, Fig.8). Receptors displayed different adaptation properties namely rapidly-adapting or slowly-adapting, intrinsic properties used to classify responding sensory neurons.

The Piezo actor was used to apply the Velocity protocol: a series of mechanical indentations with increasing velocity but constant indentation force (of approximately 45mN). Action potentials generated in the dynamic phase of the stimulation were analyzed. 25Hz sinusoidal vibrations of increasing force were used to determine the mechanical threshold. The stimulation rod of the Piezo actor as well as the Nanomotor were connected to a force sensor with a calibrated conversion factor of Volt to Milinewton (in my case: value in Volt * 130 = threshold in Milinewton). The Nanomotor was used to apply the Ramp and Hold protocol: a series of 6 consecutive indentations with a doubling of exerted force from between 50 – 400mN and a 10s static phase duration with a constant velocity (in later experiments the exerted force was adjusted to produce more stimulations in the force range of 20 – 250mN). Action potentials in the static phase of the stimulation were analyzed (until the discovery of dynamic-phase coding properties in C-fibers following neuropathic injury, afterwards all action potentials from the onset of the stimulus were analyzed).

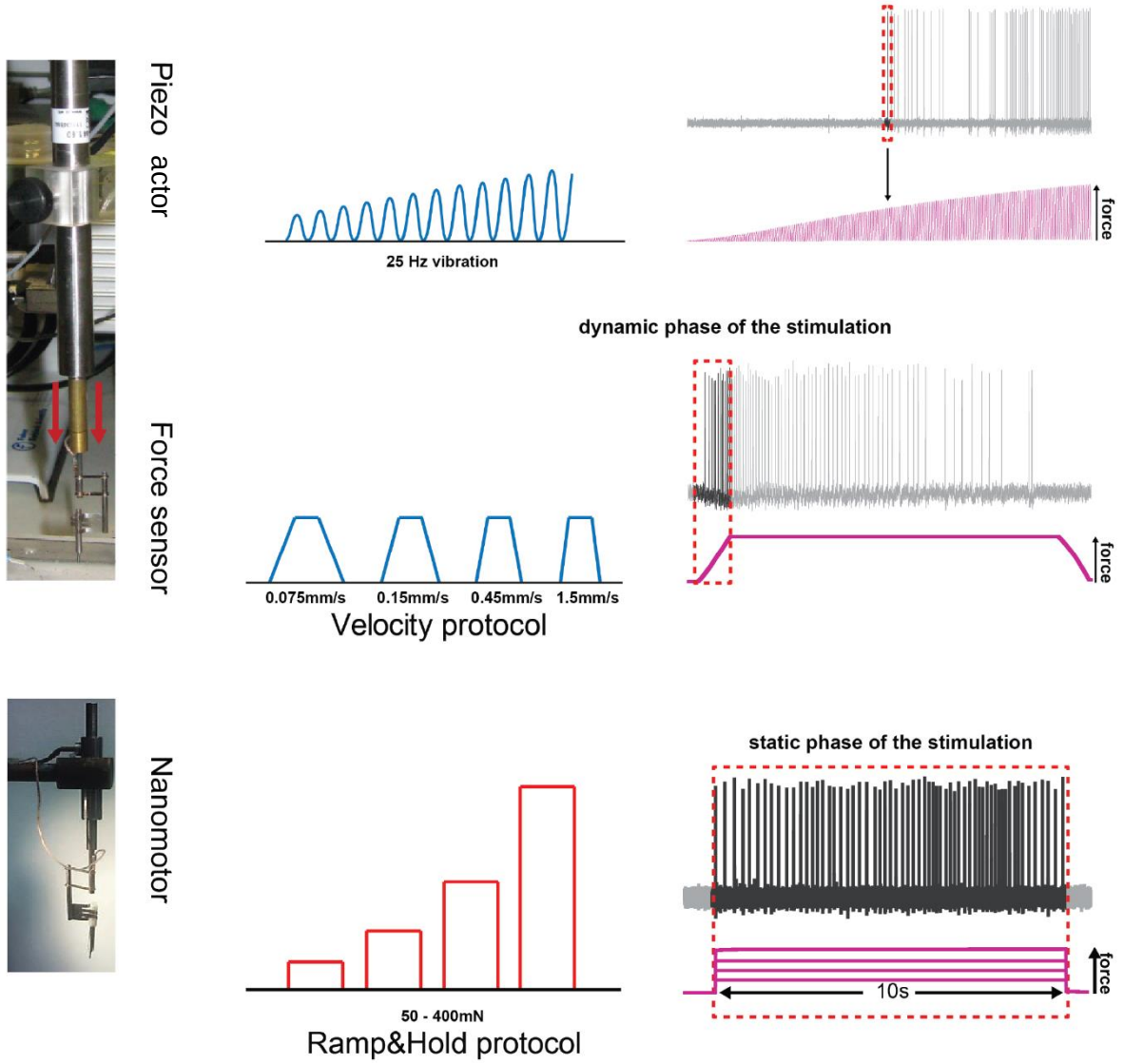

Figure 8 – Stimulation devices- and protocols used to characterize mechanoreceptors and nociceptors in the skin nerve preparation

Schematic drawing of the stimulation protocols and the devices used to apply them. The Piezo actor was used to apply the velocity protocol: a series of mechanical indentations with increasing velocity (0.075mm/s, 0.15mm/s,0.45mm/s, 1.5mm/s and 15mm/s (last velocity not shown)) but constant indentation force (of approximately 45mN). Action potentials generated in the dynamic phase of the stimulation were analyzed. 25Hz sinusoidal vibrations with increasing force were used to determine the mechanical threshold. The stimulation rod of the Piezo actor as well as Nanomotor were connected to a force sensor with a calibrated conversion factor of Volt to Milinewton (in my case: value in Volt * 130 = threshold in Milinewton). The Nanomotor was used to apply the Ramp and Hold protocol: a series of 6 consecutive indentations with a doubling of the exerted force of between 50 – 400mN and a 10s static phase duration with a constant velocity (in later experiments the exerted force was adjusted to produce more stimulations in the force range of 20 – 250mN). Action potentials in the static phase of the stimulation were analyzed (until the discovery of dynamic-phase coding, afterwards all action potentials from the onset of the stimulus were analyzed). (Illustration modified from Jan Walcher)

2.8 Statistics

2.8.1.1 von Frey Assay

The Chaplan modification of the Dixon approach was applied. Monofilaments with a defined force are used to stimulate the animal's hindpaw. If the animal responds (aversive behaviour such as lifting of the paw) the force will be decreased in the consecutive stimulation (description of the experimental paradigm in previous section). A two-way ANOVA was used to test differences in paw-withdrawal threshold after CCI. Thresholds of the affected paw vs. the unaffected paw as well as before and after surgery of the same paw were compared.

2.8.1.2 Mouse walk

The evaluation of the animals' walks using a Mathlab algorithm created by Cesar Mendes et al. produces a summary matrix of various parameters characterizing gait. There are dynamic and static parameters, i.e. parameters influenced by the velocity of the animal (or not). This is taken into account by filtering the dataset using the duty factor. The duty factor is a ratio created by dividing the stance time by swing time (i.e. the time the animal is in contact with the walkway divided by the time the animal moves its' paw – no contact to the walkway). Ratios below 0.5 are classified as runs, and those above 0.5 are classified as walks. In addition, every parameter is attributed with discrete values that can be compared between groups with an unpaired or paired t-test, depending on the experimental paradigm. Pawprint area, for example, is a static parameter created by summation of every illuminated pixel belonging to one of the four paws.

2.8.1.3 Anatomy

Unpaired t-tests were used to calculate possible differences between groups (for example: number of myelinated fibers in constricted vs naïve tibial nerve).

2.8.1.4 Electrophysiology

Activity values (responses of receptors to a given stimulus) displayed as frequencies or number of action potentials (#spikes) were compared using ANOVAs. If a three-group comparison was performed, a repeated measures ANOVA with Dunnett's multiple comparison test was calculated. The Dunnett's test allows the experimenter to decide against which dataset the other two shall be compared, so a baseline measurement could be compared against measurements after pain-inducing surgery in different genotypes. If a comparison of two groups was performed, a two-way ANOVA with Bonferroni post-hoc test was applied.

Mechanical threshold data was initially analyzed regarding its distribution type using the Kolmogorov-Smirnov-, D'Agostino and Pearson omnibus normality- and Shapiro-Wilk normality test. Data was taken to be normally distributed if at least two of the three tests indicated a normal distribution. If data was normally distributed an unpaired t-test was used to investigate statistical differences, for non-parametric data a Mann-Whitney test was used to investigate statistical differences.

Asterisks in figures and text indicate statistical significance: *p<0.05, **p<0.01, ***p<0.001

3 Results

3.1 Mechanical hypersensitivity following surgery (behaviour)

3.1.1 von Frey

3.1.1.1 New von Frey method: Dixon approach / Chaplan modification

The “gold-standard” in measuring pain hypersensitivity is the von Frey assay. In this assay, monofilaments with a range of exerted forces are applied to the animal’s paw. If the animal retracts its paw following stimulation, the experimenter progresses to presentation of the next smaller filament in the sequence with a reduction in applied force. Multiple versions of this assay have been developed. This work utilizes the Chaplan modification (Chaplan et al., 1994) of the classical Dixon up-down method (Dixon, 1980) which reduces stimulations to a necessary minimum and presents a robust statistical outcome. An example of the von Frey assay with Chaplan modification in naïve vs. CCI treated animals is displayed in Fig.9A,B. Animals display a robust mechanical hypersensitivity 7 days after CCI ($p<0.001$, two-way ANOVA) i.e. smaller filaments are sufficient to evoke aversive behaviour. In this cohort the 0.07g filament was on average sufficient to induce paw-withdrawal, in non-operated animals the threshold for paw-withdrawal ranges between 0.4g and 0.6g.

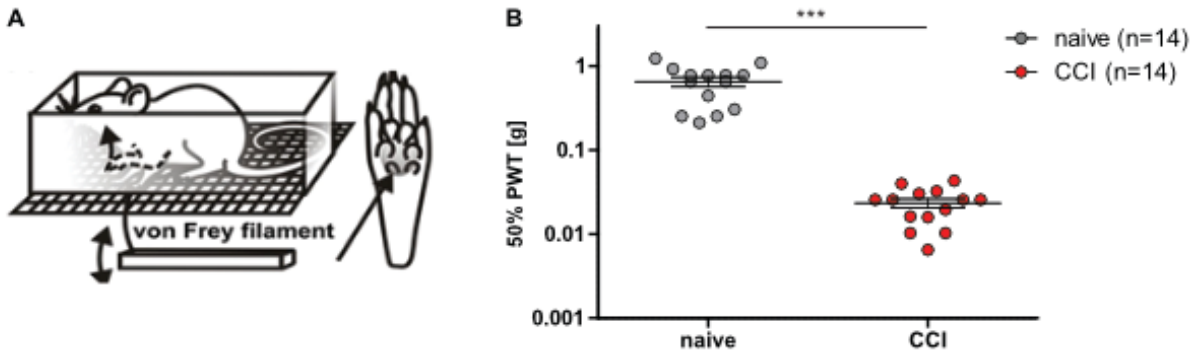

Figure 9 – Classical von Frey assay demonstrates mechanical hypersensitivity of experimental animals following CCI

A illustrates the classical von Frey assay (taken from Yu et al., 2013). Filaments are applied to the hindpaw before and after CCI, The Chaplan modification of the Dixon approach is used to calculate a possible difference using k (tabular value) and the applied force of the filament used last. B: after CCI the animals are hypersensitive to mechanical stimulation. A two-way ANOVA is used to calculate the difference, here $p<0.001$.

3.1.1.2 Initial applications of the von Frey method

A total of 28 C57BL6/N (wildtype) mice were used for the electrophysiological characterization of sensory neurons innervating the hindpaw glabrous skin. For the first half of this cohort a different, simpler von Frey approach was applied. In this simple paradigm the von Frey filaments 0.6g, 0.4g, 0.16g, 0.07g and 0.04g were applied to the animals' hindpaw 5 times each. Animals were classified as having acquired mechanical hypersensitivity if they displayed aversive behaviour following stimulation with the 0.07g and 0.04g von Frey filament.

3.1.2 Mouse walk

The experimental configuration is illustrated in Fig.10A. The illumination of the paws is used to annotate their position in relation to the center of the body and along with the head and base of the tail are used to characterize the animal's gait. Numerous parameters can be evaluated, the static parameters paw area and paw pressure (pixel intensity / area) have proven to be most valuable. A reduction of the pawprint of the affected side can be seen in Fig.10B. CCI is a unilateral procedure always applied to the right sciatic nerve. The animals develop a robust hypersensitivity to mechanical stimulations and therefore try to minimize any stimulation to the hypersensitive paw i.e. while walking they minimize the contact time of the paw with the ground. Furthermore, only the tips of their toes make contact with the walkway but not the running pads (Fig.10B). This behaviour was quantified by calculating a ratio of the area of the right hindpaw (affected) divided by the area of the left hindpaw. Before CCI this ratio was 1, after CCI it dropped to 0.4 (Fig.10C) whereas the pressure of the affected paw dropped from 1 to 0.7 (Fig.10D) (both significant differences $p<0.001$, paired t-test).

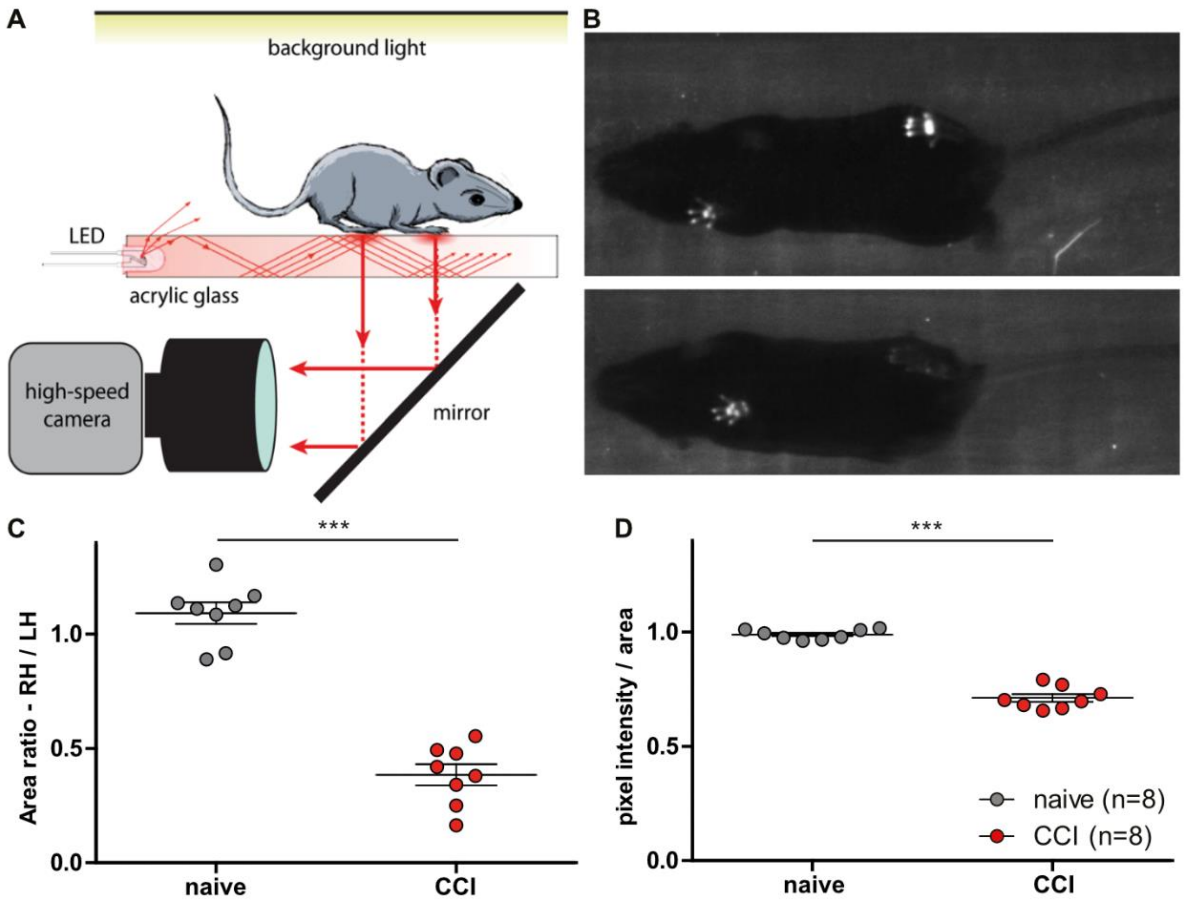

Figure 10 – Behavioural characterization of neuropathic animals using gait analysis

Animals walk across an 80cm long acrylic-glass walkway which is transilluminated with white LED lights (A, from Mendes et al. 2015). Contact of a paw with the walkway results in illumination (fTIR effect, B) – the step pattern is recorded with a high-speed camera and fed into an algorithm that enables the quantification of approximately 26 gait parameters. Also shown in B, the reduction in pawprint area of the right hindpaw following neuropathic injury (top panel is the control, bottom 7 days after CCI). The quantification is shown in C – before CCI the ratio of the pawprint area right hindpaw / left hindpaw is approximately 1. After CCI the ratio drops to 0.4 illustrating the contact minimization of the affected paw ($p<0.001$, paired t-test). On the right the pixel intensity per area is quantified, after CCI the intensity (i.e. pressure) drops to 0.7, again illustrating the animals' change in behaviour to minimize load on the affected paw ($p<0.001$, paired t-test).

3.2 Loss of myelinated fibers after surgery (as assessed by light microscopy)

On the 10th post-operative day animals were perfused with 4% PFA and tibial nerve tissue proximal- and distal to the constriction site was taken for electron microscopy. Additional tissue for semi-thin sections was taken from another 6 animals (that were later used for electrophysiology), unfortunately 2 samples from the contralateral side were lost in the process.

The semi-thin sections were stained with toluidine blue and used for a quantitative assessment of myelinated fibers (A-fibers). A-fibers were counted in injured and uninjured tibial nerves and then compared. A-fibers without a clearly visible “lumen” were categorized as degenerated (or degenerating) since EM pictures confirmed, that neurons lacking defined “lumen” had undergone Wallerian degeneration and were therefore no longer functional.

The quantification of A-fiber abundance shows that following CCI approximately 50% of myelinated fibers disappear. This is illustrated in Fig.11. Healthy tibial nerves contained on average 1150 myelinated fibers, on the injured side only 590 could be found and an additional 278 were observed to be undergoing Wallerian degeneration. Measuring the circumference of the nerves also showed that injured nerves were swollen i.e. their perimeter was significantly increased ($p<0.05$, unpaired t-test) – a phenomenon that to my knowledge was previously only described for parts of the nerve proximal to the injury.

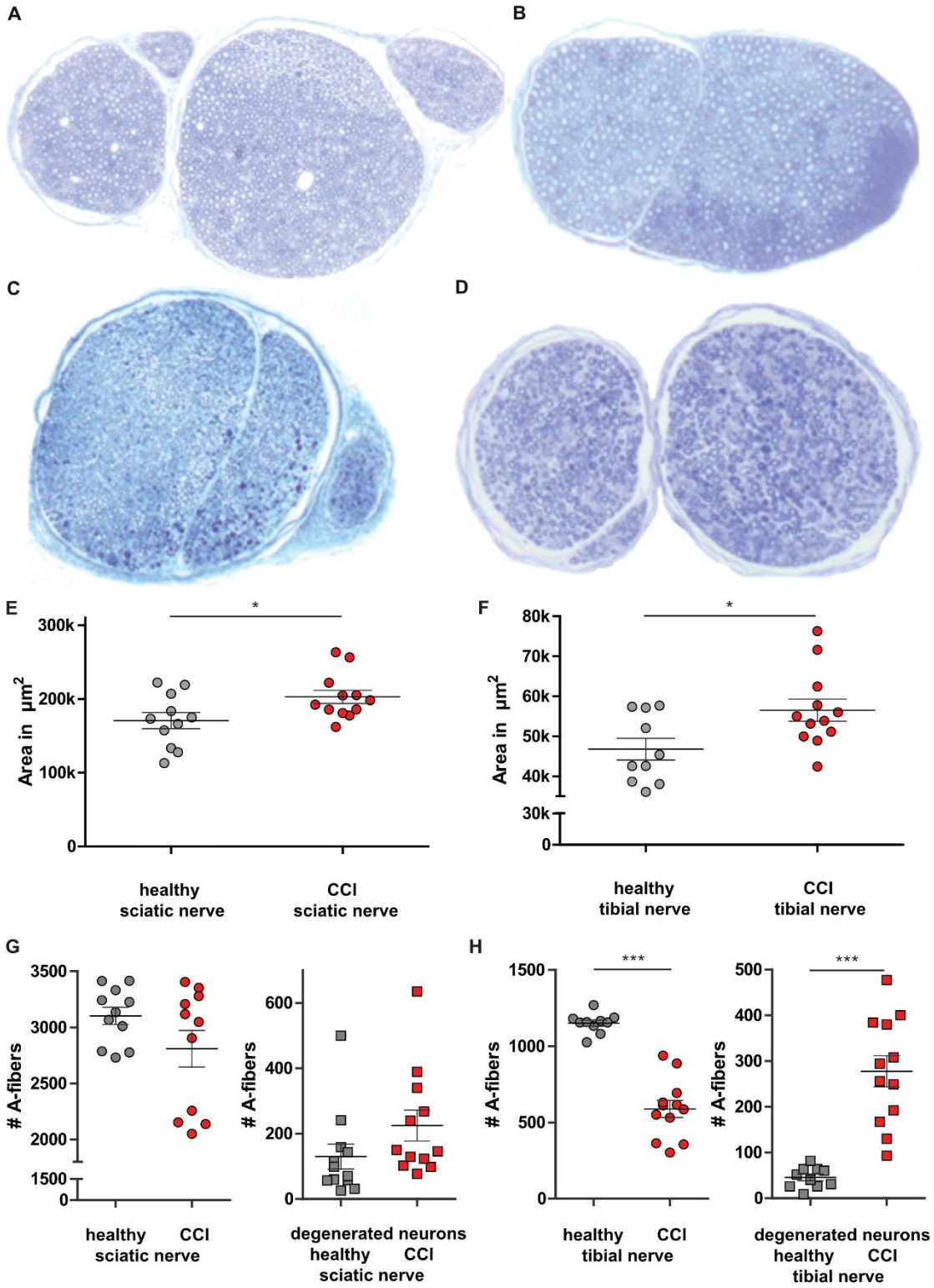

Figure 11 – CCI results in degeneration of approximately 50% of myelinated fibers

Semi-thin sections of sciatic nerves (A and C) and tibial nerves (B and D) were used to count myelinated fibers in healthy (A and B) and injured (C and D) nerves. Proximal to the injury (sciatic nerve) myelinated afferents were not observed to decay (G). The healthy tibial nerves contained on average 1150 (±64) myelinated fibers, whereas in the injured nerves only 590 (±195) fibers could still be categorized as such (H). An additional 300 fibers could be classified as “degenerating” in the injured nerves ($p<0.001$, unpaired t-test). Interestingly, axonal swelling could also be observed distal to the injury ($p<0.05$, unpaired t-test) (F).

3.3 C-fiber system unaffected (as assessed by electron microscopy)

To investigate if unmyelinated fibers (C-fibers) were affected by CCI in a similar way, I evaluated ultra-thin slices with 5600x magnification in a transmission electron microscope (TEM). C-fibers did not seem to have degenerated after surgery (Fig.12), showing elevated abundance (Fig.12D), possibly due to axonal sprouting. There was a significant increase in the C to A Ratio distal to the injury (Fig.12B $p<0.05$, unpaired t-test), this is most likely attributed to the loss of myelinated fibers as well as the emergence of C-fiber branches.

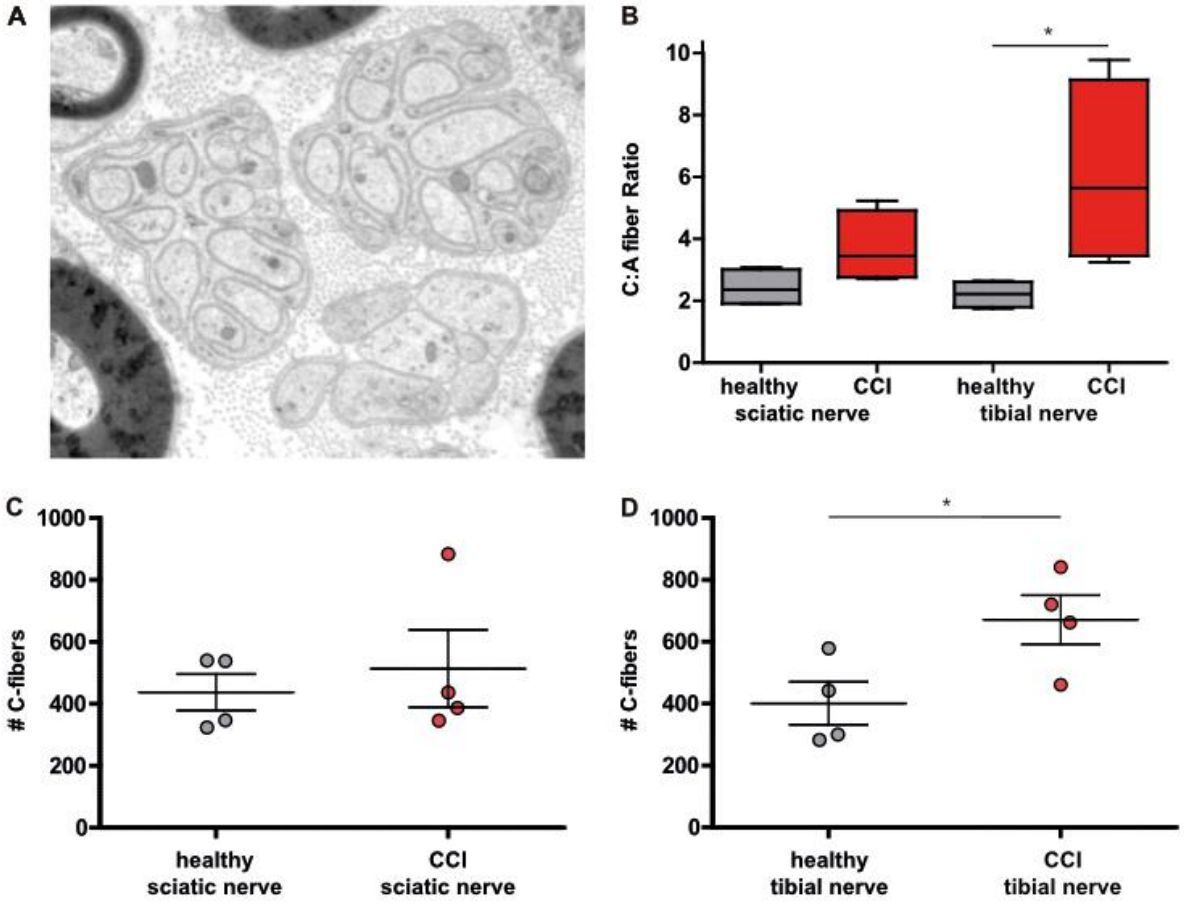

Figure 12 – C-fibers do not degenerate following CCI

To investigate a possible effect on unmyelinated fibers, ultra-thin sections from sciatic- and tibial nerves with and without CCI were produced and processed for EM. Ratios of C to A-fibers are displayed in B, depending on the source, a ratio of between 3:1 – 5:1 can be found. This ratio increased significantly distal to the injury ($p<0.05$, unpaired t-test). Proximal to the CCI a significant increase in C-fiber abundance was found, possibly illustrating the emergence of C-fiber sprouts ($p<0.05$, unpaired t-test) – ultrastructural analysis was based on samples from 4 animals.

Additional analysis was performed on myelinated axons to further characterize the CCI phenotype. Myelinated fibers were categorized by axonal diameter and a distribution of small to large diameter axons plotted.

In the tibial nerve (distal to the CCI injury) the abundance of large myelinated fibers with a diameter of more than 4µm was significantly lower (Fig.13F, χ^2-test, $p<0.0001$) compared to the contralateral side.

This indicates, that following CCI mainly large neurons with thick myelin-sheets may have degenerated – this population of neurons is known to be associated with mechanoreceptors (and proprioceptors). G-Ratios, which measure axon integrity (Hildebrand & Hahn, 1978), were calculated by dividing the inner diameter by the outer diameter of the myelin-sheet (Fig.13G and H). A shift in this ratio would indicate, that neurons might display slower conduction velocities during signal propagation and would pose a problem for the categorisation of sensory afferents in the electrophysiology experiments. No shift in this ratio could be observed, it was 0.7 for controls as well as injured nerves consistent with g-Ratios calculated in non-operated animals from colleagues in the lab. This analysis confirmed that neurons recorded in the following electrophysiology experiments could be categorized using conduction velocity. Thickly myelinated neurons associated with low-threshold mechanoreceptors (LTMRs) display CVs >10m/s. Thus, healthy neurons exist in peripheral nerves after nerve-constriction and can be recorded from and their physiological properties investigated.

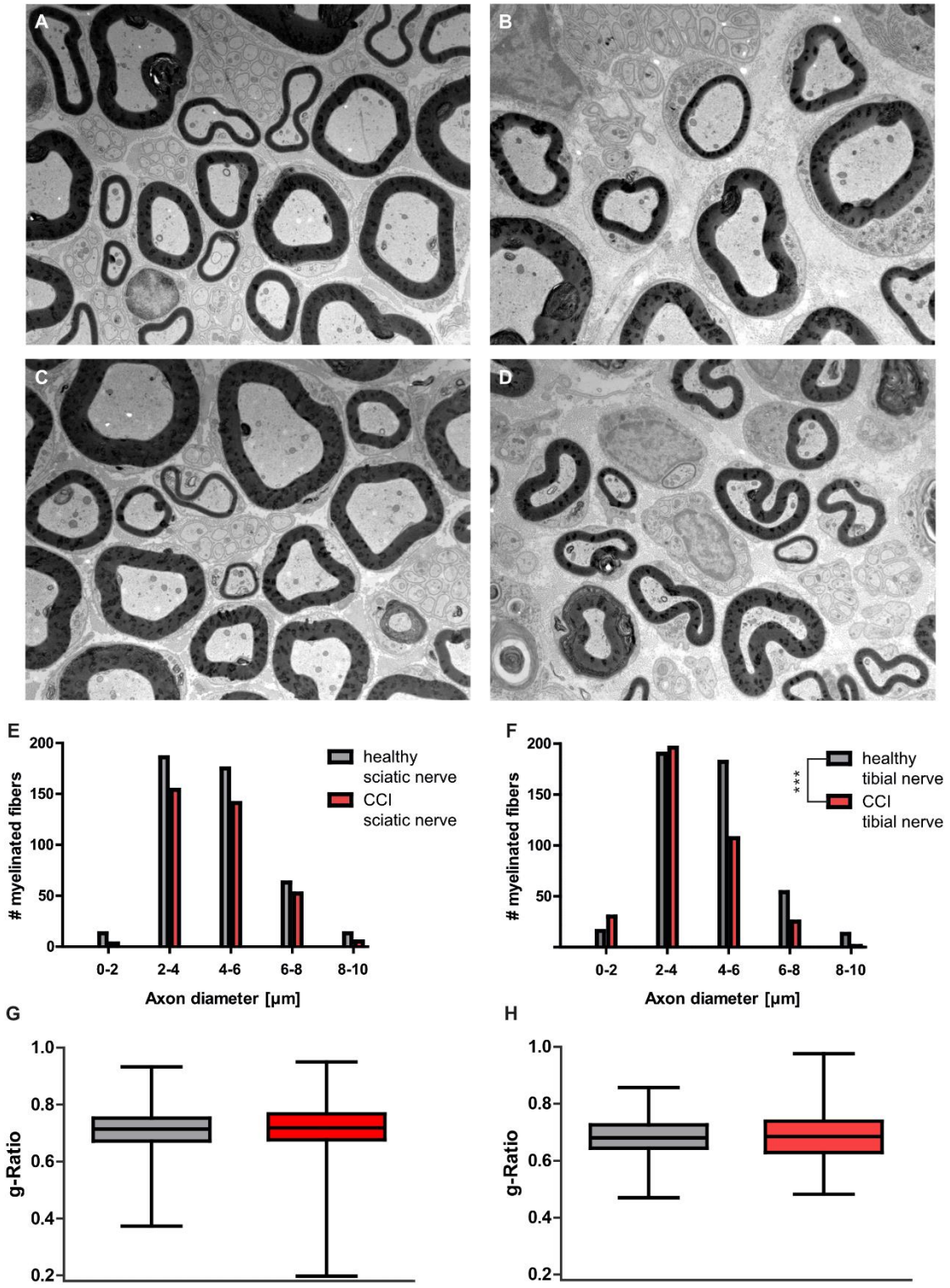

Figure 13 – Degenerating axons following CCI are mainly of large-diameter

Ultra-thin sections of sciatic nerves (A and C) and tibial nerves (B and D) were used to perform additional analysis of myelinated fibers in healthy and injured nerves. Myelinated axons were categorized by axonal diameter and a distribution of small to large diameter axons plotted. A significant decrease in abundance of large myelinated fibers with a diameter >4µm was found (F, χ^2-test, $p<0.0001$). G-Ratios were calculated to investigate the integrity of the myelin-sheet of axons of the sciatic nerve (G) and tibial nerve (H). No abnormality could be found in peripheral nerves after constriction injury.

3.4 Physiological properties of LTMRs after surgery are unaltered

In a pilot experiment I attempted to record primary afferents from a recording site proximal to the neuropathic injury (between ligatures and DRGs, the usual recording site was distal to the injury as indicated in Fig.6). This experiment was executed to prove that indeed following CCI there are intact sensory afferents transmitting information through the ligation site and therefore peripheral input can indeed be a driving force of behavioural changes observed after surgery such as reduced paw-withdrawal thresholds. I succeeded in recording a D-hair as well as A-mechanonociceptors (AM), but the process of cutting off the ligatures (necessary in order to be able to guide the nerve from the buffer- into the insulated recording chamber) was laborious and damaging to the nervous tissue. Recordings were only possible within a short timeframe afterwards, so in all subsequent experiments I removed the ligation site to maximize the length of available recording time. If sensory neurons survived the injury, that must mean they transmit through the ligation site and the electron microscopy proved that proximal and distal to the injury there are indeed numerous thickly myelinated afferents present. On the other hand, if a sensory neuron was damaged or destroyed (the connection from peripheral terminal to cell body in the DRG was severed) it would have undergone degeneration, making it unlikely that recordings could be made from axons distal to the injury. In the following section I will present the physiological properties of intact LTMRs following CCI.

3.4.1 Rapidly-adapting mechanoreceptors (RAMs)

RAMs are so-called velocity-indicators. They respond to moving stimuli by producing action potentials. Very fast stimuli are encoded with more action potentials than slower moving stimuli. Thickly myelinated neurons terminate in the glabrous skin and connect to specialized end-organs, the Meissner's corpuscle. The neurons belong to the A-ß category allowing for information-transmission speed of more than 10m/s. A cartoon of the corpuscle as well as its rapidly-adapting property is presented in Fig.14A. RAMs are present in the hairy skin as well – similar physiological properties are observed, but produced by a different type of receptor – the hair follicle afferent.

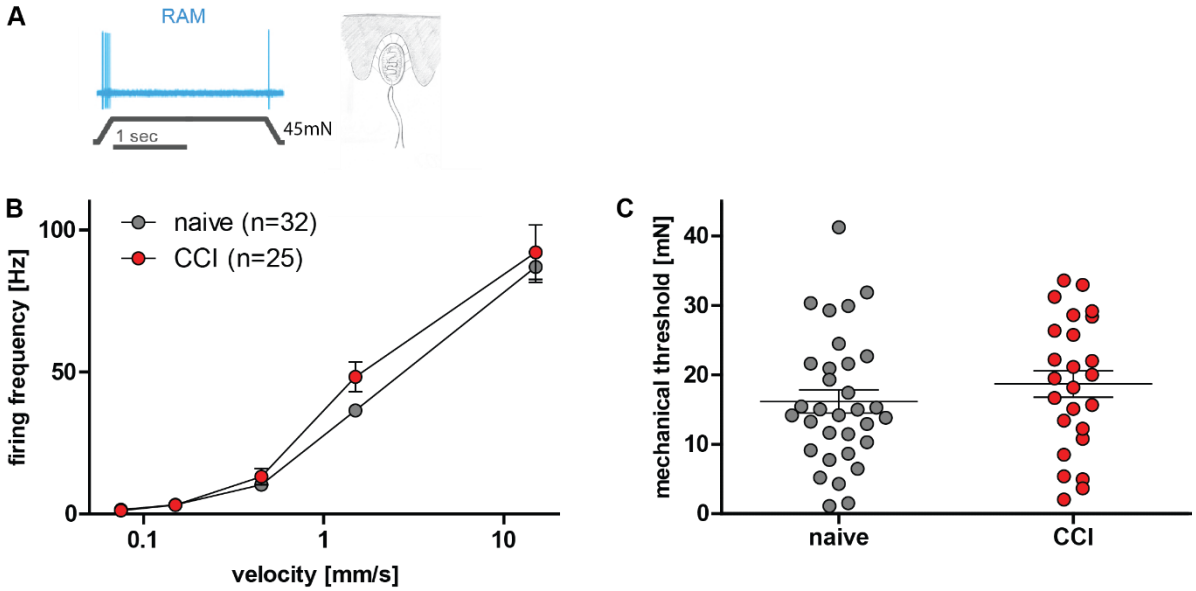

Figure 14 – Physiological properties of rapidly-adapting mechanoreceptors are not altered following CCI

A shows an illustration of the Meissner's corpuscle as well as an example of a rapidly-adapting receptor. Action potentials are only produced in the dynamic (on- or off-) phase of the stimulation, but not in the static phase. RAMs in the naive condition and following CCI were stimulated in the glabrous hindpaw skin with the „velocity protocol". Action potentials in response to the consecutive probe velocities were counted and divided by the length of the dynamic phase to calculate firing frequencies [Hz]. Following CCI, RAMs did not display altered physiological properties (B, two-way ANOVA). Mechanical thresholds [mN] calculated from ramp stimulations were unaltered as well (C, unpaired t-test).

In this study, I recorded 32 RAMs from C57BL6/N animals and compared their physiological properties to 25 RAMs recorded from C57BL6/N animals following CCI. Each receptor was stimulated with a protocol that increased the velocity of the ramp with every consecutive stimulation (velocity-protocol), starting with a probe velocity of 0.075mm/s and ending at 15mm/s (see Methods for a more detailed description). The indentation force was kept constant at about 45mN. Action potentials evoked in the dynamic phase of the stimulation were analyzed and divided by the length of the dynamic phase to calculate firing frequencies [Hz].

The mechanical threshold of the first action potential of every velocity step was used to calculate the mean mechanical threshold in [mN] of the receptors. As illustrated in Fig.14B slow velocities (0.075mm/s and 0.15mm/s) are not sufficient to evoke action potentials in RAMs in the naïve or CCI group (with very few exceptions). From a velocity of 0.45mm/s over 1.5mm/s to 15mm/s there is a linear increase in the receptor's activity. This physiological characteristic was observed in naïve and CCI RAMs. No difference could be found between the two groups. The same was true for the mechanical threshold of the receptors.

3.4.2 Slowly-adapting mechanoreceptors (SAMs)

SAMs provide information about the texture of objects and respond to moving- as well as static stimuli. Thickly myelinated neurons terminate in the glabrous skin and connect to specialized end-organs, the Merkel cells. The neurons belong to the A-ß category allowing for information-transmission speed of more than 10m/s. A cartoon of the end-organ as well as its slowly-adapting property is presented in Fig.15A.

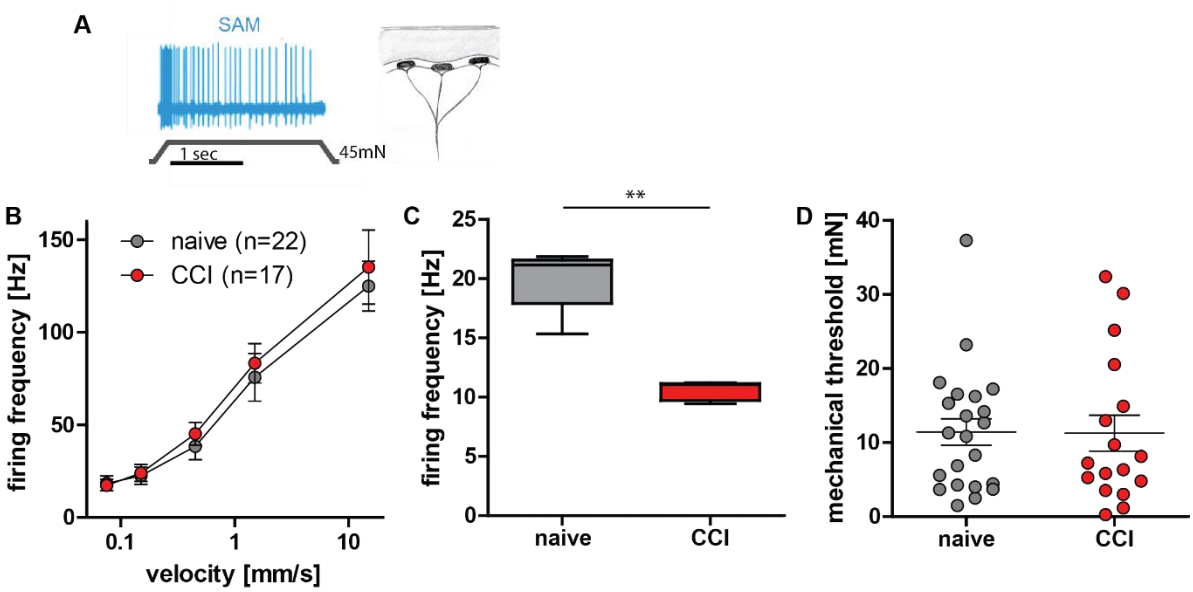

Figure 15 – Physiological properties of slowly-adapting mechanoreceptors, static phase transduction is impaired

A shows an illustration of the Merkel cells as well as an example of a slowly-adapting receptor. SAMs in the naive condition and following CCI were stimulated in the glabrous hindpaw skin with the „velocity protocol". Action potentials in response to the consecutive probe velocities in the dynamic phase of the stimulation were counted and divided by the length of the dynamic phase to calculate firing frequencies [Hz], APs in the static phase of the stimulus were counted and firing frequencies calculated (C). Following CCI, SAMs did not display altered dynamic-phase physiological properties (B, two-way ANOVA), however in the static phase of the stimulation SAMs fired significantly less APs than controls (C, $p<0.01$, two-way ANOVA). Mechanical thresholds [mN] calculated from ramp stimulations were unaltered (D, Mann-Whitney test).

In this study, I recorded 22 SAMs from C57BL6/N animals and compared their physiological properties to 17 SAMs recorded from C57BL6/N animals following CCI. Each receptor was stimulated with the “velocity protocol” as described in the previous section. Additionally, APs in the static phase were counted, firing frequencies calculated and compared between the two conditions. The mechanical threshold of the first action potential of every velocity step was used to calculate the mean mechanical threshold in [mN] of the receptors. As illustrated in Fig.15B slow velocities (0.075mm/s and 0.15mm/s) are already sufficient to evoke action potentials in SAMs in the naïve and CCI group. From a velocity of 0.45mm/s to 1.5mm/s and 15mm/s there is a linear increase in the receptor’s activity. This physiological characteristic was observed in naïve and CCI SAMs. No difference in mechanical threshold could be found between the two groups. But the static phase response of SAMs was significantly lower (Fig.15C).

3.4.3 D-hair mechanoreceptors

D-hairs are the most sensitive mechanoreceptors with huge receptive fields and two specializations distinguishing them from other LTMRs: they do not make a connection to a specialized end-organ such as the Meissner’s corpuscle or Merkel cell – they are hair-follicle afferents associated with down-hairs present in the center of the glabrous skin (a cartoon of the hair-follicle as well as its rapidly-adapting property is presented in Fig.16A). Furthermore, they are not associated with myelinated neurons of the A-ß category but with neurons of the A-δ category, therefore their transmission speed is slower than 10m/s. They are rapidly-adapting like RAMs but produce more action potentials when challenged with the same stimuli. Furthermore, directional sensitivity was recently described for these receptors (Rutlin et al., 2014; Walcher et al., 2018). When stimulating the down-hair with the direction of the hair growth opposed to orthogonal to the growth, the D-hair produces significantly more action potentials.

In this study, I recorded 19 D-hairs from C57BL6/N animals and compared their physiological properties to 32 D-hairs recorded from C57BL6/N animals following CCI. Each receptor was stimulated with the “velocity protocol” (described before). As illustrated in Fig.16B slow velocities (0.075mm/s and 0.15mm/s) are already sufficient to evoke action potentials in D-hairs in the naïve and CCI group. From a velocity of 0.45mm/s to 1.5mm/s and 15mm/s there was a linear increase in the receptor’s activity in the naïve condition. In the CCI group there seemed to be a decay of activity when challenged with the last stimulation. In controls a mean firing frequency of 180Hz was measured, whereas following CCI the activity declines to 145Hz. The Bonferroni post-hoc test of the two-way ANOVA yields a significant difference between the two groups in this bin ($p<0.001$); however, the overall activity of these receptors was

statistically not different. The same was true for the mechanical threshold of the receptors. D-hairs following CCI seemed to have an increased transduction threshold, but again the difference was not significant.

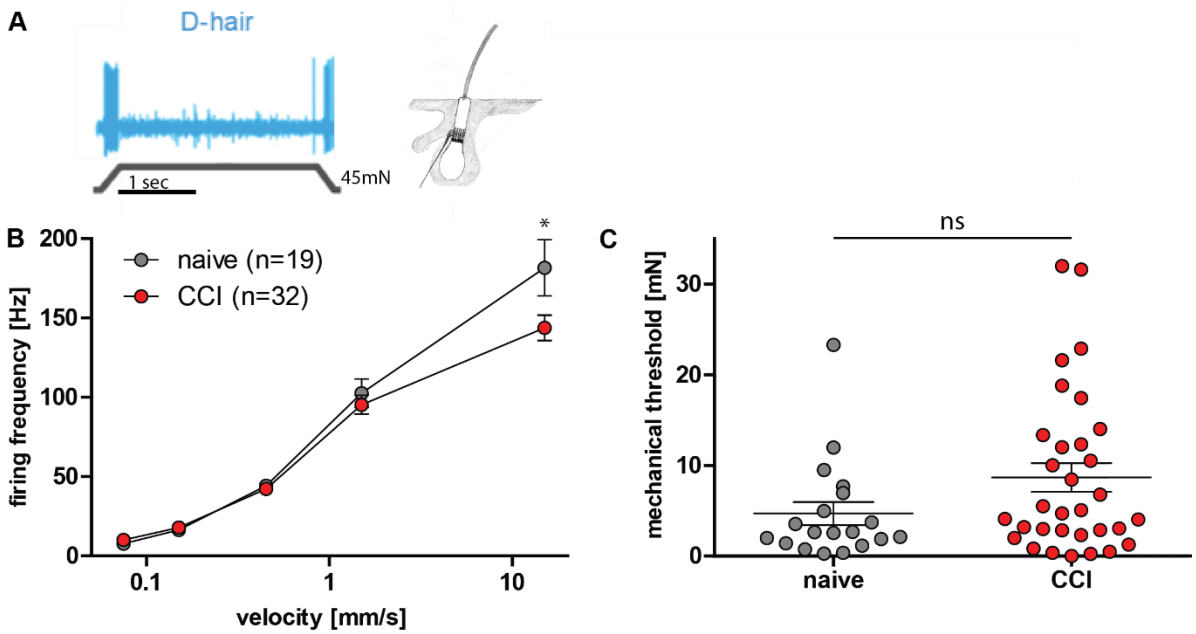

Figure 16 – Physiological properties of D-hair mechanoreceptors are not altered following CCI

A shows an illustration of the down-hair follicle as well as an example of a rapidly-adapting receptor. D-hairs in the naive condition and following CCI were stimulated in the glabrous hindpaw skin with the „velocity protocol“. Action potentials in response to the consecutive probe velocities were counted and divided by the length of the dynamic phase to calculate firing frequencies [Hz]. Following CCI, D-hairs did not display altered physiological properties (B, two-way ANOVA). The Bonferroni post-hoc test yields a significant difference in activity between the two groups in the last/ fastest velocity stimulus, however the overall activity was not different. Mechanical thresholds [mN] calculated from ramp stimulations were unaltered as well (C, Mann-Whitney test) even though a trend towards increased transduction thresholds is visible.

To summarise these findings so far, the physiological properties of LTMRs are not substantially altered following CCI, except for a diminished static phase activity in SAMs. I could not find evidence for a peripheral driver such as threshold reduction (sensitization) or increased activity.

The TEM analysis showed a decreased abundance in myelinated neurons associated with the receptors investigated so far. But the receptors of these categories were physiologically unaltered if still intact. However, this cannot disprove that a loss of LTMRs might be centrally translated into neuropathic pain.

3.5 Physiological properties of nociceptors following neuropathic injury

In the following section I will present the physiological properties of HTMRs or nociceptors following CCI. In brief, our nociceptive system consists of two distinct fiber systems terminating

in free nerve endings in the periphery, tightly associated with nociceptive Schwann-cells (a specialized type of glia-cell). These Schwann-cells were demonstrated to have a direct excitatory function on sensory neurons (mainly nociceptors) and might therefore play an important role in initiation of nociceptive activity (Abdo et al., 2019). There are myelinated nociceptors with neurons of the A-δ category and information transmission speed of less than 10m/s. They are responsible for the perception of the so-called first pain (Ploner et al., 2002; Price, 1972, 1977; Taylor, 1950; Torebjörk & Hallin, 1973), which is a fast, sharp sensation allowing the person or animal experiencing it to withdraw from the source of the tissue damage and therefore prevent further damage. The second system consists of unmyelinated nociceptors called C-fibers and is a very diverse system. C-fibers do not only transduce mechanical stimuli, there are at least 4 different subgroups in which in addition to mechanical stimuli, heat, cold or both can excite the receptor and therefore induce the generation of action potentials (Fleischer et al., 1983; Kress et al., 1992; G. R. Lewin & Mendell, 1994; Paricio-Montesinos et al., 2020). C-fibers have axonal conduction velocities of up to 1.3m/s and are associated with the perception of the so-called second pain – a long-lasting blunt, pulsating sensation (Ploner et al., 2002; Price, 1972, 1977; Taylor, 1950). The second pain is a very complex phenomenon and can be adapting (the sensation can decay over time) or not (e.g. as for tooth-pain). Is neuropathic pain driven by physiological changes in one or both of these fiber systems? This question will be addressed in the next section.

3.5.1 A-mechanonociceptors (AM)

AMs are slowly-adapting high-threshold nociceptors that generate action potentials when challenged with static indentations once their transduction threshold is reached (a cartoon of the free nerve ending as well as the AMs slowly-adapting property is presented in Fig.17A). The more force applied to the receptive field the larger the activity of the receptor. In this study, I recorded 27 AMs from C57BL6/N animals and compared their physiological properties to 53 AMs recorded from C57BL6/N animals following CCI. Each receptor was stimulated with a ramp and hold protocol that consisted of 10s stimuli with a doubling in applied force with each consecutive stimulus. The speed of the ramp was a constant 2mm/s. Evoked action potentials were analyzed (depending on the strength of the stimulus the receptor already generated activity in the dynamic phase if its threshold was reached) and divided by the length of the stimulus to calculate firing frequencies [Hz]. The mechanical threshold for the first action potential of every indentation step was used to calculate the mean mechanical threshold in [mN] for each receptor.

As illustrated in Fig.17B indentation forces from ~ 50 - 200mN are transduced with a linear increase in firing frequency by the receptor. At forces between 200 - 400mN the increase in

activity begins to saturate. In the CCI group there seems to be a reduction in activity at applied forces of between 100 - 200mN however, the overall activity of these receptors was statistically not different (two-way ANOVA). The same was true for the mechanical threshold of the receptors. AMs following CCI seemed to have a slightly decreased transduction threshold (Fig.12C), which would be expected in the state of injury induced sensitization, but again the difference was not significant (Mann-Whitney test).

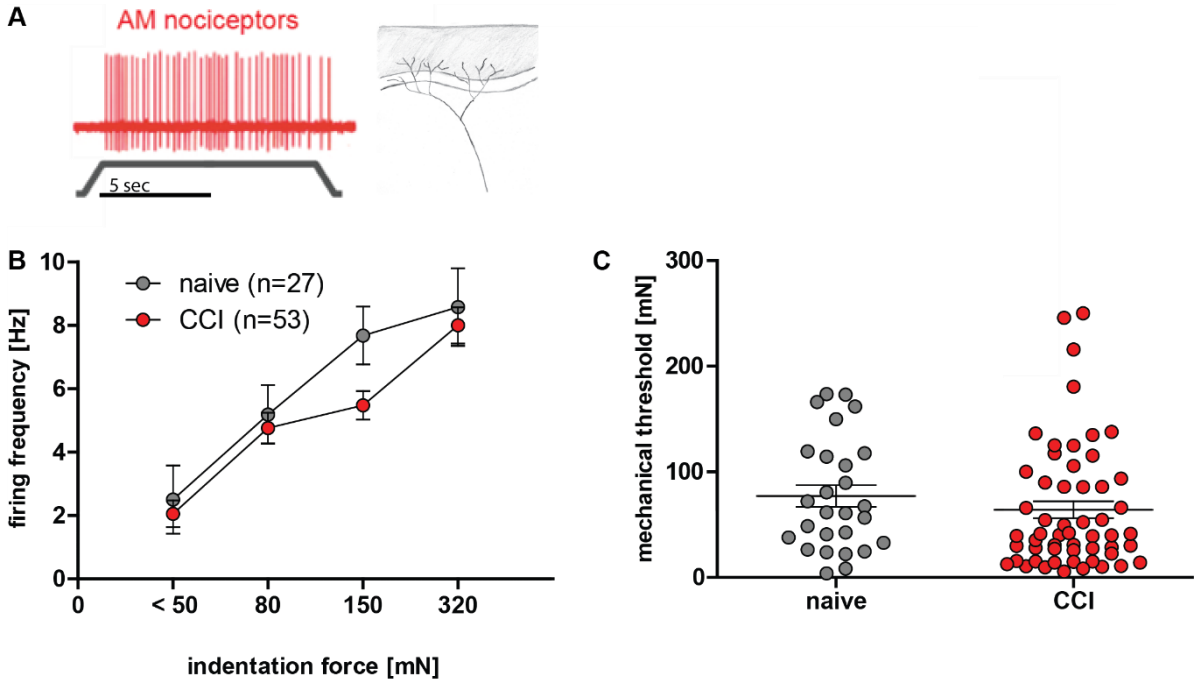

Figure 17 – Physiological properties of A-mechanonociceptors are not altered following CCI

A shows an illustration of the free nerve ending as well as an example of a slowly-adapting receptor. AMs in the naive condition and following CCI were stimulated in the glabrous hindpaw skin with a ramp and hold protocol. Action potentials generated in response to the consecutive indentation forces were counted and divided by the length of the stimulus to calculate firing frequencies [Hz]. Following CCI, AMs did not display altered physiological properties (B, two-way ANOVA). Mechanical thresholds [mN] were unaltered as well (C, Mann-Whitney test) even though a slight trend towards decreased transduction thresholds is discernable.

3.5.2 C-fiber nociceptors

C-fibers are slowly-adapting high-threshold nociceptors that generate action potentials when challenged with static indentations once their transduction threshold is reached (a cartoon of the free nerve ending as well as the slowly-adapting property of a C-mechanonociceptor is presented in Fig.18A). The more force applied to the receptive field the larger the activity of the receptor. In this study, I recorded 29 C-fibers from C57BL6/N animals and compared their physiological properties to 42 C-fibers recorded from C57BL6/N animals following CCI. Each receptor was stimulated with a ramp and hold protocol as described above. The mechanical

threshold for the first action potential of every indentation step was used to calculate the mean mechanical threshold in [mN] of the receptors.

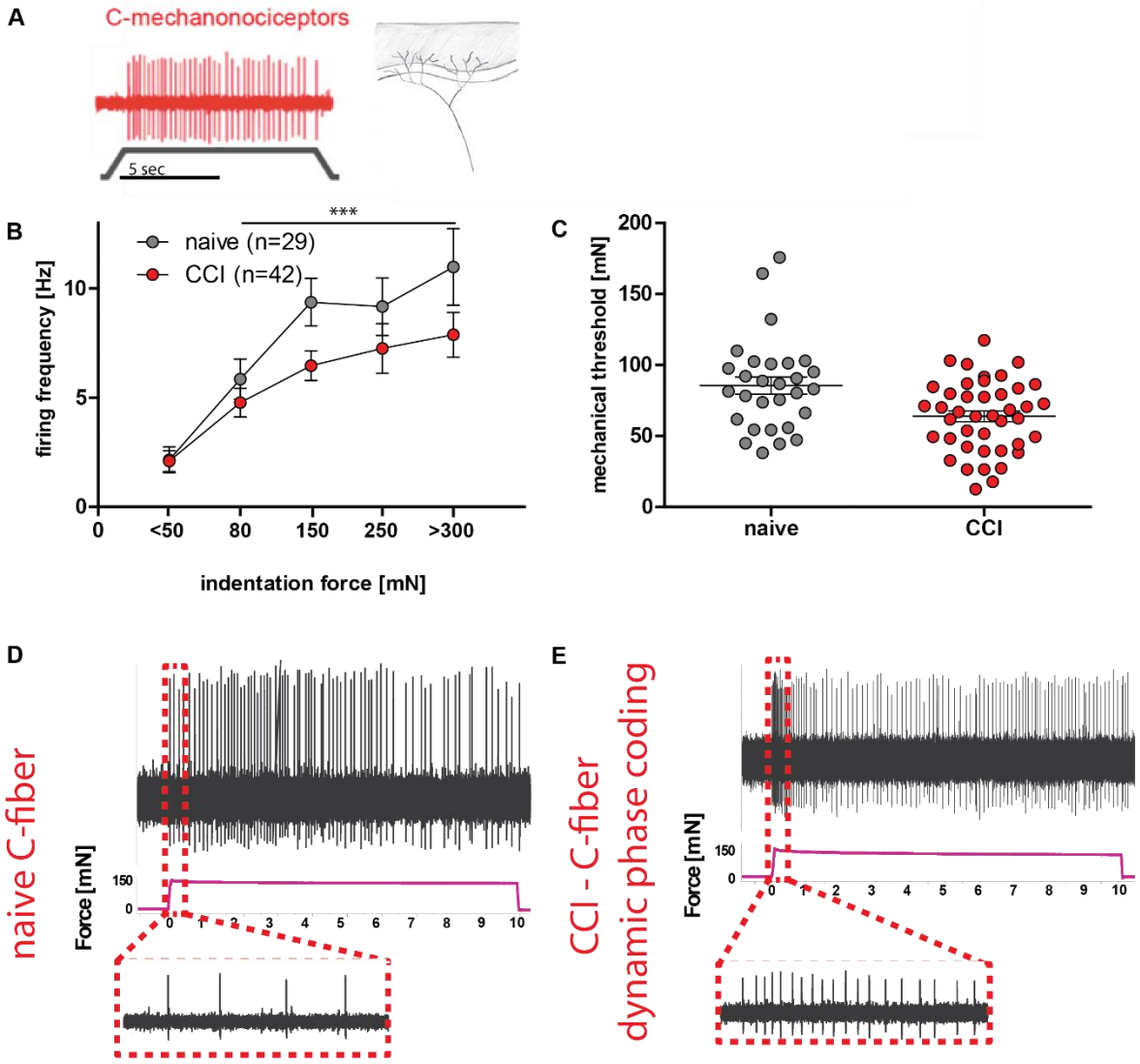

Figure 18 – Physiological properties of C-fibers following CCI

A shows an illustration of the free nerve ending as well as an example of a slowly-adapting C-mechanonociceptor. C-fibers in the naive condition and following CCI were stimulated in the glabrous hindpaw skin with a ramp and hold protocol. Action potentials generated in response to the consecutive indentation forces were counted and divided by the length of the stimulus to calculate firing frequencies [Hz]. Following CCI, C-fibers display a significant reduction in activity (B, $p<0.001$, two-way ANOVA). Mechanical thresholds [mN] were unaltered, (C, unpaired t-test) even though a trend towards decreased transduction thresholds is visible. D and E show a comparison of physiological traces. Following CCI, C-fibers acquire dynamic-phase coding properties. A strong increase in activity in the first 500ms of the stimulus is observed.

The recorded C-fibers were not sub-classified according to their thermal sensitivity with heat- and cold stimuli. True mechanonociceptive C-fibers display more regular firing properties, similar to those of AMs, whereas polymodal C-fibers (those which transduce heat, cold or heat and cold in addition to mechanical stimuli) display more bursting spike patterns. Not dividing

the C-fibers into sub-populations and knowing what kind of percentage belongs to which population makes proving differences in activity difficult.

As illustrated in Fig.18B indentation forces from ~ 50 - 200mN are transduced with a linear increase in firing frequency by the naïve receptors. At forces between 200 - 400mN the increase in activity begins to saturate. The C-fibers following CCI are less active during the static phase compared to naïve C-fibers ($p<0.001$, two-way ANOVA, Fig.18B). Additionally, C-fibers following CCI displayed a trend towards decreased transduction thresholds (Fig.18C), which would be expected in the state of injury induced sensitization but again the difference was not significant (unpaired t-test). However, examining the individual recordings and transduction thresholds, sensitized C-fibers with very low transduction thresholds were recorded following CCI. Another interesting characteristic emerged from the recordings: the acquisition of dynamic-phase coding properties. Fig.18D shows a physiological trace of a naïve C-fiber, next to it in Fig.18E a trace of a C-fiber following neuropathic injury, both with magnifications of the first 500ms of the stimulus. A strong increase in activity in the dynamic phase of the stimulus is visible in C-fibers of the neuropathic group. This phenomenon required a more in-depth analysis of the physiological properties of these sensory afferents.

The data was re-binned to achieve a higher resolution in the transduction range of between 40 - 200mN. Individual thresholds per indentation-strength as well as action potentials generated in the first 500ms of the stimulation were analyzed. In order to explain acquired mechanical hypersensitivity following neuropathic injury, the investigation of stimulation-strengths in the low- to medium indentation force spectrum seemed more reasonable. Fig.19 shows three indentation strengths of mean applied force in the static phase of the stimulus (40 – 80mN, 80 – 130mN and 130 – 200mN) in A,C and E. A light-grey line is drawn at 50mN for visual purposes. In the naïve condition, up to 3 (out of 14) control C-fibers start transducing action potentials with thresholds below 50mN, meaning there is virtually no activity. Following CCI, there is a significant number of recorded C-fibers transducing stimuli with applied force of less than 50mN. Considering the 40 – 80mN stimulus: more than 50% of C-fibers were active, 80 - 130mN: roughly 40% of C-fibers were active and 130 – 200mN: around a third of C-fibers were active. The corresponding transduction thresholds are shown in Fig.19B,D and F. Following CCI C-fibers are sensitized to smaller indentation forces as demonstrated by a significant reduction in transduction threshold to the first (40 – 80mN, $p<0.001$, unpaired t-test) and third (130 – 200mN, $p<0.01$, unpaired t-test) stimulation strengths.

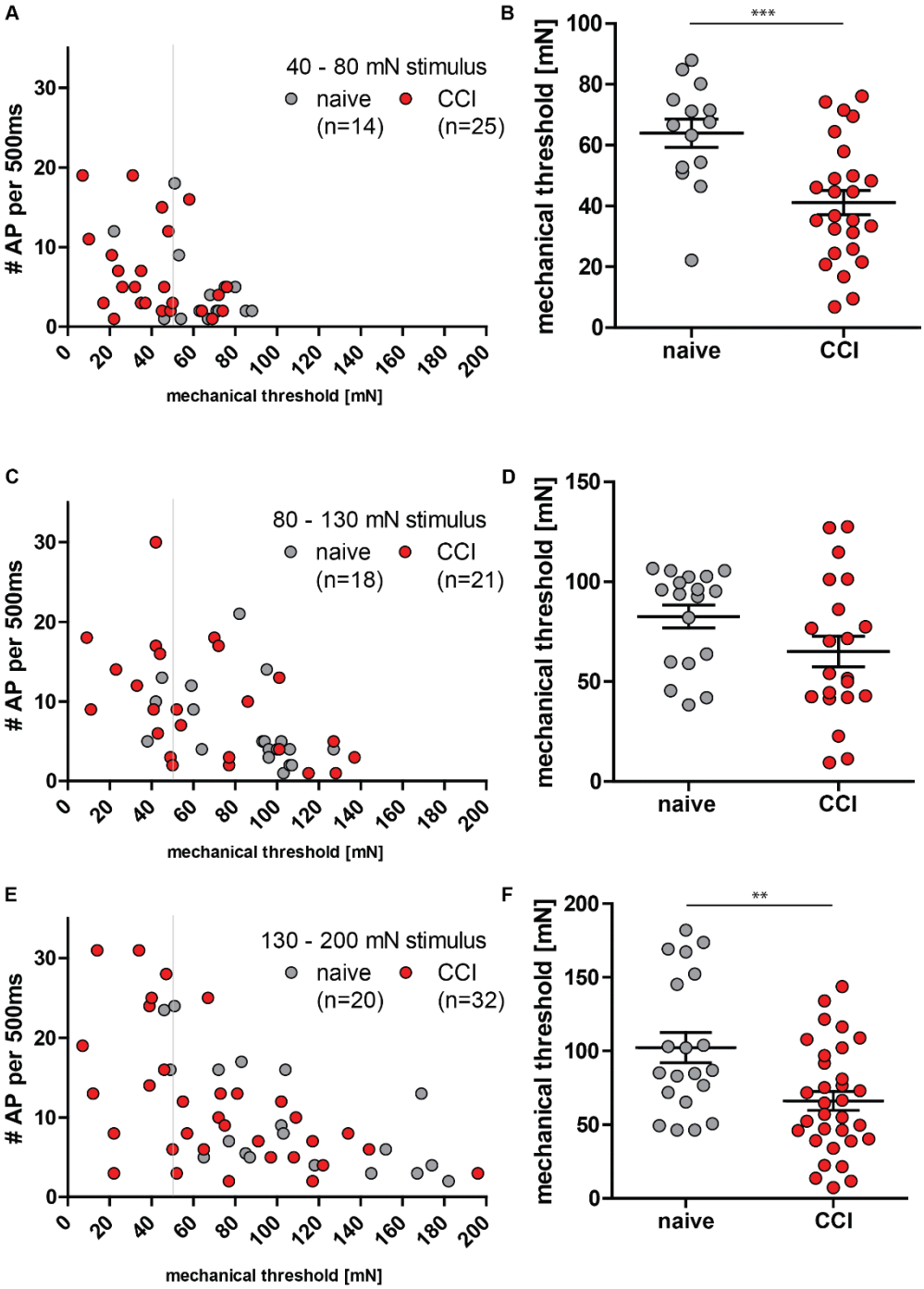

Figure 19 – C-fibers are sensitized to smaller indentation forces following CCI

Three indentation strengths of mean applied force in the static phase of the stimulus (40 – 80mN, 80 – 130mN and 130 – 200mN) are shown in A,C and E. A light-grey line is drawn at 50mN for visual purposes. The corresponding transduction thresholds are shown in B,D and F. Following CCI, C-fibers are sensitized to smaller indentations demonstrated by a significant reduction in mechanical threshold displayed in B ($p<0.001$, unpaired t-test) and F ($p<0.01$, unpaired t-test). Additionally, there was increased activity in CCI C-fibers below 50mN indentation force. A, 40 – 80mN: more than 50% of C-fibers were active. C, 80 -130mN: roughly 40% of C-fibers were active and 130 – 200mN: ~a third of C-fibers were active.

The mean mechanical force transduction thresholds of the recorded C-fibers were calculated using data only from stimuli of up to 200mN (using the 40 – 80mN, 80 – 130mN and 130 – 200mN stimuli shown in Fig.19). And indeed, considering this force spectrum, a significant reduction in transduction threshold ($p<0.001$, unpaired t-test) was observed (Fig.20). A fraction of sensitized C-fibers displayed mechanical thresholds similar to RAM-LTMRs (blue box in Fig.20).

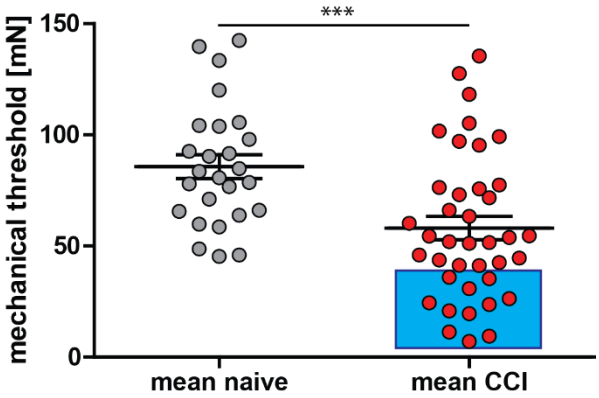

Figure 20 – Mechanical thresholds of C-fibers are sensitized to transduce smaller indentation forces following CCI at stimulation strengths up to 200mN

The experiment shown in Fig.19B,D and F is summarized here. The force thresholds of C-fibers stimulated with indentations of up to 200mN were used to calculate their mean mechanical thresholds. Following CCI, C-fibers are sensitized to smaller indentations as shown by a significant reduction in mechanical threshold ($p<0.001$, unpaired t-test). For visual purposes, a light blue box is drawn around a fraction of the C-fibers. Those have mechanical thresholds below 40mN and are in this respect very similar to RAM LTMRs shown in Fig.14.

The second interesting phenomenon apart from the sensitization of the receptors' transduction threshold was the emergence of dynamic-phase coding properties, shown initially in Fig.18E. In order to further investigate this increase in activity to moving stimuli the receptors' activity over the entire stimulation length was investigated. For an overview, 1s bins were chosen to depict the physiological response characteristics in its entirety (shown in Fig.21A,C and E, the force bins are the same used in the analysis underlying Fig.19). In a second step smaller bins (of 200ms) were chosen to specifically highlight the activity in response to the dynamic phase of the ramp- and hold stimulus (this is visualized in Fig.21B,D and F). There is increased activity in sensitized C-fiber nociceptors in the first second of the stimulation (which includes the dynamic phase) independent of the magnitude of the indentation strength, visible in Fig.21A,C and E, followed by a drop in activity. The remaining 9s were characterized by an approximately constant frequency of action potentials. In the naïve condition at least at forces up to 130mN the C-fibers respond with an approximately constant frequency from the beginning of the stimulus. Considering the indentation force from 130 – 200mN, both naïve and sensitized C-fibers display increased activity in the first second of the stimulation (including

the dynamic phase). The adaptation of the naïve C-fibers was slower, whereas the sensitized nociceptors showed a fast drop in activity and a faster return to their base-frequency.

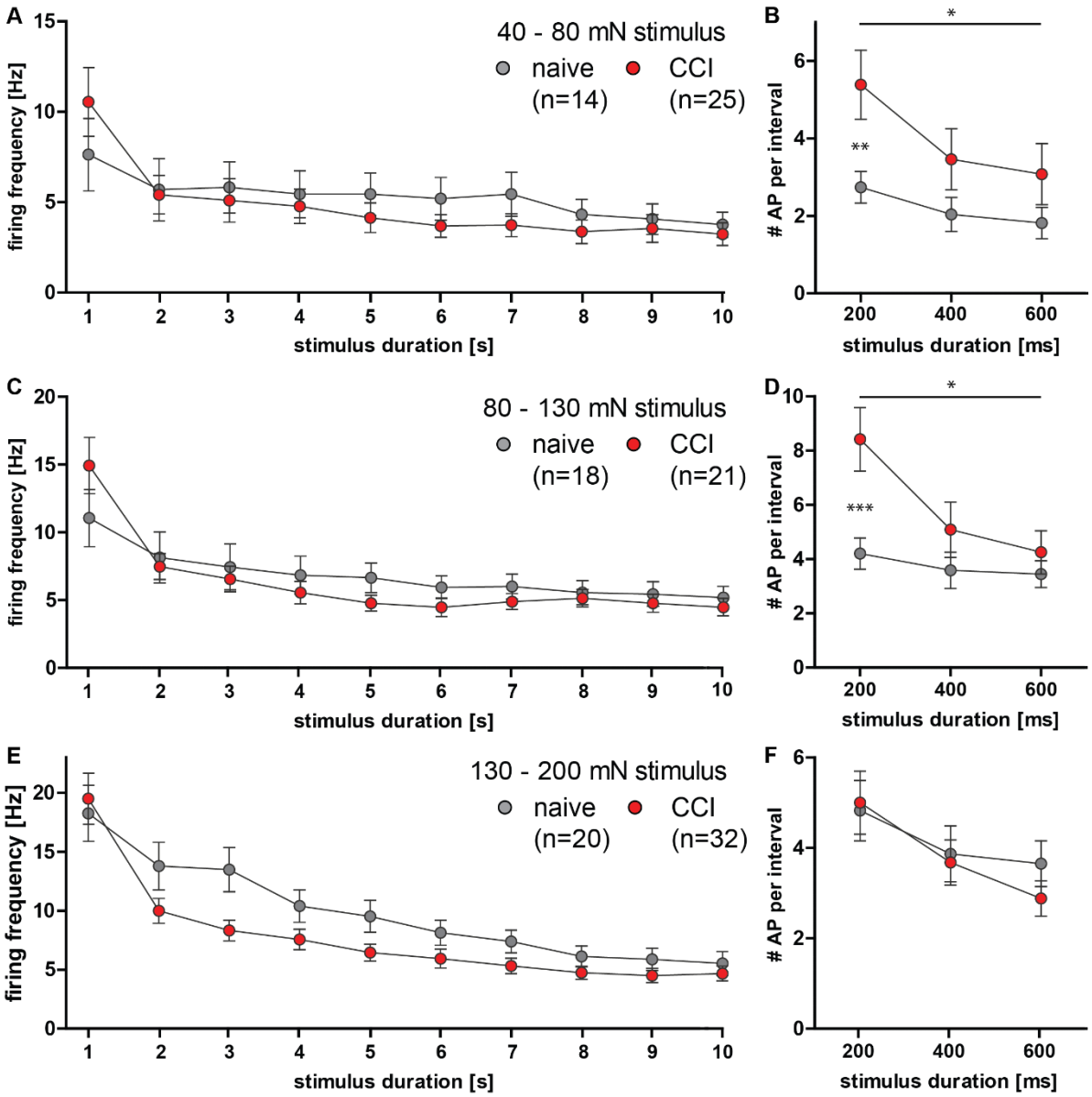

Figure 21 – Dynamic-phase coding properties of C-fibers emerge following CCI

Histograms of the stimulus transduction properties were created. An overview of the entire stimulus is shown for the respective indentation forces in A,C and E. The adjacent panels B,D and F highlight the activity in response to the dynamic phase of the ramp- and hold stimulus. Following CCI, C-fibers display a significant increase in activity in the dynamic-phase (at stimulation strengths of up to 130mN) – Fig.16B and D ($p<0.05$, two-way ANOVA with Bonferroni post-hoc test). The main change between the 2 groups result from the first 200ms of the stimulation, indicated by the asterisks between the activity curves of the two conditions (Fig.21B, $p<0.01$ and Fig.21D, $p<0.001$ – results from the Bonferroni post-hoc test).

Considering the receptors' activity in the dynamic-phase of the stimulus in response to indentations of up to 130mN, there is a significant increase in activity in C-fibers following CCI (Fig 21B and D, $p<0.05$, two-way ANOVA with Bonferroni post-hoc test). The main change

between the 2 groups was observed in first 200ms of the stimulus, indicated by the asterisks between the activity curves of the two conditions (Fig.21B, $p<0.01$ and Fig.21D, $p<0.001$ – results from the Bonferroni post-hoc test).

To summarise: the physiological properties of LTMRs are not altered following CCI, except for a diminished static phase response of SAMs shown in Fig.15C.

Investigating nociceptors, firstly AMs did not display any physiological differences in the neuropathic state. However, sensitization following neuropathic injury could be shown in C-fibers. Investigating stimulation forces of up to 200mN revealed a significant reduction in transduction thresholds (Fig.20) as well as emerging dynamic-phase coding properties (Fig.21) that resulted from the chronic constriction injury. These alterations in physiological properties could explain in part the phenomenon of mechanical allodynia. Stimuli that would under normal circumstances not induce activity in the nociceptive C-fiber system, now do so following CCI.

In this set of experiments recordings were performed from every afferent neuron that could be found (in the naïve and CCI condition). The proportions of mechanoreceptors and nociceptors was calculated using a Chi-square test. In the naïve condition recordings from 147 neurons were performed – and compared to 153 separate recordings performed following CCI. Indeed, following CCI a significant shift ($p<0.05$, χ^2-test) towards the abundance of nociceptors could be found. This reflects the anatomical data displayed in Fig.12 and Fig.13F. Following CCI approximately 50% of myelinated afferents are subjected to degeneration, whereas there was no decrease in the abundance of C-fibers. Therefore, it is plausible that following neuropathic injury proportionately more nociceptors are activated by low intensity mechanical stimuli, and that nociceptive input plays a more pronounced role in the overall sensory barrage into the spinal cord in animals with neuropathic pain.

3.6 Mechanical hypersensitivity following overexpression of STOML3 (Behaviour)

Previous studies from the lab investigated the role of stomatin-like protein 3 (STOML3) in neuropathic pain (Wetzel et al., 2007, 2017). Following CCI STOML3 is upregulated in sensory neurons and their axons, proven by increased STOML3 abundance in the injured ipsilateral sciatic nerve compared to that of the internal control side (contralateral, no ligation). This interesting finding as well as the idea to use tagged STOML3 to look for new interaction partners and possibly new mechanosensitive ion channels inspired James Hall (PhD-thesis) to create a transgenic animal to overexpress STOML3 *in vivo* in all sensory neurons upon induction of the Cre/ERT2 system using Tamoxifen injections (Fig.22).

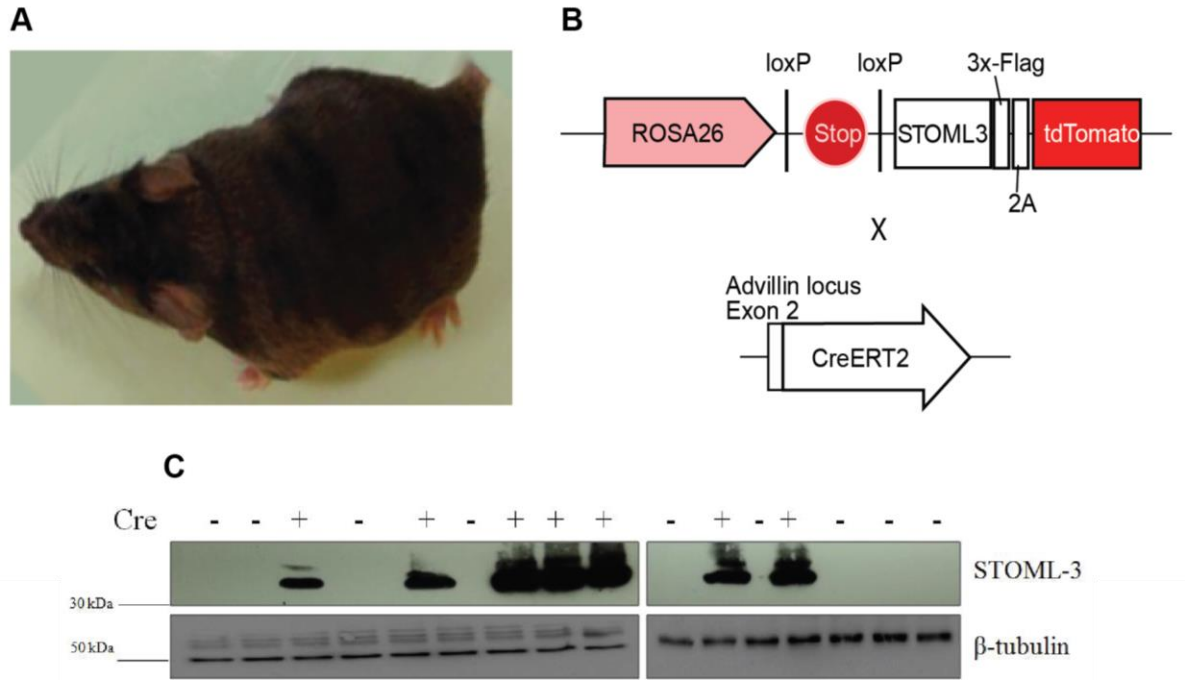

Figure 22 – Inducible *in vivo* overexpression of STOML3 in sensory neurons

In A, the first offspring is shown crossing *stoml3*$^{fl/fl}$ animals with AdvilinCre/ERT2 animals. B: STOML3 was flag-tagged, a 2A sequence was introduced as well as the red reporter tdTomato. Lox-P sites are flanking the Stop-cassette, the locus of recombination is the ROSA26 locus. Upon injection of Tamoxifen (an artificial estrogen analogue), the Cre-recombinase cuts the loxP-sites excising the Stop-cassette. STOML3 is then expressed under the rosa26 promoter. C shows a western blot detecting STOML3 in mice overexpressing STOML3 but not in littermates lacking the Cre (James Hall, PhD thesis).

I performed a thorough characterization of these animals testing if overexpression of STOML3 alone would be sufficient to reproduce the symptoms of neuropathic pain without having to actually induce nerve injury. Initially, the animals were analyzed behaviourally. The von Frey assay as well as Mouse walk experiments were performed to acquire baseline paw-withdrawal thresholds and gait-patterns. Mouse walk data will not be shown here, since there was no

difference or interesting changes in gait parameters following the overexpression of STOML3. Since the overexpression occurred globally in the animals and not unilaterally like after CCI, this was not unexpected.

3.6.1 Behavioural assessment of paw-withdrawal thresholds using the von Frey assay in *in vivo* STOML3 overexpressors

In order to induce the *in vivo* overexpression of STOML3 (Fig.23B), animals were injected with 100µl of Tamoxifen (solubilized in corn oil, 20mg/ml) for 5 consecutive days. The following week they were left in their home cages without any handling. This time was necessary in order to achieve a maximum amount of recombination and therefore overexpression of STOML3. The following week the animals were evaluated for their 50% paw-withdrawal threshold in the von Frey assay. Both left- and right hindpaw were stimulated and compared to baseline values before Tamoxifen injection. A two-way ANOVA was used to compare the paw-withdrawal threshold and we found a highly significant decrease after overexpression of STOML3 ($p<0.001$). On average, the 0.04g von Frey filament was sufficient to produce aversive behaviour in the left hindpaw (LH), for the right hindpaw (RH) it was the 0.07g filament (Fig.23D). This experiment is shown in Fig.23 in contrast to the von Frey experiments on animals after CCI (already shown in Fig.9). Comparing these two experiments shows that the paw-withdrawal threshold of neuropathic animals decreased in a quantitatively similar manner to animals that overexpress STOML3 in sensory neurons but have not been subjected to neuropathic injury.

Having established that experimental animals overexpressing STOML3 acquire mechanical hypersensitivity similar to that in the neuropathic condition we next asked how the hypersensitivity arises. Are there changes in sensory neuron physiology similar to those observed in neuropathic animals? Since the overexpression of STOML3 was sensory neuron specific, once again the *ex-vivo* skin nerve technique was applied to investigate LTMR- and nociceptor physiology to uncover the physiological basis of the induced behavioural hypersensitivity.

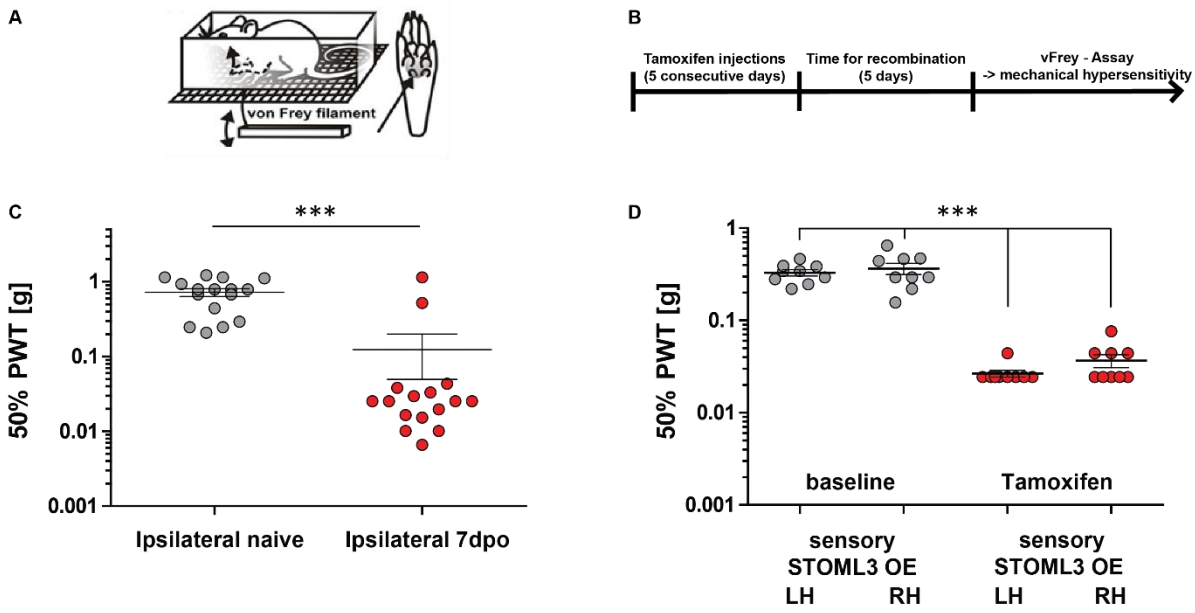

Figure 23 – The *in vivo* overexpression of STOML3 produces robust mechanical hypersensitivity similar to neuropathic injury

Fig.23 shows von Frey experiments in neuropathic animals after CCI and animals that overexpress STOML3 in sensory neurons. A shows a cartoon of the classic von Frey assay (taken from Yu et al., 2013). Special monofilaments calibrated to exert a specific force upon bending are used to stimulate experimental animals‘ hindpaws. In C paw-withdrawal thresholds before and after CCI are compared, following CCI animals develop a robust mechanical hypersensitivity, illustrated by the drop in 50% PWT from around 400 – 600mg to 40 - 60mg ($p<0.001$, two-way ANOVA, two outliers excluded from statistical analysis). In D the same drop in 50% PWT was measured but just by overexpressing STOML3 in sensory neurons. The drop from 400 – 600mg to 40 – 60mg ($p<0.001$, two-way ANOVA) seems even more severe than in CCI. In fact, the results are exactly the same, excluding the two outliers that didn’t develop mechanical hypersensitivity following CCI in C. To overexpress STOML3 AvilCre/ERT2::LSLstoml3-Flag animals were injected with 100µl Tamoxifen (20mg/ml, in corn oil) 5 times (D). After a week of recombination animals were investigated and displayed robust mechanical hypersensitivity – same as following neuropathic injury.

3.6.1.1 Rapidly-adapting mechanoreceptors (RAMs)

In this study, I recorded 28 RAMs from AvilCre/ERT2::LSLstoml3-Flag or LSLstoml3-Flag animals injected with vehicle (controls) and compared their physiological properties to 21 RAMs recorded from AvilCre/ERT2::LSLstoml3-Flag animals after Tamoxifen treatment (termed: induced overexpression of STOML3 or sensory STOML3 OE). Each receptor was stimulated with the “velocity protocol”. The indentation force was kept constant at 45mN. Action potentials evoked in the dynamic phase of the stimulation were analyzed, counting the actual number of action potentials generated during each ramp stimulus. The mechanical threshold of the first action potential of every velocity step was used to calculate the mean mechanical threshold in [mN] of the receptors.

As shown in Fig.14B, for naïve RAMs slow velocities (0.075mm/s) are not sufficient to evoke action potentials (with very few exceptions, in this case ~10%, shown in Fig.24B). Increasing the velocity of the stimulation increases receptor activity. The same physiological properties can be observed in the control RAMs recorded for this set of experiments. However, there was a large significant difference in the activity of RAMs from induced STOML3-overexpression animals ($p<0.01$, two-way ANOVA).

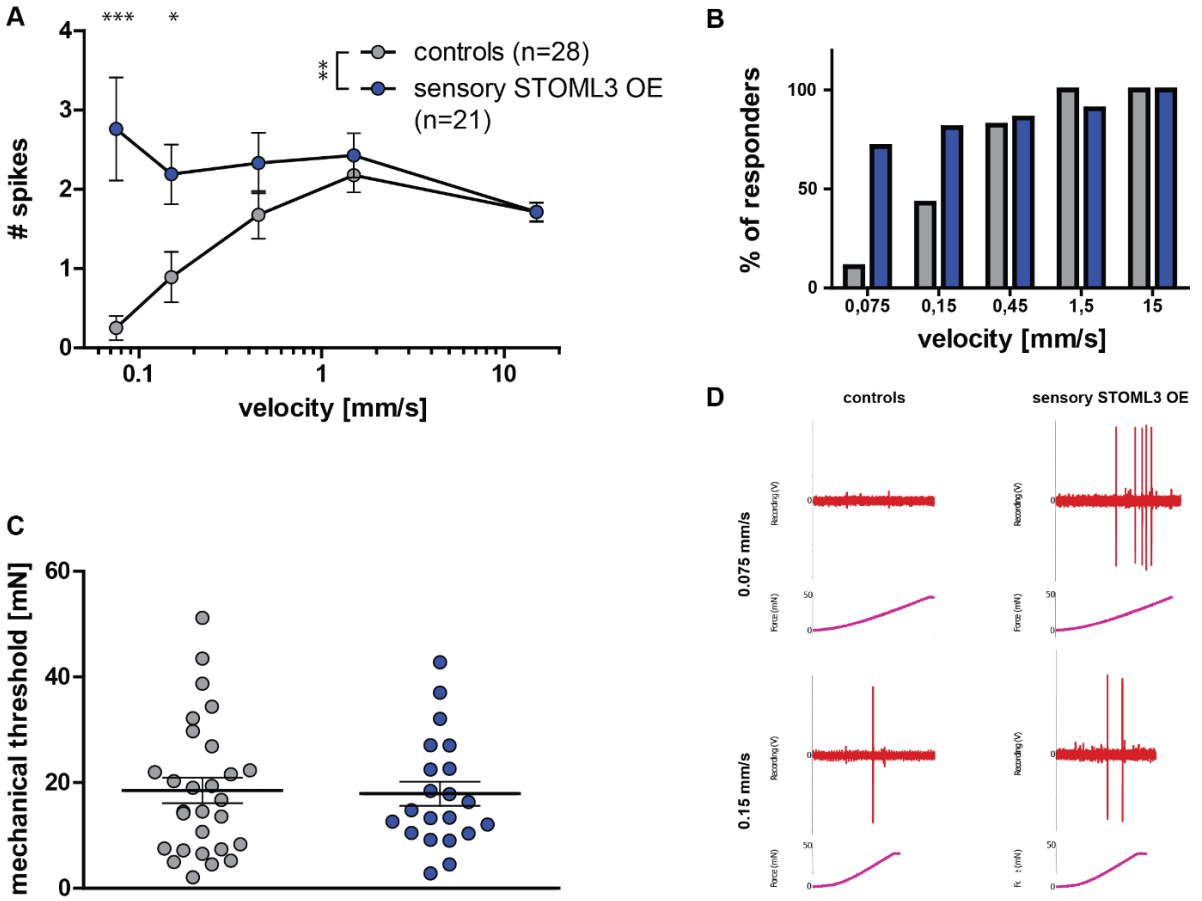

Figure 24 – The *in vivo* overexpression of STOML3 sensitizes rapidly-adapting mechanoreceptors to slow moving stimuli

RAMs in the control condition and following the overexpression of STOML3 in sensory neurons were stimulated in the glabrous hindpaw skin with the „velocity protocol“. Action potentials were counted and shown as actual number of spikes in A. Following the overexpression of STOML3 RAMs become sensitized to slower velocities ($p<0.01$, two-way ANOVA with Bonferroni post-hoc test) – the main change results from the increase in activity in the first two velocity-stimuli indicated by asterisks (bin1: $p<0.001$, bin2: $p<0.05$). The proportion of receptors encoding the consecutive velocities has changed as well, slow velocities are being encoded by significantly more receptors after overexpression of STOML3 ($p<0.001$, χ^2-test), shown in B. This sensitization is achieved without a reduction in mean transduction threshold (C). Examples of the physiology are shown in D, the slowest velocity is not transduced by RAMs in the control condition, in the second the RAMs start transducing (in ~43% of the cases) with little activity. This is opposed to high activity in 71% and 81% percent of receptors after STOML3 overexpression. Controls: LSLstoml3-Flag treated with vehicle; sensory STOML3 OE: AvilCre/ERT2::LSLstoml3-Flag treated with Tamoxifen.

The RAMs are sensitized towards slower velocities reflected by their spike-patterns illustrated in Fig.24A and B. Already the slowest velocity of 0.075mm/s is sufficient to generate on average 2.76 action potentials (opposed to 0.25 in controls, an 11-fold increase after overexpression). Furthermore, changes were observed in the percentage of receptors transducing this velocity stimulus, 71% of RAMs after induced overexpression of STOML3 displayed this physiological property (opposed to 11% in controls) yielding a significant difference in the proportion of receptors transducing slow velocities ($p<0.001$, χ^2-test). The second velocity step showed similar characteristics. After overexpression of STOML3 RAMs generate on average 2.19 spikes being challenged with velocities of 0.15mm/s (opposed to 0.89 in controls, a 2.5-fold increase after overexpression). 81% of RAMs behave like this compared to 43% in the control group. From the third velocity step on, the two groups displayed comparable physiological properties, the percentage of responses was also not different with faster velocities. Interestingly, this change in physiology occurred in the absence of actual threshold reduction (Fig.24C). Examples of this astonishing sensitization towards slower moving stimuli are shown in Fig.24D. The first two velocities are compared, and example physiological traces are shown for the two groups.

3.6.1.2 Slowly-adapting mechanoreceptors (SAMs)

I recorded 22 SAMs from control animals (LSLstoml3-Flag) and compared their physiological properties to 13 SAMs recorded from AvilCre/ERT2::LSLstoml3-Flag animals after Tamoxifen treatment (termed: induced overexpression of STOML3 or sensory STOML3 OE). Each receptor was stimulated with the “velocity protocol” as described before.

SAMs are very sensitive and do not require a certain speed to start encoding stimuli, they start to fire once their threshold is reached. Therefore, the highest activity can be seen in the slowest velocity ramp (since it is the longest). Following the overexpression of STOML3, SAMs become sensitized, resulting in a significant difference in activity regarding SAMs from STOML3-overexpression animals ($p<0.05$, two-way ANOVA). The main change was an increase in activity to the first velocity stimulus (0.075mm/s).

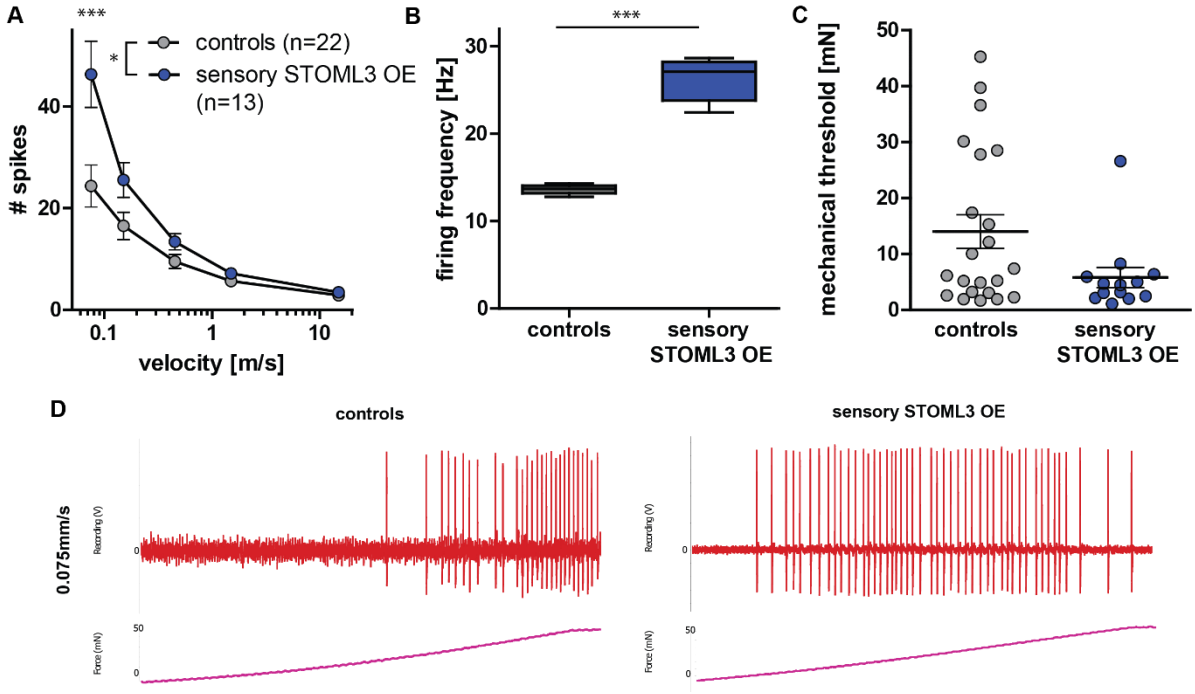

Figure 25 – The *in vivo* overexpression of STOML3 sensitizes slowly-adapting mechanoreceptors

SAMs in the control condition and following the overexpression of STOML3 in sensory neurons were stimulated in the glabrous hindpaw skin with the „velocity protocol“. Action potentials were counted and shown as actual number of spikes in A. Following the overexpression of STOML3 SAMs become sensitized ($p<0.05$, two-way ANOVA with Bonferroni post-hoc test) – the main change results from the increase in activity to the first velocity-stimulus indicated by asterisks ($p<0.001$). Drastically increased continuous activity was observed in the static phase of the stimuli additionally (B, $p<0.001$, two-way ANOVA). This sensitization is accompanied by a trend towards reduction in mean mechanical threshold (C), though not significant. Examples of the physiology are shown in D, the slowest velocity is coded by SAMs with approximately double the amount of action potentials after overexpression of STOML3. This increased activity and tendency towards a reduced transduction threshold is visualized in example traces. Controls: LSLstoml3-Flag treated with vehicle; sensory STOML3 OE: AvilCre/ERT2::LSLstoml3-Flag treated with Tamoxifen.

On average SAMs fired 46 action potentials to the first stimulus ramp following overexpression of STOML3, compared to 24 in the control population (Fig.25A). Increased activity to slow ramps was accompanied by a strong (though not statistically significant) tendency towards reduced mechanical thresholds (Fig.25C) and a drastically increased continuous activity in the static phase of the stimuli (Fig.25B). In animals overexpressing STOML3 the mean mechanical threshold was 5.8mN compared to 14mN in the controls. The increased activity and reduction in threshold can be seen in Fig.25C. The slowest velocity (0.075mm/s) is displayed in Fig. 25D, following the overexpression of STOML3 SAMs start transducing earlier after stimulus onset and produce more action potentials per stimulus.

3.6.1.3 D-hair mechanoreceptors

A total of 15 D-hairs from control animals (LSLstoml3-Flag) were recorded and their physiological properties compared to 23 D-hairs from AvilCre/ERT2::LSLstoml3-Flag animals after Tamoxifen treatment (termed: induced overexpression of STOML3 or sensory STOML3 OE). Each receptor was stimulated with the “velocity protocol” (described above).

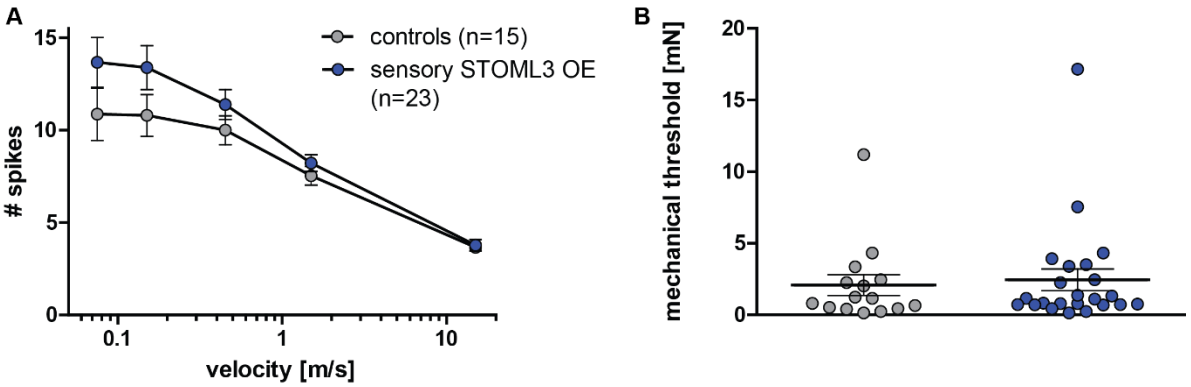

Figure 26 – The *in vivo* overexpression of STOML3 did not sensitize D-hair LTMRs

D-hairs in the control condition and following the overexpression of STOML3 in sensory neurons were stimulated in the glabrous hindpaw skin with the „velocity protocol“. Action potentials were counted and shown as actual number of spikes in A. A slight increase in activity (not significant) can be seen in Fig.26A. Mechanical thresholds are unchanged from controls (Fig.26B). Controls: LSLstoml3-Flag treated with vehicle; sensory STOML3 OE: AvilCre/ERT2::LSLstoml3-Flag treated with Tamoxifen.

As illustrated in Fig.26, D-hairs are incredibly sensitive LTMRs. Slow velocities are sufficient to evoke action potentials in D-hairs – in this respect they are more similar to SAMs than RAMs. They do not require faster velocity stimuli for activation, they become active once their threshold is reached and are therefore most active in the slow velocity ramps, since those stimuli are the longest. There seemed to be a slight increase in overall activity when overexpressing STOML3 in sensory neurons (however not statistically significant). The mechanical threshold of the receptors was not significantly different from controls after Tamoxifen treatment.

3.6.2 Sensitization of nociceptors after STOML3 overexpression

3.6.2.1 A-mechanonociceptors (AM)

I recorded from 32 AMs in control animals (LSLstoml3-Flag) and compared their properties to 29 AMs recorded from AvilCre/ERT2::LSLstoml3-Flag animals after Tamoxifen treatment (termed: induced overexpression of STOML3 or sensory STOML3 OE). Each receptor was stimulated with a ramp and hold protocol, the number of spikes are shown as well as the peak firing frequency of the receptors. Finally, the mechanical threshold of the first action potential of every indentation step was used to calculate the mean mechanical threshold in [mN].

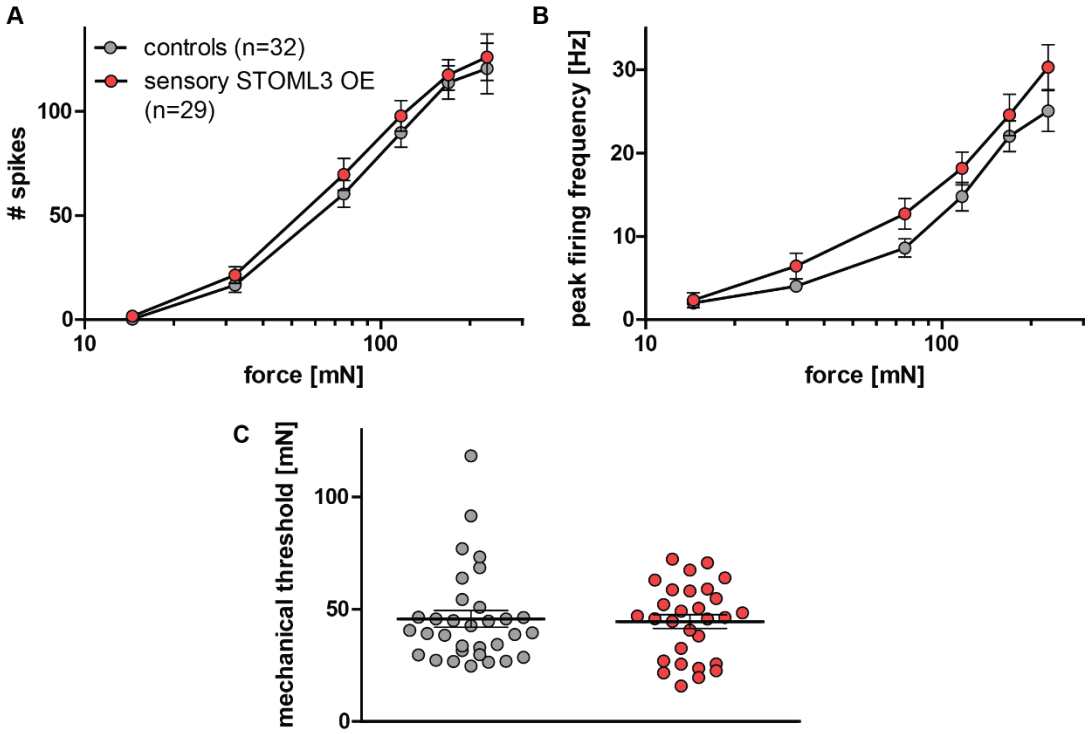

Figure 27 – The *in vivo* overexpression of STOML3 did not sensitize A-mechanonociceptors

AMs in the control condition and following the overexpression of STOML3 in sensory neurons were stimulated in the glabrous hindpaw skin with the ramp and hold protocol. Action potentials were counted and shown as actual number of spikes in A. Peak firing frequencies were calculated and compared in B and mechanical thresholds in C. Regardless of the comparison, there was no difference in AMs after the overexpression of STOML3. Controls: LSLstoml3-Flag treated with vehicle; sensory STOML3 OE: AvilCre/ERT2::LSLstoml3-Flag treated with Tamoxifen.

As in Fig.17B, indentation forces from ~ 50 - 200mN are coded with a linear increase in firing frequency. For forces between 200 - 400mN the increase in activity begins to saturate. However, in these and in following experiments the force spectrum of stimulations for nociceptors was redesigned to increase the number of stimulations in the range of ~20 – 250mN. This was done to address the hypothesis, that peripheral sensitization might occur

(shown in C-fiber nociceptors following CCI) and that acquired mechanical hypersensitivity should be reflected in the physiological properties of sensory neurons to mild to medium forces.

Overall activity (Fig.27A), peak firing frequency (Fig.27B) and mean mechanical threshold (Fig.27C) were completely unaltered after overexpression of STOML3. However further analyzes were applied. As in the CCI experiments in C-fibers, for every stimulation strength transduction histograms as well as individual force thresholds were calculated and compared to probe for more subtle phenotypes. Every analysis undertaken indicated that there was no difference in A-mechanonociceptors after STOML3 overexpression.

3.6.2.2 C-fiber nociceptors

Finally, C-fiber nociceptors were investigated. Initially a summary of this heterogeneous group of nociceptors will be shown. But as already addressed in the C-fiber section of the CCI experiments, in this set of experiments to improve C-fiber classification, the C-fibers were additionally stimulated with hot (50°C) or cold (5°C) SIF buffer and in a second analysis step divided into true mechanonociceptive C-fibers (CM) and polymodal C-fibers (C-MH, C-MC and C-MHC). CMs were classified as such if they did not fire action potentials while being challenged with thermal stimuli and as polymodal C-fibers if they did. This classification was applied due to the similar firing patterns in the polymodal group that is vastly different to the CM group. CMs display physiological properties similar to AMs namely a very regular firing pattern whereas polymodal C-fibers display bursting spike patterns when challenged with constant mechanical force (Milenkovic, Wetzel, Moshourab, & Lewin, 2008; Moshourab, Wetzel, Martinez-Salgado, & Lewin, 2013).

The physiological properties of 26 C-fibers from control animals (LSLstoml3-Flag) were compared to those of 29 C-fibers from AvilCre/ERT2::LSLstoml3-Flag animals after Tamoxifen treatment (termed: induced overexpression of STOML3 or sensory STOML3 OE). Each receptor was stimulated with a ramp and hold protocol, activity is shown as number of spikes. Finally, the mechanical threshold of the first action potential of every indentation step was used to calculate the mean mechanical threshold in [mN].

For C-fibers the overall activity (Fig.28A) and mean mechanical thresholds (Fig.28B) were not significantly different after overexpression of STOML3. In controls a maximum mean activity of 89 spikes with the maximal indentation force in these experiments (~230mN) was in contrast to 128 spikes in animals overexpressing STOML3. The Bonferroni post-hoc test of the two-way ANOVA yields a significant difference between the two groups to this indentation force ($p<0.01$); however the overall stimulus response of these receptors was statistically not

different. A similar observation was made for the mechanical thresholds. A trend towards sensitization (reduced thresholds) can be seen (mean: 73mN vs 58mN in STOML3 overexpressing animals), however this was not statistically significant. Peristimulus time histograms for every stimulation strength as well as individual force thresholds were calculated and compared to uncover subtle phenotypes (results not shown). Each analysis showed no differences and therefore no effect of excess STOML3 on C-fibers. However, this only held when analyzing all C-fibers together. In the following section, I repeated the same analysis but this time the C-fibers were divided into into true mechanonociceptive C-fibers and polymodal C-fibers.

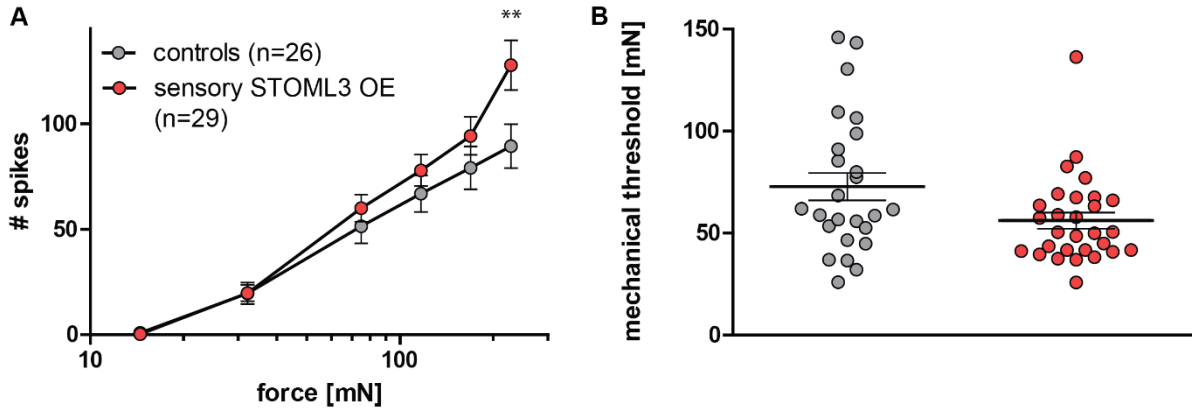

Figure 28 – The *in vivo* overexpression of STOML3 did not sensitize C-fibers on the population level

C-fibers in the control condition and following the overexpression of STOML3 in sensory neurons were stimulated in the glabrous hindpaw skin with the ramp and hold protocol. Action potentials were counted and shown as actual number of spikes in A and mechanical thresholds in B. A tendency towards increased activity was observed regarding the maximal indentation strength in A ($p<0.01$, Bonferroni post-hoc test of the two-way ANOVA) as well as reduced transduction thresholds in B ($p=0.0712$, Mann-Whitney test), however not significant. Controls: LSLstoml3-Flag treated with vehicle; sensory STOML3 OE: AvilCre/ERT2::LSLstoml3-Flag treated with Tamoxifen.

3.6.2.3 Polymodal C-fibers

Polymodal C-fibers were clearly sensitized following STOML3 overexpression. They displayed increased overall activity as well as significantly reduced transduction thresholds. Of all C-fibers: 11 (controls) and 18 (following overexpression of STOML3) were classified as polymodal.

Fig.29A shows the stimulus response function of the polymodal C-fibers. In the indentation range used here, a mean maximal activity of 43 generated action potentials was found. This was in contrast to 103 generated action potentials following the overexpression of STOML3.

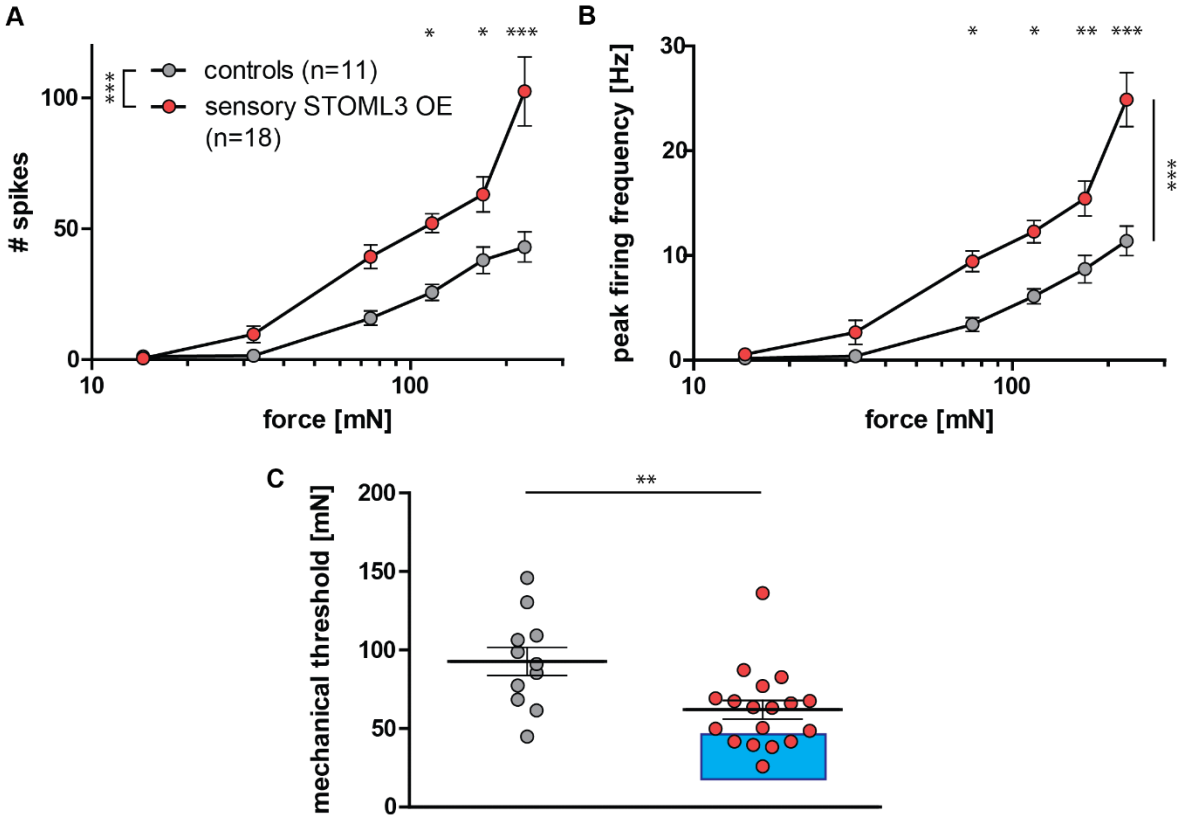

Figure 29 – The *in vivo* overexpression of STOML3 sensitizes polymodal C-fibers

The subpopulation of polymodal C-fibers from the previously shown analysis in Fig.28 is shown. A highly significant increased overall activity is shown in A ($p<0.001$, two-way ANOVA with Bonferroni post-hoc test), the main change results from the increase in activity to the 4th, 5th and 6th stimuli (the force range of ~120 – 230mN) indicated by asterisks (bin4: $p<0.05$, bin5: $p<0.05$ and bin6: $p<0.001$). The difference in activity is even more pronounced when comparing the peak firing frequencies in panel B. Polymodal C-fibers are able to reach much higher firing frequencies after STOML3 overexpression, at highly significant levels ($p<0.001$, two-way ANOVA with Bonferroni post-hoc test), the main change is resulting from the increased peak firing frequencies to the 3rd, 4th, 5th and 6th stimuli (the force range of ~75 – 230mN) indicated by asterisks (bin3: $p<0.05$, bin4: $p<0.05$, bin5: $p<0.01$ and bin 6: $p<0.001$). Sensitization because of excess STOML3 is also visible in the significantly reduced mechanical thresholds ($p<0.01$, Mann-Whitney test) shown in C, again a light blue box highlights mechanical thresholds similar to LTMRs recorded in this set of experiments, see Fig.24 and 25. Controls: LSLstoml3-Flag treated with vehicle; sensory STOML3 OE: AvilCre/ERT2::LSLstoml3-Flag treated with Tamoxifen.

Following STOML3 overexpression, increased activity can be seen at all stimulation strengths starting already with ~35mN. The difference in activity was highly significant ($p<0.001$, two-way ANOVA with Bonferroni post-hoc test), the main change resulted from the increase in activity to the 4th, 5th and 6th stimuli (the force range of ~120 – 230mN) indicated by asterisks (bin4: $p<0.05$, bin5: $p<0.05$ and bin6: $p<0.001$). The receptors peak firing frequencies were compared in Fig.29B. The difference in activity is even more pronounced than in panel A. Polymodal C-fibers are able to reach much higher firing frequencies after STOML3 overexpression, a highly significant result ($p<0.001$, two-way ANOVA with Bonferroni post-hoc test), where the main change occurs due to the increased peak firing frequencies to the 3rd,

4^{th}, 5^{th} and 6^{th} stimuli (the force range of ~75 – 230mN) indicated by asterisk (bin3: $p<0.05$, bin4: $p<0.05$, bin5: $p<0.01$ and bin6:$p<0.001$).

Sensitization as a result of STOML3 overexpression is also reflected in significantly reduced mechanical thresholds shown in Fig.29C, again a fraction of C-fibers displayed mechanical thresholds similar to LTMRs (highlighted by blue box). Mean mechanical thresholds of controls were 93mN compared to 63mN after overexpression of STOML3, again a highly significant difference was observed ($p<0.01$, Mann-Whitney test). The following analysis addresses the question if the overexpression of STOML3 might be a causative factor for the emergence of dynamic-phase coding properties observed in C-fibers following CCI.

Peristimulus time histograms were created for each stimulus strength and compared between controls and following the overexpression of STOML3. Mechanical thresholds to each stimulus strength were also calculated.

Dynamic-phase coding properties were shown to emerge after overexpression of STOML3. Fig.30 shows peristimulus time histograms and mechanical thresholds for indentation strengths between ~75 – 230mN. Increased activity especially in the first second of the stimulus that includes the dynamic phase is seen at each stimulus strength. The effect of excess STOML3 on polymodal C-fiber nociceptors was marked. A doubling in activity in the intervals shown as well as in some cases (Fig.30C and D) a significant reduction in mechanical threshold of this nociceptor sub-population. In the following section the same analysis was made for C-mechanonociceptors.

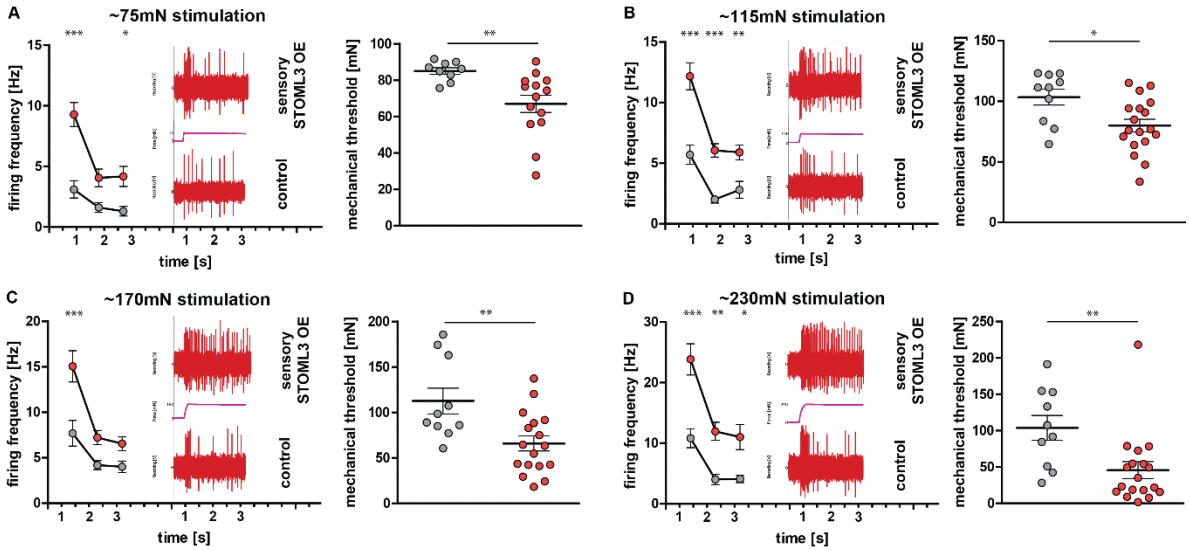

Figure 30 – Dynamic-phase coding properties emerged in sensitized polymodal C-fibers after overexpression of STOML3

Peristimulus time histograms were created as well as individual mechanical thresholds per indentation strength and compared between controls and following the overexpression of STOML3, here shown with physiological examples from recorded receptors in the applied force range between ~75 - 230mN. The first 3 seconds of the stimulus histograms are displayed as a quantification of the firing frequency on the left and corresponding examples of receptor activity on the right (the first second includes activity in the dynamic-phase). To indicate the increased activity in polymodal C-fiber nociceptors after overexpression of STOML3, traces belonging to that experimental group are shown on top of controls. Highly significant increased activity especially in the first second of the stimulation is seen in all panels. A (75mN stimulation): ($p<0.01$, two-way ANOVA with Bonferroni post-hoc test) 1st second: $p<0.001$ and 3rd second: $p<0.05$. The mechanical threshold was significantly decreased as well ($p<0.01$, Mann-Whitney test). B (115mN stimulation): ($p<0.001$, two-way ANOVA with Bonferroni post-hoc test) 1st second: $p<0.001$, 2nd second: $p<0.001$ and 3rd second: $p<0.001$. The mechanical threshold was significantly decreased as well ($p<0.05$, Mann-Whitney test). C (170mN stimulation): ($p<0.05$, two-way ANOVA with Bonferroni post-hoc test) 1st second: $p<0.001$. The mechanical threshold was significantly decreased as well ($p<0.01$, Mann-Whitney test). D (230mN stimulation): ($p<0.01$, two-way ANOVA with Bonferroni post-hoc test) 1st second: $p<0.001$, 2nd second: $p<0.01$ and 3rd second: $p<0.05$. The mechanical threshold was significantly decreased as well ($p<0.01$, Mann-Whitney test). Dynamic-phase coding and sensitization to smaller indentation strengths emerged in polymodal C-fibers after STOML3 overexpression. Controls: LSLstoml3-Flag treated with vehicle; sensory STOML3 OE: AvilCre/ERT2::LSLstoml3-Flag treated with Tamoxifen.

3.6.2.4 Mechanonociceptive C-fibers (CMs)

A mild sensitization of mechanonociceptive C-fibers was observed following the overexpression of STOML3. They displayed an increased overall activity but no significant reduction in mechanical thresholds. From the initial 26 controls (LSLstoml3-Flag) and 29 AvilCre/ERT2::LSLstoml3-Flag after Tamoxifen treatment (termed: induced overexpression of STOML3 or sensory STOML3 OE) C-fibers, 15 (controls) and 11 (sensory STOML3 OE) were categorized as CMs. Fig.31A shows the stimulus response function of the receptors. CMs increase their activity with the force applied to their receptive field. In the indentation range

used in these experiments there was a mean maximal activity of 120 generated action potentials. This was in contrast to 169 generated action potentials following the overexpression of STOML3. This example clearly demonstrates the strong effect of excess STOML3 on these receptors. A slight increase can already be seen with stimulation strengths of ~75mN, which becomes significant at 170mN ($p<0.05$, two-way ANOVA with Bonferroni post-hoc test), with the main change resulting from the increase in activity to the 5th and 6th stimulations (the force range of ~170 – 230mN) indicated by asterisks (bin5: $p<0.05$ and bin6: $p<0.01$). Peak firing frequencies for CMs were compared in Fig.31B. The difference in activity was not significant ($p=0.0653$, two-way ANOVA with Bonferroni post-hoc test), however a clear trend can be seen. This increase in activity was observed without sensitizing effect on mechanical threshold Fig.31C.

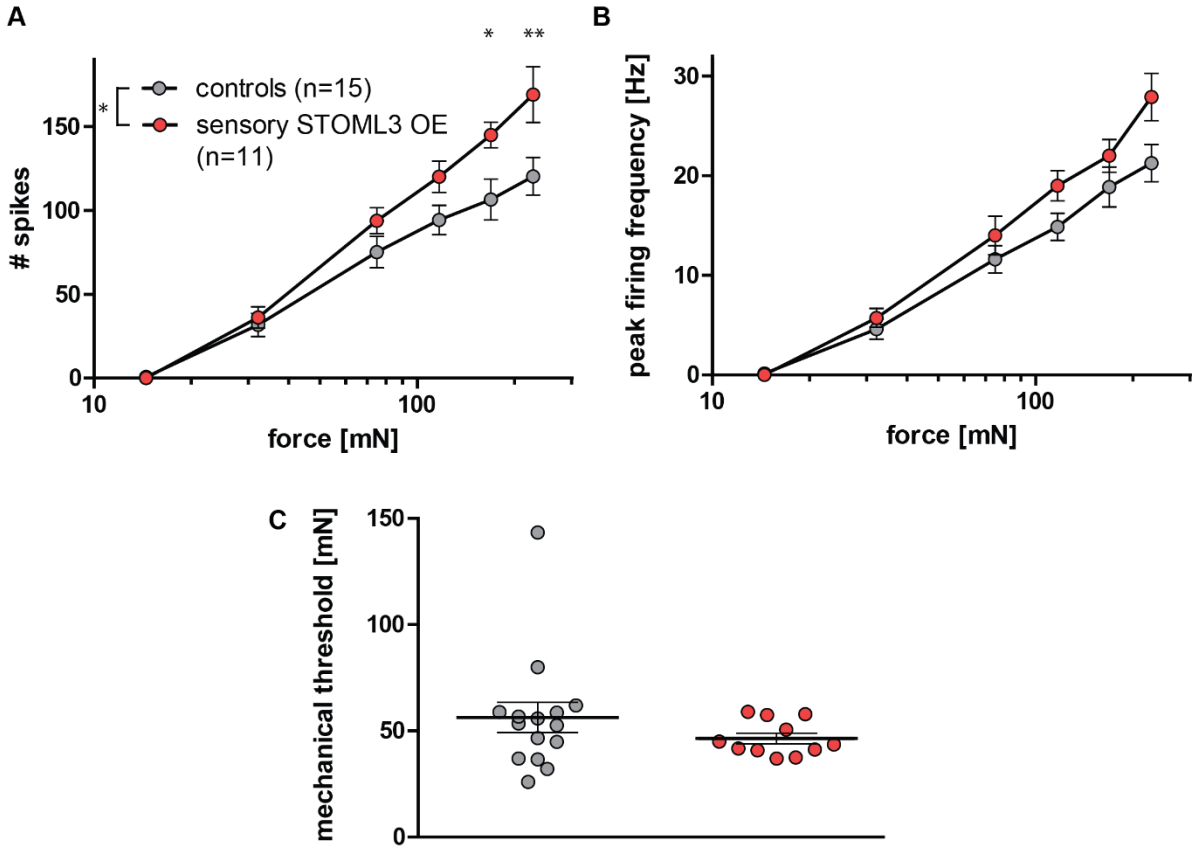

Figure 31 – The *in vivo* overexpression of STOML3 sensitized mechanonociceptive C-fibers

The subpopulation of CMs from the previously shown analysis in Fig.28 is reanalyzed here. A significantly increased overall activity is observed in A ($p<0.05$, two-way ANOVA with Bonferroni post-hoc test), the main change results from the increase in activity to the 5th and 6th stimuli (the force range of ~170 – 230mN) indicated by asterisks (bin5: $p<0.05$ and bin6:$p<0.01$). A strong trend towards increased peak firing frequencies can be seen in panel B ($p=0.0653$, two-way ANOVA with Bonferroni post-hoc test. The Bonferroni post-hoc test of the two-way ANOVA yields a significant difference between the two groups in the 6th bin ($p<0.05$), however the overall peak firing frequency of these receptors was statistically not different. This increase in activity was observed without sensitizing effect on mechanical threshold (C). Controls: LSLstoml3-Flag treated with vehicle; sensory STOML3 OE: AvilCre/ERT2::LSLstoml3-Flag treated with Tamoxifen.

Finally, peristimulus time plots were created as well as individual mechanical thresholds per indentation strength and compared between controls and following the overexpression of STOML3 to address the question if excess STOML3 might induce dynamic-phase coding properties in these receptors as well.

An increase in the dynamic-phase coding properties along with increases in overall activity appeared after overexpression of STOML3. However, this increased activity became apparent only with suprathreshold force stimuli. Fig.32 shows peristimulus time plots and mechanical thresholds for indentation strengths between ~170 – 230mN.

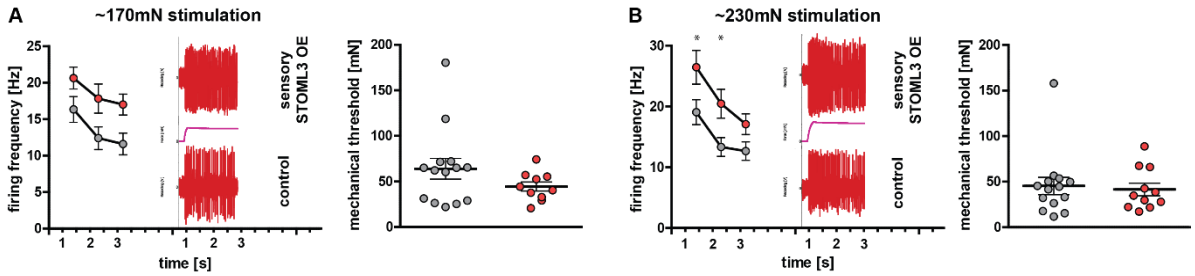

Figure 32 – Increased dynamic-phase coding properties emerged in sensitized mechanonociceptive C-fibers after overexpression of STOML3

Peristimulus time plots were created along with individual mechanical thresholds per indentation strength and compared between controls and following the overexpression of STOML3, here shown with physiological examples from recorded receptors in the applied force range between ~170 - 230mN. The first 3 seconds of the stimulus histograms are displayed as a quantification of the firing frequency on the left and corresponding examples of receptor activity on the right (the first second includes activity in the dynamic-phase). To indicate the increased activity in CMs after overexpression of STOML3, traces belonging to that experimental group are shown on top of controls. The overall increased activity is already almost significant in the 115mN stimulation strength ($p=0.0575$, two-way ANOVA with Bonferroni post-hoc test; data not shown). Starting with ~170mN, the difference becomes significant and obvious in A: ($p<0.05$, two-way ANOVA with Bonferroni post-hoc test). However, like in the summary (Fig.26C), the mechanical threshold was not decreased. With ~230mN stimulation strength in B, the biggest difference is shown ($p<0.05$, two-way ANOVA with Bonferroni post-hoc test) 1st second: $p<0.05$ and 2nd second: $p<0.05$. Again, the mechanical threshold was not decreased. CMs were different from polymodal C-fibers. Overall, their physiological properties were not changed drastically, just elevated. The increased activity especially in the first second of the stimulation was present, but not to scale with polymodals, where a doubling (or even slightly more) in activity was observed. Controls: LSLstoml3-Flag treated with vehicle; sensory STOML3 OE: AvilCre/ERT2::LSLstoml3-Flag treated with Tamoxifen.

To summarize this set of experiments.:

The *in vivo* overexpression of STOML3 has immense effects on the physiological properties of mechanoreceptors and nociceptors.

LTMRs (RAMs and SAMs) were clearly sensitized. The effect on RAMs was very large, resulting not simply from an increase in activity or function, but sensitization towards slower velocity stimuli (Fig.24A) which was also reflected in the percentage of responding receptors to the slowest moving stimuli. Fig.24B shows, that the slowest velocity (0.075mm/s) was only being encoded in ~10% of the control RAMs, with the overexpression of STOML3 this percentage increased to 71%. SAMs displayed an increase in activity most prominently during the slow velocity stimulation (Fig.25A) accompanied by a trend towards reduced mechanical thresholds and significantly more activity in the static phase of the stimulus (Fig.25B). This was not surprising (if some form of sensitization was assumed), since the slow velocity is the longest stimulus allowing for more time for spike activity. The receptors innervated by A-δ neurons did not display sensitization phenotypes. D-hairs and AMs (Fig.26A and Fig.27A) were not significantly affected by STOML3 overexpression.

Finally, C-fibers displayed prominent changes in their mechanosensitivity. Analyzing the C-fiber population as a whole masked pronounced effects of STOML3 overexpression. Polymodal C-fibers displayed marked sensitization phenotypes. Increased activity, lowered mechanical thresholds (some displayed mechanical thresholds similar to LTMRS) as well as dynamic-phase coding properties after induced STOML3 overexpression. CMs increased their activity as well but only for the largest suprathreshold force stimuli.

Overall, the overexpression of STOML3 in sensory neurons phenocopied the physiological changes emerging following CCI. Animals acquired mechanical hypersensitivity and the changes in the C-fiber nociceptive system were very similar.

3.7 *stoml3* conditional deletion prevents C-fiber nociceptors from being sensitized after surgery

After investigating the effects of STOML3 overexpression in sensory neurons and finding a remarkably robust sensitization effect, I examined ablation of *stoml3* to explore what physiological process might explain the lack of development of mechanical hypersensitivity initially described by Wetzel et al. 2007. Previous studies from the Lewin group used transgenic animals in which *stoml3* was knocked out globally. These animals were protected from neuropathic pain, they did not develop behavioural mechanical hypersensitivity after CCI. Recently, a conditional knockout of *stoml3* was created, in these animals *stoml3* is knocked out only in neurons expressing the wnt1-Cre recombinase (neural crest specific) and therefore this knockout was sensory neuron specific. Firstly, I investigated these animals using the von Frey- and Mouse walk behavioural assays to determine if these animals were protected from developing pain behaviour.

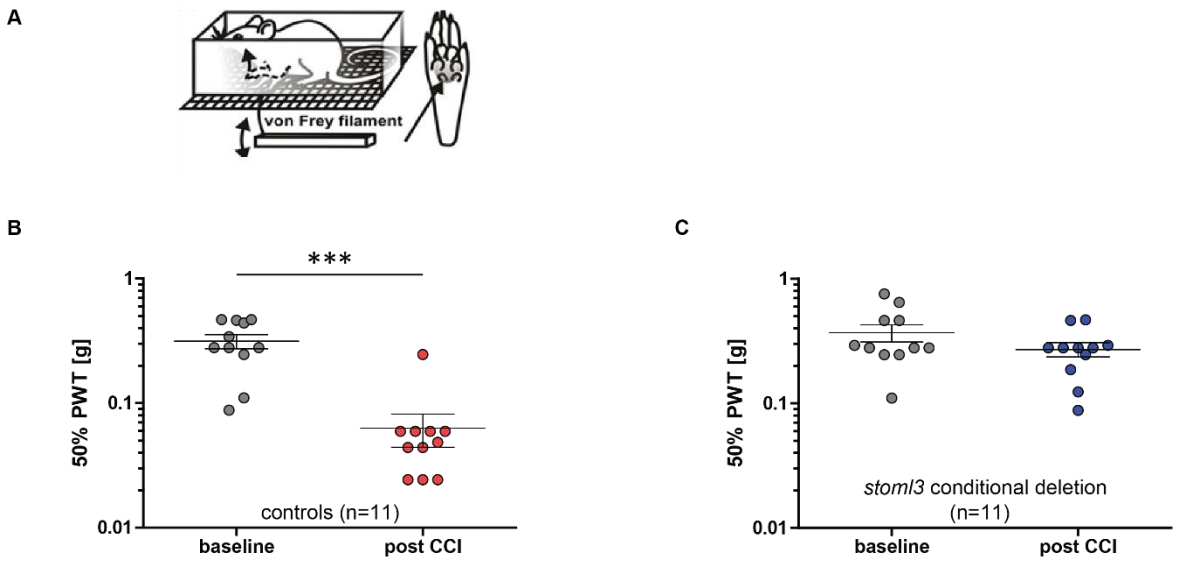

Figure 33 – The neural crest specific conditional knockout of *stoml3* prevents experimental animals from developing mechanical hypersensitivity following CCI

A illustrates the classical von Frey assay (taken from Yu et al., 2013). Filaments are applied to the hindpaw before and after CCI, the Chaplan modification of the Dixon approach is used to calculate a possible difference using k (tabular value) and the applied force of the filament used last. B: after CCI the control animals not expressing the wnt1-Cre recombinase were hypersensitive to mechanical stimulation ($p<0.001$, two-way ANOVA). In conditional knockouts, no mechanical hypersensitivity could be observed, shown in C. Controls: *stoml3*$^{fl/fl}$; *stoml3* conditional deletion: wnt1-cre::*stoml3*$^{fl/fl}$.

The same timeline was used as in the original experiments (see above, section 3.1 (pp.41-43)). Animals were assayed the day before surgery for baseline PWTs, then operated on and 7 days post-CCI evaluated again for the experimental thresholds.

Experimental animals that possessed the floxed *stoml3* allele but did not express the wnt1-Cre recombinase were used as controls. Since these animals did not express the Cre, the floxed allele was not excised making them essentially wildtype animals. These animals were compared to littermates expressing the Cre (conditional deletion or knockouts). The von Frey assay showed that following CCI experimental animals lacking STOML3 were protected from mechanical hypersensitivity (Fig.33C). This was in contrast to the littermate controls shown in Fig.33B. These animals developed mechanical hypersensitivity as also observed in the initial CCI cohort.

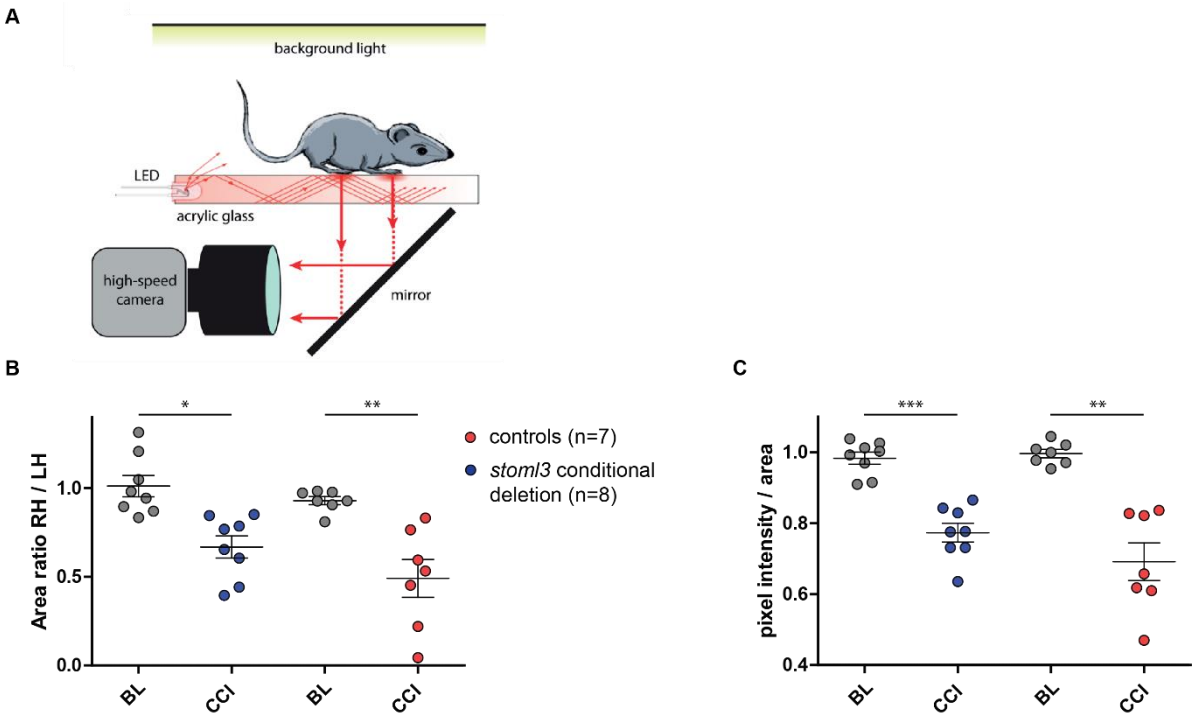

Figure 34 – The conditional *stoml3* deletion animals present a less severe gait phenotype following CCI

Animals walk across an 80cm long acrylic-glass walkway which is transilluminated with white LED lights (A, from Mendes et al. 2015). Contact of a paw with the walkway results in illumination (fTIR effect) – the step pattern is recorded with a high-speed camera and fed to an algorithm that enables the quantification of approximately 26 gait parameters. Before CCI the ratio of the pawprint area right hindpaw / left hindpaw is approximately 1. Following CCI the ratio drops to 0.49 ($p<0.01$, paired t-test) in control animals, but only to 0.69 ($p<0.05$, paired t-test) in conditional knockouts of STOML3. On the right the pixel intensity per area is quantified, after CCI the intensity (i.e. pressure) drops to 0.77, illustrating the animals' change in behaviour to minimize load on the affected paw ($p<0.001$, paired t-test), the intensity ratio in littermate controls dropped to 0.69 ($p<0.01$) a larger net effect, but due to smaller sample size statistically less significant. BL: baseline; CCI: chronic constriction injury. Controls: *stoml3*$^{fl/fl}$; *stoml3* conditional deletion: wnt1-cre::*stoml3*$^{fl/fl}$.

Following the von Frey evaluation of paw withdrawal thresholds a gait analysis was carried out using the Mouse walk assay. The reduction of the pawprint on the operated side can be seen in Fig.34 in both genotypes, however to a lesser degree in the conditional knockout animals.

Before CCI this ratio was 1 (mean of the conditional knockout population), after CCI it dropped to 0.69 (Fig.34B $p<0.05$, paired t-test) whereas the pressure ratio of the affected paw dropped from 0.97 to 0.77 (Fig.34C $p<0.001$, paired t-test). Compared to the initial pawprint ratios shown in Fig.10 (a drop from 1 to 0.4), the change was not as severe in *stoml3* conditional deletion animals.

In littermate controls, prior to CCI the pawprint ratio was 0.94 (mean of the control population), and after CCI it dropped to 0.49 (Fig.34B $p<0.01$, paired t-test), a larger difference compared to that of the knockouts and on the same scale as the initial CCI experiments on C57BL6/N mice. The pressure ratio of the affected paw dropped from 1 to 0.69 (Fig.34C $p<0.01$, paired t-test) again a larger net difference, however statistically less significant, as the sample size was smaller. After CCI not every animal was successfully recorded, this accounts for the difference in sample size between the von Frey (n=11) and Mouse walk assays (*stoml3* conditional deletion n=8, littermate controls n=7). However, the collected data and calculated paw-print ratios were constant over different experiments (see again Fig.10) and the net change was smaller in *stoml3* conditional deletion animals – which indicates a less severe pain phenotype.

These behavioural observations indicated that the *stoml3* conditional deletion animals displayed the same behavioural phenomena observed in global knockouts nearly 15 years ago and in experiments repeated by Wetzel et. al 2017. STOML3 seems to play an essential role in the genesis of mechanical hypersensitivity following neuropathic injury. And sensory neurons are likely the driver of this condition because the animals investigated here were sensory neuron specific knockouts. Since the initial CCI experiments showed a sensitization phenotype in C-fibers following neuropathic injury I chose to perform CCI on *stoml3* conditional deletion animals (wnt1-cre::*stoml3*$^{fl/fl}$) and littermate controls (*stoml3*$^{fl/fl}$) as well as record a new naïve C-fiber dataset to investigate the effect of ablated *stoml3* on C-fiber mechanosensitivity. These experiments were designed to ask whether STOML3 expression in sensory neurons is required for C-fiber sensitization seen after CCI.

Similar to the structure of the previous section addressing the effects of STOML3 overexpression on sensory neuron physiology, I will present the effect of *stoml3* conditional deletion on C-fiber mechanosensitivity firstly on the population level before dividing this heterogenous group into polymodal- and true mechanonociceptive C-fibers.

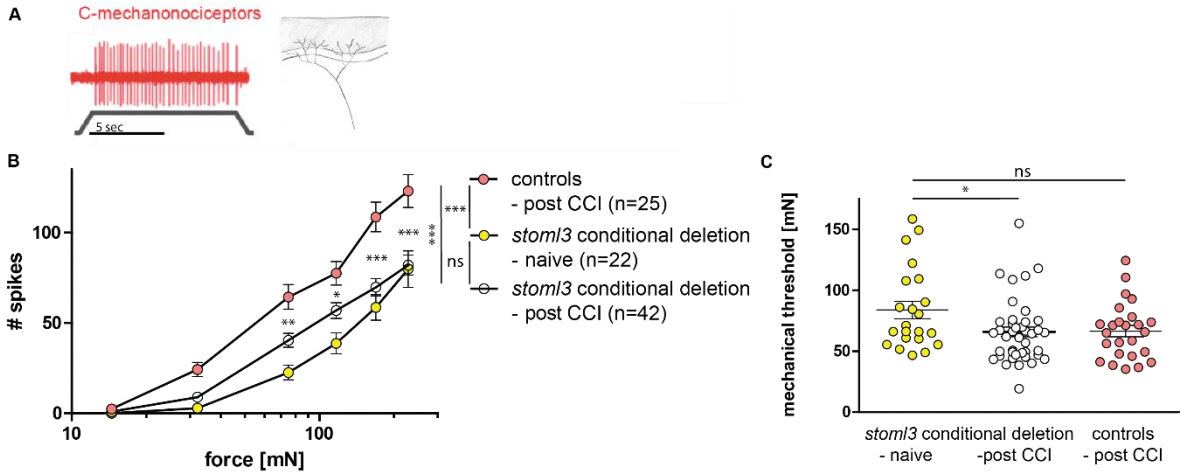

Figure 35 – Absence of STOML3 prevents C-fiber sensitization following neuropathic injury

C-fibers from *stoml3* conditional deletion and control animals in the naive condition and following CCI were stimulated in the glabrous hindpaw skin with the ramp and hold protocol. Action potentials were counted and shown as actual number of spikes in B and mechanical thresholds in C. Drastically increased activity was observed following CCI in the presence of STOML3 ($p<0.001$, repeated measures ANOVA with Dunnett's multiple comparison test). In the conditional knockouts of *stoml3* no increase in activity could be found. Subsequently both genotypes were compared to each other following CCI yielding once again a highly significant difference between C-fibers recorded from animals expressing STOML3 and those who lack it ($p<0.001$, two-way ANOVA with Bonferroni post-hoc test: 75mN: $p<0.01$, 115mN: $p<0.05$, 170mN: $p<0.001$ and 230mN: $p<0.001$). Mean mechanical thresholds were reduced in both groups following CCI, but only in the conditional knockouts of *stoml3* to a significant degree (due to the larger sample size, Fig.35C $p<0.05$, Mann-Whitney test). The actual transduction threshold values following CCI were 66mN on the population level for both genotypes. Controls: *stoml3*$^{fl/fl}$; *stoml3* conditional deletion: wnt1-cre::*stoml3*$^{fl/fl}$.

I recorded from 22 C-fibers in *stoml3* conditional deletion animals to illustrate C-fiber physiology in the naïve condition. Physiological properties were compared to C-fibers recorded from *stoml3* conditional deletion animals (42 recordings) and controls not expressing the Cre (essentially wildtype animals, 25 recordings) following neuropathic injury to investigate the role of STOML3 in peripheral sensitization. Each receptor was stimulated with a ramp and hold protocol, activity is shown as number of spikes. The mechanical threshold of the first action potential of every indentation step was used to calculate the mean mechanical threshold in [mN].

The overall activity (Fig.35B) of C-fibers following CCI increased drastically, but only if we consider the comparison between naïve vs. cre-negative animals (controls) ($p<0.001$, repeated measures ANOVA with Dunnett's multiple comparison test (the control dataset for the comparison was the naïve dataset)). After conditional deletion of *stoml3*, there was no significant increase in overall activity. In a second analysis step a two-way ANOVA was used to compare the activity of the two genotypes following CCI. Conditional *stoml3* knockouts and their littermate controls displayed highly significant differences in stimulus response function ($p<0.001$, two-way ANOVA with Bonferroni post-hoc test) with stimulation intensities of 75mN

and higher (individual significances from the post-hoc test are indicated by asterisks in Fig.35B). Mean mechanical thresholds were reduced in both groups following CCI (Fig.35C $p<0.05$, Mann-Whitney test). The actual mechanical threshold values following CCI were 66mN on the population level for both genotypes. In naïve *stoml3* conditional deletion animals a maximum mean activity of 82 spikes was generated to the largest indentation force (~230mN), this was in contrast to 123 spikes in animals expressing STOML3 following CCI and 82 spikes in animals with *stoml3* conditional deletion respectively (no increase in activity).

Peristimulus time histograms for every stimulation strength as well as individual force thresholds were calculated, plotted and compared to investigate dynamic-phase coding properties. However, this analysis will not be shown on the population level. Fig.35 provides an introduction and summary of this set of experiments and was included to highlight the robust effect of *stoml3* conditional deletion on C-fiber physiology. In previous experiments (overexpression) differences in C-fiber physiology were most obvious after dividing these sensory neurons further into polymodal- and true mechanonociceptive C-fibers. In the following section I show a more detailed analysis of C-fiber physiology for polymodals and CMs.

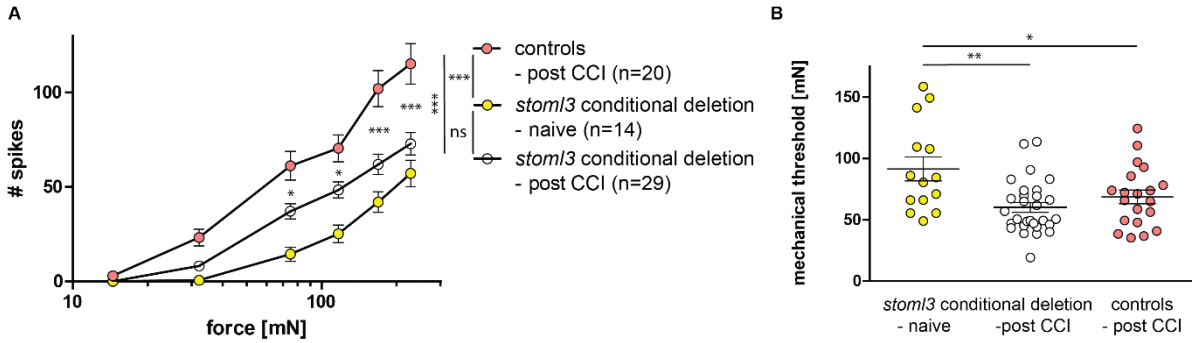

Figure 36 – Absence of STOML3 prevents sensitization of polymodal C-fibers following neuropathic injury

The subpopulation of polymodal C-fibers from the previous analysis in Fig.35 is further analyzed here. Drastically increased activity was observed following CCI in the presence of STOML3 ($p<0.001$, repeated measures ANOVA with Dunnett's multiple comparison test). In the *stoml3* conditional deletion no significant increase in activity could be found (A). Subsequently both genotypes were compared to each other following CCI yielding once again a highly significant difference between C-fibers recorded from animals expressing STOML3 and those with ablated *stoml3* ($p<0.001$, two-way ANOVA with Bonferroni post-hoc test: 75mN: $p<0.05$, 115mN: $p<0.05$, 170mN: $p<0.001$ and 230mN: $p<0.001$). Mean mechanical thresholds were reduced in both groups following CCI (C: $p<0.01$ for the conditional knockouts and $p<0.05$ for the controls, Mann-Whitney test). Controls: *stoml3*$^{fl/fl}$; *stoml3* conditional deletion: wnt1-cre::*stoml3*$^{fl/fl}$.

Polymodal C-fibers are thus markedly sensitized following CCI in the presence of STOML3. They display increased overall activity as well as significantly reduced mechanical thresholds. Sensory neuron specific ablation of *stoml3* prevents polymodal C-fibers from being sensitized,

no significant increase in overall activity could be measured. Comparing the conditional *stoml3* deletion to their controls lacking the Cre with a two-way ANOVA demonstrated significant differences in activity ($p<0.001$, two-way ANOVA with Bonferroni post-hoc test) from stimulation intensities of 75mN and higher (individual significances from the post-hoc test are indicated by asterisks in Fig.36A). Mean mechanical thresholds were reduced in both groups following CCI, due to the larger sample size the calculated difference was larger in the conditional *stoml3* deletion group (Fig.36B $p<0.01$, Mann-Whitney test for *stoml3* conditional deletion and $p<0.05$, Mann-Whitney test for the littermate controls). The actual mean transduction threshold values following CCI were very similar for both genotypes (60mN vs. 68mN compared to 92mN in the naïve condition). In the naïve *stoml3* conditional deletion group a maximum mean activity of 57 spikes was generated at the maximal indentation force (~230mN), this was opposed to 115 spikes in animals expressing STOML3 following CCI and 73 spikes in animals with *stoml3* conditional deletion respectively (no increase in activity).

To illustrate the differences in C-fiber physiology following neuropathic injury and its dependence on STOML3, peristimulus time histograms for every stimulation strength (starting with 35mN) as well as individual force thresholds were calculated and compared to investigate dynamic-phase coding properties.

Polymodal C-fibers become sensitized following neuropathic injury. Small mechanical indentations (35mN, Fig.37A) are transduced with significantly more action potentials than in the naïve condition. This effect appeared regardless of the presence or absence of STOML3, however the magnitude of the sensitization phenotype was significantly decreased if *stoml3* was genetically ablated. From stimulation intensities of 75mN (Fig.38A) and higher sensitized polymodal C-fiber nociceptors started displaying dynamic-phase coding properties. A burst of activity was generated in the beginning of the mechanical stimulation (this was true for both genotypes), however, in the presence of STOML3 this initial increase in activity was followed by a slower adaptation, meaning that spiking activity remained high. If *stoml3* was conditionally deleted, this initial burst of activity was followed by a huge drop in activity, displaying intermediate activity levels between naïve and knockouts not expressing Cre. With higher stimulation intensities this effect became more pronounced. At 115mN (Fig.39A) the initial peak activity was very similar regardless of the presence or absence of STOML3, the following 3 seconds were characteristic of normal neuropathic C-fibers, however the final 6 seconds of the stimulation showed physiology more comparable to naïve recordings in the conditional deletion of *stoml3*. High intensity stimulations (170mN, Fig.40A and 230mN, Fig, 41A) showed an even faster adaptation phenotype in the *stoml3* conditional deletion group. The dynamic-phase activity was elevated similar to the littermate controls; however, this increased activity

was only observed in the first 2 seconds of the mechanical stimulus. Following that polymodal C-fibers from the conditional deletion animals displayed physiology similar to the naïve condition.

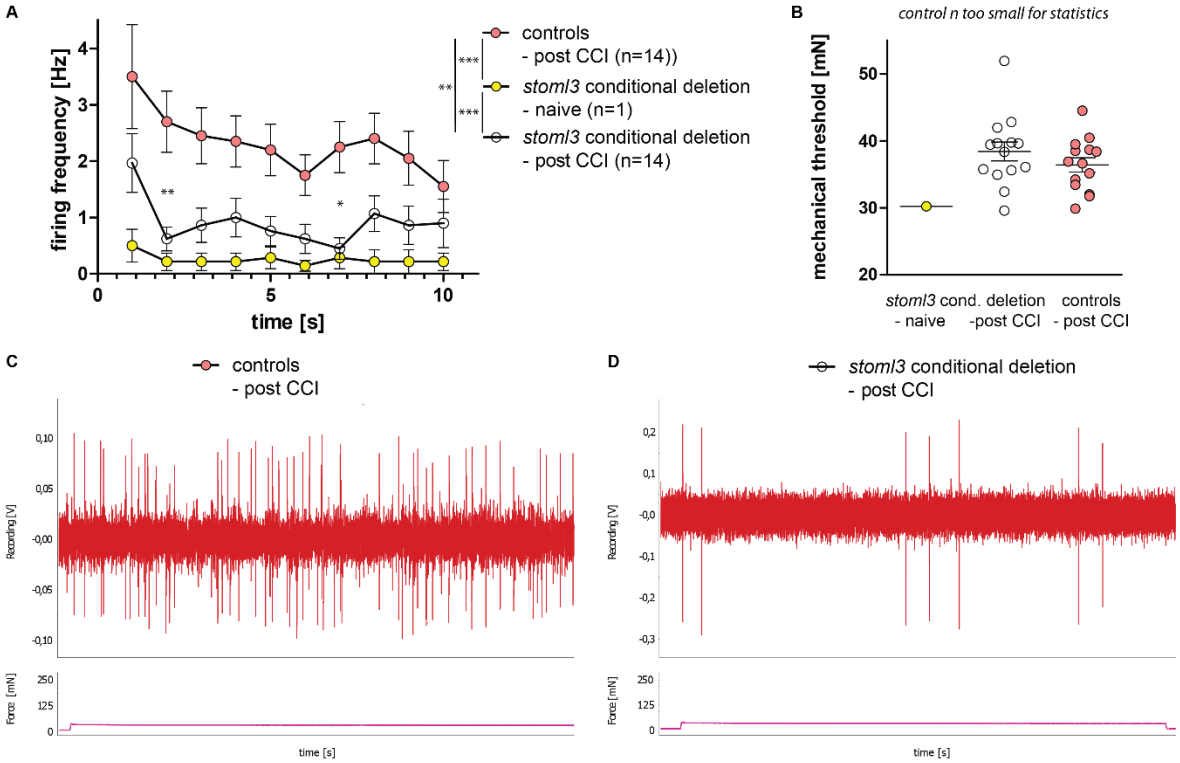

Figure 37 – Peristimulus time histogram of 35mN response of polymodal C-fibers following CCI in the presence and absence of STOML3 - STOML3 is essential for peripheral sensitization Drastically increased activity was observed following CCI in the presence and absence of STOML3 ($p<0.001$, repeated measures ANOVA with Dunnett's multiple comparison test) (A). However, comparing the two genotypes following CCI yielded a highly significant difference between C-fibers recorded from animals with and without STOML3 ($p<0.01$, two-way ANOVA with Bonferroni post-hoc test: 2s: $p<0.01$ and 7s: $p<0.05$). Mean mechanical thresholds (B) could not be compared to the naïve condition, since only 1 C-fiber responded to stimulations of this intensity. Exemplary physiological traces are shown in C (littermate controls lacking the Cre) and D (*stoml3* conditional deletion) to illustrate the difference in activity. Interestingly the mean dynamic-phase response was elevated in the *stoml3* conditional deletion animals as well. Controls: *stoml3*$^{fl/fl}$; *stoml3* conditional deletion: wnt1-cre::*stoml3*$^{fl/fl}$.

Another interesting characteristic was observed using this analysis. High intensity mechanical stimulations (170mN and 230mN) are also transduced with increased dynamic-phase activity in naïve C-fibers, however this physiological characteristic emerged earlier and was more severe in the neuropathic condition.

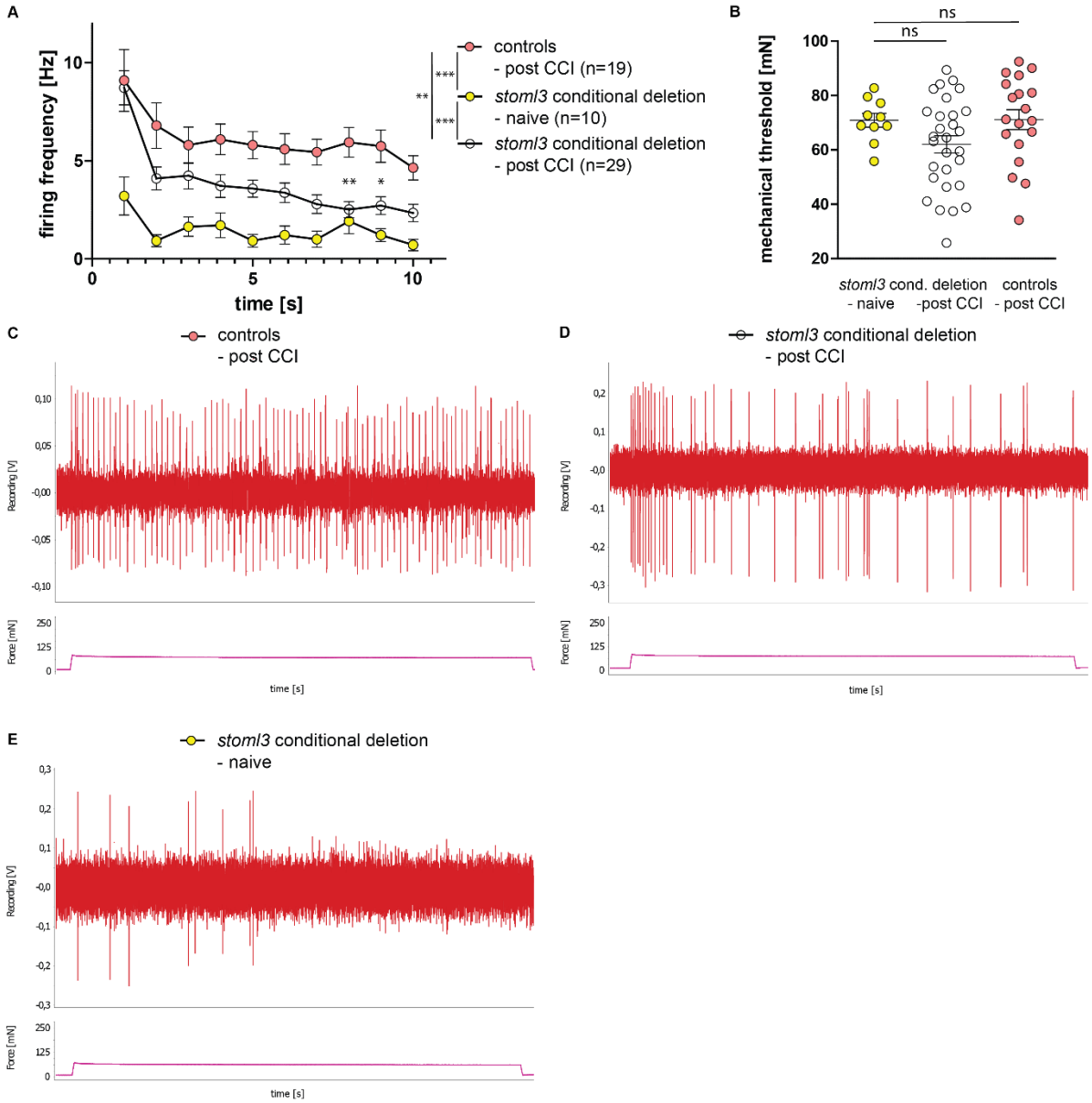

Figure 38 – Peristimulus time histogram of 75mN response of polymodal C-fibers following CCI in the presence and absence of STOML3 - STOML3 is essential for peripheral sensitization
Drastically increased activity was observed following CCI in the presence and absence of STOML3 ($p<0.001$, repeated measures ANOVA with Dunnett's multiple comparison test) (A). However, comparing the two genotypes following CCI yielded a highly significant difference between C-fibers recorded from animals with and without STOML3 ($p<0.01$, two-way ANOVA with Bonferroni post-hoc test: 8s: $p<0.01$ and 9s: $p<0.05$). Mean mechanical thresholds (B) were not decreased. Exemplary physiological traces are shown in C (littermate controls lacking the Cre), D (*stoml3* conditional deletion) and E (*stoml3* conditional deletion in the naïve condition) to illustrate the difference in activity. Interestingly the mean dynamic-phase response was elevated in the *stoml3* conditional deletion animals to the same degree than in the littermate controls, after the initial burst of activity the stimulus coding response declined. Naïve polymodal C-fibers are hardly active being stimulated with only 75mN of force. Controls: *stoml3*$^{fl/fl}$; *stoml3* conditional deletion: wnt1-cre::*stoml3*$^{fl/fl}$.

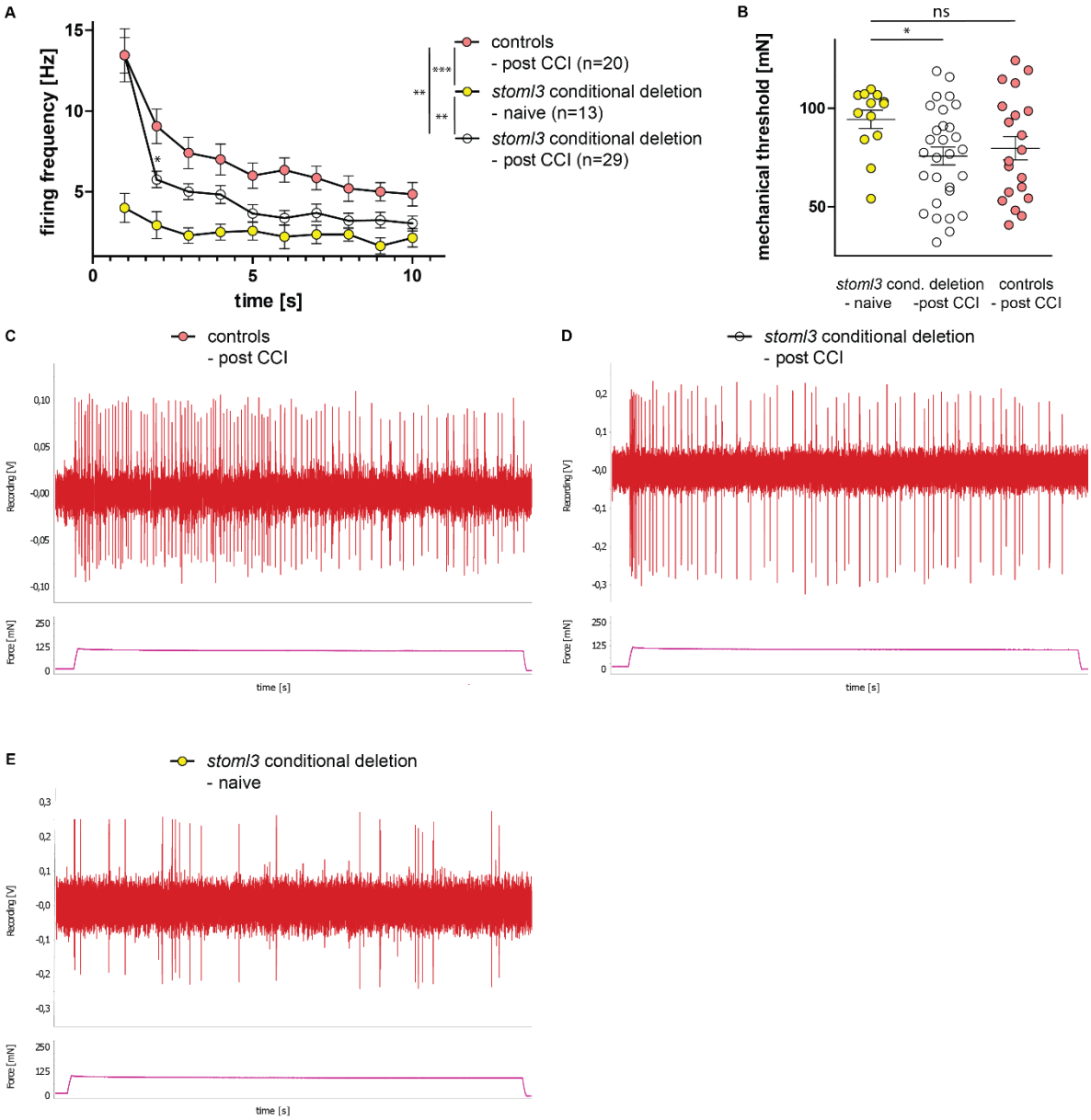

Figure 39 – Peristimulus time histogram of 115mN response of polymodal C-fibers following CCI in the presence and absence of STOML3 - STOML3 is essential for peripheral sensitization
Drastically increased activity was observed following CCI in the presence and absence of STOML3 ($p<0.001$ for the littermate controls and $p<0.01$ for the *stoml3* conditional deletion animals, repeated measures ANOVA with Dunnett's multiple comparison test) (A). However, comparing the two genotypes following CCI yielded a highly significant difference between C-fibers recorded from animals with and without STOML3 ($p<0.01$, two-way ANOVA with Bonferroni post-hoc test: 2s: $p<0.05$). Mean mechanical thresholds (B) were decreased in the *stoml3* conditional deletion animals ($p<0.05$, Mann-Whitney test) however not significantly in the littermate controls even though a drop in threshold could be observed in both groups (to 75mN and 80mN from the naïve 95mN). Exemplary physiological traces are shown in C (littermate controls lacking the Cre), D (*stoml3* conditional deletion animals) and E (*stoml3* conditional deletion animals in the naïve condition) to illustrate the difference in activity. The mean dynamic-phase response was elevated in the *stoml3* conditional deletion animals to the same degree than in the littermate controls, after the initial burst of activity the stimulus coding response declined. Naïve polymodal C-fibers are still hardly active being stimulated with 115mN of force. Controls: *stoml3*$^{fl/fl}$; *stoml3* conditional deletion: wnt1-cre::*stoml3*$^{fl/fl}$.

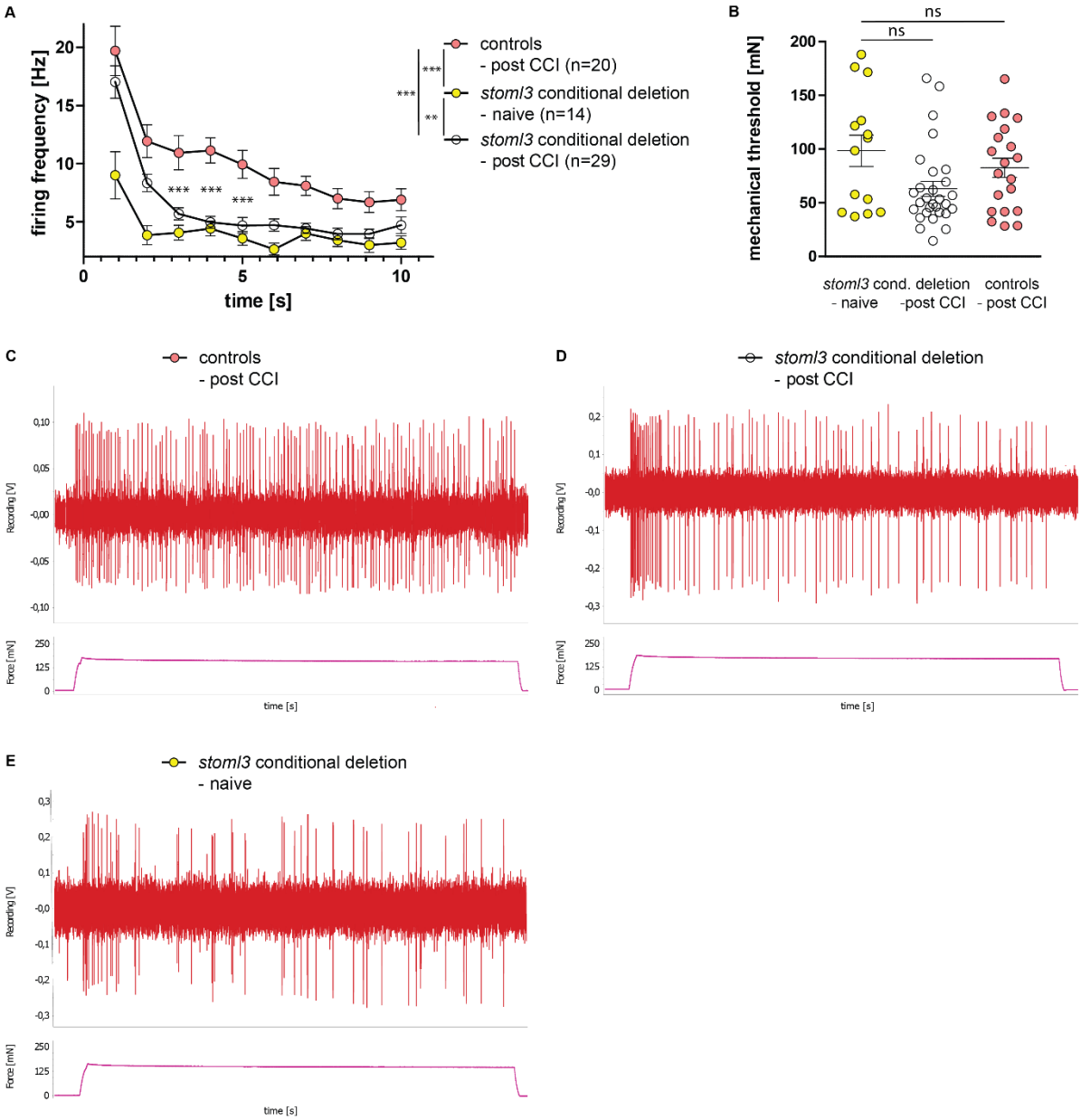

Figure 40 – Peristimulus time histogram of 170mN response of polymodal C-fibers following CCI in the presence and absence of STOML3 - STOML3 is essential for peripheral sensitization
Drastically increased activity was observed following CCI in the presence and absence of STOML3 ($p<0.001$ for the littermate controls and $p<0.01$ for the *stoml3* conditional deletion animals, repeated measures ANOVA with Dunnett's multiple comparison test) (A). However, comparing the two genotypes following CCI yielded a highly significant difference between C-fibers recorded from animals with and without STOML3 ($p<0.001$, two-way ANOVA with Bonferroni post-hoc test: 3s: $p<0.001$, 4s: $p<0.001$ and 5s: $p<0.001$). Mean mechanical thresholds (B) were not decreased significantly in the *stoml3* conditional deletion animals (though an obvious reduction is visible) or the littermate controls. Exemplary traces are shown in C (littermate controls lacking Cre), D (*stoml3* conditional deletion animals) and E (*stoml3* conditional deletion animals in naïve condition) to illustrate the difference in activity. The mean dynamic-phase response was elevated in the *stoml3* conditional deletion animals to the same degree as in the littermate controls, after the initial burst of activity the stimulus coding response declined. Naïve polymodal C-fibers are far less active being stimulated with 170mN of force, interestingly they started displaying increased dynamic-phase responses as well starting with this indentation force. Controls: *stoml3*$^{fl/fl}$; *stoml3* conditional deletion: wnt1-cre::*stoml3*$^{fl/fl}$.

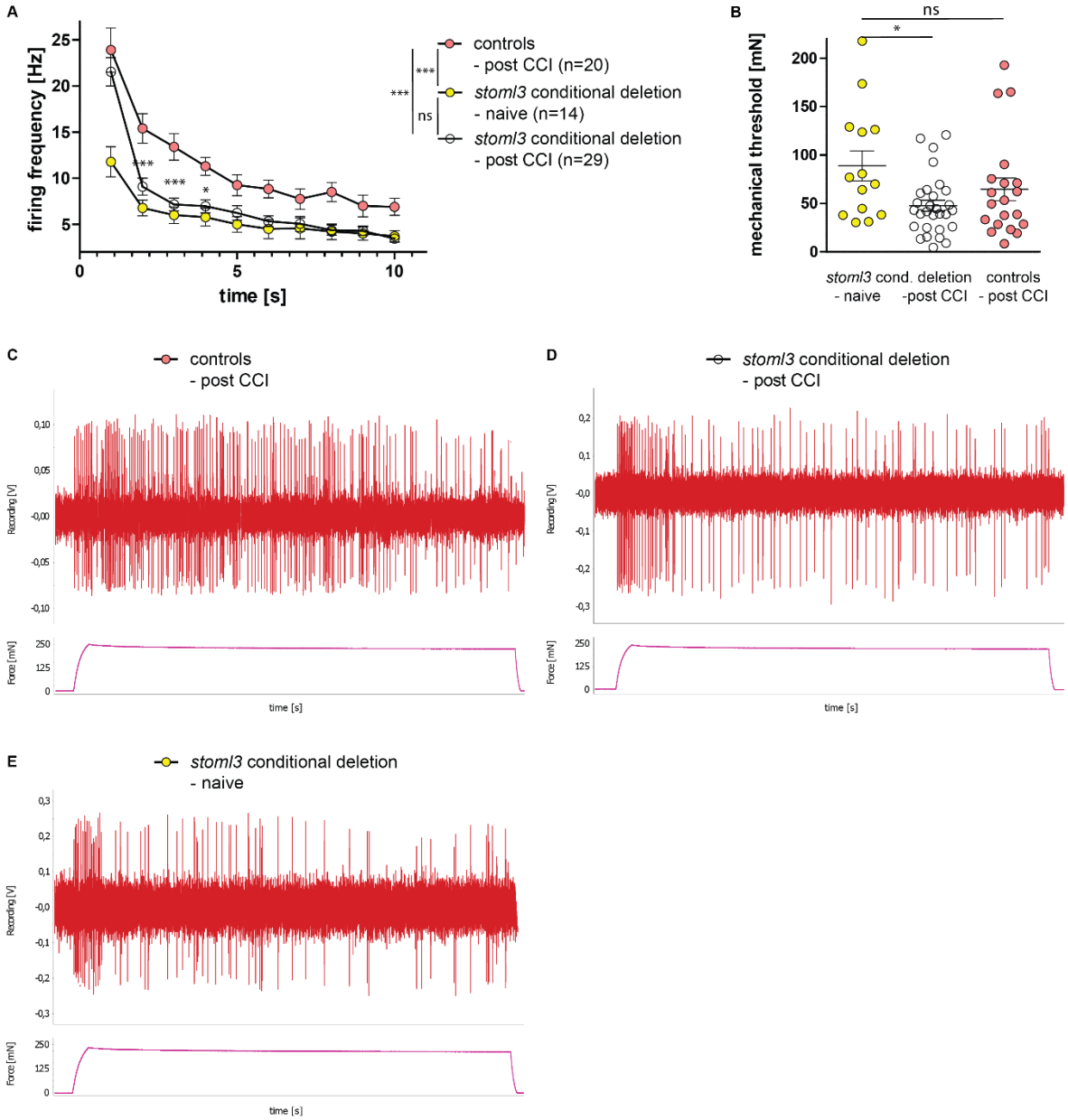

Figure 41 – Peristimulus time histogram of 230mN response of polymodal C-fibers following CCI in the presence and absence of STOML3 - STOML3 is essential for peripheral sensitization
Drastically increased activity was observed following CCI, but only in the presence of STOML3 ($p<0.001$ for the littermate controls, repeated measures ANOVA with Dunnett's multiple comparison test) (A). Comparing the two genotypes following CCI yielded a highly significant difference between C-fibers recorded from animals with and without STOML3 ($p<0.001$, two-way ANOVA with Bonferroni post-hoc test: 2s: $p<0.001$, 3s: $p<0.001$ and 4s: $p<0.05$). Mean mechanical thresholds (B) were decreased significantly in the *stoml3* conditional deletion animals ($p<0.05$, Mann-Whitney test) however not significant in the littermate controls even though a drop in threshold could be observed in both groups (to 45mN and 65mN from the naïve 89mN). Exemplary traces are shown in C (littermate controls lacking Cre), D (*stoml3* conditional deletion animals) and E (*stoml3* conditional deletion animals in the naïve condition) to illustrate the difference in activity. The mean dynamic-phase response was elevated in the *stoml3* conditional deletion animals to the same degree as in the littermate controls, after the initial burst of activity the stimulus coding response declined. Naïve polymodal C-fibers are far less active being stimulated with 230mN of force but they continued displaying increased dynamic-phase responses. Controls: *stoml3*$^{fl/fl}$; *stoml3* conditional deletion: wnt1-cre::*stoml3*$^{fl/fl}$.

In general, small (as well as intermediate and large) tactile stimuli induce increased activity in this part of the C-fiber system and the absence of STOML3 yielded significantly less active polymodal C-fibers following CCI. Force thresholds of the two groups were reduced compared to naïve controls though not always significantly even in the absence of STOML3. Therefore, STOML3 likely has multiple functions beyond the determination of transduction thresholds or the initial dynamic-phase activity and its roles may be influenced by several factors in addition to the mechanical sensitivity in this subset of neurons.

Below the results for the true mechanonociceptive C-fibers are shown. There was no sensitization following CCI in the absence of STOML3, in the presence of STOML3 however sensitization similar to that seen in polymodal C-fibers was found. CMs displayed increased overall activity.

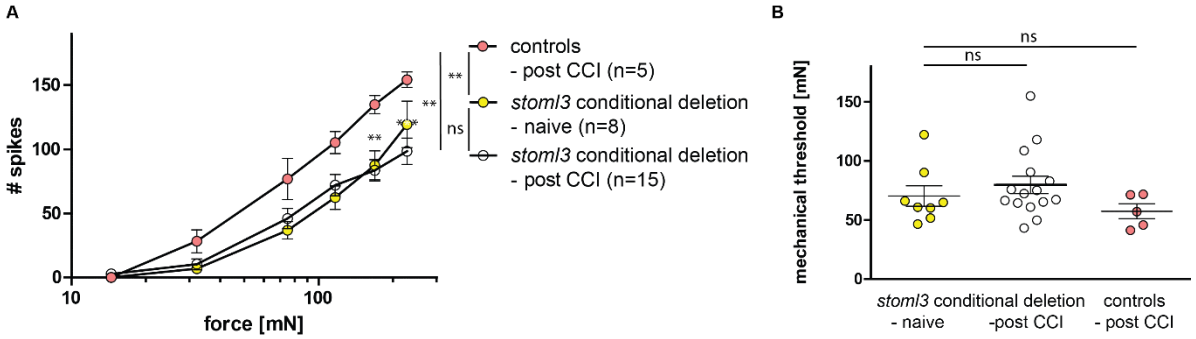

Figure 42 – Absence of STOML3 prevents true mechanonociceptive C-fibers from being sensitized following neuropathic injury

The subpopulation of CMs from the previously shown analysis in Fig.35 is shown again here. Highly increased activity was observed following CCI in the presence of STOML3 ($p<0.01$, repeated measures ANOVA with Dunnett's multiple comparison test). In the *stoml3* conditional deletion animals no significant increase in activity could be found (A). Subsequently both genotypes were compared to each other following CCI yielding once again a highly significant difference between C-fibers recorded from animals with and without STOML3 ($p<0.01$, two-way ANOVA with Bonferroni post-hoc test: 170mN: $p<0.01$ and 230mN: $p<0.001$). Mean mechanical thresholds were slightly reduced in littermate controls expressing STOML3, a trend towards increased mechanical thresholds could be observed in the *stoml3* conditional deletion animals, however it was not significant. Controls: *stoml3*$^{fl/fl}$; *stoml3* conditional deletion: wnt1-cre::*stoml3*$^{fl/fl}$.

Conditional ablation of *stoml3* prevented CMs from being sensitized, no significant increase in overall activity could be measured. Comparing the *stoml3* conditional deletion animals to controls lacking the Cre with a two-way ANOVA showed significant differences in activity ($p<0.01$, two-way ANOVA with Bonferroni post-hoc test) from stimulation intensities of 170mN and greater (individual significances from the post-hoc test are indicated by asterisks in Fig.42A). In naïve *stoml3* conditional deletion animals a maximum mean activity of 120 spikes was generated at the maximal indentation force in these experiments (~230mN), this is opposed to 154 spikes in animals expressing STOML3 following CCI and 98 spikes in animals

with ablated *stoml3* respectively (no increase in activity). To illustrate the differences in C-fiber physiology following neuropathic injury and its dependence on STOML3, peristimulus time histograms for every stimulation strength (starting with 35mN) as well as individual force thresholds were calculated and compared to investigate dynamic-phase coding properties.

True mechanonociceptive C-fibers become sensitized following neuropathic injury. Small mechanical indentations (35mN, Fig.43A) are transduced with significantly more action potentials than in the naïve condition. This effect was observed only in the presence of STOML3 (this being the main difference of polymodal C-fibers and CMs). From the very beginning of the force stimulation range sensitized CMs started displaying dynamic-phase coding properties, but once again only if STOML3 was present.

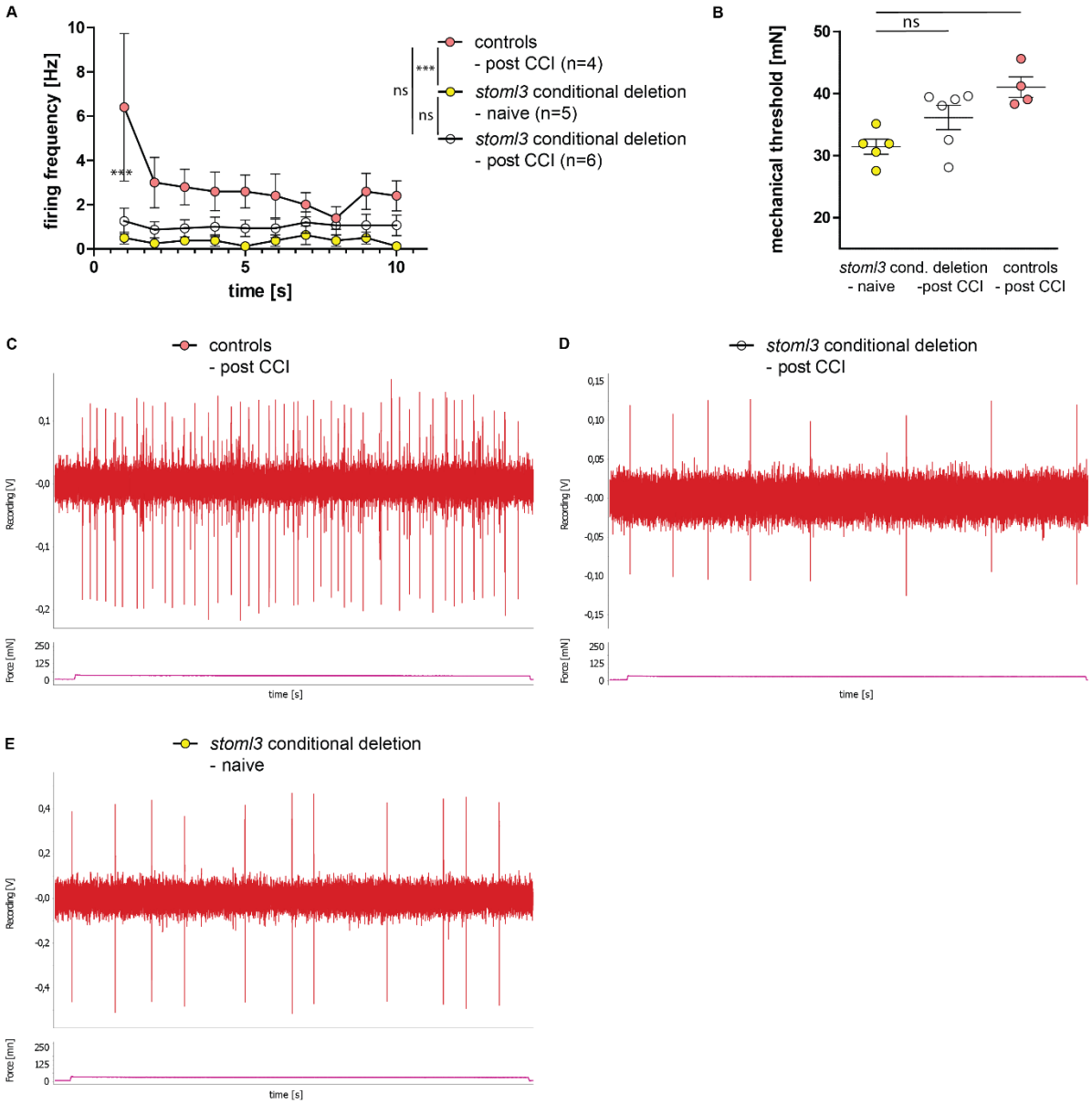

Figure 43 – Peristimulus time histogram of 35mN response of CMs following CCI in the presence and absence of STOML3 - STOML3 is essential for peripheral sensitization
Drastically increased activity was observed following CCI in the presence of STOML3 ($p<0.001$, repeated measures ANOVA with Dunnett's multiple comparison test) (A). Mean mechanical thresholds (B) were elevated in CMs, however not significantly. Exemplary physiological traces are shown in C (littermate controls lacking the Cre), D (*stoml3* conditional deletion animals) and E (*stoml3* conditional deletion animals in the naïve condition) to illustrate the difference in activity. CM activity from *stoml3* conditional deletion animals following neuropathic injury was indistinguishable from naive controls. Controls: *stoml3*$^{fl/fl}$; *stoml3* conditional deletion: wnt1-cre::*stoml3*$^{fl/fl}$.

Beginning with very small stimuli, CMs recorded from *stoml3* conditional deletion animals were no different than those recorded in the naïve condition. The largest indentation even yielded a significantly decreased activity (Fig.47). Highly increased activity was generated in the beginning of the mechanical stimulation in the presence of STOML3.

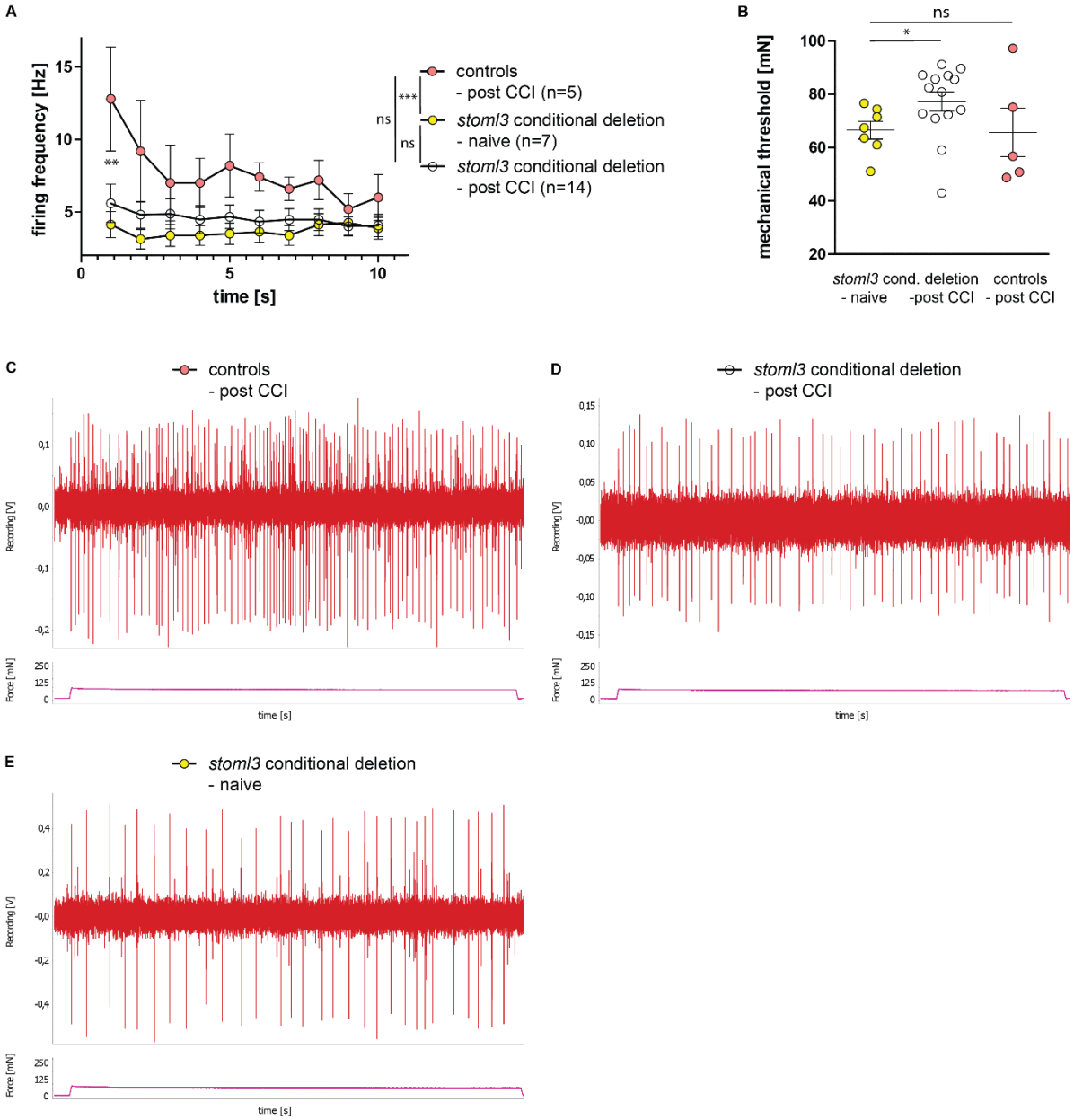

Figure 44 – Peristimulus time histogram of 75mN response of CMs following CCI in the presence and absence of STOML3 - STOML3 is essential for peripheral sensitization
Drastically increased activity was observed following CCI in the presence of STOML3 ($p<0.001$, repeated measures ANOVA with Dunnett's multiple comparison test) (A). Mean mechanical thresholds (B) were elevated in CMs recorded from the *stoml3* conditional deletion animals ($p<0.05$, Mann-Whitney test). Exemplary physiological traces are shown in C (littermate controls lacking the Cre), D (*stoml3* conditional deletion animals) and E (*stoml3* conditional deletion animals in the naïve condition) to illustrate the difference in activity. CM activity from *stoml3* conditional deletion animals following neuropathic injury was indistinguishable from naive controls. Controls: *stoml3*$^{fl/fl}$; *stoml3* conditional deletion: wnt1-cre::*stoml3*$^{fl/fl}$.

This initial increase in activity was followed by a slow adaptation, meaning that the level of activity or generated action potentials remained high. The duration of increased activity increased with the stimulation intensity.

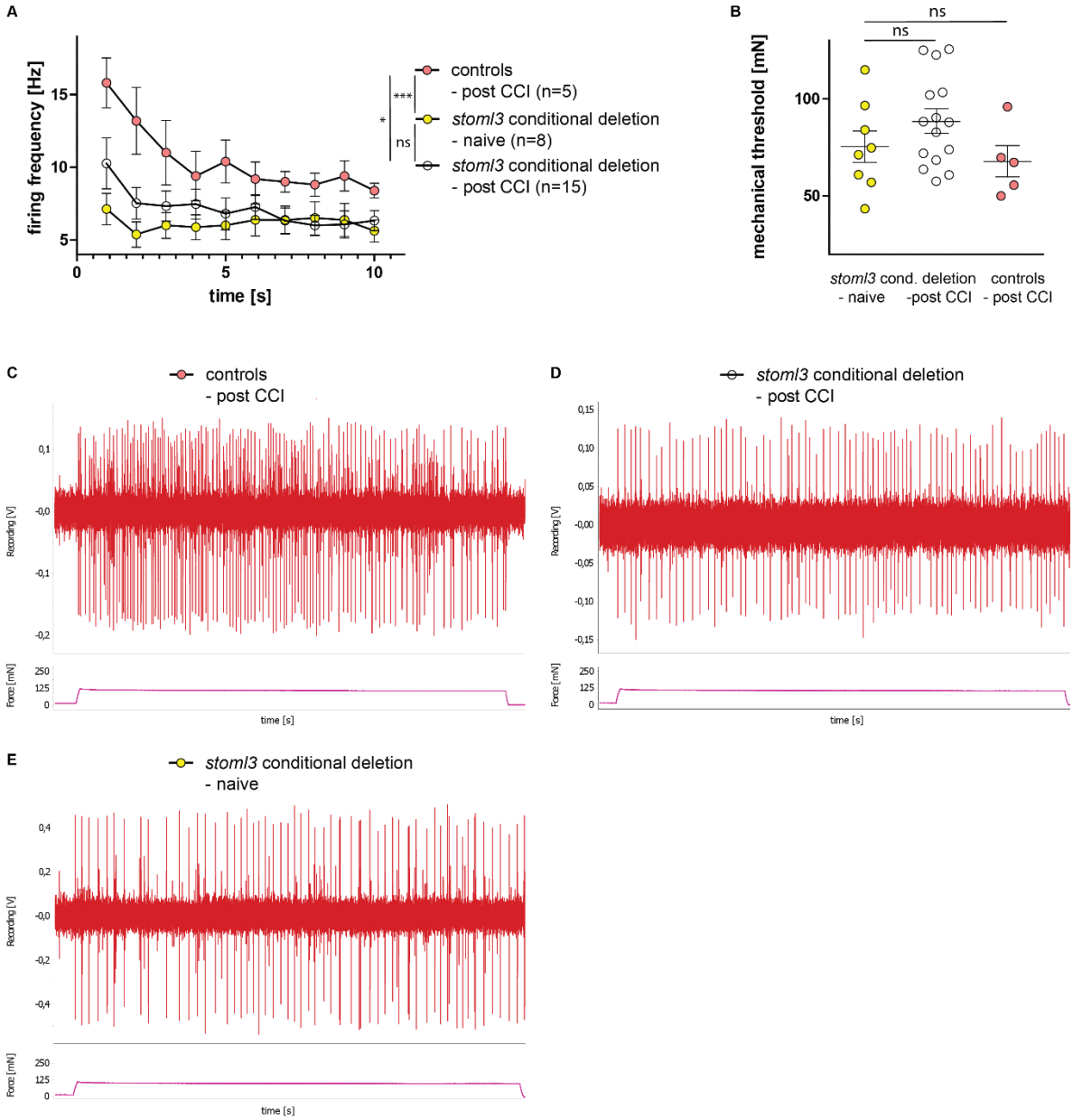

Figure 45 – Peristimulus time histogram of 115mN response of CMs following CCI in the presence and absence of STOML3 - STOML3 is essential for peripheral sensitization
Drastically increased activity was observed following CCI in the presence of STOML3 ($p<0.001$, repeated measures ANOVA with Dunnett's multiple comparison test) (A). Comparing the two genotypes following CCI yielded a significant difference between C-fibers recorded from animals with and without STOML3 ($p<0.05$, two-way ANOVA with Bonferroni post-hoc test). Mean mechanical thresholds (B) were elevated in CMs recorded from the *stoml3* conditional deletion animals (though not significantly). Exemplary physiological traces are shown in C (littermate controls lacking the Cre), D (*stoml3* conditional deletion animals) and E (*stoml3* conditional deletion animals in the naïve condition) to illustrate the difference in activity. CM activity from *stoml3* conditional deletion animals following neuropathic injury was indistinguishable from naive controls. Controls: *stoml3*$^{fl/fl}$; *stoml3* conditional deletion: wnt1-cre::*stoml3*$^{fl/fl}$.

The highest intensity (230mN, Fig.47A) yielded an even larger initial response followed by a drop in activity, however the consecutive 5 seconds still displayed increased activity before adapting to basal level (for this stimulus).

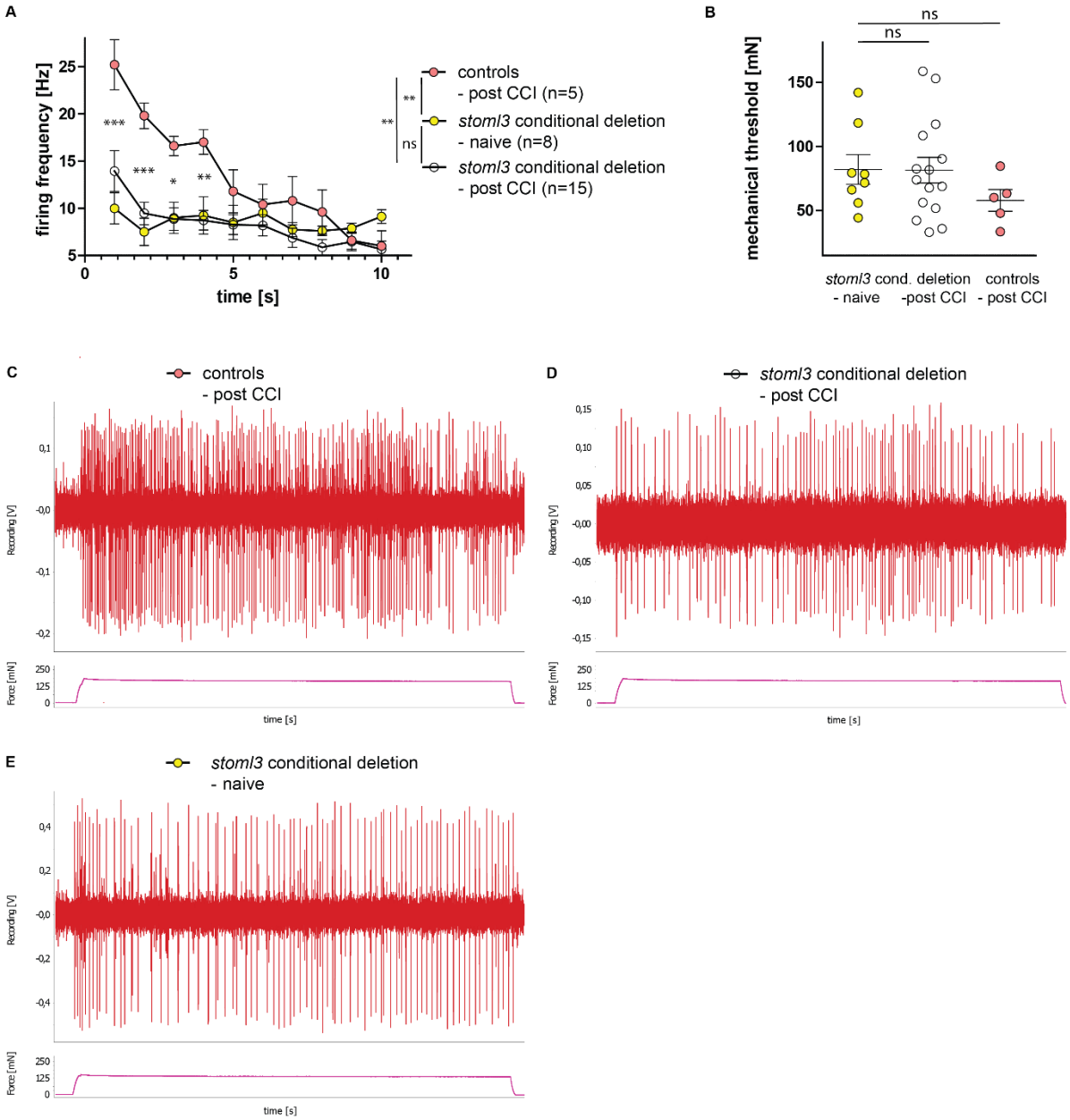

Figure 46 – Peristimulus time histogram of 170mN response of CMs following CCI in the presence and absence of STOML3 - STOML3 is essential for peripheral sensitization
Highly increased activity was observed following CCI in the presence of STOML3 ($p<0.01$, repeated measures ANOVA with Dunnett's multiple comparison test) (A). Comparing the two genotypes following CCI yielded a significant difference between C-fibers recorded from animals with and without STOML3 ($p<0.01$, two-way ANOVA with Bonferroni post-hoc test: 1s: $p<0.001$, 2s: $p<0.001$, 3s: $p<0.05$ and 4s: $p<0.01$). Mean mechanical thresholds (B) were not different. Exemplary physiological traces are shown in C (littermate controls lacking the Cre), D (*stoml3* conditional deletion animals) and E (*stoml3* conditional deletion animals in the naïve condition) to illustrate the difference in activity. CM activity from *stoml3* conditional deletion animals following neuropathic injury was indistinguishable from naive controls. Controls: *stoml3*$^{fl/fl}$; *stoml3* conditional deletion: wnt1-cre::*stoml3*$^{fl/fl}$.

If *stoml3* was genetically ablated, there was no initial burst of activity at mild stimulation strengths and only a slightly increased firing frequency in the first second of the stimulation

using stronger stimuli. The *stoml3* conditional deletion animals displayed wild-type like physiology.

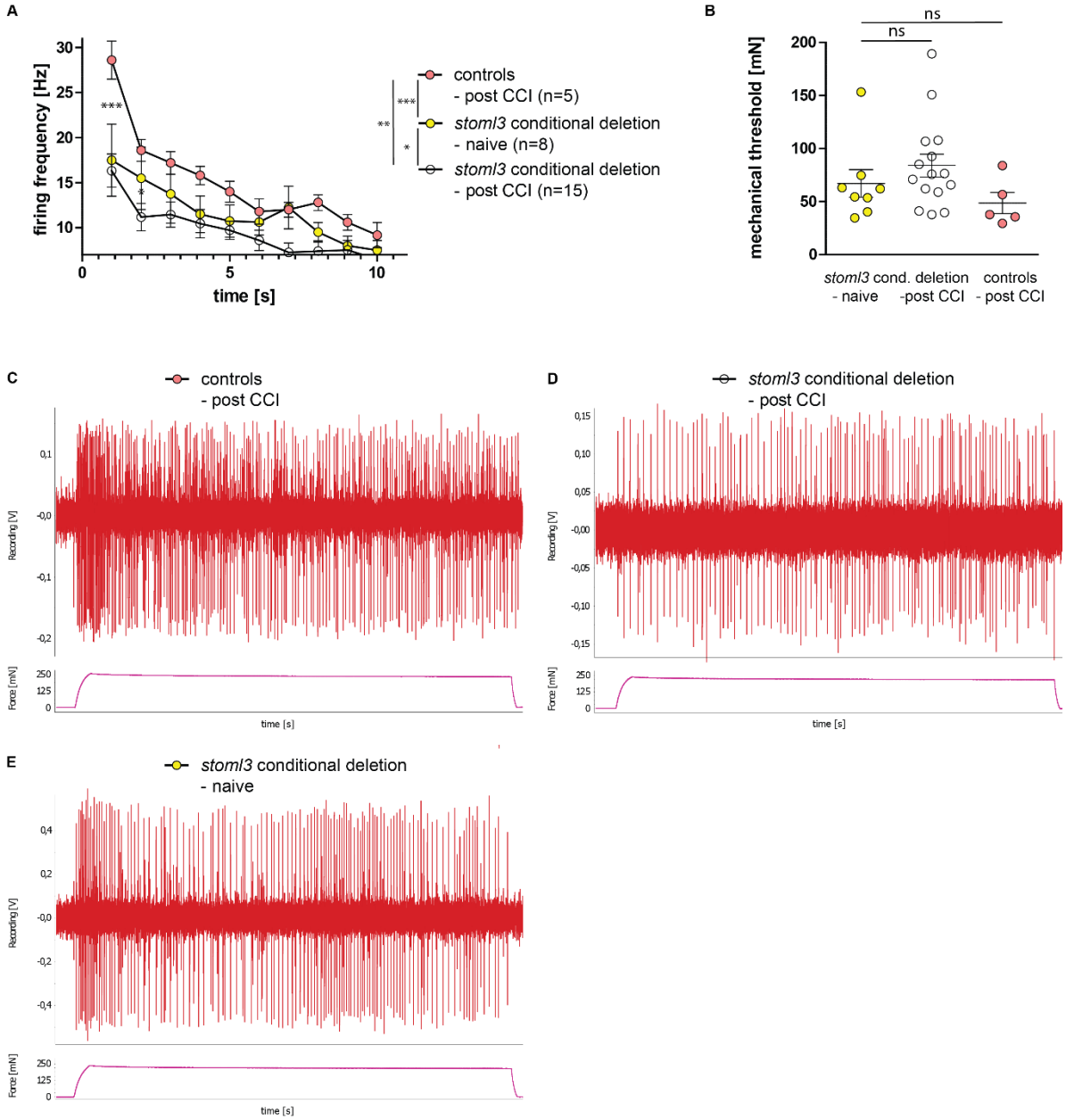

Figure 47 – Peristimulus time histogram of 230mN response of CMs following CCI in the presence and absence of STOML3 - STOML3 is essential for peripheral sensitization

Drastically increased activity was observed following CCI in the presence of STOML3 ($p<0.001$, repeated measures ANOVA with Dunnett's multiple comparison test) (A). Interestingly the analysis also yielded a significant decrease in activity in the *stoml3* conditional deletion animals compared to naïve controls ($p<0.05$). Comparing the two genotypes following CCI yielded a significant difference between C-fibers recorded from animals with and without STOML3 ($p<0.01$, two-way ANOVA with Bonferroni post-hoc test: 1s: $p<0.001$ and 2s: $p<0.05$). Mean mechanical thresholds (B) were not different but seemed elevated in the absence of STOML3. Exemplary physiological traces are shown in C (littermate controls lacking the Cre), D (*stoml3* conditional deletion animals) and E (*stoml3* conditional deletion animals in the naïve condition) to illustrate the difference in activity. CM activity from *stoml3* conditional deletion animals following neuropathic injury was decreased even below the activity levels of naive controls. Controls: *stoml3*$^{fl/fl}$; *stoml3* conditional deletion: wnt1-cre::*stoml3*$^{fl/fl}$.

In general, small (as well as intermediate and large) mechanical stimuli induce increased activity in this part of the C-fiber system and the absence of STOML3 provided complete protection from the emerging sensitization phenotype. In some cases, the force thresholds of CMs from *stoml3* conditional deletion animals were even elevated. If activity in CMs is linked to paw-withdrawal responses in experimental animals, this change in physiology provides an explanation for the lack of aversive behaviour observed in *stoml3* conditional deletion animals following neuropathic injury.

Finally, I wanted to investigate in more detail the dynamic-phase coding properties. I stimulated the C-fibers of the last experimental cohort with a vibration-step protocol.

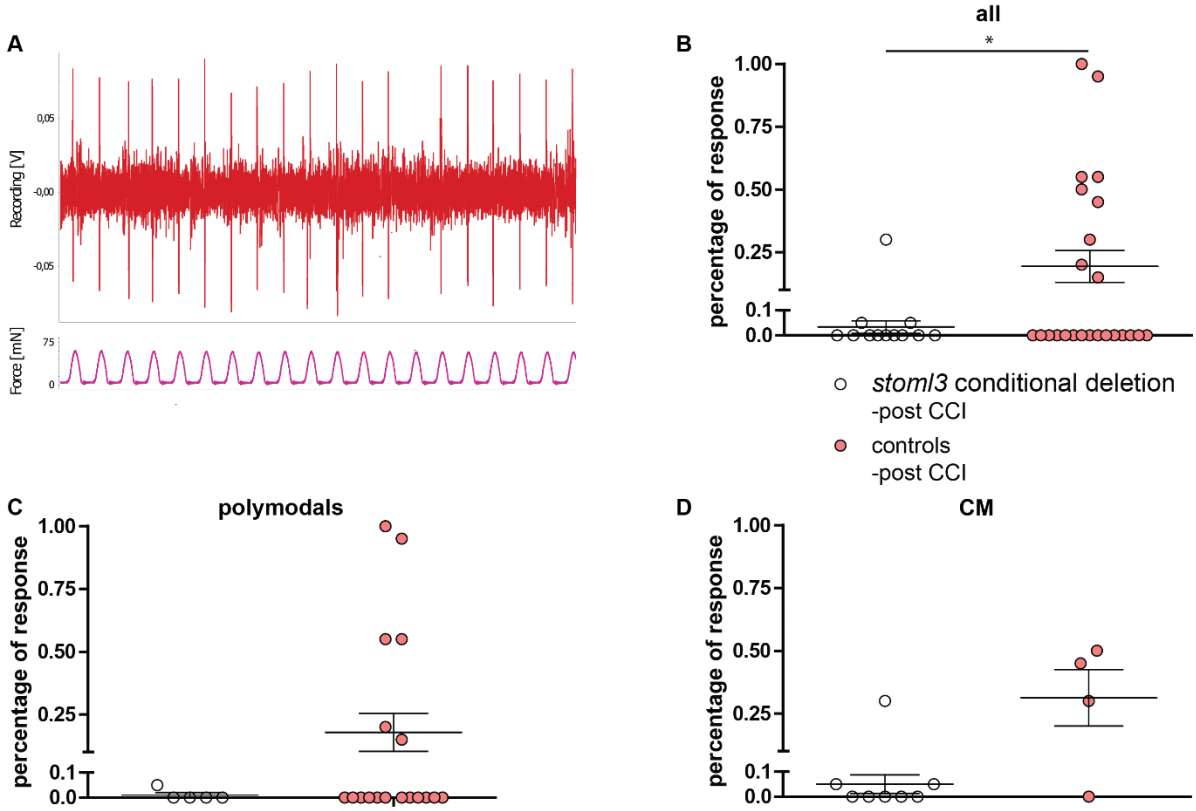

Figure 48 – Sensitized C-fiber nociceptors gain dynamic-phase coding properties in the neuropathic condition – vibration encoding

C-fibers in the neuropathic condition (*stoml3* conditional deletion animals and littermate controls) were stimulated with a vibration-step protocol consisting of 20 indentations with a frequency of 5Hz (shown in A) in 6 cycles with increasing indentation force – in this case 55mN. B shows the summary of occurring responses. Genetic ablation of *stoml3* prevents C-fibers from following this kind of stimulation. Only one C-fiber followed a few vibrations (every third wave). However, over a third of C-fibers (9 out of 24) followed these slow vibrations and few examples even displayed phase-locking. Using a Fisher's exact test on the responders and the percentage of response yielded a significant difference between the two groups ($p<0.05$). Polymodals and CMs were not analyzed separately since the n-number was too small. An example of the accuracy with which this stimulus is being encoded is shown in A. In C (polymodal C-fibers) and D (true mechanonociceptive C-fibers) the C-fiber population was divided to investigate if this phenomenon could be attributed to a specific subset of receptors – both polymodal C-fibers and CMs can follow vibrations in the sensitized state. Controls: *stoml3*$^{fl/fl}$; *stoml3* conditional deletion: wnt1-cre::*stoml3*$^{fl/fl}$.

20 indentations with a frequency of 5Hz in 6 cycles with increasing indentation force were used to stimulate C-fibers following neuropathic injury (from the *stoml3* conditional deletion animals and the littermate controls). C-fibers should not transduce these vibrations. Here, I will present data from the two last stimulation intensities, 55mN and 70mN (the force spectrum that is around threshold for most of the C-fibers following neuropathic injury).

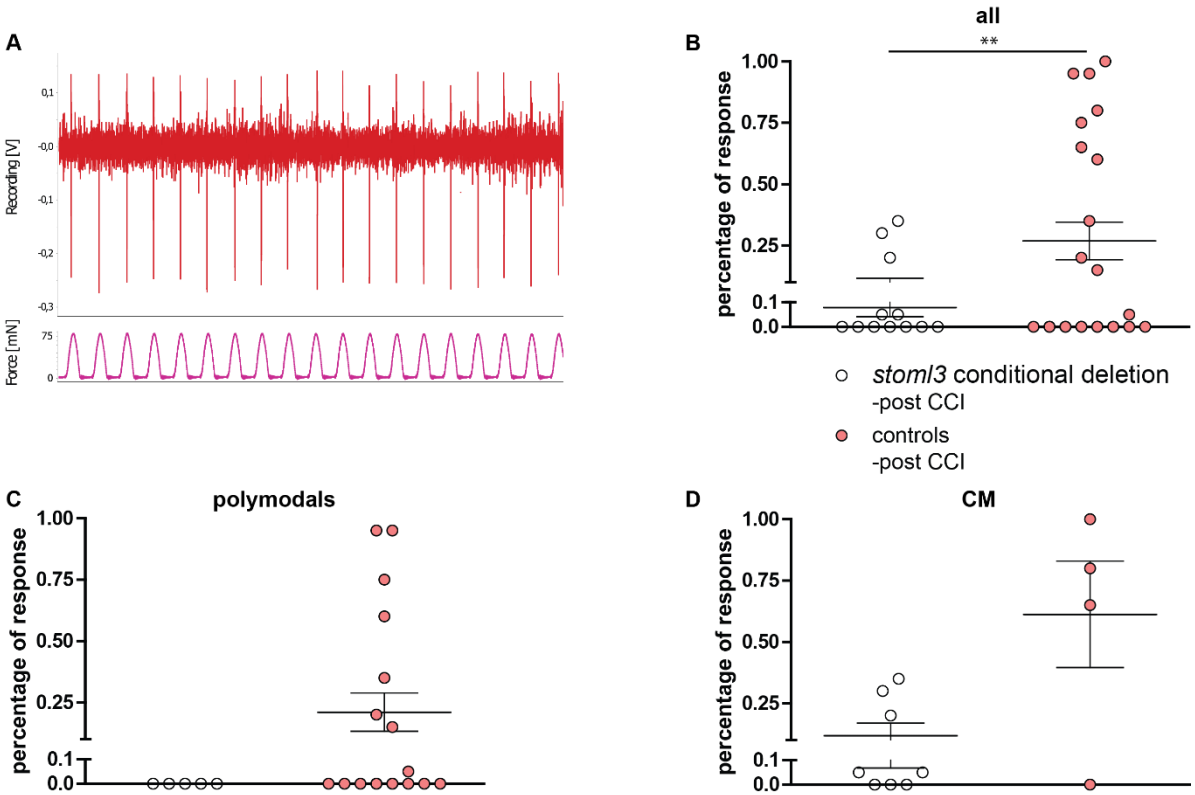

Figure 49 – Sensitized C-fiber nociceptors gain dynamic-phase coding properties in the neuropathic condition – vibration encoding with higher intensity

C-fibers in the neuropathic condition (*stoml3* conditional deletion animals and littermate controls) were stimulated with a vibration-step protocol consisting of 20 indentations with a frequency of 5Hz (shown in A) in 6 cycles with increasing indentation force – in this case 70mN. B shows the summary of observed responses. With increasing intensity more C-fibers from the *stoml3* conditional deletion animals followed the vibration to some extent (approximately every 5th wave) – interestingly these C-fibers were all CMs (see C and D). However, with this intensity around 50% (10 of 19) of the C-fibers from the littermate controls followed these slow vibrations and few examples even displayed phase-locking. Using a Fisher's exact test on the responders and the percentage of response yielded a significant difference between the two groups ($p<0.01$). Polymodals and CMs were not analyzed separately since the n-number was too small. An example of the accuracy with which this stimulus is being encoded is shown in A. In C (polymodal C-fibers) and D (true mechanonociceptive C-fibers) the C-fiber population was divided to investigate if this phenomenon could be attributed to a specific subset of receptors – both polymodal C-fibers and CMs can follow vibrations in the sensitized state. However, it seemed that most of the CMs gain the ability to transduce vibration, whereas for polymodal C-fibers only between a third and half of the population acquired this ability. Controls: *stoml3*$^{fl/fl}$; *stoml3* conditional deletion: wnt1-cre::*stoml3*$^{fl/fl}$.

As shown in Fig.48 with a 55mN stimulation intensity, over a third of C-fibers (9 out of 24) followed these slow vibrations and few examples even displayed phase-locking shown in

Fig.48B. Genetic *stoml3* ablation prevents C-fibers from following this stimulation. Only one C-fiber followed a few vibrations (every third wave). Using a Fisher's exact test with the responders and the percentage of response yielded a significant difference between the two groups ($p<0.05$). Dividing the C-fiber population into polymodal C-fibers and true mechanonociceptive C-fibers showed, that in principle both sub-populations can acquire the ability to follow vibration stimuli.

Increasing the stimulation intensity increased the percentage of units transducing the vibrations and also the percentage of responses to the 20 waves. With 70mN intensity around 50% (10 out of 19) of C-fibers from the littermate controls followed these slow vibrations and few examples even displayed phase-locking. More C-fibers from the *stoml3* conditional deletion animals followed the vibration to some extent as well (approximately every 5^{th} wave) – interestingly these C-fibers were all CMs (see Fig.49C and D). Using a Fisher's exact test with the responders and the percentage of response yielded a significant difference between the two groups ($p<0.01$) Both polymodal C-fibers and CMs can follow vibrations in the sensitized state. However, it seemed that most of the CMs gain the ability to transduce vibration, whereas for polymodal C-fibers only between a third and half of the population acquired this ability.

To summarize this set of experiments: STOML3 is essential for the emerging sensitization of C-fibers following neuropathic injury. C-fibers after CCI displayed a drastic increase in activity (be it from polymodal C-fibers or CMs). The overall population additionally displayed reduced force thresholds, characteristic of peripheral sensitization. The *stoml3* conditional deletion animals also displayed reduced mechanical thresholds, however their physiological activity was not elevated (for CMs) or showed intermediate phenotypes (polymodal C-fibers). Dynamic-phase coding properties re-emerged in these experiments. In the *stoml3* conditional deletion animals polymodal C-fibers also showed increased activity in the first second of the stimulation, however in CMs, this physiological abnormality was completely abolished. STOML3 seems to be essential for proper CM mechanotransduction and for polymodal C-fibers it seems to at least be involved in activity maintenance. However, there must be another mechanism or influence on the onset of mechanical transduction response in these receptors, since in the *stoml3* conditional deletion animals the initial elevated dynamic-phase response was not abolished or even modulated. Finally, I showed that sensitized C-fibers acquired the ability to follow low frequency (5Hz) vibrations. In some cases, to the extent of phase-locking, and in some cases with less accuracy. High stimulation strengths were necessary to induce activity in CMs in the *stoml3* conditional deletion animals, polymodal C-fibers lacking STOML3

did not respond to this type of stimulation at all, further evidence that STOML3 is important for regulating dynamic mechanosensitivity of C-fibers.

4 Discussion

4.1 Assessing targeted modulation of sensory mechanotransduction to wind down neuropathic pain using CCI

Neuropathic pain is a consequence of partial- or complete lesion of somatosensory afferents (Decosterd & Woolf, 2000). In this thesis I have shown that a consequence of applying the chronic constriction injury (CCI) to the sciatic nerve is that experimental animals display mechanical hypersensitivity. I acquired data that describes the behaviour of affected animals as well as the underlying physiological changes in sensory afferents. Neuropathic animals showed a drastic decrease in paw-withdrawal thresholds in the classical von Frey assay as well as an asymmetrical gait with reduced ipsilateral weight bearing, determined by gait analysis. *Ex-vivo* skin nerve recordings showed a reduction in mechanical threshold for C-fiber nociceptors as well as the acquisition of dynamic-phase coding properties that are completely atypical for these sensory receptors. Still an important question remains as to whether these findings are specific to the CCI model.

Currently, there is some disagreement in the field as how to best model neuropathic pain. Several models to produce neuropathic pain in experimental animals have been developed to study the disease mechanism. The CCI model was invented first (Bennett & Xie, 1988), followed by modifications of the methodology. In the CCI model loose ligations of the entire sciatic nerve are used, whereas the Seltzer model (Seltzer et al., 1990) applies a tight ligation to only a part of the sciatic nerve and the spinal nerve ligation (SNL) (Kim & Chung, 1992) ligates an entire spinal segmental nerve. These models all produce constriction, but not transection of peripheral nerves – meaning that there will always be intact as well as degenerating or degenerated neurons abundant in the nerve and that there is possible crosstalk between these populations. In 2000 the so-called spared-nerve injury model (SNI) (Decosterd & Woolf, 2000) was introduced. The SNI model involves a transection of two of the three sciatic branches, the tibial nerve and the common peroneal nerve while the sural nerve is left intact. It results in prolonged mechanical hypersensitivity and the authors describe its main advantage over previously existing models as “prevention of crosstalk between injured and intact axons in the peripheral nerve”. This approach is not without drawbacks. For example, it remains unclear whether limiting crosstalk between intact and degenerating axons is really advantageous if one wants to create a globally applicable disease model to investigate its mechanism (e.g. a component of the disease might result from crosstalk). Altered peripheral input after nerve injury might be one of the main drivers of the emerging pain-phenotype.

Eliminating this component might then obscure crucial information needed to develop effective treatments.

Most traumatic nerve injuries in the human population are due to stretch-related injuries, laceration or compression (Althagafi & Nadi, 2019). According to the Sunderland grading system (Sunderland, 1951), nerve injuries are categorized by the degree of changes induced in the normal structure of the nerve from 1 to 5. 1 represents preserved axonal continuity and 5 a completely severed nerve trunk. Categories 3 and 4 include axonal Wallerian degeneration and ultimately present with a disorganized internal structure in which nervous tissue is ultimately transformed to connective tissue. Based on our own anatomical investigation of nerve tissue following CCI, I would categorize the effect of the CCI on peripheral nerve tissue as Sunderland category 2 to 3. However, ultrastructural analysis revealed the presence of healthy axons in these damaged nerves as well (Fig.13). A study evaluating traumatic injuries in 5.777 patients (Noble, Munro, Prasad, & Midha, 1998) over a decade (1986 - 1996) categorized the incidence of peripheral nerve injury according to Sunderland and found that 48 cases could be classified as category 5, however, 44 cases were classified as category 1, 66 as category 2 and 39 as category 3 and 4. Thus complete transections as modelled by the SNI were rare and therefore one must ask if it is really a suitable model to gain generalized insights into pathological processes occurring in neuropathic conditions. One needs to carefully evaluate the research question and apply the model most suited to it. Our efforts to develop novel analgesics targeting sensory mechanotransduction pathways to alleviate neuropathic pain required the use of a model in which intact sensory afferents are present. Mechanical hypersensitivity observed in behavioural experiments is likely caused by abnormal sensory input which is relayed to higher-order integrative centers in the brain, producing ongoing pain. Targeting this exaggerated input using SNI would not be possible, since the connection of the peripheral sense organ (the skin) and the spinal cord is severed. Nevertheless, the development of therapeutic interventions will benefit from a comprehensive understanding of pain aetiology, across multiple injury models, making it valuable to consider not only the mechanisms at play in CCI, but also in SNI.

4.2 How does pain emerge in the spared-nerve injury model?

The emergence of pain in the SNI model is most likely due in part to central sensitization: “the increased responsiveness of nociceptive neurons in the central nervous system to their normal or subthreshold afferent input” (M Koltzenburg et al., 1994; Sandkühler, 2009; Ziegler, Magerl, Meyer, & Treede, 1999). One study by Stucky and colleagues (Smith, O’Hara, & Stucky, 2013) tried to assess the contribution of cutaneous sensory afferents to SNI-induced mechanical

hypersensitivity. They performed *ex-vivo* skin nerve recordings on the sural nerve (which is the intact branch of the sciatic nerve in SNI) and found enhanced suprathreshold firing in A-mechanonociceptors (AM) and C-fibers. However, mechanical thresholds of SNI and control (naïve) C-fibers were the same and sham thresholds were elevated to almost double that of controls. An increased activity in this study could be attributed to the lack of classification of C-fibers. As I demonstrated in this thesis work, it is crucial to classify C-fibers further into CMs and polymodals, since their responses to mechanical stimuli differ drastically (Milenkovic, Wetzel, Moshourab, & Lewin, 2008; Moshourab, Wetzel, Martinez-Salgado, & Lewin, 2013). An increase in activity observed in this study could be due to more recorded CMs in the SNI group compared to more polymodal C-fibers in the controls. Smith et al. also found a decrease in the abundance of SA-LTMRs but provide no explanation. The intact nerve should not differ in its abundance of fiber types since no neurons were degenerating because no direct damage was imposed on the tissue. In general, the changes reported in this study were of very small amplitude and statistically borderline.

In this thesis I present data indicating that neuropathic pain using CCI as a model, is associated with the sensitization of receptors in the periphery (peripheral sensitization) and that attenuation of harmful sensory input can alleviate pain responses in experimental animals. This mechanism is dependent on STOML3, specifically the inhibition of STOML3 self-oligomerisation (Wetzel et al., 2017). Mechanically gated ion channels are sensitized to matrix deflection by STOML3 (Poole, Herget, Lapatsina, Ngo, & Lewin, 2014) via membrane stiffening in a cholesterol-dependent manner (Qi et al., 2015a). Preventing the sensitization of mechanically gated ion channels inhibiting STOML3 can be a promising mechanism to alleviate pain.

4.3 Description of the CCI, evaluation of neuropathic behaviour, anatomy and electrophysiological changes

The initial investigation of CCI effects on peripheral nerves was done on the anatomical level. Nerve counts from myelinated afferents were performed using light microscopy. Approximately 50% of myelinated fibers were found to be degenerating or have degenerated and subjected to Wallerian degeneration (Fig.11 and 52). These are similar numbers to reports in previously published studies. The amount of reported damage to myelinated axons varies from “a significant amount” in large myelinated fibers and a “varying degree” in small myelinated fibers (Basbaum et al., 1991) to a reported diminished axon density to approximately 64% following CCI (Surchev & Surcheva, 2011). A different study investigated the relation between fiber damage and number of surgical sutures applied, 60 to 80% of axons survived the surgery

using 1 to 3 surgical sutures respectively (Gopalsamy et al., 2019). I could thoroughly and accurately quantify degeneration in peripheral nerves since myelinated fibers are big enough to investigate using light-microscopy and hence whole nerves were evaluated in sections and repeated in 12 animals. The investigation of the C-fiber system was more difficult. Electron microscopy was applied to investigate unmyelinated C-fibers. The increased resolution enables the experimenter to visualize tiny structures, but it is expensive and laborious which resulted in a reduced number of samples investigated (n=4). Ultimately only approximately 2% of the nerve cross-section was investigated. My results showed no degeneration of small fibers following neuropathic injury. Distal to the constriction site more C-fibers in the injured side were observed compared to the contralateral control, resulting in an increased C:A fiber Ratio (Fig.12).

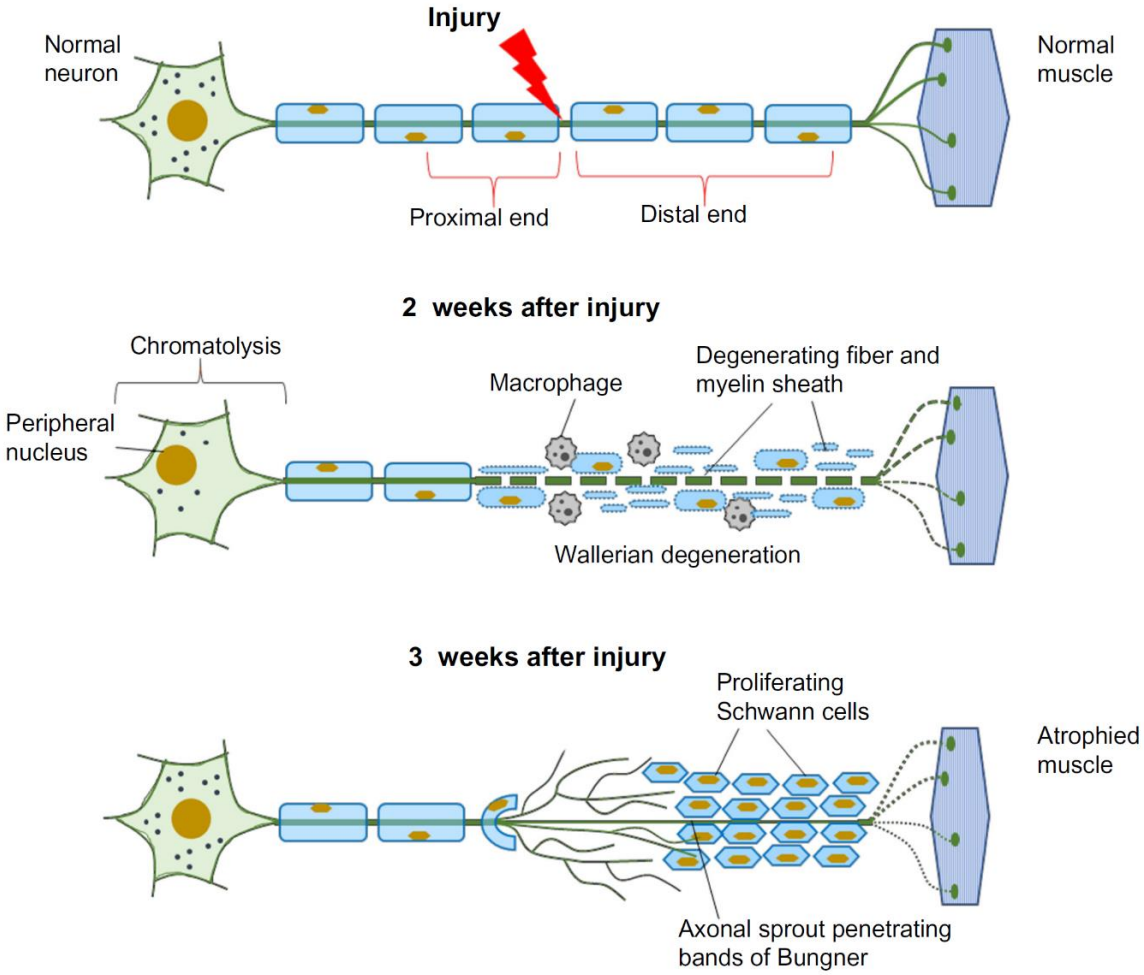

Figure 50 – Physiological cascade following peripheral nerve injury

Peripheral nerve injury results in de-afferentiation. Shortly after injury onset, macrophage-infestation and degeneration of myelin-sheaths (predominantly of large myelinated axons) can be observed (Wallerian degeneration). Following degeneration, the nervous system attempts to regenerate missing connections to peripheral tissue (in this example muscle, scheme taken from Arslantunali, Dursun, Yucel, Hasirci, & Hasirci, 2014) by regrowing axons from the proximal nerve stump, so-called axonal sprouts can be detected.

It is possible, that some regrowing axonal sprouts (Fig.52) were mistaken for C-fibers (there is no way to distinguish them) increasing the count on the ipsilateral side, distal to the injury.

Earlier studies investigating anatomical changes in peripheral nervous tissue found degeneration in the C-fiber system in addition to myelinated fibers (Basbaum et al., 1991). Constriction of the sciatic nerve and thereby induced damage does not injure the nerve in a homogeneously distributed fashion. There are fascicles that are devastated next to fascicles that appear almost normal despite injury (Fig.53). Yet a continual confound in both this study and our own is the low percentage of the cross-sections investigated. Depending on where the EM-pictures are taken, samples can display only thickly myelinated fibers, or myelinated fibers with C-fiber Remak-bundles in varying abundance.

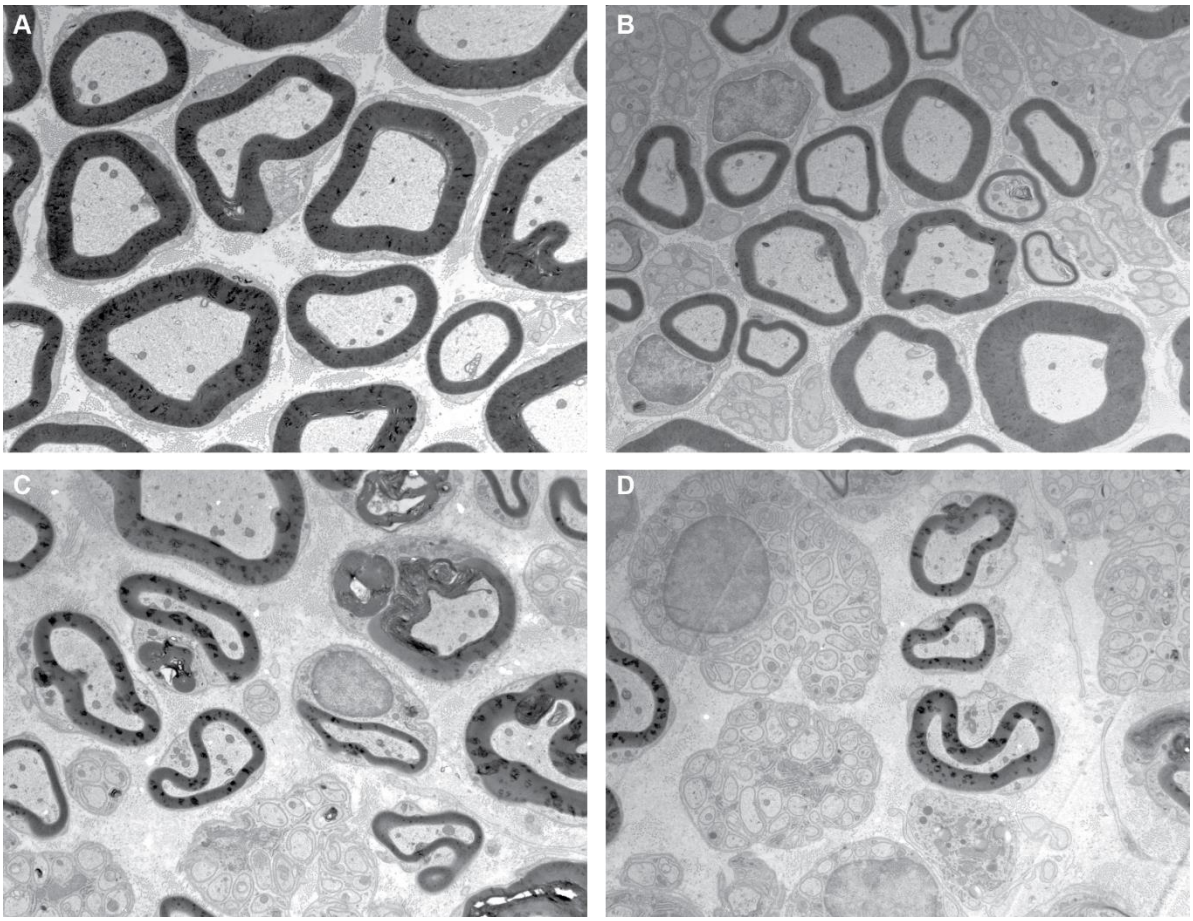

Figure 51 – Damage to peripheral nerve fascicles is not homogeneous – varying degree of degeneration

The disadvantage of electron microscopy in investigating peripheral damage following CCI. Pictures A and B are examples of healthy nerves. Depending on where the image is taken, only myelinated fibers are displayed (A) or myelinated fibers as well as C-fibers can be investigated (B). C and D show peripheral nerves after CCI, varying degrees of degeneration can be observed. In C there are thickly- and thinly myelinated fibers as well as some C-fibers, whereas D only contains few thinly myelinated fibers and many C-fibers. As only approximately 2% of the entire cross-section was investigated, the increased abundance of C-fibers following CCI could be coincidental, due to the small sample area.

Solely due to the sampling design it is very possible to detect varying numbers of C-fibers both before and after injury, irrespective of injury-induced effects.

There is only one way to definitively assess the degree of damage the unmyelinated C-fiber system was subjected to: Entire nerve cross-sections after constriction would have to be investigated using image-stitching algorithms to reproduce EM pictures of the entire cross-section. Regardless, the fact remains that following CCI there are myelinated fibers as well as C-fibers left anatomically intact. These neurons project through the constriction site and can therefore transmit information (spikes) from mechanoreceptors and nociceptors to the central nervous system. I investigated if this peripheral input was modulated and if such modulation (peripheral sensitization) could provide an explanation for behavioural phenomena such as allodynia.

Following anatomical characterization, experimental animals were investigated using the classical nociceptive behavioural assay: von Frey. The von Frey assay has been extensively used beginning with the original CCI characterization (Bennett & Xie, 1988) to confirm that following CCI animals develop mechanical hyperalgesia and allodynia. While the von Frey assay is therefore very useful it is not automated, but experimenter dependent. During experimenter stimulation of the animals' paw: duration of application, number of repeated stimulations required until a satisfactory response is scored and the introduction of a dynamic vibrating component of the filament are all possible ways to influence the experimental outcome and "produce" aversive responses that may reflect allodynia. Independent of experimenter error, experimental animals (especially when in pain) sometimes do not respond to stimuli (painful or not). They might be in an apathetic state or because of excessive paw-guarding (animals put their paw onto their tail or retract the paw towards the body) their paw might not be accessible for stimulation. Therefore, the assay is susceptible to experimenter bias. For this reason, we established gait analysis in the lab, to have an automated, experimenter-independent assay with which to make unbiased assessments of experimental animals pain states. The Mouse walk (Mendes et al., 2015) is an open source version of Catwalk technology (Bozkurt et al., 2008; Melorose, Perroy, & Careas, 2003). Animals with CCI use decreased pressure when placing the affected paw on the Mouse walk walkway, a parameter I also chose to evaluate to determine the pain state of mice following neuropathic injury. Recently Kang et al., 2017 evaluated CCI with the newest Catwalk technology and also described a reduced paw-print area ratio of the affected paw in addition to pressure (for details see online JOVE, Kang et al., 2017). This provides further confirmation that these parameters I independently chose are suitable for the evaluation of pain states.

Gait analysis is also not without drawbacks. The initial Catwalk paper found that in rats the reduced paw-pressure following neuropathic injury was only detectable for 8 weeks after injury. Also, possible changes in gait parameters describing the actual gait (and not static parameters such as pressure and area) may be influenced by the injury. During CCI it is possible to nick muscles of the leg such as the biceps femoris, which could possibly introduce a limp in the animals' gait. However, studies using inflammatory pain models such as intra-articular (knee-joint) injection of CFA (complete Freund's adjuvants, inactivated and dried *Mycobacterium tuberculosis*) to model arthritic pain used gait analysis to characterize the emerging pain behaviour and possible analgesic effects of indomethacin using the paw-print area parameter as well (Parvathy & Masocha, 2013). Crucially, they found that paw print area and pressure intensity could be used to monitor developing arthritic pain and indomethacin-mediated analgesia. In this assay, there is no muscle component that could affect these static parameters and therefore I believe it is reasonable to use them for the assessment of the neuropathic status.

4.4 What causes allodynia after CCI?

In initial experiments, the electrophysiological investigation of constricted peripheral nerves, revealed that recording from primary afferents proximal to the neuropathic injury (between ligatures and DRGs as opposed to the usual recording site, which was distal to the injury as indicated in Fig.6) was possible. This experiment was undertaken to prove that indeed following CCI there are intact sensory afferents that conduct information through the ligation site and therefore proving that peripheral input could drive behavioural changes observed after surgery such as reduced paw-withdrawal thresholds. If sensory neurons survived the injury, that must mean they conduct APs through the ligation site and the electron microscopy (discussed in the previous section) proved that proximal and distal to the injury there are indeed numerous healthy looking thickly- and thinly myelinated afferents as well as unmyelinated C-fibers present. On the other hand, if a sensory axon was damaged or destroyed (the connection from peripheral terminal to cell body in the DRG was severed) it would undergo degeneration and no recordings at sites distal to the injury could be possible.

I found that the physiological properties of LTMRs were not altered following CCI, except for a diminished static phase activity in SAMs (Fig.15C). I could not find evidence for a peripheral driver such as threshold reduction (sensitization) or increased activity for mechanical allodynia or hyperalgesia investigating LTMRs (see Figures: 14,15 and 16). Electron microscopy demonstrated a decreased abundance of myelinated neurons associated with LTMRs, but the receptors were physiologically unaltered. This cannot eliminate the possibility that loss of

LTMRs might be centrally translated into neuropathic pain, but based on the results presented here, I would argue against LTMR contributions in the periphery for the emergence of pain that were postulated to be causal for neuropathic pain by earlier studies such as (Clifford J. Woolf & Doubell, 1994). They argued that C-fiber activation increased the excitability of spinal neurons and consecutively low intensity stimulations usually mediated by LTMRs would produce painful sensations (allodynia) through altered connectivity or sprouting of Aβ-fiber terminals from Lamina IV to Lamina II in the dorsal horn (Koerber, Mirnics, Brown, & Mendell, 1994; Kohno et al., 2003; Clifford J. Woolf, Shortland, & Coggeshall, 1992). Through this mechanism LTMR input would gain direct access to the central pain pathway. Although, subsequent experimental studies have failed to confirm this anatomical plasticity, making it unlikely that an altered LTMR connection to Lamina II is a key/main contributor to the onset of neuropathic pain.

Investigation of nociceptors revealed that firstly AMs did not display any physiological alterations in the neuropathic state (Fig.17). However, sensitization following neuropathic injury could be shown in C-fibers. Testing stimulation forces of up to 200mN revealed a significant reduction in mechanical thresholds (Fig.20) as well as emerging dynamic-phase coding properties (Fig.21) that resulted from the chronic constriction injury. These alterations in physiological properties could explain in part the phenomenon of mechanical allodynia. Stimuli that would under normal circumstances not induce activity in the nociceptive C-fiber system now do so following CCI. This was indicated in Fig.20 and 29, where C-fiber thresholds below approximately 45mN were highlighted by a blue box, since they exhibited mechanical thresholds comparable to RAM-LTMRs.

In the initial physiological characterization of physiological properties of somatosensory afferents following neuropathic injury, recordings were performed from every afferent neuron that was encountered (in the naïve and CCI condition). This enabled me to investigate if the proportions of mechanoreceptors and nociceptors in both conditions were altered. In naïve conditions recordings from 147 neurons were performed – and compared to 153 separate recordings performed following CCI. Indeed, following CCI a significant shift ($p<0.05$, χ^2-test) towards the numbers of nociceptors could be found. This reflects the anatomical data displayed in Fig.12 and Fig.13F. Following CCI approximately 50% of myelinated afferents degenerate, whereas no decrease in the number of C-fibers was observed. Therefore, it is plausible that following neuropathic injury proportionately more nociceptors were recorded, and that nociceptive input plays a more pronounced role in the overall sensory input of animals experiencing neuropathic pain.

How do these findings apply to theories explaining pain emergence?

4.4.1 Theories explaining the emergence of pain sensation

Research aimed at understanding, conceptualize and explain the emergence of pain is ongoing for a long time. One of the first theories, now termed “intensity theory”, is based on observations from historical scholars Plato and Aristotle. It was postulated that pain resulted from excessive stimulation of the sense of touch (intensity and central summation in the dorsal horn were stated as defining factors of emerging pain) by Erb (1874, Fig.54A) referenced in (Chen, 2011; Moayedi & Davis, 2013; E. R. Perl, 2007). “Specificity theory” by von Frey (1895, Fig.54B - again referenced in Chen, 2011; Moayedi & Davis, 2013; E. R. Perl, 2007) argued that the body has specific sensors for pain (nociceptors) that would upon stimulation send information about the painful stimulus to higher order centers in the brain. Contrasting that, the “pattern theory” ignored the abundance of specialized receptors for modality-specific stimuli and argued that there were no separate systems for pain and other components of somatosensation (Fig.54C). Pain emerges as a consequence of activity in receptors transducing innocuous- as well as painful and thermal stimuli by the temporal pattern of signals sent to the nervous system. Certain patterns of neural activity would thus be the explanation for painful sensations according to Goldschneider (1884, again referenced in (Chen, 2011; Moayedi & Davis, 2013; E. R. Perl, 2007). A few more experimental and theoretical additions to the development of theoretical explanations for pain emergence were made consecutively, leading to the at that time very controversially discussed theory – the Gate Control Theory (Fig.54D, Melzack, 1996; Melzack & Wall, 1967). Painful stimuli are mediated by small-caliber fibers with slow conduction velocities, relaying information to the dorsal horn of the spinal cord where they synapse onto so-called transmission cells (T-cells in the substantia gelatinosa, Lamina II), that further relay information to higher order centers in the brain. These T-cells serve as a “gate”, information can pass through or flow of information can be inhibited, for instance through activity in the large-fiber system (LTMRs). The state of the “gate” is influenced by the amount of activity in the small-fiber system, the amount of activity in the large-fiber system and descending modulatory input from the brain. The stronger the noxious stimulus, the more likely that modulatory input from the brain or simultaneous input from the large-fiber system would be overcome and transmission of nociceptive information to the brain occurs. This model also gave rise to a more recent theory, the so-called neuromatrix (Melzack, 1996) since it could not explain the emergence of certain pain conditions like phantom-limb pain. Therein it was proposed that the body-perception of humans resulted from sensory input and that these percepts form an intrinsic imprint of the body into the brain. Even if body-parts would be missing (amputations), they would still be present in our imprint and information to missing body-areas would still be created throughout life. The gate-control theory however is still used to model pain conditions to date (Ropero Peláez & Taniguchi, 2016).

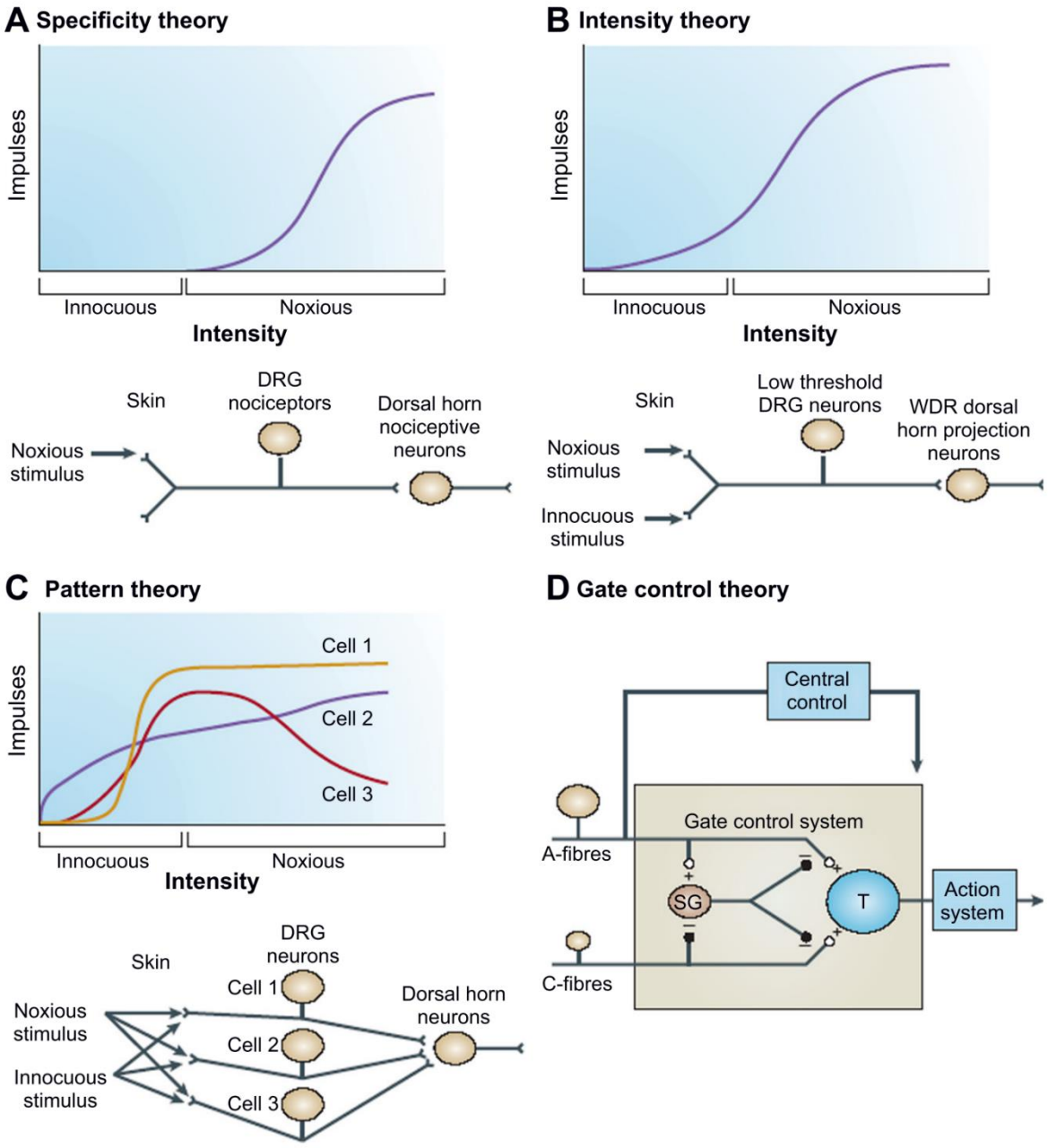

Figure 52 – Schematics of pain theories

A, specificity theory: the body has specific sensors for pain (nociceptors) that would upon stimulation send information about the painful stimulus to higher order centers in the brain. B, intensity theory: pain resulted from excessive stimulation of the sense of touch (intensity and central summation in the dorsal horn were stated as defining factors of emerging pain). C, pattern theory: Pain emerges as a consequence of activity in receptors transducing innocuous- as well as painful and thermal stimuli by the temporal pattern of signals send through the nervous system. Certain patterns of neural activity explain painful sensations. D, gate-control theory: large- and small fibers synapse onto T cells. If these transmission cells relay noxious information to higher order centers depends on the amount of activity in the small-fiber system, the amount of activity in the large-fiber system and descending modulatory input from the brain. The stronger the noxious stimulus, the more likely that modulatory input from the brain or simultaneous input from the large-fiber system is overcome, resulting in pain perception (Taken from E. R. Perl, 2007).

Applying a parsimonious computational model successfully yielded no “pain-relay” if mechanoreceptor input alone was fed to the gate circuit or when mechanoreceptor- and nociceptor inputs were both presented. Challenging their system with non-standard parameters to model various pain conditions was successful. The only edits to the original gate-control theory that were considered were an excitatory only afferent input to the “gate”.

I will also argue that according to gate-control theory, emergence of pain following CCI can be understood and explained well. Since my data showed a definitive loss of LTMR input following CCI and C-fibers gain dynamic-phase coding properties it is therefore plausible that the baseline tonic state of the “Gate” might be more easily influenced by the small fiber system input to relay information being perceived as painful (again taking into account that there is a significant increase in the abundance of nociceptors vs. mechanoreceptors recorded following neuropathic injury). Specifically, the dynamic-phase coding properties observed result from an increased activity generation in C-fiber nociceptors to the stimulus onset and therefore are reminiscent of neural activity usually generated by rapidly-adapting LTMRs. Thus, mechanical stimuli that are usually only detected by RAMs are now being detected and relayed by sensitized C-fiber nociceptors creating the sensory paraesthesia: allodynia. Additional support for this hypothesis comes from the vibration-sensitivity experiment shown in Fig.48 and 49. Sensitized C-fiber nociceptors (especially CMs) were in some cases even phase-locked to low-frequency vibrations. A physiological characteristic observed in RA-LTMRs, which is rarely observed in C-fiber nociceptors.

4.5 How can sensory neuron physiology be modulated?

When applying a surgical technique to induce neuropathic pain an obvious concern is the associated inflammation response and possible effects of inflammatory mediators or cytokines on sensory neuron physiology. Nociceptor sensitivity especially, is largely modulated by inflammatory mediators. The second messengers cAMP and Protein Kinase A (PKA) were implicated in sensitization of nociceptors (Kress, Rödl, & Reeh, 1996) and activators of Protein Kinase C (PKC), which was also found to depolarize and activate nociceptors (Burgess, Mullaney, McNeill, Dunn, & Rang, 1989) mimicking the effect of bradykinin. True inflammatory mediators: bradykinin (Cesare & Mcnaughton, 1996), tumor necrosis factor alpha (TNFa) (Parada, Yeh, Joseph, & Levine, 2003), carrageenan, epinephrine (Khasar, Mccarter, & Levine, 1999) as well as protease-activated receptor (PAR2) (Amadesi et al., 2006) amongst others mediate nociceptor sensitization to thermal- and mechanical stimuli. Nerve growth factor (NGF) signalling is crucial for the functional maintenance of nociceptors and is involved in emerging heat- and mechanical hyperalgesia in inflammation (Fig.53, Gary R. Lewin &

Nykjaer, 2014). Many sensory neurons express and produce neurotrophins and proNeurotrophins (such as NGF or BDNF, proNGF or proBDNF, Ernfors, Wetmore, Olson, & Persson, 1990; Pang et al., 2004; Teng et al., 2005; N. H. Woo et al., 2005) and the release of neuropeptides mediated by BDNF (enhanced by elevated levels of NGF induced by inflammatory processes (Balkowiec & Katz, 2000; Lever et al., 2001)) from sensory neurons may strengthen or weaken spinal synapses (Seybold, 2009).

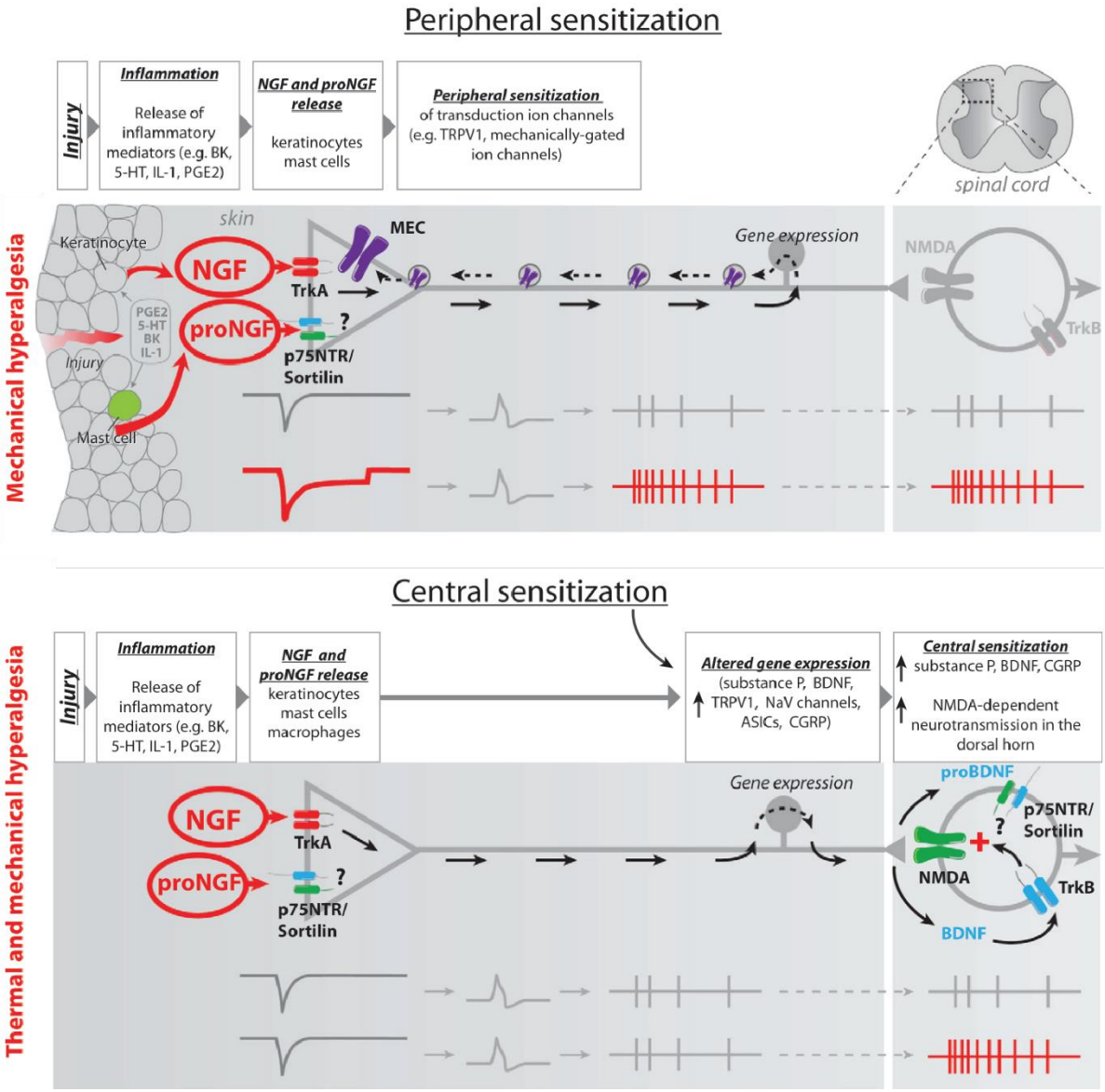

Figure 53 – Mechanisms contributing to neuropathic pain sensory phenotypes

A, peripheral sensitization is dependent on NGF secretion after injury (such as neuropathic injury). NGF may sensitize nociceptors to mechanical stimuli, transduction currents of sensory neurons may be increased, leading to increase firing rates in response to mechanical stimuli. Additionally, NGF may induce increased synthesis and trafficking of mechanosensitive ion channels from the cell body to the periphery. B, central sensitization: also dependent on NGF signalling may increase the expression of sensory neuron proteins in the cell body. NGF-induced BDNF signalling then can affect the physiology of neurons of the dorsal horn leading to central sensitization (taken from Gary R. Lewin & Nykjaer, 2014).

Release of BDNF from nociceptor central terminals might be causal for NMDA receptor sensitization (Kerr et al., 1999) via phosphorylation of its NR1 subunit (Pezet & McMahon, 2006) and enhances synaptic transmission (Garraway, Petruska, & Mendell, 2003).

Inflammation is also known to activate spinal microglia which release BDNF or proNeurotrophins (Srinivasan, Roque, Hempstead, Al-Ubaidi, & Roque, 2004) modulating dorsal horn neuron excitability, rendering inhibitory interneurons ineffective (Coull et al., 2005). Activated microglia are crucial for the initiation of neuropathic symptoms (Tsuda, Beggs, Salter, & Inoue, 2013; Tsuda et al., 2003) such as allodynia. Confined mechanical hyperalgesia was produced by rhNGF injections into skin (Rukwied et al., 2010; Obreja et al., 2011; Weinkauf, Obreja, Schmelz, & Rukwied, 2012) indicating peripheral sensitization processes through nociceptor sensitization (Gary R. Lewin & Moshourab, 2004), however this must be in a STOML3 independent manner, since STOML3 was not implicated in inflammatory pain (Wetzel et al., 2017).

Anti-NGF antibodies can reduce inflammatory pain (Gary R. Lewin, Lechner, & Smith, 2014; Gary R. Lewin, Rueff, & Mendell, 1994), leading to the generation of the only new analgesic established in the clinic in the past decades, tanezumab, which was proven to be effective in the treatment of osteoarthritic pain (Lane et al., 2010) providing pain relief and functional improvement with only mild to moderate side-effects. Anti-NGF therapy in rats following chronic constriction injury proved to be effective in abolishing heat- and cold hyperalgesia and reduced autotomy behaviour (Long Sun Ro, Chen, Tang, & Jacobs, 1999) and it reduces bone cancer pain and central- as well as peripheral sensitization markers (Sevcik et al., 2005).

4.5.1 Inflammatory- and immune mechanisms in neuropathic pain

Inflammatory and immune mechanisms play an important role in the peripheral nervous system and must also be considered in order to fully understand changes in sensory neuron excitability and overall physiology occurring during disease states. Nervous system damage causes the infiltration of inflammatory cells (macrophages, mast cells, neutrophils; Lindborg, Mack, & Zigmond, 2017). Neutrophils were found to be the cells clearing myelin debris after axon degeneration and are therefore the main phagocytotic cells and not macrophages as formerly thought. The activation of resident immune cells (T-lymphocytes, microglia, astrocytes) contributes to the production and secretion of the aforementioned cytokines. Especially microglia, as described above, play a specific role in central sensitization. Some cytokines directly sensitize nociceptors by acting on neuronal receptors (Pitchford & Levine, 1991) and directly influence pain behaviour in animal models for inflammation and neuropathic pain (Cook, Christensen, Tewari, McMahon, & Hamilton, 2018; White, Bhangoo, & Miller,

2005). On the other hand, nociceptors secrete neuropeptides that modulate adaptive- and innate immune cell activity (Baral, Mills, Pinho-Ribeiro, & Chiu, 2016; Baral, Udit, & Chiu, 2019; Chiu, Von Hehn, & Woolf, 2012; Pinho-Ribeiro, Verri, & Chiu, 2017). Increased sensitivity to mechanical- (or thermal) stimuli in peripheral sensitization is induced by inflammatory cells and -mediators, which requires nociceptors to express receptors to detect them (Cook et al., 2018; Pinho-Ribeiro et al., 2017). Ultimately, activity from inflammatory mediators results in membrane conductance property modification and altered gating properties of ion channels. In the dorsal horn of the spinal cord membrane excitability and synaptic transmission are altered.

TNF injections into joints of experimental animals induced mechanical hypersensitivity (Richter et al., 2010) and application to DRG neurons increased their excitability downstream of the receptor (TNFR1) through p38 signalling and TTX-resistant sodium channels (Jin, 2006). Blocking of p38 signalling prevented hyperalgesia. In the CNS, TNF is secreted by microglia and astrocytes, increasing excitatory postsynaptic currents and synaptic transmission in the dorsal horn (Ji, Xu, & Gao, 2014; Zhang et al., 2011). Another cytokine, IL-1ß, was found to increase the generation of APs in nociceptors in response to thermal- and mechanical stimuli (Fukuoka, Kawatani, Hisamitsu, & Takeshige, 1994) through Na_V 1.8 sensitization (Binshtok et al., 2008). Again, microglia produce this cytokine mediating central sensitization in the dorsal horn. IL-17A produced hyperalgesia in mice, a process found to be depending on neutrophil recruitment and TNF signalling (McNamee et al., 2011).

Modified ion channel activity is a key process in pain emergence, implicated are $Na_V1.7$ (TTX-sensitive), $Na_V1.8$ and $Na_V1.9$ (both TTX-resistant), which are highly enriched in nociceptors and underlie AP generation (Dib-Hajj, Cummins, Black, & Waxman, 2010). These sodium channels are phosphorylated to facilitate open probability through NGF- and IL-1ß signalling (Binshtok et al., 2008; Jin, 2006; S. Talbot, Foster, & Woolf, 2016). Furthermore, inflammation produced via CFA injection resulted in upregulated expression of $Na_V1.7$ and $Na_V1.8$ (Black, Liu, Tanaka, Cummins, & Waxman, 2004; Strickland et al., 2008). Upregulated ion channel abundance, modified ion channel activity and central sensitization all act together to produce complex pain phenotypes such as allodynia or hyperalgesia in neuropathic conditions.

It is known that the originally applied surgical suture (chromic-gut) by itself (Maves et al., 1993) introduced inflammation in experimental animals, no such observation is known to me using silk-gut sutures. A study comparing the emergence and persistence of pain-symptoms in mice described that using CFA to produce inflammation, pain symptoms can only be evaluated for 4 days post application, whereas using CCI symptoms were easily detectable for at least 20 days (Krzyzanowska et al., 2011) post-operation. This time-course of attenuated inflammatory

responses is important for the experiments performed in this thesis-work. It is clear that an injection of CFA is not really comparable to a surgical procedure in inducing inflammatory responses. However, it provides a range in which the animals' metabolism deals with inflammation and how long it usually takes for inflammatory pain to decline. Since the sutures are left in the animals and have been implicated in the immune response it might be, that CCI has an inherent inflammatory and immunological component. Peak responses to inflammatory pain are observed up to 4 days after injury, so by investigating experimental animals' pain state 7 days post-surgery and performing the earliest recordings from sensory neurons using the *ex-vivo* skin nerve technique 8 days post-op, we can be confident that the initial inflammatory response resulting from the surgical insult had subsided at the time of recording. Thus, induced sensitization of C-fiber nociceptors that we found to be aetiological for the emergence of pain was caused by a process other than inflammation. Several studies have proven that experimentally induced inflammation using CFA induces only mild sensitization of nociceptors and can therefore not be exclusively responsible for the observed pronounced and ongoing sensitization shown in this thesis work. Sensitization of C-fiber nociceptors upon CFA mediated inflammation returned to baseline 4 days after treatment (Djouhri, Dawbarn, Robertson, Newton, & Lawson, 2001), sensitized cultured neurons displayed reduced AP thresholds as well as increased sensitivity to GABA and capsaicin but only for a maximum of 48 hours (Chakrabarti et al., 2018) and behavioural signs of CFA mediated hypersensitivity like guarding behaviour diminished 4 days after CFA treatment (Okun et al., 2011). We hypothesize that mechanical hypersensitivity arises due to STOML3s exaggerated effect on mechanosensitive ion channels in the periphery (with a possible continuous inflammatory drive). STOML3 was found to be localized in mobile transport vesicles in sensory neuron axons (Liudmila Lapatsina, Jira, et al., 2012) thus, upon nerve injury upregulated STOML3 could be transported anterogradely from DRG neuron soma to the periphery where it then sensitizes mechanically-gated ion channels. It might as well be, that inflammatory- or immune responses following neuropathic injury are the reason for increased STOML3 translation and subsequent trafficking to the peripheral terminals of somatosensory afferents. However, this would have to happen in an NGF-independent manner, since NGF injections into *Stoml3*$^{-/-}$ mice produced mechanical- and heat hyperalgesia independent of STOML3 (Wetzel et al., 2017).

4.5.2 Upregulation of ion channels modulating electrical properties of sensory neuron physiology

Electrical hyperexcitability of sensory neurons can manifest as ectopic firing (abnormal, erratic excitability of C-fiber sprouts at the injury site (referred to as the neuroma, Patrick D. Wall & Gutnick, 1974; Zimmermann, 2001)). Increased activity in injured fibers is not all that

contributes to the pathology. There is crosstalk between injured and uninjured neurons, rendering the uninjured fibers hyperexcitable (irritable nociceptors) (Fields et al., 1998; Tesfaye, Boulton, et al., 2013). These irritable nociceptors are thought to be the cause of ongoing and evoked pain in patients. The application of so-called nerve blocks (lidocaine patch, blocks VGSCs) yields pain relief (Haroutounian, 2014; Kleggetveit, 2012; Serra, 2011; Vaso et al., 2014) suggesting that peripheral input is a driver for neuropathic pain (Fig.5). Peripheral input in neuropathic cases induces the release of neuropeptides and amino acids (excitatory) leading to phosphorylation of NMDA and AMPA receptors that cause increased thalamic activity (Patel & Dickenson, 2016; Peyron, 2016). A second possible mechanism is the loss of GABAergic interneurons generating an overall loss of inhibition, contributing to emerging hypersensitivity (Gagnon et al., 2013).

Increased STOML3 expression in the periphery was discovered and described by Wetzel et al., 2017 and was the reason for generating experimental animals in which STOML3 was overexpressed *in vivo* using an inducible Cre/ERT2 system. In this work, I discovered, that the *in vivo* overexpression of STOML3 has large and robust effects on the physiological properties of mechanoreceptors and nociceptors. Specifically, that LTMRs (RAMs and SAMs) are sensitized. The effect on RAMs was very large, resulting not simply from an increase in activity or function, but to sensitization towards slower velocity stimuli (Fig.24A). SAMs displayed an increase in activity most prominently during the slowest stimuli (Fig.25A) accompanied by heightened static phase activity and a trend towards reduced mechanical thresholds.

Finally, STOML3 induced a large change in physiological properties of C-fibers. Polymodal C-fibers displayed a robust sensitization phenotype (Fig.29), with a more than doubling in maximal activity. Increased activity, lowered mechanical thresholds as well as dynamic-phase coding properties emerged after induced sensory-neuron specific STOML3 overexpression. CMs increased their activity as well albeit not as dramatically as the polymodal sub-population.

Overall, the overexpression of STOML3 in sensory neurons phenocopied the physiological changes emerging following CCI, we successfully produced allodynia without nerve injury. Animals acquired mechanical hypersensitivity and the changes in the C-fiber nociceptive system are similar to those discovered following neuropathic injury. The actual extent of this effect even appears larger in the STOML3 overexpression experiments. Taken together I believe it is very likely that increased STOML3 is a driver of pain behaviour such as allodynia through sensitization of unmyelinated C-fiber nociceptors, since the behavioural assessment of experimental animals yielded similar results and dynamic-phase coding properties were discovered only when overexpressing STOML3 in sensory neurons.

4.6 What about the LTMRs?

In the initial CCI experiments no sensitization in LTMRs was observed (only a decreased static phase response in SAMs). However, since overexpressing STOML3 in the periphery induced sensitization in RAMs and SAMs (Fig.24 and 25), why were these effects not observed in the initial characterisation of the CCI must be addressed. The anatomical investigation of constricted peripheral nerves showed degeneration of about 50% in the myelinated fibers. Furthermore, when recording from sensory afferents, not every unit displays the exaggerated (or attenuated) phenotype. This can generate very puzzling results. For instance in the investigation of Piezo2s contribution to sensory neuron mechanosensitivity (Murthy, Loud, et al., 2018a), we did not observe an abnormal RAM phenotype in all recorded units. Some displayed completely normal signal transduction properties (an unexpected result, considering Piezo2 was postulated to be the mechanosensitive ion channel essential for the mediation of low threshold mechanical stimuli). Since approximately 50% of LTMRs have degenerated following CCI, it may be that a sensitization phenotype was simply not observed.

STOML3 appears to be absolutely essential for C-fiber sensitization as shown by *stoml3* ablation experiments. C-fibers following neuropathic injury displayed a drastic increase in activity (be it from polymodal C-fibers or CMs, Fig.36 and 42). These experiments also confirmed the initial sensitization phenotype in C-fibers discovered in wildtype C57BL6/N mice. The overall population of C-fibers displayed reduced force thresholds, characteristic of peripheral sensitization. The conditional knockouts of *stoml3* also displayed reduced mechanical thresholds, however their physiological activity was not elevated (for CMs) or they showed intermediate phenotypes (polymodal C-fibers). Dynamic-phase coding properties were again observed in these experiments. In the *stoml3* knockouts polymodal C-fibers also showed increased activity in the first second of the stimulation, however in CMs, this physiological abnormality was completely abolished (Fig.42 - 47). Thus, STOML3 seems to be essential for the sensitization of CM mechanotransduction and for polymodal C-fibers it seems to at least be involved in maintenance of elevated activity. However, there must be another mechanism that influences the onset of mechanical transduction response in polymodal C-fibers, since in the conditional knockouts of *stoml3* the initial elevated dynamic-phase response was not abolished or even modulated. It might be, that nociceptive Schwann cells are more important for activity initiation in polymodal C-fibers compared to CMs (Abdo et al., 2019). The onset sensitization in polymodal C-fibers might be independent of STOML3 and driven by this Schwann cell population of the glio-neural network. Sustained activity in polymodal C-fibers was attenuated in *stoml3* ablated animals following neuropathic injury like in CMs and therefore probably largely dependent on STOML3. Finally, I showed that sensitized C-fibers acquired

the ability to follow low frequency (5Hz) vibration (Fig.48 and 49). In some cases, to the extent of phase-locking, and in other cases with less accuracy. High stimulation strengths were necessary to induce activity in CMs in the *stoml3* conditional knockouts, polymodal C-fibers lacking STOML3 did not respond to this type of stimulation at all, further evidence that STOML3 is necessary for abnormal nociceptor activity after CCI.

4.7 Possible role of Piezo channels in neuropathic pain?

The role of Piezo2 in nociception became of interest recently and might be of importance to the results shown in this study. It was already introduced that Piezo2 mediates sensitivity to mechanical pain in experimental animals (Murthy, Loud, et al., 2018b; Szczot et al., 2018b). Furthermore, inflammatory signals such as bradykinin were shown to enhance Piezo2-mediated mechanosensitive currents (Dubin et al., 2012). In general, inflammatory mediators can enhance the excitability of DRG neurons (Ma, Greenquist, & LaMotte, 2006). Spinal GABA-signalling becomes excitatory through a more depolarized resting membrane potential of (for instance) small- to medium size capsaicin-sensitive neurons (nociceptors) (Zhu, Lu, & Gold, 2012). A previous study from our lab (Moroni, Servin-Vences, Fleischer, Sánchez-Carranza, & Lewin, 2018) revealed that under normal conditions, only approximately 10% of all Piezo2 channels are available for activation. Piezo channels are modulated by voltage and neuropathic conditions associated with the abundance of inflammatory mediators might sensitize Piezo2 in a sense that the membranes of peripheral terminals incorporating Piezo2 might become more depolarized. Therefore, a larger percentage of Piezo2 channels might be recruited upon mechanical stimulation contributing to exaggerated activity as physiological basis of symptoms such as allodynia and/or hyperalgesia. My data suggests that the observed sensitization in the C-fiber nociceptive system shown in this study is due to exactly these processes. STOML3 is upregulated, transported anterogradely from soma to the peripheral terminal of sensory neurons (Liudmila Lapatsina, Smith, et al., 2012), where it localizes to membrane scaffolds incorporating mechanosensitive ion channels and through the modification of the membrane (more STOML3 yields a more stiff membrane (Qi et al., 2015b)) sensitizes Piezo2. At the same time inflammatory mediators produce a more depolarized resting membrane potential enabling more Piezo2 channels to be recruited upon mechanical stimulation ultimately potentiating the sensitization effect. This might be the physiological basis for exaggerated pain responses observed in neuropathic conditions.

The last Figure of my thesis (Fig.54) is intended to summarize the most important experimental findings:

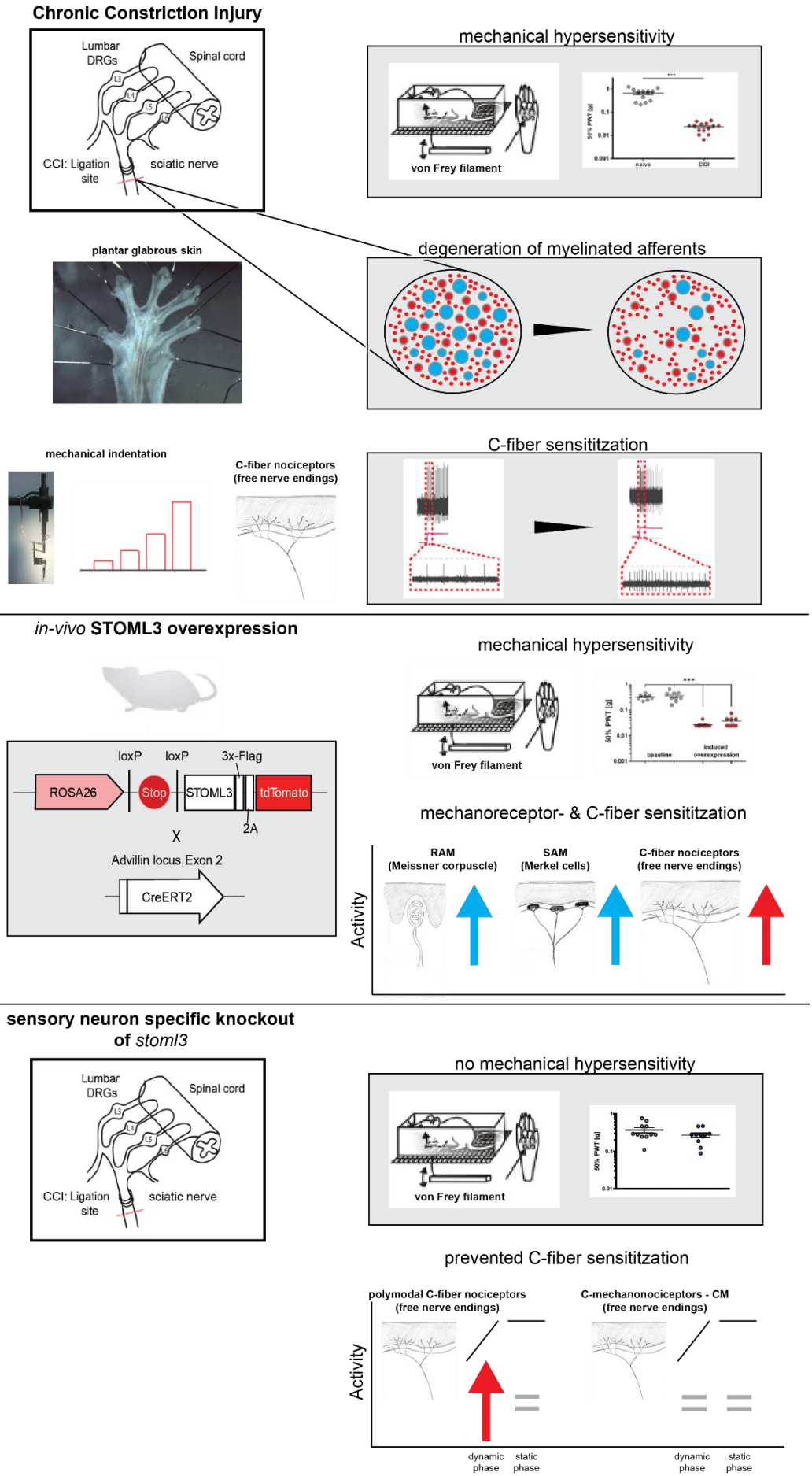
Chronic Constriction Injury
Lumbar DRGs
Spinal cord
CCI: Ligation site
sciatic nerve
mechanical hypersensitivity
von Frey filament
naive
CCI
plantar glabrous skin
degeneration of myelinated afferents
mechanical indentation
C-fiber nociceptors (free nerve endings)
C-fiber sensititzation
in-vivo STOML3 overexpression
mechanical hypersensitivity
von Frey filament
baseline
induced overexpression
loxP
loxP
3x-Flag
ROSA26
Stop
STOML3
tdTomato
2A
X
Advillin locus, Exon 2
CreERT2
mechanoreceptor- & C-fiber sensititzation
RAM (Meissner corpuscle)
SAM (Merkel cells)
C-fiber nociceptors (free nerve endings)
Activity
sensory neuron specific knockout of stoml3
Lumbar DRGs
Spinal cord
CCI: Ligation site
sciatic nerve
no mechanical hypersensitivity
von Frey filament
prevented C-fiber sensititzation
polymodal C-fiber nociceptors (free nerve endings)
C-mechanonociceptors - CM (free nerve endings)
Activity
dynamic phase
static phase
dynamic phase
static phase

Figure 54 – Summary of experimental findings

Neuropathic pain modelled by applying CCI produces mechanical hypersensitivity in experimental animals. Large myelinated fibers degenerate and C-fibers become sensitized. Upregulation of STOML3 is associated with neuropathic pain, therefore we overexpressed STOML3 *in vivo* in sensory neurons and observed again mechanical hypersensitivity in experimental animals as well as sensitization in LTMRs and C-fibers. Using a sensory neuron specific knockout of STOML3 we found that these animals are protected from mechanical hypersensitivity following CCI and also that the physiology of C-fiber mechanotransduction was for CMs comparable to naïve control and for polymodal C-fibers attenuated.

Neuropathic pain modelled by applying CCI produces mechanical hypersensitivity in experimental animals. Large myelinated fibers degenerate and C-fibers become sensitized. Upregulation of STOML3 is associated with neuropathic pain, therefore we overexpressed STOML3 *in vivo* in sensory neurons and observed again mechanical hypersensitivity in experimental animals as well as sensitization in LTMRs and C-fibers. Using a sensory neuron specific knockout of *stoml3* we found that these animals are protected from mechanical hypersensitivity following CCI and also that the physiology of C-fiber mechanotransduction was for CMs comparable to naïve controls and for polymodal C-fibers attenuated. Thus, sensitization of CMs might be the driver for allodynia emerging in neuropathic conditions and STOML3 is essential for the emerging exaggerated activity in nociceptive sensory neurons probably by sensitization of Piezo2.

5 References

Abdo, H., Calvo-Enrique, L., Lopez, J. M., Song, J., Zhang, M.-D., Usoskin, D., … Ernfors, P. (2019). Specialized cutaneous Schwann cells initiate pain sensation. *Science*, *365*(6454), 695–699. https://doi.org/10.1126/science.aax6452

Adriaensen, H., Gybels, J., Handwerker, H. O., & Van Hees, J. (1983). Response properties of thin myelinated (A-δ) fibers in human skin nerves. *Journal of Neurophysiology*, *49*(1), 111–122. https://doi.org/10.1152/jn.1983.49.1.111

Alcaino, C., Knutson, K., Gottlieb, P. A., Farrugia, G., & Beyder, A. (2017). Mechanosensitive ion channel Piezo2 is inhibited by D-GsMTx4. *Channels*, *11*(3), 1–9. https://doi.org/10.1080/19336950.2017.1279370

Althagafi, A., & Nadi, M. (2019). *Acute Nerve Injury*. Retrieved from http://europepmc.org/books/NBK549848

Amadesi, S., Cottrell, G. S., Divino, L., Chapman, K., Grady, E. F., Bautista, F., … Bunnett, N. W. (2006). Protease-activated receptor 2 sensitizes TRPV1 by protein kinase Cε- and A-dependent mechanisms in rats and mice. *Journal of Physiology*, *575*(2), 555–571. https://doi.org/10.1113/jphysiol.2006.111534

Arslantunali, D., Dursun, T., Yucel, D., Hasirci, N., & Hasirci, V. (2014). Peripheral nerve conduits: Technology update. *Medical Devices: Evidence and Research*, *7*, 405–424. https://doi.org/10.2147/MDER.S59124

Bae, C., Sachs, F., & Gottlieb, P. A. (2011). The mechanosensitive ion channel Piezo1 is inhibited by the peptide GsMTx4. *Biochemistry*, *50*(29), 6295–6300. https://doi.org/10.1021/bi200770q

Balkowiec, A., & Katz, D. M. (2000). Activity-dependent release of endogenous brain-derived neurotrophic factor from primary sensory neurons detected by ELISA in situ. *Journal of Neuroscience*, *20*(19), 7417–7423. https://doi.org/10.1523/jneurosci.20-19-07417.2000

Baral, P., Mills, K., Pinho-Ribeiro, F. A., & Chiu, I. M. (2016). Pain and Itch: Beneficial or Harmful to Antimicrobial Defense? *Cell Host and Microbe*, *19*(6), 755–759. https://doi.org/10.1016/j.chom.2016.05.010

Baral, P., Udit, S., & Chiu, I. M. (2019). Pain and immunity: implications for host defence. *Nature Reviews Immunology*, *19*(7), 433–447. https://doi.org/10.1038/s41577-019-0147-2

Barik, A., Saade, D., Chesler, A. T., Liljencrantz, J., Necaise, A., Szczot, M., … Bönnemann, C. G. (2018). PIEZO2 mediates injury-induced tactile pain in mice and humans. *Science Translational Medicine*, *10*(462), eaat9892. https://doi.org/10.1126/scitranslmed.aat9892

Baron, R. (2006). Mechanisms of disease: neuropathic pain--a clinical perspective. *Nature Clinical Practice. Neurology*, *2*(2), 95–106. https://doi.org/10.1038/ncpneuro0113

Baron, R., Hans, G., & Dickenson, A. H. (2013). Peripheral input and its importance for central sensitization. *Annals of Neurology*, *74*(5), 630–636. https://doi.org/10.1002/ana.24017

Basbaum, a I., Gautron, M., Jazat, F., Mayes, M., & Guilbaud, G. (1991). The spectrum of fiber loss in a model of neuropathic pain in the rat: an electron microscopic study. *Pain*, *47*(3), 359–367.

Beaulieu-Laroche, L., Christin, M., Donoghue, A., Agosti, F., Yousefpour, N., Petitjean, H., … Sharif-Naeini, R. (2020). TACAN Is an Ion Channel Involved in Sensing Mechanical Pain. *Cell*, *180*(5), 956-967.e17. https://doi.org/10.1016/j.cell.2020.01.033

Bennett, G. J., & Xie, Y. K. (1988). A peripheral mononeuropathy in rat that produces disorders of pain sensation like those seen in man. *Pain*, *33*(1), 87–107. https://doi.org/10.1016/0304-3959(88)90209-6

Berrier, C., Pozza, A., De Lacroix De Lavalette, A., Chardonnet, S., Mesneau, A., Jaxel, C., … Ghazi, A. (2013). The purified mechanosensitive channel TREK-1 is directly sensitive to membrane tension. *Journal of Biological Chemistry*, *288*(38), 27307–27314. https://doi.org/10.1074/jbc.M113.478321

Binder, A., Bruxelle, J., Rogers, P., Hans, G., Bösl, I., & Baron, R. (2009). Topical 5% lidocaine (lignocaine) medicated plaster treatment for post-herpetic neuralgia: Results of a double-blind, placebo-controlled, multinational efficacy and safety trial. *Clinical Drug Investigation*, *29*(6), 393–408. https://doi.org/10.2165/00044011-200929060-00003

Binshtok, A. M., Wang, H., Zimmermann, K., Amaya, F., Vardeh, D., Shi, L., … Samad, T. A. (2008). Nociceptors are interleukin-1β sensors. *Journal of Neuroscience*, *28*(52), 14062–14073. https://doi.org/10.1523/JNEUROSCI.3795-08.2008

Black, J. A., Liu, S., Tanaka, M., Cummins, T. R., & Waxman, S. G. (2004). Changes in the expression of tetrodotoxin-sensitive sodium channels within dorsal root ganglia neurons in inflammatory pain. *Pain*, *108*(3), 237–247. https://doi.org/10.1016/j.pain.2003.12.035

Blake, D. T., Hsiao, S. S., & Johnson, K. O. (1997). Neural coding mechanisms in tactile pattern

recognition: The relative contributions of slowly and rapidly adapting mechanoreceptors to perceived roughness. *Journal of Neuroscience*, *17*(19), 7480–7489. https://doi.org/10.1523/jneurosci.17-19-07480.1997

Bouhassira, D., Lantéri-Minet, M., Attal, N., Laurent, B., & Touboul, C. (2008). Prevalence of chronic pain with neuropathic characteristics in the general population. *Pain*, *136*(3), 380–387. https://doi.org/10.1016/j.pain.2007.08.013

Bourquin, A. F., Süveges, M., Pertin, M., Gilliard, N., Sardy, S., Davison, A. C., … Decosterd, I. (2006). Assessment and analysis of mechanical allodynia-like behavior induced by spared nerve injury (SNI) in the mouse. *Pain*, *122*(1–2), 14.e1-14.e14. https://doi.org/10.1016/j.pain.2005.10.036

Bozkurt, A., Deumens, R., Scheffel, J., O'Dey, D. M., Weis, J., Joosten, E. A., … Pallua, N. (2008). CatWalk gait analysis in assessment of functional recovery after sciatic nerve injury. *Journal of Neuroscience Methods*, *173*(1), 91–98. https://doi.org/10.1016/j.jneumeth.2008.05.020

Brand, J., Smith, E. S. J., Schwefel, D., Lapatsina, L., Poole, K., Omerbašić, D., … Daumke, O. (2012). A stomatin dimer modulates the activity of acid-sensing ion channels. *The EMBO Journal*, *31*(17), 3635–3646. https://doi.org/10.1038/emboj.2012.203

Brohawn, S. G., Campbell, E. B., & MacKinnon, R. (2014). Physical mechanism for gating and mechanosensitivity of the human TRAAK K+ channel. *Nature*, *516*(729), 126–130. https://doi.org/10.1038/nature14013

Brown, B. Y. A. G., & Iggo, A. (1967). *From the Department of Veterinary Physiology , University of Edinburgh*. 707–733.

Burgess, G. M., Mullaney, I., McNeill, M., Dunn, P. M., & Rang, H. P. (1989). Second messengers involved in the mechanism of action of bradykinin in sensory neurons in culture. *Journal of Neuroscience*, *9*(9), 3314–3325. https://doi.org/10.1523/jneurosci.09-09-03314.1989

Cain, D. M., Khasabov, S. G., & Simone, D. A. (2001). Response properties of mechanoreceptors and nociceptors in mouse glabrous skin: An in vivo study. *Journal of Neurophysiology*, *85*(4), 1561–1574. https://doi.org/10.1152/jn.2001.85.4.1561

Canning, B. J., & Spina, D. (2009). Sensory nerves and airway irritability. In *Handbook of Experimental Pharmacology* (Vol. 194). https://doi.org/10.1007/978-3-540-79090-7_5

Carlton, S. M., Dougherty, P. M., Pover, C. M., & Coggeshall, R. E. (1991). Neuroma formation and numbers of axons in a rat model of experimental peripheral neuropathy. *Neuroscience Letters*, *131*(1), 88–92. https://doi.org/10.1016/0304-3940(91)90343-R

Caterina, M. J., Leffler, A., Malmberg, A. B., Martin, W. J., Trafton, J., Petersen-Zeitz, K. R., … Julius, D. (2000). Impaired nociception and pain sensation in mice lacking the capsaicin receptor. *Science (New York, N.Y.)*, *288*(5464), 306–313.

Cauna, N. (1881). *Nerve supply and nerve endings i n meissner's corpuscles*. (1873).

Cesare, P., & Mcnaughton, P. (1996). A novel heat-activated current in nociceptive neurons and its sensitization by bradykinin. *Proceedings of the National Academy of Sciences of the United States of America*, *93*(26), 15435–15439. https://doi.org/10.1073/pnas.93.26.15435

Chakrabarti, S., Pattison, L. A., Singhal, K., Hockley, J. R. F., Callejo, G., St, E., & Smith, J. (2018). Neuropharmacology Acute in fl ammation sensitizes knee-innervating sensory neurons and decreases mouse digging behavior in a TRPV1-dependent manner. *Neuropharmacology*, *143*(June), 49–62. https://doi.org/10.1016/j.neuropharm.2018.09.014

Chaplan, S. R., Bach, F. W., Pogrel, J. W., Chung, J. M., & Yaksh, T. L. (1994). Quantitative assessment of tactile allodynia in the rat paw. *Journal of Neuroscience Methods*, *53*(1), 55–63. https://doi.org/10.1016/0165-0270(94)90144-9

Chen, J. (2011). History of pain theories. *Neuroscience Bulletin*, *27*(5), 343–350. https://doi.org/10.1007/s12264-011-0139-0

Chiu, I. M., Von Hehn, C. A., & Woolf, C. J. (2012). Neurogenic inflammation and the peripheral nervous system in host defense and immunopathology. *Nature Neuroscience*, *15*(8), 1063–1067. https://doi.org/10.1038/nn.3144

Christin, M., & Agosti, F. (2019). *TACAN is an essential component of the mechanosensitive ion channel responsible for pain sensing Nuclear Platelet-activating Factor Receptor View project Onirographe View project*. https://doi.org/10.1101/338673

Cook, A. D., Christensen, A. D., Tewari, D., McMahon, S. B., & Hamilton, J. A. (2018). Immune Cytokines and Their Receptors in Inflammatory Pain. *Trends in Immunology*, *39*(3), 240–255. https://doi.org/10.1016/j.it.2017.12.003

Corey, D. P., & Hudspeth, A. J. (1979). Response latency of vertebrate hair cells. *Biophysical*

Journal, *26*(3), 499–506. https://doi.org/10.1016/S0006-3495(79)85267-4

Coste, B., Mathur, J., Schmidt, M., Earley, T. J., Ranade, S., Petrus, M. J., … Patapoutian, A. (2010). Piezo1 and Piezo2 are essential components of distinct mechanically activated cation channels. *Science*, *330*(6000), 55–60. https://doi.org/10.1126/science.1193270

Coull, J. A. M., Beggs, S., Boudreau, D., Boivin, D., Tsuda, M., Inoue, K., … De Koninck, Y. (2005). BDNF from microglia causes the shift in neuronal anion gradient underlying neuropathic pain. *Nature*, *438*(7070), 1017–1021. https://doi.org/10.1038/nature04223

Cox, C. D., Bae, C., Ziegler, L., Hartley, S., Nikolova-Krstevski, V., Rohde, P. R., … Martinac, B. (2016). Removal of the mechanoprotective influence of the cytoskeleton reveals PIEZO1 is gated by bilayer tension. *Nature Communications*, *7*, 1–13. https://doi.org/10.1038/ncomms10366

Cunningham, C. L., Qiu, X., Wu, Z., Zhao, B., Peng, G., Kim, Y.-H., … Müller, U. (2020). TMIE Defines Pore and Gating Properties of the Mechanotransduction Channel of Mammalian Cochlear Hair Cells. *Neuron*, 1–18. https://doi.org/10.1016/j.neuron.2020.03.033

Danielian, P. S., Muccino, D., Rowitch, D. H., Michael, S. K., & McMahon, a P. (1998). Modification of gene activity in mouse embryos in utero by a tamoxifen-inducible form of Cre recombinase. *Current Biology : CB*, *8*(24), 1323–1326. https://doi.org/10.1016/S0960-9822(07)00562-3

De Vry, J., Kuhl, E., Franken-Kunkel, P., & Eckel, G. (2004). Pharmacological characterization of the chronic constriction injury model of neuropathic pain. *European Journal of Pharmacology*, *491*(2–3), 137–148. https://doi.org/10.1016/j.ejphar.2004.03.051

Decosterd, I., & Woolf, C. J. (2000). Spared nerve injury: An animal model of persistent peripheral neuropathic pain. *Pain*, *87*(2), 149–158. https://doi.org/10.1016/S0304-3959(00)00276-1

Dib-Hajj, S. D., Cummins, T. R., Black, J. A., & Waxman, S. G. (2010). Sodium channels in normal and pathological pain. *Annual Review of Neuroscience*, *33*, 325–347. https://doi.org/10.1146/annurev-neuro-060909-153234

Dixon, W. J. (1980). Efficient Analysis of Experimental Observations. *Ann. Rev. Pharcol. Toxicol*, *20*, 441–462.

Djouhri, L., Dawbarn, D., Robertson, A., Newton, R., & Lawson, S. N. (2001). *Time Course and Nerve Growth Factor Dependence of Inflammation-Induced Alterations in*

Electrophysiological Membrane Properties in Nociceptive Primary Afferent Neurons. *21*(22), 8722–8733.

Dowdall, T., Robinson, I., & Meert, T. F. (2005). Comparison of five different rat models of peripheral nerve injury. *Pharmacology Biochemistry and Behavior*, *80*(1), 93–108. https://doi.org/10.1016/j.pbb.2004.10.016

Driscoll, M., & Tavernarakis, N. (1997). Molecules that mediate touch transduction in the nematode Caenorhabditis elegans. *Gravitational and Space Biology Bulletin : Publication of the American Society for Gravitational and Space Biology*, Vol. 10, pp. 33–42.

Driskell, R. R., Giangreco, A., Jensen, K. B., Mulder, K. W., & Watt, F. M. (2009). Sox2-positive dermal papilla cells specify hair follicle type in mammalian epidermis. *Development*, *136*(16), 2815–2823. https://doi.org/10.1242/dev.038620

Dry, F. W. (1926). The coat of the mouse (Mus musculus). *Journal of Genetics*, *16*(3), 287–340. https://doi.org/10.1007/BF02983004

Dubin, A. E., Schmidt, M., Mathur, J., Petrus, M. J., Xiao, B., Coste, B., & Patapoutian, A. (2012). Inflammatory Signals Enhance Piezo2-Mediated Mechanosensitive Currents. *Cell Reports*, *2*(3), 511–517. https://doi.org/10.1016/j.celrep.2012.07.014

Duverger, O., & Morasso, M. I. (2009). Epidermal patterning and induction of different hair types during mouse embryonic development. *Birth Defects Research Part C - Embryo Today: Reviews*, *87*(3), 263–272. https://doi.org/10.1002/bdrc.20158

Ernfors, P., Wetmore, C., Olson, L., & Persson, H. (1990). Identification of cells in rat brain and peripheral tissues expressing mRNA for members of the nerve growth factor family. *Neuron*, *5*(4), 511–526. https://doi.org/10.1016/0896-6273(90)90090-3

Fields, H. L., Rowbotham, M., & Baron, R. (1998). Postherpetic neuralgia: Irritable nociceptors and deafferentation. *Neurobiology of Disease*, *5*(4), 209–227. https://doi.org/10.1006/nbdi.1998.0204

Finnerup, N. B., Attal, N., Haroutounian, S., McNicol, E., Baron, R., Dworkin, R. H., … Wallace, M. (2015). Pharmacotherapy for neuropathic pain in adults: A systematic review and meta-analysis. *The Lancet Neurology*, *14*(2), 162–173. https://doi.org/10.1016/S1474-4422(14)70251-0

Fleischer, E., Handwerker, H. O., & Joukhadar, S. (1983). Unmyelinated nociceptive units in two skin areas of the rat. *Brain Research*, *267*(1), 81–92. https://doi.org/10.1016/0006-

8993(83)91041-7

Florez-Paz, D., Bali, K. K., Kuner, R., & Gomis, A. (2016). A critical role for Piezo2 channels in the mechanotransduction of mouse proprioceptive neurons. *Scientific Reports*, *6*, 1–9. https://doi.org/10.1038/srep25923

Fukuoka, H., Kawatani, M., Hisamitsu, T., & Takeshige, C. (1994). Cutaneous hyperalgesia induced by peripheral injection of interleukin-1β in the rat. *Brain Research*, *657*(1–2), 133–140. https://doi.org/10.1016/0006-8993(94)90960-1

Gagnon, M., Bergeron, M. J., Lavertu, G., Castonguay, A., Tripathy, S., Bonin, R. P., … De Koninck, Y. (2013). Chloride extrusion enhancers as novel therapeutics for neurological diseases. *Nature Medicine*, *19*(11), 1524–1528. https://doi.org/10.1038/nm.3356

Garell, P. C., McGillis, S. L. B., & Greenspan, J. D. (1996). Mechanical response properties of nociceptors innervating feline hairy skin. *Journal of Neurophysiology*, *75*(3), 1177–1189. https://doi.org/10.1152/jn.1996.75.3.1177

Garraway, S. M., Petruska, J. C., & Mendell, L. M. (2003). BDNF sensitizes the response of lamina II neurons to high threshold primary afferent inputs. *European Journal of Neuroscience*, *18*(9), 2467–2476. https://doi.org/10.1046/j.1460-9568.2003.02982.x

Gingras, J., Smith, S., Matson, D. J., Johnson, D., Nye, K., Couture, L., … McDonough, S. I. (2014). Global Nav1.7 knockout mice recapitulate the phenotype of human congenital indifference to pain. *PLoS ONE*, *9*(9). https://doi.org/10.1371/journal.pone.0105895

Gold, M. S., & Gebhart, G. F. (2010). Nociceptor sensitization in pain pathogenesis. *Nature Medicine*, *16*(11), 1248–1257. https://doi.org/10.1038/nm.2235

Gopalsamy, B., Sambasevam, Y., Zulazmi, N. A., Chia, J. S. M., Omar Farouk, A. A., Sulaiman, M. R., … Perimal, E. K. (2019). Experimental Characterization of the Chronic Constriction Injury-Induced Neuropathic Pain Model in Mice. *Neurochemical Research*, *44*(9), 2123–2138. https://doi.org/10.1007/s11064-019-02850-0

Green, J. B., & Young, J. P. W. (2008). Slipins: Ancient origin, duplication and diversification of the stomatin protein family. *BMC Evolutionary Biology*, *8*(1), 1–12. https://doi.org/10.1186/1471-2148-8-44

Guinard, D., Usson, Y., Guillermet, C., & Saxod, R. (2000). PS-100 and NF 70-200 double immunolabeling for human digital skin meissner corpuscle 3D imaging. *Journal of Histochemistry and Cytochemistry*, *48*(2), 295–302.

https://doi.org/10.1177/002215540004800215

Handwerker, H. O., Forster, C., & Kirchhoff, C. (1991). Discharge patterns of human C-fibers induced by itching and burning stimuli. *Journal of Neurophysiology*, *66*(1), 307–315. https://doi.org/10.1152/jn.1991.66.1.307

Haroutounian, S. (2014). Primary afferent input is critical for maintaining spontaneous pain in peripheral neuropathy. *Pain*. https://doi.org/13277545

Hartschuh, W., & Weihe, E. (1980). Fine structural analysis of the synaptic junction of Merkel cell-axon-complexes. *Journal of Investigative Dermatology*, *75*(2), 159–165. https://doi.org/10.1111/1523-1747.ep12522555

Hildebrand, C., & Hahn, R. (1978). Relation between myelin sheath thickness and axon size in spinal cord white matter of some vertebrate species. *Journal of the Neurological Sciences*, *38*(3), 421–434. https://doi.org/10.1016/0022-510X(78)90147-8

Hu, J., & Lewin, G. R. (2006). Mechanosensitive currents in the neurites of cultured mouse sensory neurones. *The Journal of Physiology*, *577*(3), 815–828. https://doi.org/10.1113/jphysiol.2006.117648

Huang, M., Gu, G., Ferguson, E. L., & Chalfiet, M. (1995). *A stomatin · like protein*. *378*(November), 292–295.

Huang, X., & Saint-Jeannet, J. P. (2004). Induction of the neural crest and the opportunities of life on the edge. *Developmental Biology*, *275*(1), 1–11. https://doi.org/10.1016/j.ydbio.2004.07.033

Huber, T. B., Schermer, B., Muller, R. U., Hohne, M., Bartram, M., Calixto, A., … Benzing, T. (2006). Podocin and MEC-2 bind cholesterol to regulate the activity of associated ion channels. *Proceedings of the National Academy of Sciences*, *103*(46), 17079–17086. https://doi.org/10.1073/pnas.0607465103

Iggo, B. Y. A. (1960). *of Physiology, University of Edinburgh*. 337–353.

Ikeda, R., Cha, M., Ling, J., Jia, Z., Coyle, D., & Gu, J. G. (2014). Merkel cells transduce and encode tactile stimuli to drive aβ-Afferent impulses. *Cell*, *157*(3), 664–675. https://doi.org/10.1016/j.cell.2014.02.026

Ji, R. R., Xu, Z. Z., & Gao, Y. J. (2014). Emerging targets in neuroinflammation-driven chronic pain. *Nature Reviews Drug Discovery*, *13*(7), 533–548. https://doi.org/10.1038/nrd4334

Jia, Y., Zhao, Y., Kusakizako, T., Wang, Y., Pan, C., Zhang, Y., … Yan, Z. (2020). TMC1 and TMC2 Proteins Are Pore-Forming Subunits of Mechanosensitive Ion Channels. *Neuron*, *105*(2), 310-321.e3. https://doi.org/10.1016/j.neuron.2019.10.017

Jin, X. (2006). Acute p38-Mediated Modulation of Tetrodotoxin-Resistant Sodium Channels in Mouse Sensory Neurons by Tumor Necrosis Factor- . *Journal of Neuroscience*, *26*(1), 246–255. https://doi.org/10.1523/JNEUROSCI.3858-05.2006

Johansson, R. S., & Westling, G. (1984). <*Johansson and Westling 1984.pdf*>. 550–564. https://doi.org/10.1007/BF00237997

Johnson, K. O. (2001). The roles and functions of cutaneous mechanoreceptors. *Current Opinion in Neurobiology*, *11*(4), 455–461. https://doi.org/10.1016/S0959-4388(00)00234-8

Joong Woo Leem, Willis, W. D., & Jin Mo Chung. (1993). Cutaneous sensory receptors in the rat foot. *Journal of Neurophysiology*, *69*(5), 1684–1699. https://doi.org/10.1152/jn.1993.69.5.1684

Kang, D. W., Choi, J. G., Moon, J. Y., Kang, S. Y., Ryu, Y., Park, J. B., & Kim, H. W. (2017). Automated gait analysis in mice with chronic constriction injury. *Journal of Visualized Experiments*, *2017*(128), 1–5. https://doi.org/10.3791/56402

Kauppila, T. (1998). Correlation between autotomy-behavior and current theories of neuropathic pain. *Neuroscience and Biobehavioral Reviews*, *23*(1), 111–129. https://doi.org/10.1016/S0149-7634(98)00038-4

Kelly, M. B., & Strifling, M. S. (2006). *Analysis of Upper and Lower Extremity Peripheral*.

Kerr, B. J., Bradbury, E. J., Bennett, D. L. H., Trivedi, P. M., Dassan, P., French, J., … Thompson, S. W. N. (1999). Brain-derived neurotrophic factor modulates nociceptive sensory inputs and NMDA-evoked responses in the rat spinal cord. *Journal of Neuroscience*, *19*(12), 5138–5148. https://doi.org/10.1523/jneurosci.19-12-05138.1999

Khasar, S. G., Mccarter, G., & Levine, J. D. (1999). Epinephrine produces a β-adrenergic receptor-mediated mechanical hyperalgesia and in vitro sensitization of rat nociceptors. *Journal of Neurophysiology*, *81*(3), 1104–1112. https://doi.org/10.1152/jn.1999.81.3.1104

Kim, S. H., & Chung, J. M. (1992). An experimental model for peripheral neuropathy produced by segmental spinal nerve ligation in the rat. *Pain*, *50*(3), 355–363. https://doi.org/10.1016/0304-3959(92)90041-9

Kleggetveit, I. (2012). High spontaneous activity of C-nociceptors in painful polyneuropathy. *Pain*. https://doi.org/13277545

Koerber, H. R., Mirnics, K., Brown, P. B., & Mendell, L. M. (1994). Central sprouting and functional plasticity of regenerated primary afferents. *Journal of Neuroscience*, *14*(6), 3655–3671. https://doi.org/10.1523/jneurosci.14-06-03655.1994

Kohno, T., Moore, K. A., Baba, H., & Woolf, C. J. (2003). Peripheral nerve injury alters excitatory synaptic transmission in laminal II of the rat dorsal horn. *Journal of Physiology*, *548*(1), 131–138. https://doi.org/10.1113/jphysiol.2002.036186

Koltzenburg, M, Torebjörk, H. E., & Wahren, L. K. (1994). Nociceptor modulated central sensitization causes mechanical hyperalgesia in acute chemogenic and chronic neuropathic pain. *Brain : A Journal of Neurology*, *117 (Pt 3*, 579–591. https://doi.org/10.1093/brain/117.3.579

Koltzenburg, Martin, Stucky, C. L., & Lewin, G. R. (1997). Receptive properties of mouse sensory neurons innervating hairy skin. *Journal of Neurophysiology*, *78*(4), 1841–1850. https://doi.org/10.1152/jn.1997.78.4.1841

Komori, N., Takemori, N., Hee, K. K., Singh, A., Hwang, S. H., Foreman, R. D., … Matsumoto, H. (2007). Proteomics study of neuropathic and nonneuropathic dorsal root ganglia: Altered protein regulation following segmental spinal nerve ligation injury. *Physiological Genomics*, *29*(2), 215–230. https://doi.org/10.1152/physiolgenomics.00255.2006

Kress, M., Koltzenburg, M., Reeh, P. W., & Handwerker, H. O. (1992). Responsiveness and functional attributes of electrically localized terminals of cutaneous C-fibers in vivo and in vitro. *Journal of Neurophysiology*, *68*(2), 581–595. https://doi.org/10.1152/jn.1992.68.2.581

Kress, M., Rödl, J., & Reeh, P. W. (1996). Stable analogues of cyclic AMP but not cyclic GMP sensitize unmyelinated primary afferents in rat skin to heat stimulation but not to inflammatory mediators, in vitro. *Neuroscience*, *74*(2), 609–617. https://doi.org/10.1016/0306-4522(96)00181-9

Kruger, L., Perl, E. R., & Sedivec, M. J. (1981). Fine structure of myelinated mechanical nociceptor endings in cat hairy skin. *Journal of Comparative Neurology*, *198*(1), 137–154. https://doi.org/10.1002/cne.901980112

Krzyzanowska, A., Pittolo, S., Cabrerizo, M., Sánchez-López, J., Krishnasamy, S., Venero, C.,

& Avendaño, C. (2011). Assessing nociceptive sensitivity in mouse models of inflammatory and neuropathic trigeminal pain. *Journal of Neuroscience Methods*, *201*(1), 46–54. https://doi.org/10.1016/j.jneumeth.2011.07.006

Kuner, R., & Flor, H. (2016). Structural plasticity and reorganisation in chronic pain. *Nature Reviews Neuroscience*, *18*(1), 20–30. https://doi.org/10.1038/nrn.2016.162

LaBuda, C. J., & Little, P. J. (2005). Pharmacological evaluation of the selective spinal nerve ligation model of neuropathic pain in the rat. *Journal of Neuroscience Methods*, *144*(2), 175–181. https://doi.org/10.1016/j.jneumeth.2004.11.008

Lane, N. E., Schnitzer, T. J., Birbara, C. A., Mokhtarani, M., Shelton, D. L., Smith, M. D., & Brown, M. T. (2010). Tanezumab for the treatment of pain from osteoarthritis of the knee. *New England Journal of Medicine*, *363*(16), 1521–1531. https://doi.org/10.1056/NEJMoa0901510

Lapatsina, Liudmila, Jira, J. A., Smith, E. S. J., Poole, K., Kozlenkov, A., Bilbao, D., … Heppenstall, P. A. (2012). Regulation of ASIC channels by a stomatin/STOML3 complex located in a mobile vesicle pool in sensory neurons. *Open Biology*, *2*(JUNE). https://doi.org/10.1098/rsob.120096

Lapatsina, Liudmila, Smith, E. S. J., Poole, K., Kozlenkov, A., Lewin, G. R., Jira, J. A., … Heppenstall, P. A. (2012). Regulation of ASIC channels by a stomatin/STOML3 complex located in a mobile vesicle pool in sensory neurons. *Open Biology*, *2*(JUNE). https://doi.org/10.1098/rsob.120096

Lapatsina, Liudmilla, Brand, J., Poole, K., Daumke, O., & Lewin, G. R. (2012). Stomatin-domain proteins. *European Journal of Cell Biology*, *91*(4), 240–245. https://doi.org/10.1016/j.ejcb.2011.01.018

Lau, J., Minett, M. S., Zhao, J., Dennehy, U., Wang, F., Wood, J. N., & Bogdanov, Y. D. (2011). Temporal control of gene deletion in sensory ganglia using a tamoxifen-inducible Advillin-Cre-ERT2 recombinase mouse. *Molecular Pain*, *7*, 1–13. https://doi.org/10.1186/1744-8069-7-100

Lee, W., Leddy, H. A., Chen, Y., Lee, S. H., Zelenski, N. A., McNulty, A. L., … Liedtke, W. B. (2014). Synergy between Piezo1 and Piezo2 channels confers high-strain mechanosensitivity to articular cartilage. *Proceedings of the National Academy of Sciences of the United States of America*, *111*(47), E5114–E5122. https://doi.org/10.1073/pnas.1414298111

Lett, A. R. F., Sukharev, S. I., Blount, P., Martinac, B., Blattnert, F. R., & Kung, C. (1994). *mscL and mscS*. *368*(March), 265–268.

Lever, I. J., Bradbury, E. J., Cunningham, J. R., Adelson, D. W., Jones, M. G., McMahon, S. B., … Malcangio, M. (2001). Brain-derived neurotrophic factor is released in the dorsal horn by distinctive patterns of afferent fiber stimulation. *Journal of Neuroscience*, *21*(12), 4469–4477. https://doi.org/10.1523/jneurosci.21-12-04469.2001

Lewin, G. R., & Mendell, L. M. (1994). Regulation of cutaneous C-fiber heat nociceptors by nerve growth factor in the developing rat. *Journal of Neurophysiology*, *71*(3), 941–949. https://doi.org/10.1152/jn.1994.71.3.941

Lewin, Gary R., Lechner, S. G., & Smith, E. S. J. (2014). Nerve growth factor and nociception: From experimental embryology to new analgesic therapy. In *Handbook of Experimental Pharmacology* (Vol. 220). https://doi.org/10.1007/978-3-642-45106-5_10

Lewin, Gary R., & Moshourab, R. (2004). Mechanosensation and pain. *Journal of Neurobiology*, *61*(1), 30–44. https://doi.org/10.1002/neu.20078

Lewin, Gary R., & Nykjaer, A. (2014). Pro-neurotrophins, sortilin, and nociception. *European Journal of Neuroscience*, *39*(3), 363–374. https://doi.org/10.1111/ejn.12466

Lewin, Gary R., Rueff, A., & Mendell, L. M. (1994). Peripheral and Central Mechanisms of NGF-induced Hyperalgesia. *European Journal of Neuroscience*, *6*(12), 1903–1912. https://doi.org/10.1111/j.1460-9568.1994.tb00581.x

Li, L., & Ginty, D. D. (2014). The structure and organization of lanceolate mechanosensory complexes at mouse hair follicles. *ELife*. https://doi.org/10.7554/eLife.01901.001

Lin, C. S., Tsaur, M. L., Chen, C. C., Wang, T. Y., Lin, C. F., Lai, Y. L., … Cheng, J. K. (2007). Chronic Intrathecal Infusion of Minocycline Prevents the Development of Spinal-Nerve Ligation-Induced Pain in Rats. *Regional Anesthesia and Pain Medicine*, *32*(3), 209–216. https://doi.org/10.1016/j.rapm.2007.01.005

Lindborg, J. A., Mack, M., & Zigmond, R. E. (2017). Neutrophils are critical for myelin removal in a peripheral nerve injury model of wallerian degeneration. *Journal of Neuroscience*, *37*(43), 10258–10277. https://doi.org/10.1523/JNEUROSCI.2085-17.2017

Luo, Z. D., Chaplan, S. R., Higuera, E. S., Sorkin, L. S., Stauderman, K. A., Williams, M. E., & Yaksh, T. L. (2001). Upregulation of dorsal root ganglion α2δ calcium channel subunit and its correlation with allodynia in spinal nerve-injured rats. *Journal of Neuroscience*,

21(6), 1868–1875. https://doi.org/10.1523/JNEUROSCI.21-06-01868.2001

M, C., MA, D., & MX, H. (1993). Degenerin similarities. *Nature*, *361*(February), 504–1993.

Ma, C., Greenquist, K. W., & LaMotte, R. H. (2006). Inflammatory mediators enhance the excitability of chronically compressed dorsal root ganglion neurons. *Journal of Neurophysiology*, *95*(4), 2098–2107. https://doi.org/10.1152/jn.00748.2005

Macefield, V. G., Häger-Ross, C., & Johansson, R. S. (1996). Control of grip force during restraint of an object held between finger and thumb: Responses of cutaneous afferents from the digits. *Experimental Brain Research*, *108*(1), 155–171. https://doi.org/10.1007/BF00242913

Maingret, F., Fosset, M., Lesage, F., Lazdunski, M., & Honoré, E. (1999). TRAAK is a mammalian neuronal mechano-gated K+ channel. *Journal of Biological Chemistry*, *274*(3), 1381–1387. https://doi.org/10.1074/jbc.274.3.1381

Maingret, F., Patel, A. J., Lesage, F., Lazdunski, M., & Honoré, E. (1999). Mechano- or acid stimulation, two interactive modes of activation of the TREK-1 potassium channel. *Journal of Biological Chemistry*, *274*(38), 26691–26696. https://doi.org/10.1074/jbc.274.38.26691

Maksimovic, S., Nakatani, M., Baba, Y., Nelson, A. M., Marshall, K. L., Wellnitz, S. A., … Lumpkin, E. A. (2014). Epidermal Merkel cells are mechanosensory cells that tune mammalian touch receptors. *Nature*, *509*(7502), 617–621. https://doi.org/10.1038/nature13250

Mannsfeldt, A. G., Carroll, P., Stucky, C. L., & Lewin, G. R. (1999). Stomatin, a MEC-2 like protein, is expressed by mammalian sensory neurons. *Molecular and Cellular Neurosciences*, *13*(6), 391–404. https://doi.org/10.1006/mcne.1999.0761

Maricich, S. M., Morrison, K. M., Mathes, E. L., & Brewer, B. M. (2012). Rodents rely on Merkel cells for texture discrimination tasks. *Journal of Neuroscience*, *32*(10), 3296–3300. https://doi.org/10.1523/JNEUROSCI.5307-11.2012

Martinez-Salgado, C., Benckendorff, A. G., Chiang, L.-Y., Wang, R., Milenkovic, N., Wetzel, C., … Lewin, G. R. (2007). Stomatin and Sensory Neuron Mechanotransduction. *Journal of Neurophysiology*, *98*(6), 3802–3808. https://doi.org/10.1152/jn.00860.2007

Maves, T. J., Pechman, P. S., Gebhart, G. F., & Meller, S. T. (1993). Possible chemical contribution from chromic gut sutures produces disorders of pain sensation like those seen in man. *Pain*, *54*(1), 57–69. https://doi.org/10.1016/0304-3959(93)90100-4

McNamee, K. E., Alzabin, S., Hughes, J. P., Anand, P., Feldmann, M., Williams, R. O., & Inglis, J. J. (2011). IL-17 induces hyperalgesia via TNF-dependent neutrophil infiltration. *Pain*, *152*(8), 1838–1845. https://doi.org/10.1016/j.pain.2011.03.035

Meacham, K., Shepherd, A., Mohapatra, D. P., & Haroutounian, S. (2017). Neuropathic Pain: Central vs. Peripheral Mechanisms. *Current Pain and Headache Reports*, *21*(6). https://doi.org/10.1007/s11916-017-0629-5

Melorose, J., Perroy, R., & Careas, S. (2003). "Catwalk" automated quantitative gait analysis ... *Statewide Agricultural Land Use Baseline 2015*, *1*, 203–209. https://doi.org/10.1017/CBO9781107415324.004

Melzack, R. (1996). Gate control theory: On the evolution of pain concepts. *Pain Forum*, *5*(2), 128–138. https://doi.org/10.1016/S1082-3174(96)80050-X

Melzack, R., & Wall, P. D. (1967). Pain mechanisms: a new theory. *Survey of Anesthesiology*, Vol. 11, p. 89. https://doi.org/10.1126/science.150.3699.971

Mendes, C. S., Bartos, I., Márka, Z., Akay, T., Márka, S., & Mann, R. S. (2015). Quantification of gait parameters in freely walking rodents. *BMC Biology*, *13*, 50. https://doi.org/10.1186/s12915-015-0154-0

Merkel, F. (1875). Tastzellen und Tastkörperchen bei den Hausthieren und beim Menschen. *Archiv Für Mikroskopische Anatomie*, *11*(1 Supplement), 636–652. https://doi.org/10.1007/BF02933819

Metzger, D., & Chambon, P. (2001). Site- and time-specific gene targeting in the mouse. *Methods*, *24*(1), 71–80. https://doi.org/10.1006/meth.2001.1159

Meyer, R. A., Davis, K. D., Cohen, R. H., Treede, R. D., & Campbell, J. N. (1991). Mechanically insensitive afferents (MIAs) in cutaneous nerves of monkey. *Brain Research*, *561*(2), 252–261. https://doi.org/10.1016/0006-8993(91)91601-V

Milenkovic, N., Wetzel, C., Moshourab, R., & Lewin, G. R. (2008). Speed and temperature dependences of mechanotransduction in afferent fibers recorded from the mouse saphenous nerve. *Journal of Neurophysiology*, *100*(5), 2771–2783. https://doi.org/10.1152/jn.90799.2008

Millard, C. L., & Woolf, C. J. (1988). Sensory innervation of the hairs of the rat hindlimb: A light microscopic analysis. *Journal of Comparative Neurology*, *277*(2), 183–194. https://doi.org/10.1002/cne.902770203

Minett, M. S., Nassar, M. A., Clark, A. K., Passmore, G., Dickenson, A. H., Wang, F., … Wood, J. N. (2012). Distinct Nav1.7-dependent pain sensations require different sets of sensory and sympathetic neurons. *Nature Communications*, *3*. https://doi.org/10.1038/ncomms1795

Mitchell, V. A., White, D. M., & Cousins, M. J. (1999). The long-term effect of epidural administration of butamben suspension on nerve injury-induced allodynia in rats. *Anesthesia and Analgesia*, *89*(4), 989–994. https://doi.org/10.1097/00000539-199910000-00031

Moayedi, M., & Davis, K. D. (2013). Theories of pain: From specificity to gate control. *Journal of Neurophysiology*, *109*(1), 5–12. https://doi.org/10.1152/jn.00457.2012

Moroni, M., Servin-Vences, M. R., Fleischer, R., Sánchez-Carranza, O., & Lewin, G. R. (2018). Voltage gating of mechanosensitive PIEZO channels. *Nature Communications*, *9*(1), 1–15. https://doi.org/10.1038/s41467-018-03502-7

Morrison, K. M., Miesegaes, G. R., Lumpkin, E. A., & Maricich, S. M. (2009). Mammalian Merkel cells are descended from the epidermal lineage. *Developmental Biology*, *336*(1), 76–83. https://doi.org/10.1016/j.ydbio.2009.09.032

Moshourab, R. a, Wetzel, C., Martinez-Salgado, C., & Lewin, G. R. (2013). Stomatin-domain protein interactions with acid-sensing ion channels modulate nociceptor mechanosensitivity. *The Journal of Physiology*, *591*(Pt 22), 5555–5574. https://doi.org/10.1113/jphysiol.2013.261180

Muir, A. R. (1969). *Veterinary Studies, University of*. *1882*, 763–796.

Murnion, B. P. (2018). Neuropathic pain: Current definition and review of drug treatment. *Australian Prescriber*, *41*(3), 60–63. https://doi.org/10.18773/austprescr.2018.022

Murthy, S. E., Dubin, A. E., & Patapoutian, A. (2017). Piezos thrive under pressure: Mechanically activated ion channels in health and disease. *Nature Reviews Molecular Cell Biology*, *18*(12), 771–783. https://doi.org/10.1038/nrm.2017.92

Murthy, S. E., Dubin, A. E., Whitwam, T., Jojoa-Cruz, S., Cahalan, S. M., Mousavi, S. A. R., … Patapoutian, A. (2018). OSCA/TMEM63 are an evolutionarily conserved family of mechanically activated ion channels. *ELife*, *7*, 1–17. https://doi.org/10.7554/eLife.41844

Murthy, S. E., Loud, M. C., Daou, I., Marshall, K. L., Schwaller, F., Kühnemund, J., … Patapoutian, A. (2018a). The mechanosensitive ion channel Piezo2 mediates sensitivity

to mechanical pain in mice. *Science Translational Medicine*, *10*(462). https://doi.org/10.1126/scitranslmed.aat9897

Murthy, S. E., Loud, M. C., Daou, I., Marshall, K. L., Schwaller, F., Kühnemund, J., … Patapoutian, A. (2018b). The mechanosensitive ion channel Piezo2 mediates sensitivity to mechanical pain in mice. *Science Translational Medicine*, *10*(462). https://doi.org/10.1126/scitranslmed.aat9897

Nassar, M. A., Stirling, L. C., Forlani, G., Baker, M. D., Matthews, E. A., Dickenson, A. H., & Wood, J. N. (2004). Nociceptor-specific gene deletion reveals a major role for Na. *Pnas*, *101*(34), 12706–12711.

Noble, J., Munro, C. A., Prasad, V. S. S. V., & Midha, R. (1998). Analysis of upper and lower extremity peripheral nerve injuries in a population of patients with multiple injuries. *Journal of Trauma - Injury, Infection and Critical Care*, *45*(1), 116–122. https://doi.org/10.1097/00005373-199807000-00025

Nonomura, K., Woo, S. H., Chang, R. B., Gillich, A., Qiu, Z., Francisco, A. G., … Patapoutian, A. (2017). Piezo2 senses airway stretch and mediates lung inflation-induced apnoea. *Nature*, *541*(7636), 176–181. https://doi.org/10.1038/nature20793

O. van Hecke. (2013). Neuropathic pain in the general populace: A systematic review of epidemiological studies. *Pain*. https://doi.org/13277545

Obreja, O., Kluschina, O., Mayer, A., Hirth, M., Schley, M., Schmelz, M., & Rukwied, R. (2011). NGF enhances electrically induced pain, but not axon reflex sweating. *Pain*, *152*(8), 1856–1863. https://doi.org/10.1016/j.pain.2011.04.002

Okun, A., Defelice, M., Eyde, N., Ren, J., Mercado, R., King, T., & Porreca, F. (2011). Transient inflammation-induced ongoing pain is driven by TRPV1 sensitive afferents. *Molecular Pain*, *7*(1), 4. https://doi.org/10.1186/1744-8069-7-4

Pang, P. T., Teng, H. K., Zaitsev, E., Woo, N. T., Sakata, K., Zhen, S., … Lu, B. (2004). Cleavage of proBDNF by tPA/plasmin is essential for long-term hippocampal plasticity. *Science*, *306*(5695), 487–491. https://doi.org/10.1126/science.1100135

Parada, C. A., Yeh, J. J., Joseph, E. K., & Levine, J. D. (2003). Tumor necrosis factor receptor type-1 in sensory neurons contributes to induction of chronic enhancement of inflammatory hyperalgesia in rat. *European Journal of Neuroscience*, *17*(9), 1847–1852. https://doi.org/10.1046/j.1460-9568.2003.02626.x

Paré, M., Elde, R., Mazurkiewicz, J. E., Smith, A. M., & Rice, F. L. (2001). The Meissner corpuscle revised: A multiafferented mechanoreceptor with nociceptor immunochemical properties. *Journal of Neuroscience*, *21*(18), 7236–7246. https://doi.org/10.1523/jneurosci.21-18-07236.2001

Paricio-Montesinos, R., Schwaller, F., Udhayachandran, A., Rau, F., Walcher, J., Evangelista, R., … Lewin, G. R. (2020). The Sensory Coding of Warm Perception. *Neuron*, *106*(5), 830-841.e3. https://doi.org/10.1016/j.neuron.2020.02.035

Parvathy, S. S., & Masocha, W. (2013). Gait analysis of C57BL/6 mice with complete Freund's adjuvant-induced arthritis using the CatWalk system. *BMC Musculoskeletal Disorders*, *14*(1), 14. https://doi.org/10.1186/1471-2474-14-14

Patel, R., & Dickenson, A. H. (2016). Neuronal hyperexcitability in the ventral posterior thalamus of neuropathic rats: Modality selective effects of pregabalin. *Journal of Neurophysiology*, *116*(1), 159–170. https://doi.org/10.1152/jn.00237.2016

Patkunarajah, A., Stear, J. H., Moroni, M., Schroeter, L., Blaszkiewicz, J., Tearle, J. L. E., … Poole, K. (2020). TMEM87a/Elkin1, a component of a novel mechanoelectrical transduction pathway, modulates melanoma adhesion and migration. *ELife*, *9*, 1–25. https://doi.org/10.7554/eLife.53308

Perl, E. R. (2007). Ideas about pain, a historical view. *Nature Reviews Neuroscience*, *8*(1), 71–80. https://doi.org/10.1038/nrn2042

Perl, P. R. B. and E. R. (1972). *From the Department of Physiology , University of Utah Biological Sciences Group , University of Connecticut ,*. 691–713.

Peyron, R. (2016). Functional brain imaging: What has it brought to our understanding of neuropathic pain? A special focus on allodynic pain mechanisms. *Pain*, *157*(2), S67–S71. https://doi.org/10.1097/j.pain.0000000000000387

Pezet, S., & McMahon, S. B. (2006). Neurotrophins: Mediators and modulators of pain. *Annual Review of Neuroscience*, *29*, 507–538. https://doi.org/10.1146/annurev.neuro.29.051605.112929

Pinho-Ribeiro, F. A., Verri, W. A., & Chiu, I. M. (2017). Nociceptor Sensory Neuron–Immune Interactions in Pain and Inflammation. *Trends in Immunology*, *38*(1), 5–19. https://doi.org/10.1016/j.it.2016.10.001

Pitchford, S., & Levine, J. D. (1991). Prostaglandins sensitize nociceptors in cell culture.

Neuroscience Letters, *132*(1), 105–108. https://doi.org/10.1016/0304-3940(91)90444-X

Ploner, M., Gross, J., Timmermann, L., & Schnitzler, A. (2002). Cortical representation of first and second pain sensation in humans. *Proceedings of the National Academy of Sciences of the United States of America*, *99*(19), 12444–12448. https://doi.org/10.1073/pnas.182272899

Poole, K., Herget, R., Lapatsina, L., Ngo, H.-D., & Lewin, G. R. (2014a). Tuning Piezo ion channels to detect molecular-scale movements relevant for fine touch. *Nature Communications*, *5*, 1–14. https://doi.org/10.1038/ncomms4520

Poole, K., Herget, R., Lapatsina, L., Ngo, H.-D., & Lewin, G. R. (2014b). Tuning Piezo ion channels to detect molecular-scale movements relevant for fine touch. *Nature Communications*, *5*, 1–14. https://doi.org/10.1038/ncomms4520

Poole, K., Moroni, M., & Lewin, G. R. (2014). Sensory mechanotransduction at membrane-matrix interfaces. *Pfl??Gers Archiv - European Journal of Physiology*, 121–132. https://doi.org/10.1007/s00424-014-1563-6

Prato, V., Taberner, F. J., Hockley, J. R. F., Callejo, G., Arcourt, A., Tazir, B., … Lechner, S. G. (2017). Functional and Molecular Characterization of Mechanoinsensitive "Silent" Nociceptors. *Cell Reports*, *21*(11), 3102–3115. https://doi.org/10.1016/j.celrep.2017.11.066

Price, D. D. (1972). Characteristics of second pain and flexion reflexes indicative of prolonged central summation. *Experimental Neurology*, *37*(2), 371–387. https://doi.org/10.1016/0014-4886(72)90081-7

Price, D. D. (1977). *Mechanism of first and second pain in the peripheral and central nervous system.pdf*.

Qi, Y., Andolfi, L., Frattini, F., Mayer, F., Lazzarino, M., & Hu, J. (2015a). Membrane stiffening by STOML3 facilitates mechanosensation in sensory neurons. *Nature Communications*, *6*, 8512. https://doi.org/10.1038/ncomms9512

Qi, Y., Andolfi, L., Frattini, F., Mayer, F., Lazzarino, M., & Hu, J. (2015b). Membrane stiffening by STOML3 facilitates mechanosensation in sensory neurons. *Nature Communications*, *6*, 1–13. https://doi.org/10.1038/ncomms9512

Qiu, Z., Dubin, A. E., Mathur, J., Tu, B., Reddy, K., Miraglia, L. J., … Patapoutian, A. (2014). SWELL1, a plasma membrane protein, is an essential component of volume-regulated

anion channel. *Cell*, *157*(2), 447–458. https://doi.org/10.1016/j.cell.2014.03.024

Ranade, S. S., Qiu, Z., Woo, S.-H., Hur, S. S., Murthy, S. E., Cahalan, S. M., … Patapoutian, A. (2014). Piezo1, a mechanically activated ion channel, is required for vascular development in mice. *Proceedings of the National Academy of Sciences of the United States of America*, *111*(28), 10347–10352. https://doi.org/10.1073/pnas.1409233111

Retailleau, K., Duprat, F., Arhatte, M., Ranade, S. S., Peyronnet, R., Martins, J. R., … Honoré, E. (2015). Piezo1 in Smooth Muscle Cells Is Involved in Hypertension-Dependent Arterial Remodeling. *Cell Reports*, *13*(6), 1161–1171. https://doi.org/10.1016/j.celrep.2015.09.072

Richter, F., Natura, G., Löser, S., Schmidt, K., Viisanen, H., & Schaible, H. G. (2010). Tumor necrosis factor causes persistent sensitization of joint nociceptors to mechanical stimuli in rats. *Arthritis Care and Research*, *62*(12), 3806–3814. https://doi.org/10.1002/art.27715

Ro, L. S., & Jacobs, J. M. (1993). The role of the saphenous nerve in experimental sciatic nerve mononeuropathy produced by loose ligatures: a behavioural study. *Pain*, *52*(3), 359–369. https://doi.org/10.1016/0304-3959(93)90170-T

Ro, Long Sun, Chen, S. T., Tang, L. M., & Jacobs, J. M. (1999). Effect of NGF and anti-NGF on neuropathic pain in rats following chronic constriction injury of the sciatic nerve. *Pain*, *79*(2–3), 265–274. https://doi.org/10.1016/S0304-3959(98)00164-X

Ropero Peláez, F. J., & Taniguchi, S. (2016). The gate theory of pain revisited: Modeling different pain conditions with a parsimonious neurocomputational model. *Neural Plasticity*, *2016*. https://doi.org/10.1155/2016/4131395

Roselli, S., Gribouval, O., Boute, N., Sich, M., Benessy, F., Attié, T., … Antignac, C. (2002). Podocin localizes in the kidney to the slit diaphragm area. *American Journal of Pathology*, *160*(1), 131–139. https://doi.org/10.1016/S0002-9440(10)64357-X

Rukwied, R., Mayer, A., Kluschina, O., Obreja, O., Schley, M., & Schmelz, M. (2010). NGF induces non-inflammatory localized and lasting mechanical and thermal hypersensitivity in human skin. *Pain*, *148*(3), 407–413. https://doi.org/10.1016/j.pain.2009.11.022

Rutlin, M., Ho, C. Y., Abraira, V. E., Cassidy, C., Woodbury, C. J., & Ginty, D. D. (2014). The cellular and molecular basis of direction selectivity of Aδ-LTMRs. *Cell*, *159*(7), 1640–1651. https://doi.org/10.1016/j.cell.2014.11.038

Saleem, M. A., Ni, L., Witherden, I., Tryggvason, K., Ruotsalainen, V., Mundel, P., & Mathieson, P. W. (2002). Co-localization of nephrin, podocin, and the actin cytoskeleton: Evidence for a role in podocyte foot process formation. *American Journal of Pathology*, *161*(4), 1459–1466. https://doi.org/10.1016/S0002-9440(10)64421-5

Salzer, U., Ahorn, H., & Prohaska, R. (1993). Identification of the phosphorylation site on human erythrocyte band 7 integral membrane protein: implications for a monotopic protein structure. *BBA - Biomembranes*, *1151*(2), 149–152. https://doi.org/10.1016/0005-2736(93)90098-K

Sanders, K. H., & Zimmermann, M. (1986). Mechanoreceptors in rat glabrous skin: Redevelopment of function after nerve crush. *Journal of Neurophysiology*, *55*(4), 644–659. https://doi.org/10.1152/jn.1986.55.4.644

Sandkühler, J. (2009). Models and mechanisms of hyperalgesia and allodynia-2009.pdf. *Physiological Reviews*, (89), 707–758. https://doi.org/10.1152/physrev.00025.2008.

Seltzer, Z., Dubner, R., & Shir, Y. (1990). A novel behavioral model of neuropathic pain disorders produced in rats by partial sciatic nerve injury. *Pain*, *43*(2), 205–218. https://doi.org/10.1016/0304-3959(90)91074-S

Serra, J. (2011). Microneurographic identification of spontaneous activity in C-nociceptors in neuropathic pain states in humans and rats. *Pain*. https://doi.org/13277545

Seung-Hyun Woo1, Viktor Lukacs1, Joriene C. de Nooij2, 3, Dasha Zaytseva4, Connor R. Criddle4, Allain Francisco1, Thomas M. Jessell2, 3, Katherine A. Wilkinson4, and A., & Patapoutian1. (2015). Piezo2 is the principal mechanotransduction channel for proprioception. *Nat Neurosci*, *73*(4), 389–400. https://doi.org/10.1530/ERC-14-0411.Persistent

Sevcik, M. A., Ghilardi, J. R., Peters, C. M., Lindsay, T. H., Halvorson, K. G., Jonas, B. M., … Mantyh, P. W. (2005). Anti-NGF therapy profoundly reduces bone cancer pain and the accompanying increase in markers of peripheral and central sensitization. *Pain*, *115*(1–2), 128–141. https://doi.org/10.1016/j.pain.2005.02.022

Shields, S. D., Eckert, W. a., & Basbaum, A. I. (2003). Spared Nerve Injury Model of Neuropathic Pain in the Mouse: A Behavioral and Anatomic Analysis. *Journal of Pain*, *4*(8), 465–470. https://doi.org/10.1067/S1526-5900(03)00781-8

Shir, Y., & Seltzer, Z. (1991). Effects of sympathectomy in a model of causalgiform pain

produced by partial sciatic nerve injury in rats. *Pain*, *45*(3), 309–320. https://doi.org/10.1016/0304-3959(91)90056-4

Smith, A. K., O'Hara, C. L., & Stucky, C. L. (2013). Mechanical sensitization of cutaneous sensory fibers in the spared nerve injury mouse model. *Molecular Pain*, *9*, 61. https://doi.org/10.1186/1744-8069-9-61

Snyers, L., Umlauf, E., & Prohaska, R. (1998). Oligomeric nature of the integral membrane protein stomatin. *Journal of Biological Chemistry*, *273*(27), 17221–17226. https://doi.org/10.1074/jbc.273.27.17221

Srinivasan, B., Roque, C. H., Hempstead, B. L., Al-Ubaidi, M. R., & Roque, R. S. (2004). Microglia-derived pronerve growth factor promotes photoreceptor cell death via p75 neurotrophin receptor. *Journal of Biological Chemistry*, *279*(40), 41839–41845. https://doi.org/10.1074/jbc.M402872200

Strickland, I. T., Martindale, J. C., Woodhams, P. L., Reeve, A. J., Chessell, I. P., & McQueen, D. S. (2008). Changes in the expression of NaV1.7, NaV1.8 and NaV1.9 in a distinct population of dorsal root ganglia innervating the rat knee joint in a model of chronic inflammatory joint pain. *European Journal of Pain*, *12*(5), 564–572. https://doi.org/10.1016/j.ejpain.2007.09.001

Sukharev, S. I. (1994). *1-s2.0-S1046202384710073-main.pdf*.

Sunderland, S. (1951). A classification of peripheral nerve injuries producing loss of function. *Brain*, *74*(4), 491–516. https://doi.org/10.1093/brain/74.4.491

Surchev, L., & Surcheva, S. (2011). *of a Peripheral Nerve in Chronic Constriction Injury Model of Neuropathic Pain*. 25–30.

Szczot, M., Liljencrantz, J., Ghitani, N., Barik, A., Lam, R., Thompson, J. H., … Chesler, A. T. (2018a). PIEZO2 mediates injury-induced tactile pain in mice and humans. *Science Translational Medicine*, *10*(462), 1–10. https://doi.org/10.1126/scitranslmed.aat9892

Szczot, M., Liljencrantz, J., Ghitani, N., Barik, A., Lam, R., Thompson, J. H., … Chesler, A. T. (2018b). PIEZO2 mediates injury-induced tactile pain in mice and humans. *Science Translational Medicine*, *10*(462), 1–10. https://doi.org/10.1126/scitranslmed.aat9892

Takahashi-Iwanaga, H., & Shimoda, H. (2003). The three-dimensional microanatomy of Meissner corpuscles in monkey palmar skin. *Journal of Neurocytology*, *32*(4), 363–371. https://doi.org/10.1023/B:NEUR.0000011330.57530.2f

Talbot, S., Foster, S. L., & Woolf, C. J. (2016). Neuroimmunity: Physiology and Pathology. *Annual Review of Immunology*, *34*, 421–447. https://doi.org/10.1146/annurev-immunol-041015-055340

Talbot, W. H., Darian-Smith, I., Kornhuber, H. H., & Mountcastle, V. B. (1968). The sense of flutter-vibration: comparison of the human capacity with response patterns of mechanoreceptive afferents from the monkey hand. *Journal of Neurophysiology*, *31*(2), 301–334. https://doi.org/10.1152/jn.1968.31.2.301

Tavernarakis, N., Driscoll, M., & Kyrpides, N. C. (1999). The SPFH domain: Implicated in regulating targeted protein turnover in stomatins and other membrane-associated proteins. *Trends in Biochemical Sciences*, *24*(11), 425–427. https://doi.org/10.1016/S0968-0004(99)01467-X

Taylor, R. L. (1950). American association for the advancement of science. *Journal of Clinical Endocrinology and Metabolism*, *10*(10), 1361–1362. https://doi.org/10.1210/jcem-10-10-1361

Teng, H. K., Teng, K. K., Lee, R., Wright, S., Tevar, S., Almeida, R. D., … Hempstead, B. L. (2005). ProBDNF induces neuronal apoptosis via activation of a receptor complex of p75NTR and sortilin. *Journal of Neuroscience*, *25*(22), 5455–5463. https://doi.org/10.1523/JNEUROSCI.5123-04.2005

Tesfaye, S., Boulton, A. J. M., & Dickenson, A. H. (2013). Mechanisms and management of diabetic painful distal symmetrical polyneuropathy. *Diabetes Care*, *36*(9), 2456–2465. https://doi.org/10.2337/dc12-1964

Tesfaye, S., Wilhelm, S., Lledo, A., Schacht, A., Tölle, T., Bouhassira, D., … Freynhagen, R. (2013). Duloxetine and pregabalin: High-dose monotherapy or their combination? the “cOMBO-DN study” - A multinational, randomized, double-blind, parallel-group study in patients with diabetic peripheral neuropathic pain. *Pain*, *154*(12), 2616–2625. https://doi.org/10.1016/j.pain.2013.05.043

Tondera, D., Grandemange, S., Jourdain, A., Karbowski, M., Mattenberger, Y., Herzig, S., … Martinou, J. C. (2009). SlP-2 is required for stress-induced mitochondrial hyperfusion. *EMBO Journal*, *28*(11), 1589–1600. https://doi.org/10.1038/emboj.2009.89

Torebjörk, H. E., & Hallin, R. G. (1973). Perceptual changes accompanying controlled preferential blocking of A and C fibre responses in intact human skin nerves. *Experimental Brain Research*, *16*(3), 321–332. https://doi.org/10.1007/BF00233334

Tsuda, M., Beggs, S., Salter, M. W., & Inoue, K. (2013). Microglia and intractable chronic pain. *Glia*, *61*(1), 55–61. https://doi.org/10.1002/glia.22379

Tsuda, M., Shigemoto-Mogami, Y., Koizumi, S., Mizokoshi, A., Kohsaka, S., Salter, M. W., & Inoue, K. (2003). P2X4 receptors induced in spinal microglia gate tactile allodynia after nerve injury. *Nature*, *424*(6950), 778–783. https://doi.org/10.1038/nature01786

Vallbo, A. B., & Johansson, R. S. (1984). Properties of cutaneous mechanoreceptors in the human hand related to touch sensation. *Human Neurobiology*, *3*(1), 3–14.

Vaso, A., Adahan, H. M., Gjika, A., Zahaj, S., Zhurda, T., Vyshka, G., & Devor, M. (2014). Peripheral nervous system origin of phantom limb pain. *Pain*, *155*(7), 1384–1391. https://doi.org/10.1016/j.pain.2014.04.018

Vega-Bermudez, F., & Johnson, K. O. (1999a). SA1 and RA receptive fields, response variability, and population responses mapped with a probe array. *Journal of Neurophysiology*, *81*(6), 2701–2710. https://doi.org/10.1152/jn.1999.81.6.2701

Vega-Bermudez, F., & Johnson, K. O. (1999b). Surround suppression in the responses of primate SA1 and RA mechanoreceptive afferents mapped with a probe array. *Journal of Neurophysiology*, *81*(6), 2711–2719. https://doi.org/10.1152/jn.1999.81.6.2711

Walcher, J., Ojeda-Alonso, J., Haseleu, J., Oosthuizen, M. K., Rowe, A. H., Bennett, N. C., & Lewin, G. R. (2018). Specialized mechanoreceptor systems in rodent glabrous skin. *Journal of Physiology*, *596*(20), 4995–5016. https://doi.org/10.1113/JP276608

Wall, P. D., Devor, M., Inbal, R., Scadding, J. W., Schonfeld, D., Seltzer, Z., & Tomkiewicz, M. M. (1979). Autotomy following peripheral nerve lesions: experimental anesthesia dolorosa. *Pain*, *7*(2), 103–113. https://doi.org/10.1016/0304-3959(79)90002-2

Wall, Patrick D., & Gutnick, M. (1974). Ongoing activity in peripheral nerves: The physiology and pharmacology of impulses originating from a neuroma. *Experimental Neurology*, *43*(3), 580–593. https://doi.org/10.1016/0014-4886(74)90197-6

Wang, S. P., Chennupati, R., Kaur, H., Iring, A., Wettschureck, N., & Offermanns, S. (2016). Endothelial cation channel PIEZO1 controls blood pressure by mediating flow-induced ATP release. *Journal of Clinical Investigation*, *126*(12), 4527–4536. https://doi.org/10.1172/JCI87343

Weinkauf, B., Obreja, O., Schmelz, M., & Rukwied, R. (2012). Differential effects of lidocaine on nerve growth factor (NGF)-evoked heat- and mechanical hyperalgesia in humans.

European Journal of Pain (London, England), *16*(4), 543–549. https://doi.org/10.1016/j.ejpain.2011.08.004

Wellnitz, S. A., Lesniak, D. R., Gerling, G. J., & Lumpkin, E. A. (2010). The regularity of sustained firing reveals two populations of slowly adapting touch receptors in mouse hairy skin. *Journal of Neurophysiology*, *103*(6), 3378–3388. https://doi.org/10.1152/jn.00810.2009

Westling, G., & Johansson, R. S. (1984). Factors influencing the force control during precision grip. *Experimental Brain Research*, *53*(2), 277–284. https://doi.org/10.1007/BF00238156

Wetzel, C., Hu, J., Riethmacher, D., Benckendorff, A., Harder, L., Eilers, A., … Lewin, G. R. (2007). A stomatin-domain protein essential for touch sensation in the mouse. *Nature*, *445*(7124), 206–209. https://doi.org/10.1038/nature05394

Wetzel, C., Pifferi, S., Picci, C., Gök, C., Hoffmann, D., Bali, K. K., … Lewin, G. R. (2017). Small-molecule inhibition of STOML3 oligomerization reverses pathological mechanical hypersensitivity. *Nature Neuroscience*, *20*(2), 209–218. https://doi.org/10.1038/nn.4454

White et al. (1986). *TH E S T R U C T U R E OF TH E N ER V O U S SYSTEM OF*. *340*, 1–340.

White, F. A., Bhangoo, S. K., & Miller, R. J. (2005). Chemokines: Integrators of pain and inflammation. *Nature Reviews Drug Discovery*, *4*(10), 834–844. https://doi.org/10.1038/nrd1852

Woo, N. H., Teng, H. K., Siao, C. J., Chiaruttini, C., Pang, P. T., Milner, T. A., … Lu, B. (2005). Activation of p75NTR by proBDNF facilitates hippocampal long-term depression. *Nature Neuroscience*, *8*(8), 1069–1077. https://doi.org/10.1038/nn1510

Woo, S.-H., Ranade, S., Weyer, A. D., Dubin, A. E., Baba, Y., Qiu, Z., … Patapoutian, A. (2014). Piezo2 is required for Merkel-cell mechanotransduction. *Nature*, *509*(7502), 622–626. https://doi.org/10.1038/nature13251

Woolf, C J, & Salter, M. W. (2000). Neuronal plasticity: increasing the gain in pain. *Science (New York, N.Y.)*, *288*(5472), 1765–1769. https://doi.org/10.1126/science.288.5472.1765

Woolf, Clifford J. (2011). Central sensitization: Implications for the diagnosis and treatment of pain. *Pain*, *152*(SUPPL.3). https://doi.org/10.1016/j.pain.2010.09.030

Woolf, Clifford J., & Doubell, T. P. (1994). The pathophysiology of chronic pain - increased

sensitivity to low threshold Aβ-fibre inputs. *Current Opinion in Neurobiology*, *4*(4), 525–534. https://doi.org/10.1016/0959-4388(94)90053-1

Woolf, Clifford J., Shortland, P., & Coggeshall, R. E. (1992). Peripheral nerve injury triggers central sprouting of myelinated afferents. *Nature*, *355*(6355), 75–78. https://doi.org/10.1038/355075a0

Woolf, Clifford J, & Mannion, R. J. (1999). *Neuropathic pain : aetiology , s y m p t o m s , m e c h a n i s m s , a n d m a n a g e m e n t*. *353*, 1959–1964.

Yamamoto, T. (1966). The fine structure of the palisade-type sensory endings in relation to hair follicles. *Journal of Electron Microscopy*, *15*(3), 158–166. https://doi.org/10.1093/oxfordjournals.jmicro.a049523

Yang, Y., Wang, Y., Li, S., Xu, Z., Li, H., Ma, L., … Shen, Y. (2004). Mutations in SCN9A, encoding a sodium channel alpha subunit, in patients with primary erythermalgia. *Journal of Medical Genetics*, *41*(3), 171–174. https://doi.org/10.1136/jmg.2003.012153

Yoon, C., Young Wook, Y., Heung Sik, N., Sun Ho, K., & Jin Mo, C. (1994). Behavioral signs of ongoing pain and cold allodynia in a rat model of neuropathic pain. *Pain*, *59*(3), 369–376. https://doi.org/10.1016/0304-3959(94)90023-X

Yu, D., Thakor, D. K., Han, I., Ropper, A. E., Haragopal, H., Sidman, R. L., … Teng, Y. D. (2013). Alleviation of chronic pain following rat spinal cord compression injury with multimodal actions of huperzine A. *Proceedings of the National Academy of Sciences of the United States of America*, *110*(8), 1–10. https://doi.org/10.1073/pnas.1300083110

Zhang, L., Berta, T., Xu, Z. Z., Liu, T., Park, J. Y., & Ji, R. R. (2011). TNF-alpha contributes to spinal cord synaptic plasticity and inflammatory pain: Distinct role of TNF receptor subtypes 1 and 2. *Pain*, *152*(2), 419–427. https://doi.org/10.1016/j.pain.2010.11.014

Zhu, Y., Lu, S. G., & Gold, M. S. (2012). Persistent inflammation increases GABA-induced depolarization of rat cutaneous dorsal root ganglion neurons in vitro. *Neuroscience*, *220*, 330–340. https://doi.org/10.1016/j.neuroscience.2012.06.025

Ziegler, E. A., Magerl, W., Meyer, R. A., & Treede, R. D. (1999). Secondary hyperalgesia to punctate mechanical stimuli. Central sensitization to A-fibre nociceptor input. *Brain*, *122*(12), 2245–2257. https://doi.org/10.1093/brain/122.12.2245

Zimmerman, A., Bai, L., & Ginty, D. D. (2014). The gentle touch receptors of mammalian skin. *Science*, *346*(6212), 950–954. https://doi.org/10.1126/science.1254229

Zimmerman, Amanda, Bai, L., & Ginty, D. D. (2014). *of Mammalian Skin*. *346*(6212), 950–954. https://doi.org/10.1126/science.1254229

Zimmermann, M. (2001). Pathobiology of neuropathic pain. *European Journal of Pharmacology*, *429*(1–3), 23–37. https://doi.org/10.1016/S0014-2999(01)01303-6

Zotterman, Y. (1938). *CUTANEOUS SENSORY NERVES From the Physiological Laboratory , Karolinska Institutet , Stockholm of axone potentials from a phalangeal nerve preparation of the frog*. 1–28.

Acknowledgement and expression of gratitude

I would like to express my sincere gratitude to my supervisor Prof. Dr. Gary R. Lewin. He provided me with the chance to grow scientifically, experience conferences and collaborations in different countries and provided support, inspiration and critical thinking along my way of achieving the PhD. It was a pleasure to work with you, the environment you provided was very stimulating, there was never any resource you did not provide me with. Thank you for making me a part of your team! Additionally, I would like to thank Prof. Dr. Peter Robin Hiesinger for my university supervision as well as Prof. Dr. James Poulet and Prof. Dr. Simone Spuler for interesting discussion during my committee meetings.

I am also grateful to Dr. Christiane Wetzel and Dr. Jan Walcher for teaching me surgical techniques, behavioural assays, electrophysiology and being available for discussion of data and concepts. And Dr. James Hall for generating the sensory STOML3 OE animals without which our insight into STOML3s importance for sensory neuron sensitization would not be the same.

Thank you Dr. Valérie Bégay-Müller, for helping me to take care of transgenic animals as well as providing critical thought about concepts and data.

In addition, I would like to thank Dr. Bettina Purfürst and her team for helping with the electron microscopy and Dr. Alison Barker for critically reading and reviewing my thesis.

I also wish to thank the technical staff of the Lewin lab. Anke Scheer for help with taking care of mouse strains, Maria Braunschweig, Kathleen Barda and Franziska Barthel for support in producing solutions and buffers as well as lots of PCRs, which made my life a whole lot easier! Birgit Cloos and Dr. Cornelia Stärkel for helping with administrative issues and to all of them for being nice colleagues that provided smiles and a nice chat from time to time. It was really appreciated!

At last, I want to thank all remaining colleagues, the atmosphere in the lab was always nice, I did appreciate having talks with you (scientific or not) and wish all of you all the luck in the world to achieve your goals.

To end on a personal note, I wish to thank my family. They always supported me and enabled me to find my way in life. I hope the next step will be as interesting as this one was, I am excited to share it with you.

To my girlfriend: I am so very happy we met here at the institute. Thank you for coming to Berlin and for your support. I will always try to give back at least as much as I am receiving.

Eidesstattliche Erklärung

Hiermit versichere ich, dass ich die vorliegende Arbeit selbstständig verfasst und keine anderen als die angegebenen Quellen und Hilfsmittel benutzt habe. Alle Ausführungen, die anderen veröffentlichten oder nicht veröffentlichten Schriften wörtlich oder sinngemäß entnommen wurden, habe ich kenntlich gemacht.

Die Arbeit hat in gleicher oder ähnlicher Fassung noch keiner anderen Prüfungsbehörde vorgelegen.

_____ _____

Ort, Datum Unterschrift